STATE OF THE CLIMATE IN 2021

REGIONAL CLIMATES

P. Bissolli, C. Ganter, A. Mekonnen, A. Sánchez-Lugo, and Z. Zhu, Eds.

Special Online Supplement to the *Bulletin of the American Meteorological Society*, Vol. 103, No. 8, August 2022

10.1175/2022BAMSStateoftheClimate.1
Corresponding authors:
North America: Ahira Sánchez-Lugo / Ahira.Sanchez-Lugo@noaa.gov.
Central America and the Caribbean: Ahira Sánchez-Lugo / Ahira.Sanchez-Lugo@noaa.gov
South America: Ahira Sánchez-Lugo / Ahira.Sanchez-Lugo@noaa.gov
Africa: Ademe Mekonnen / amekonne@ncat.edu
Europe: Peter Bissolli / Peter.Bissolli@dwd.de
Asia: Zhiwei Zhu / zwz@nuist.edu.cn
Oceania: Catherine Ganter / Catherine.Ganter@bom.gov.au

STATE OF THE CLIMATE IN 2021
Regional Climates

Editors

Jessica Blunden
Tim Boyer

Chapter Editors

Freya Aldred
Peter Bissolli
Kyle R. Clem
Howard J. Diamond
Matthew L. Druckenmiller
Robert J. H. Dunn
Catherine Ganter
Nadine Gobron
Gregory C. Johnson
Rick Lumpkin
Ademe Mekonnen
John B. Miller
Twila A. Moon
Marilyn N. Raphael
Ahira Sánchez-Lugo
Carl J. Schreck III
Richard L. Thoman
Kate M. Willett
Zhiwei Zhu

Technical Editor

Laura Ohlmann

BAMS Special Editor for Climate

Michael A. Alexander

American Meteorological Society

Cover credit:
Flames and smoke from wildfires above the Fraser River Valley near Lytton, British Columbia, Canada, on 2 July 2021. Photographer: James MacDonald/Bloomberg ©2021 Bloomberg Finance LP - Getty

Regional Climates is one chapter from the *State of the Climate in 2021* annual report. Compiled by NOAA's National Centers for Environmental Information, *State of the Climate in 2021* is based on contributions from scientists from around the world. It provides a detailed update on global climate indicators, notable weather events, and other data collected by environmental monitoring stations and instruments located on land, water, ice, and in space. The full report is available from 10.1175/2022BAMSStateoftheClimate.1.

How to cite this document:

Citing the complete report:
Blunden, J. and T. Boyer, Eds., 2022: "State of the Climate in 2021". *Bull. Amer. Meteor. Soc.,* **103** (8), Si–S465, https://doi.org/10.1175/2022BAMSStateoftheClimate.1.

Citing this chapter:
Bissolli, P., C. Ganter, A. Mekonnen, A. Sánchez-Lugo, and Z. Zhu, Eds. 2022: Regional Climates [in "State of the Climate in 2021"]. *Bull. Amer. Meteor. Soc.*, **103** (8), S341–S453, https://doi.org/10.1175/2022BAMSStateoftheClimate_Chapter7.1.

Citing a section (example):
Koren, G., 2022: Major floods in the Amazon basin [in "State of the Climate in 2021"]. Bull. Amer. Meteor. Soc., **103** (8), S369–S370, https://doi.org/10.1175/2022BAMSStateoftheClimate_Chapter7.1.

Editor and Author Affiliations (alphabetical by name)

Abida, A., Agence Nationale de l'Aviation Civile et de la Météorologie, Union des Comores

Agyakwah, W., Climate Prediction Center, National Centers for Environmental Prediction, NOAA, College Park, Maryland

Aldeco, Laura S., Servicio Meteorológico Nacional, Buenos Aires, Argentina

Alfaro, Eric J., Center for Geophysical Research and School of Physics, University of Costa Rica, San José, Costa Rica

Allen, Teddy, Caribbean Institute for Meteorology and Hydrology, Bridgetown, Barbados

Alves, Lincoln M., Centro Nacional de Monitoramento e Alertas de Desastres Naturais CEMADEN, São Paulo, Brazil

Amador, Jorge A., Center for Geophysical Research and School of Physics, University of Costa Rica, San José, Costa Rica

Andrade, B., Seychelles Meteorological Authority, Mahe, Seychelles

Asgarzadeh, P., National Center for Climate and Drought Crisis Management, Islamic Republic of Iranian Meteorological Organization, Iran

Avalos, Grinia, Servicio Nacional de Meteorología e Hidrología del Perú, Lima, Perú

Baez, Julian, Universidad Católica Nuestra Señora de la Asunción, Asunción, Paraguay

Bardin, M. Yu., Yu. A. Izrael Institute of Global Climate and Ecology; Institute of Geography, Russian Academy of Sciences, Russia

Bekele, E., Climate Prediction Center, National Centers for Environmental Prediction, NOAA, College Park, Maryland

Bertalanic, Renato, Slovenian Environment Agency, Slovenia

Bissolli, Peter, Deutscher Wetterdienst, WMO RA VI Regional Climate Centre Network, Offenbach, Germany

Bochníček, Oliver, Slovak Hydrometeorological Institute, Slovakia

Bukunt, Brandon, NOAA/NWS Weather Forecast Office, Guam

Calderón, Blanca, Center for Geophysical Research, University of Costa Rica, San José, Costa Rica

Campbell, Jayaka D., Department of Physics, The University of the West Indies, Jamaica

Chandler, Elise, Bureau of Meteorology, Melbourne, Victoria, Australia

Charlton, Candice S, Department of Physics, The University of the West Indies, Jamaica

Cheng, Vincent Y. S., Environment and Climate Change Canada, Toronto, Ontario, Canada

Clarke, Leonardo A., Department of Physics, The University of the West Indies, Jamaica

Correa, Kris, Servicio Nacional de Meteorología e Hidrología del Perú, Lima, Perú

Cortés Salazar, Catalina R., Dirección de Meteorológica de Chile, Santiago de Chile, Chile

Costa, Felipe, Centro Internacional para la Investigación del Fenómeno de El Niño (CIIFEN), Guayaquil, Ecuador

Crhová, Lenka, Czech Hydrometeorologival Institute, Czechia

Cunha, Ana Paula, Centro Nacional de Monitoramento e Alertas de Desastres Naturais CEMADEN, São Paulo, Brazil

Demircan, Mesut, Turkish State Meteorological Service, Ankara, Türkiye

Dhurmea, K. R., Mauritius Meteorological Service, Vacoas, Mauritius

Domínguez, Diana A., Servicio Meteorológico Nacional, Buenos Aires, Argentina

Dulamsuren, Dashkhuu, Institute of Meteorology, Hydrology and Environment, National Agency for Meteorology, Ulaanbaatar, Mongolia

ElKharrim, M., Direction de la Météorologie Nationale Maroc, Rabat, Morocco

Espinoza, Jhan-Carlo, Université Grenoble Alpes, Institut des Géosciences de l'Environnement, IRD, CNRS, Grenoble INP, Grenoble, France

Fazl-Kezemi, A., National Center for Climate and Drought Crisis Management, Islamic Republic of Iranian Meteorological Organization, Iran

Fedaeff, Nava, National Institute of Water and Atmospheric Research, Ltd. (NIWA), Auckland, New Zealand

Fenimore, Chris, NOAA/NESDIS National Centers for Environmental Information, Asheville, North Carolina

Fuhrman, Steven, NOAA/NWS National Centers for Environmental Prediction, Climate Prediction Center, College Park, Maryland

Ganter, Catherine, Bureau of Meteorology, Melbourne, Victoria, Australia

Gleason, Karin, NOAA/NESDIS National Centers for Environmental Information, Asheville, North Carolina

Guard, Charles "Chip" P., Tropical Weather Sciences, Sinajana, Guam

Hagos, Samson, Pacific Northwest National Lab, Department of Energy, Washington

Hanafusa, Mizuki, Tokyo Climate Center, Japan Meteorological Agency, Japan

Heim, Jr., Richard R., NOAA/NESDIS National Centers for Environmental Information, Asheville, North Carolina

Kennedy, John, Met Office Hadley Centre, Exeter, United Kingdom

Hellström, Sverker, Swedish Meteorological and Hydrological Institute, Sweden

Hidalgo, Hugo G., Center for Geophysical Research and School of Physics, University of Costa Rica, San José, Costa Rica

Ijampy, I. A., Nigerian Meteorological Agency, Abuja, Nigeria

Im, Gyo Soon, Climate Change Monitoring Division, Korea Meteorological Administration, South Korea

Jumaux, G., Météo France, Direction Interrégionale pour l'Océan Indien, Réunion

Kabidi, K., Direction de la Météorologie Nationale Maroc, Rabat, Morocco

Kerr, Kenneth, Trinidad and Tobago Meteorological Service, Trinidad

Khalatyan, Yelena, Hydrometeorology and Monitoring Center, Armenia

Khan, Valentina, Hydrometcenter of Russia, WMO North EurAsia Climate Center, Moscow, Russia

Khiem, Mai Van, Viet Nam National Center of Hydro-Meteorology Forecasting, Viet Nam Meteorology Hydrology Administration, Viet Nam

Koch, Tobias, Soil and Water Ecosystems (SWEco), Faculty of Geography, University of Marburg, Marburg, Germany

Koren, Gerbrand, Copernicus Institute of Sustainable Development, Utrecht University, the Netherlands

Korshunova, Natalia N., All-Russian Research Institute of Hydrometeorological Information, World Data Center, Obninsk, Russia

Kruger, A. C., Climate Service, South African Weather Service, Pretoria, South Africa

Lakatos, Mónika, Climatology Unit, Hungarian Meteorological Service, Budapest, Hungary

Mamen, Jostein, Climate Division, Norwegian Meteorological Institute, Oslo, Norway

Lam, Hoang Phuc, Viet Nam National Center of Hydro–Meteorology Forecasting, Viet Nam Meteorology Hydrology Administration, Viet Nam

Lander, Mark A., University of Guam, Mangilao, Guam

Lavado-Casimiro, Waldo, Servicio Nacional de Meteorología e Hidrología del Perú, Lima, Perú

Lee, Tsz-Cheung, Hong Kong Observatory, Hong Kong, China

Leung, Kinson H. Y., Environment and Climate Change Canada, Toronto, Ontario, Canada

Liu, Xuefeng, Nanjing University of Information Science and Technology, Nanjing, China

Lu, Rui, Nanjing University of Information Science and Technology, Nanjing, China

Marengo, José A., Centro Nacional de Monitoramento e Alertas de Desastres Naturais CEMADEN, São Paulo, Brazil

Editor and Author Affiliations (alphabetical by name)

Marjan, Mohammadi, National Center for Climate and Drought Crisis Management, Islamic Republic of Iranian Meteorological Organization, Iran
Martínez, Ana E., National Meteorological Service of Mexico, Mexico City, Mexico
McBride, Charlotte, Climate Service, South African Weather Service, Pretoria, South Africa
Mekonnen, Ademe, Department of Physics, North Carolina A & T University, Greensboro, North Carolina
Mietus, Mirek, Instytut Meteorologii i Gospodarki Wodnej PIB, Poland
Misevicius, Noelia, Instituto Uruguayo de Meteorología, Montevideo, Uruguay
Moise, Aurel, Centre for Climate Research Singapore, Meteorological Service Singapore, Singapore
Molina-Carpio, Jorge, Universidad Mayor de San Andrés, La Paz, Bolivia
Mora, Natali, Center for Geophysical Research, University of Costa Rica, San José, Costa Rica
Mostafa, Awatif E., Department of Seasonal Forecast and Climate Research, Cairo Numerical Weather Prediction, Egyptian Meteorological Authority, Cairo, Egypt
Ndiaye, O., Senegalese Meteorological Service, Dakar, Senegal
Nieto, Juan J., Centro Internacional para la Investigación del Fenómeno de El Niño (CIIFEN), Guayaquil, Ecuador
Olafsdottir, Kristin, Icelandic Meteorological Service, Iceland
Pascual Ramírez, Reynaldo, National Meteorological Service of Mexico, Mexico City, Mexico
Phillips, David, Environment and Climate Change Canada, Toronto, Ontario, Canada
Porat, Amos, Israel Meteorological Service, Israel
Rodriguez Guisado, Esteban, Agencia Estatal de Meteorología, Madrid, Spain
Rajeevan, Madhavan, Earth System Science Organization, Ministry of Earth Sciences, New Delhi, India
Ramos, Andrea M., Instituto Nacional de Meteorologia, Brasilia, Brazil
Recalde Coronel, Cristina, NOAA/NWS National Centers for Environmental Prediction, Climate Prediction Center, College Park, Maryland
Reyes Kohler, Alejandra J., Dirección de Meteorológica de Chile, Santiago de Chile, Chile
Robjhon, M., Climate Prediction Center, National Centers for Environmental Prediction, NOAA, College Park, Maryland
Ronchail, Josyane, Laboratoire LOCEAN-IPSL, Paris, France
Salinas, Roberto, Dirección de Meteorología e Hidrología / Dirección Nacional de Aeronáutica Civil, Asunción, Paraguay
Sánchez-Lugo, Ahira, NOAA/NESDIS National Centers for Environmental Information, Asheville, North Carolina
Sato, Hirotaka, Tokyo Climate Center, Japan Meteorological Agency, Japan
Sato, Hitoshi, Tokyo Climate Center, Japan Meteorological Agency, Japan
Sayouri, Amal, Direction de la Météorologie Nationale Maroc, Rabat, Morocco
Sensoy, Serhat, Turkish State Meteorological Service, Ankara, Türkiye
Setiawan, Amsari Mudzakir, Division for Climate Variability Analysis, BMKG, Indonesia
Sima, F., Division of Meteorology, Department of Water Resources, Banjul, The Gambia.
Smith, Adam, NOAA/NESDIS National Centers for Environmental Information, Asheville, North Carolina
Sorel, Matthieu, Météo France, Toulouse, France
Spillane, Sandra, Met Éireann, Dublin, Ireland
Spence, Jacqueline M., Meteorological Service, Jamaica, Kingston, Jamaica
Sreejith, O. P., India Meteorological Department, Pune, India
Srivastava, A. K., India Meteorological Department, Pune, India
Stephenson, Tannecia S., Department of Physics, The University of the West Indies, Jamaica
Takahashi, Kiyotoshi, Tokyo Climate Center, Japan Meteorological Agency, Japan
Taylor, Michael A., Department of Physics, The University of the West Indies, Jamaica
Thiaw, Wassila M., NOAA/NWS National Centers for Environmental Prediction, Climate Prediction Center, College Park, Maryland
Tobin, Skie, Bureau of Meteorology, Melbourne, Victoria, Australia
Trescilo, Lidia, State Hydrometeorological Service, Moldova
Trotman, Adrian R., Caribbean Institute for Meteorology and Hydrology, Bridgetown, Barbados
Van Meerbeeck, Cedric J., Caribbean Institute for Meteorology and Hydrology, Bridgetown, Barbados
Vazifeh, A., National Center for Climate and Drought Crisis Management, Islamic Republic of Iranian Meteorological Organization, Iran
Wakamatsu, Shunya, Tokyo Climate Center, Japan Meteorological Agency, Japan
Zaheer, M. F., Afghanistan Famine Early Warning System Network, Afghanistan
Zeng, F., Pacific Northwest National Lab, Department of Energy, Washington
Zhang, Peiqun, National Climate Centre, China Meteorological Administration, Beijing, China
Zhu, Zhiwei, Nanjing University of Information Science and Technology, Nanjing, China

Editorial and Production Team

Allen, Jessicca, Graphics Support, Cooperative Institute for Satellite Earth System Studies, North Carolina State University, Asheville, North Carolina
Hammer, Gregory, Content Team Lead, Communications and Outreach, NOAA/NESDIS National Centers for Environmental Information, Asheville, North Carolina
Love-Brotak, S. Elizabeth, Lead Graphics Production, NOAA/NESDIS National Centers for Environmental Information, Asheville, North Carolina
Misch, Deborah J., Graphics Support, Innovative Consulting and Management Services, LLC, NOAA/NESDIS National Centers for Environmental Information, Asheville, North Carolina
Ohlmann, Laura, Technical Editor, Innovative Consulting and Management Services, LLC, NOAA/NESDIS National Centers for Environmental Information, Asheville, North Carolina
Riddle, Deborah B., Graphics Support, NOAA/NESDIS National Centers for Environmental Information, Asheville, North Carolina
Veasey, Sara W., Visual Communications Team Lead, Communications and Outreach, NOAA/NESDIS National Centers for Environmental Information, Asheville, North Carolina

7. Table of Contents

7. Table of Contents

*Please refer to Chapter 8 (Relevant datasets and sources) for a list of all climate variables and datasets used in this chapter for analyses, along with their websites for more information and access to the data.

7. REGIONAL CLIMATES

P. Bissolli, C. Ganter, A. Mekonnen, A. Sánchez-Lugo, and Z. Zhu, Eds.

a. Overview

This chapter provides summaries of the 2021 temperature and precipitation conditions across seven broad regions: North America, Central America and the Caribbean, South America, Africa, Europe and the Middle East, Asia, and Oceania. In most cases, summaries of notable weather events are also included. Local scientists provided the annual summary for their respective regions and, unless otherwise noted, the source of the data used is typically the agency affiliated with the authors. The base period used for these analyses in many countries is now 1991–2020, as new 30-year climate normals are being utilized (see Chapter 1 for details). However, please note that on occasion different nations, even within the same section, may use unique periods to define their normal and many countries still use the 1981–2010 base period. Section introductions typically define the prevailing practices for that section, and exceptions will be noted within the text. In a similar way, many contributing authors use languages other than English as their primary professional language. To minimize additional loss of fidelity through re-interpretation after translation, editors have been conservative and careful to preserve the voice of the author. In some cases, this may result in abrupt transitions in style from section to section.

b. North America—A. Sánchez-Lugo, Ed.

1) CANADA—K. H. Y. Leung, V. Y. S. Cheng, and D. Phillips

In Canada, 2021 was characterized by above-average winter and spring temperatures in most of southern Canada and northeastern Nunavut and by below-average winter and spring temperatures in most of the Yukon and Northwest Territories. The country also experienced above-average summer temperatures in most of western and southern Canada and below-average summer temperatures in central northern Canada. The national average temperature for autumn 2021 was the highest in the 74-year record (1948–2021).

(i) Temperature

The annual average temperature for Canada in 2021 was 1.0°C above the 1991–2020 baseline average, and the fourth-warmest year in the 74-year record (Fig. 7.1). The warmest year on record was 2010 at 1.9°C above average. Over the past 74 years (1948–2021), the national annual average temperature has exhibited a linear warming trend of +1.9°C, and three of the 10 warmest years occurred during the last decade. Annual anomalies for 2021 above +2.5°C were recorded in the northernmost parts of Canada, and anomalies

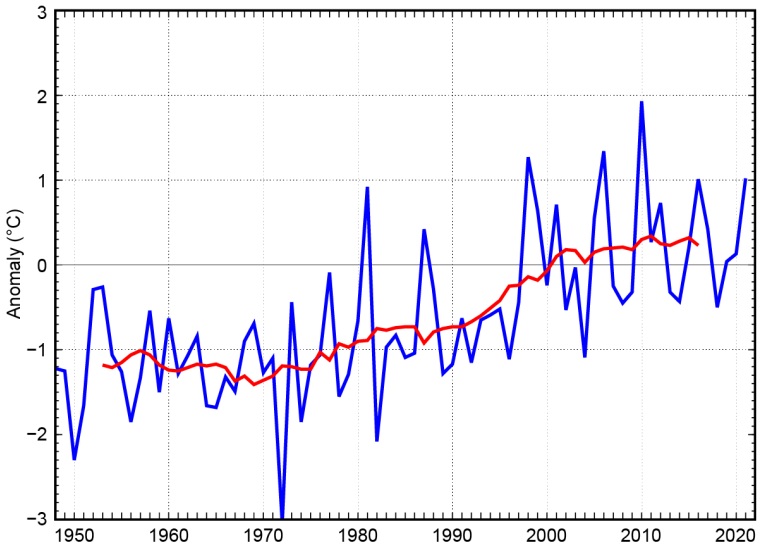

Fig. 7.1. Annual average temperature anomalies (°C; 1991–2020 base period) in Canada for the period 1948–2021. Red line is the 11-year running mean. (Source: Environment and Climate Change Canada.)

above +0.5°C were recorded in eastern Canada. Annual anomalies below −0.5°C were observed in an area centered over the southern Yukon and extending into the western Northwest Territories and northern British Columbia (Fig. 7.2). In 2021, eight provinces/territories reported an annual average temperature that was among their 10 highest on record: Newfoundland and Labrador, New Brunswick, and Quebec (second highest); Ontario and Nunavut (third highest); Nova Scotia and Prince Edward Island (fourth); and Manitoba (10th).

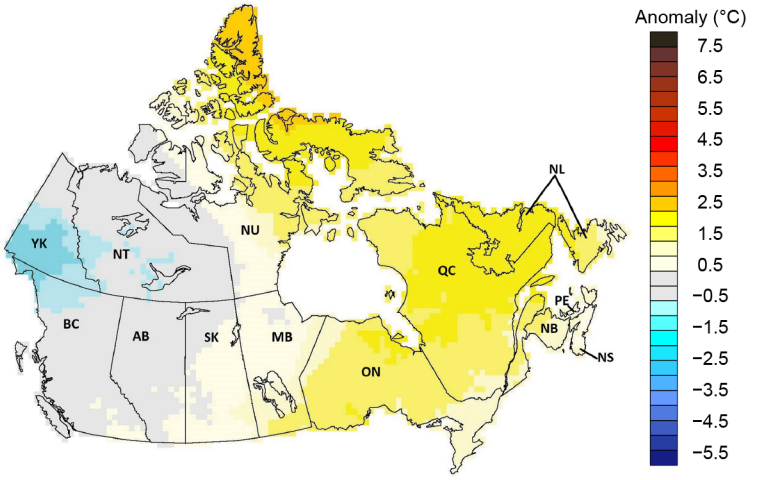

Fig. 7.2. Annual average temperature anomalies (°C; 1991–2020 base period) in Canada for 2021. (Source: Environment and Climate Change Canada.)

Seasonally, the national average temperature for the winter season (December 2020–February 2021) was 2.1°C above the 1991–2020 average, making it the fourth highest on record. The national average temperature for the winter season has increased by 3.5°C over the past 74 years. Winter anomalies of +3.0°C were recorded over eastern Quebec, eastern Nunavut, and most of the Atlantic provinces. As a result, the provinces of Nova Scotia and Prince Edward Island experienced their warmest winters on record. New Brunswick, Newfoundland and Labrador, and Quebec each experienced their second-warmest winter, while Nunavut experienced its third warmest. Below-average temperatures were observed in most of the Northwest Territories and in northern parts of the Yukon. Moreover, the month of February was among the 10 coldest on record for the Yukon, Alberta, and Saskatchewan. Some areas within those regions experienced a monthly temperature more than 5°C below average.

During spring (March–May), above-average temperatures were observed from interior British Columbia eastward to eastern and northeastern Canada, with departures above 2.0°C observed in northern Nunavut and parts of central Quebec. Below-average temperatures were recorded over northwestern Canada, with temperatures 2.0°C below average in central Yukon and eastern Northwest Territories. The national average temperature for spring 2021 was 0.6°C above average and the 14th highest in the 74-year record. Quebec and Newfoundland and Labrador both observed their seventh-warmest spring on record. The national average spring temperature has increased by 1.6°C over the past 74 years.

The national average temperature for summer (June–August) was 0.5°C above average, the fifth highest in the 74-year record. The central region of Nunavut and northern Quebec experienced summer temperatures that were 1.0°C below average. Southwestern Canada experienced summer anomalies above 1.5°C, with British Columbia having its warmest summer on record. Other provinces with temperatures among their 10 highest include Alberta and Saskatchewan (second highest); New Brunswick and Prince Edward Island (fifth highest); Newfoundland and Labrador, Nova Scotia and Yukon (sixth); Ontario (seventh); and Manitoba (ninth). The national average summer temperature has increased by 1.5°C over the past 74 years.

The national average temperature for autumn (September–November) was 2.2°C above average, the highest in the 74-year record. Most of Canada experienced temperatures at least 1.5°C above average, with Manitoba, parts of northwestern Ontario, and most of Nunavut, experiencing temperatures 2.5°C, 3.5°C, and 4.0°C above average, respectively. Only a small region between British Columbia and Yukon experienced temperatures below average. Quebec, New Brunswick, and Nunavut all experienced their highest autumn temperatures in the 74-year record. The national

average autumn temperature has increased by 1.8°C over the past 74 years. The temperature records presented above were based on adjusted and homogenized Canadian climate data.

(ii) Precipitation

Over the past decade, precipitation monitoring technology has evolved and Environment and Climate Change Canada (ECCC) and its partners implemented a transition from manual observations to the use of automatic precipitation gauges. Extensive data integration is required to link the current precipitation observations to the long-term historical manual observations. The update and reporting of historical adjusted precipitation trends and variations will be on temporary hiatus pending an extensive data reconciliation, and will be resumed thereafter. ECCC remains committed to providing credible climate data to inform adaptation decision making, while ensuring the necessary data reconciliation occurs as monitoring technology evolves.

(iii) Notable events and impacts

The record-breaking weather records in this section are based on non-homogenized station data. During the first two weeks of February, temperatures were 20°C below normal in Alberta and Saskatchewan, but 20°C above normal in southern Baffin Island. February temperatures from −35°C to −50°C were reported in parts of the Arctic and Prairies, resulting in the issuance of many extreme cold warnings. These extreme low temperatures broke minimum temperature records that dated back more than 50 years. The all-time daily minimum temperature for Edmonton International Airport reached −43.8°C, which is close to the all-time minimum of −43.9°C set in 1994 for the station.

A widespread and long-lasting dry period across western Canada from June to August 2021 was the worst on record. The southern regions between British Columbia and northwestern Ontario faced one of their driest summers in the 74-year record, with many places recording less than half of their normal rainfall in the growing season. Victoria Airport had its driest spring in 80 years. From 16 June to 6 August, Vancouver Airport recorded 53 consecutive days without a measurable rainfall event (0.2 mm or more)—the longest interval without rainfall in 35 years.

British Columbia was impacted by a historic seven atmospheric river-fueled storms in November 2021. Some of these large, wet systems featured unseasonably high temperatures (around 15°C) that were sufficient to melt snow at mid-elevations. The duration of some of these atmospheric river events ranged from two to three days instead of the usual 24 hours. According to station data, rainfall totals associated with the mid-November atmospheric river were 200–300 mm in 2.5 days, which was well above the climatological average for the entire month of November. During this storm, over 40 daily rainfall records were broken. Station data also show that rainfall totals along the south coast of British Columbia, during the last week of November, ranged from 100 mm to 350 mm, which turned valuable farm fields into wetlands. These November rain-flood storms resulted in the evacuation of almost 15,000 people from their homes and led to at least four fatalities. By the end of the month, autumn 2021 was the wettest on record for at least 10 sites across the south coast of British Columbia.

Sidebar 7.1: "Hell on Earth"—D. PHILLIPS

In the final week of June and first week of July 2021, a high-pressure ridge—an atmospheric juggernaut with incredible strength, height, scope, and persistence—built over western North America, sprawling from California to the Arctic Circle. Several factors conspired to strengthen the massive ridge and generate record blistering heat. The general circulation took a far-north arching route into northwestern Canada locking in the ridge (dome) in a slow-moving wavy pattern called an Omega Block. Clouds vanished under the dome, giving the sun an unobstructed line of sight, further warming the surface directly. As the atmospheric pressure increased under the dome, the descending air became denser and grew hotter. The air was made even hotter by the drought-stricken landscape. An exceptionally dry spring across the West led to a scarcity of soil moisture. Less soil moisture meant less solar energy being used to evaporate water, thus cooling, and instead directly heating the air and baking the ground. Timing was also crucial. The development of the ridge at the beginning of the Northern Hemisphere's summer solstice coincided with the year's highest sun angle and longest amount of daylight, further augmenting the sun's ability to heat the surface. Other dynamic factors significant in warming the air to record highs included the development of a thermal trough or "heat low" over California's Mojave Desert that spread to the California coast.

The widespread hot spell was particularly impactful as it occurred five to six weeks earlier than the typical warmest time of the year. Heat waves generally tend to be more dangerous when they occur early in the summer, before people have had time to fully acclimatize. Daytime highs were 15° to 25°C above normal with little reprieve at night as the temperature did not fall much below 20°C (Fig. SB7.1). The inferno-like heat shattered over 1000 daily maximum/minimum temperature records over 11 days, across all four Canadian western provinces and three northern territories, with over 100 records between 40° and 50°C. Lytton, a village 260 km northeast of Vancouver in British Columbia's Fraser Canyon, set a new Canadian record high temperature of 49.6°C on 28 June, nearly 24°C above normal. Two days earlier, on 26 June, Lytton first broke the previous national record of 45°C that had stood for 84 years in Saskatchewan. The new record fell again on 27 June, and again on 28 June (Fig. SB7.2). The next day, raging wildfires incinerated 90% of the village. The fire resulted in two deaths and the displacement of all 1200 residents. Lytton experienced a temperature higher than any location in the United States outside the Desert Southwest and higher than any temperature ever observed in Europe or South America. Indeed, it was the most extreme high temperature observed anywhere in the world above 45° latitude. Six other locations also observed a maximum temperature that exceeded the previous high Canadian heat record set in 1937.

At the peak of the heat wave on 28 June, Victoria (the capital city of British Columbia), with one of the most moderate climates in Canada, recorded a maximum temperature of 40°C, an all-time record for Victoria and a staggering 21°C above average. Kamloops (city in British Columbia) reported six days with maximum temperatures surpassing 40°C, significant because the city had never before observed 40°C in June. Among the thousands of temperature records broken across the Northwest was 39.9°C on 30 June in Fort Smith, Northwest Territories, the highest temperature ever recorded north of latitude 60°.

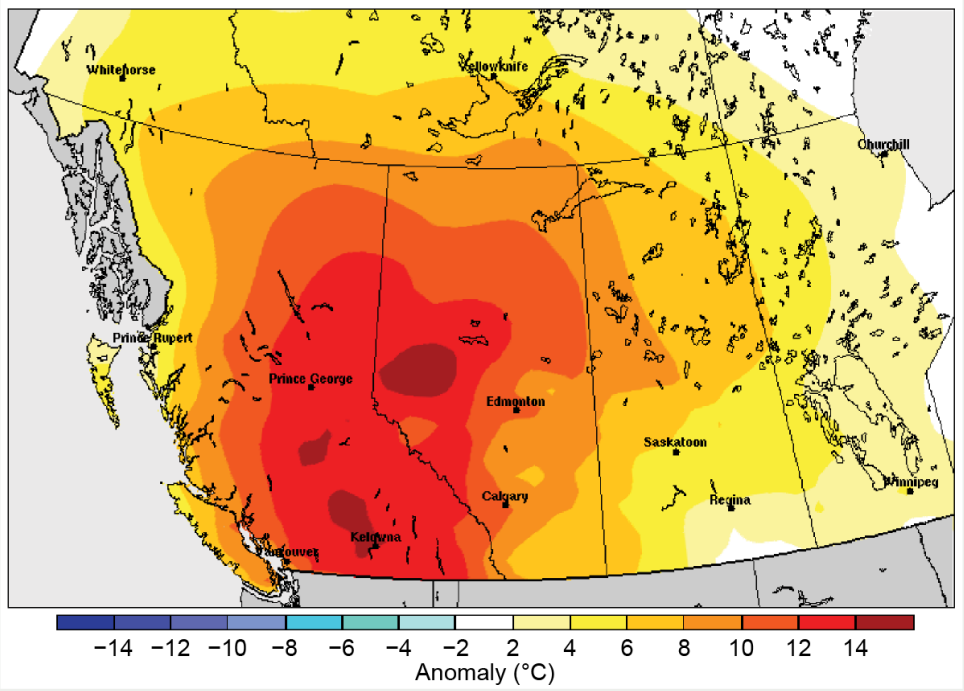

Fig. SB7.1. Surface air temperature departure (°C; 1981–2010 base period) for the period 28–30 June 2021. (Credit: National Laboratory, Central Region, Meteorological Service of Canada.)

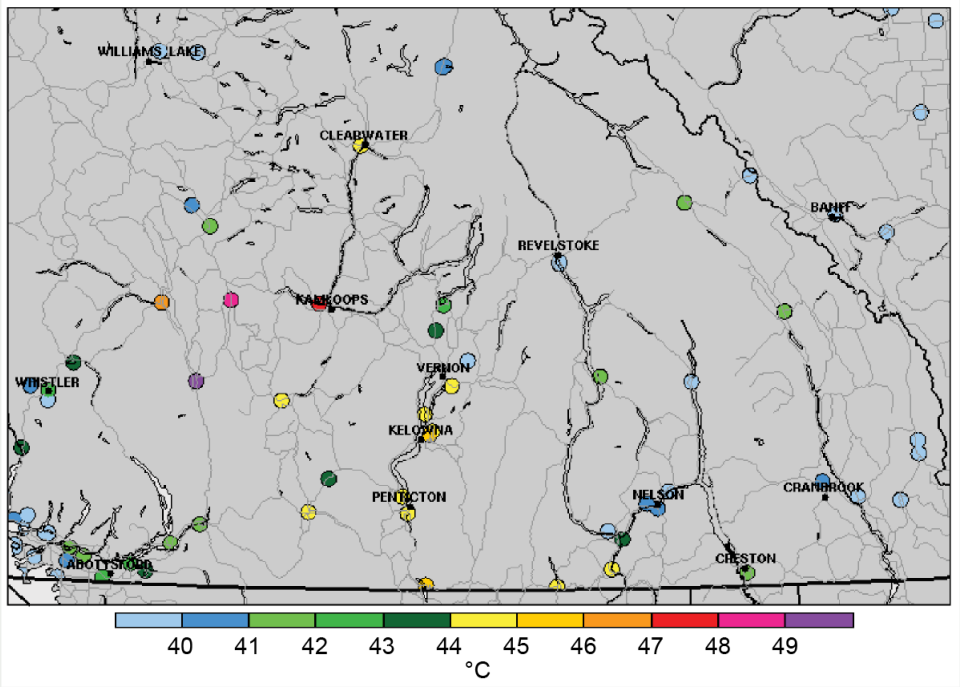

Fig. SB7.2. Highest daily maximum surface air temperature during the period of 23 June–4 July 2021. (Credit: National Laboratory, Central Region, Meteorological Service of Canada.)

The unbearable heat left millions of people overheated in western Canada. Power grids failed, asphalt melted, highways buckled, salmon cooked in hot river waters, and fruit baked on vines and trees. City workers turned on portable spray parks, added heavy misters, and converted hockey rinks into cooling centers. In Vancouver, Canada's third largest city, only 28% of households have any type of air conditioning, well below the national urban average of 60%. Officials kept shopping malls and theaters open longer to give residents additional air-conditioned comfort. Hospitals canceled outdoor COVID-19 testing and vaccination clinics or moved them indoors. Because it was almost impossible to safely go outside, people moved mattresses into basements—the coolest area of a home—to escape the heat, while others checked into air-conditioned hotels with their pets. Restaurants and bars closed after kitchen temperatures rose to potentially deadly levels. Some companies cut operating hours or suspended business, and outdoor workers opted to start before dawn and finish work at noon.

The hottest week in Canadian history was also one of the deadliest. Across Vancouver and Victoria, the historic heat wave was a contributing factor in the premature deaths of almost 600 people, with more than half occurring during 28–29 June. Alberta reported 185 heat-related fatalities. Two-thirds of the heatstroke victims were age 60 or older with underlying health conditions, socially isolated, or living alone in their homes. Emergency calls created a backlog for police and paramedic services. More than 650,000 farm animals perished. Poultry producers sprayed barn walls with cool water, but thousands of chickens were roasted alive. Dairy cows gave less milk, and raspberry crops withered on the stems. Countless wild animals and birds also perished in the record heat. The late June heat dome coincided with the lowest tides in years and some of the longest days. As a result, along the Pacific coast, a billion intertidal and marine organisms died, including mussels, clams, and fish, leaving shorelines with a foul odor for days.

2) UNITED STATES—K. Gleason, C. Fenimore, R. R. Heim Jr., and A. Smith

The annual average temperature for the contiguous United States (CONUS) in 2021 was 12.5°C, which was 0.7°C above the 1991–2020 average, the fourth highest in the 127-year record (Fig. 7.3a). Much of the northern Plains experienced temperature anomalies at least 1°C or more above average (Fig. 7.4a). Based on a linear regression of data from 1895 to 2021, the annual CONUS temperature over the 127-year record is increasing at an average rate of 0.09°C decade–1 (0.27°C decade^{-1} since 1970). Average precipitation totaled 774 mm, which is 97% of the 1991–2020 average (Fig. 7.3b). Although below average for 2021, the annual precipitation total has been increasing at an average rate of 5 mm decade^{-1} (4 mm decade^{-1} since 1970). The average annual temperature across Alaska in 2021 was 0.9°C below average. The annual temperature for Alaska over the 97-year record is increasing at an average rate of 0.17°C decade^{-1} (0.44°C decade^{-1} since 1970).

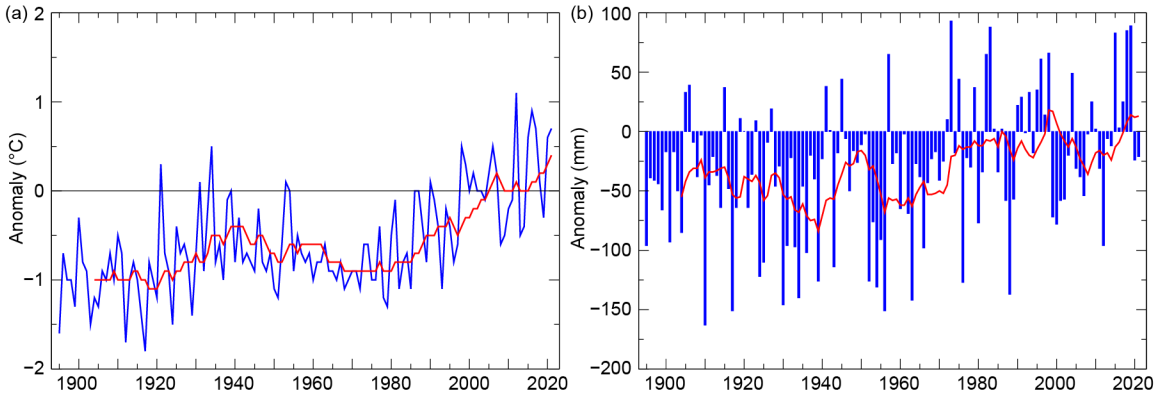

Fig. 7.3. Annual (a) mean temperature anomalies (°C) and (b) precipitation anomalies (mm) for the CONUS during 1895–2021 (1991–2020 base period). Red line is the lagged 10-year running mean. (Source: NOAA/NCEI.)

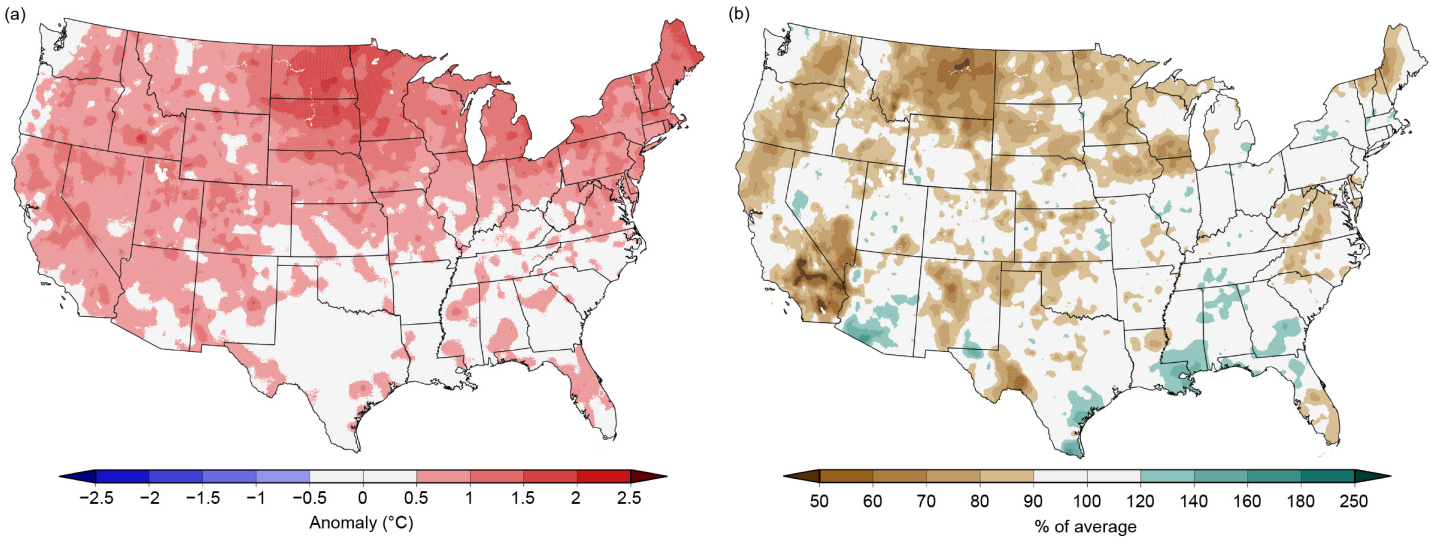

Fig. 7.4. Annual (a) average temperature anomalies (°C) and (b) total precipitation (% of average) in the CONUS for 2021 (1991–2020 base period). (Source: NOAA/NCEI.)

(i) Temperature

The winter (December–February) 2020/21 CONUS temperature was –0.2°C below average and was influenced by some of the coldest air to reach the central United States in more than 30 years, during a cold-air outbreak in February. Six states (Nebraska, Iowa, Kansas, Missouri, Oklahoma, and Arkansas) had their 10th coldest, or colder, February in the 1895–2021 record; the extreme cold, combined with icy conditions, caused widespread power outages across much of the South,

especially in Texas. Above-average warmth was present across portions of the West and from the northern Plains to the Northeast.

The CONUS spring (March–May) temperature was 0.2°C above average, with the highest anomalies occurring across parts of the Great Lakes. The summer (June–August) CONUS temperature was 0.9°C above average and virtually tied with 1936 as the warmest summer on record. California, Idaho, Nevada, Oregon, and Utah each observed their warmest summer on record.

The autumn (September–November) CONUS temperature was 1.2°C above average and was third highest on record. Temperatures were above average from the Southwest to the Great Lakes and into the Northeast, with the highest departures from average occurring across parts of the Plains. Colorado, Montana, and Wyoming each had their second-warmest autumn on record. The year ended with record warmth in the central and southern Plains and Mid- to Lower Mississippi Valley; 10 states in this region reported their warmest December, and an additional 21 states from the Rockies to the East Coast observed one of their five warmest Decembers on record. This widespread warmth resulted in the warmest December on record nationally, with a CONUS temperature anomaly of +3.7°C.

(ii) Precipitation

The weather across the contiguous United States in 2021 was driven by a pair of ridges that waxed and waned throughout the year. One ridge dominated across the North Pacific and extended over the western United States. The second ridge was situated across eastern Canada and the Northeast. This pattern brought warm, dry air to much of the West throughout the year, while an active storm track impacted the weather from the central Gulf Coast to the Great Lakes and into portions of the Northeast. In the East, Massachusetts had its ninth-wettest year on record while in the West, Montana had its ninth-driest year in 2021 (Fig. 7.4b).

Winter precipitation across the CONUS was 88% of average and ranked in the driest third of the historical record. Regionally, precipitation was above average along portions of the East Coast while dry conditions dominated much of the West, northern Plains, Great Lakes, and the South. Precipitation totals across North Dakota were third lowest on record for the season. Spring precipitation was 91% of average overall, but was above average from the central Plains to the Gulf Coast. Louisiana had its third-wettest spring on record. Precipitation was below average across much of the West, northern Plains, Great Lakes, and East Coast, resulting in the second-driest spring for Washington, Oregon, and Idaho.

Summer precipitation was 110% of average across the CONUS and ranked eighth wettest in the historical record. Above-average precipitation was observed along the southern Tier, from the Great Lakes to the Northeast, and in the summer monsoon region of the Southwest. Mississippi experienced its wettest summer on record. It was drier than average across much of the West, central Plains to Upper Mississippi Valley, and northern New England.

The autumn CONUS precipitation total was 93% of average. Drier-than-average conditions were present across parts of the northern Rockies, Southwest, South, western Great Lakes, and Mid Atlantic, while precipitation was above average across portions of the West, northern Plains, eastern Great Lakes, and Northeast.

The CONUS drought coverage remained significant and steady throughout much of 2021 with a minimum extent of 43.4% occurring on 25 May and maximum coverage of 55.5% on 7 December. Drought conditions remained intact across much of the West and northern Plains throughout the year. Excessive spring–summer dryness, coupled with record June–July (JJ) heat, rapidly intensified drought in the Pacific Northwest, and drought emerged in portions of the Lower Mississippi Valley and the Carolinas near the end of the year. Moderate (D1) to exceptional (D4) drought peaked at 94.6% of the western United States on 7 December; this is the largest drought coverage for this region in the 22-year U.S. Drought Monitor (USDM) history. Extreme (D3) and exceptional drought—the two worst categories—covered about 26.8% of the CONUS on 17 August

and marked the largest extent of D3 and D4 drought in USDM history. Moderate to exceptional drought extent grew rapidly in Hawaii during the summer months, peaking at 59% in July, and was most intense in November and early December, with extreme and exceptional drought covering nearly 11% of the islands.

(iii) Notable events and impacts

There were 20 weather and climate events across the United States during 2021 with losses each exceeding $1 billion U.S. dollars: eight severe weather events, four tropical cyclones (TC), three tornado outbreaks, two flooding events, one drought/heat wave, one winter storm/cold wave, and one wildfire event (Fig. 7.5). This was the second-highest number of events on record, with a total loss estimate of $145 billion U.S. dollars—the third highest cost on record. Hurricane Ida alone caused $75 billion U.S. dollars in damage and ranked among the five most costly U.S. hurricanes on record (since 1980; see section 4g2 and Sidebar 4.1 for more details on Ida). The total cost estimate of U.S. billion-dollar disasters over the last five years (2017–21) is in excess of $742 billion (U.S. dollars; NOAA 2022; www.ncei.noaa.gov/access/billions/).

One of these events was a cold wave during 10–19 February that produced temperature departures well below normal from Nebraska to Texas. The prolonged Arctic air caused widespread power outages in Texas, as well as other southern states, with multiple days of sustained below-freezing temperatures. At the peak of the outage, nearly 10 million people were without power. Additional impacts were frozen water pipes, which burst upon thawing, causing water damage to buildings. These extreme conditions caused or contributed to the deaths of more than 210 people in Texas alone. There were also snow and ice impacts across numerous states including Oklahoma, Arkansas, Missouri, Illinois, Kentucky, Tennessee, Louisiana, Mississippi, Colorado, Oregon, and Washington. This event is now the costliest U.S. winter storm event on record, at $24.5 billion U.S. dollars, more than doubling the inflation-adjusted cost of the 'Storm of the Century' that occurred in March 1993 (Smith 2022).

A historic heat wave developed across the Pacific Northwest from late-June into early-July, shattering numerous all-time high temperature records across the region. This prolonged heat dome was maximized over the states of Oregon and Washington and extended well into Canada (Sidebar 7.1). Hundreds of direct and indirect heat-related fatalities were reported across Oregon and Washington.

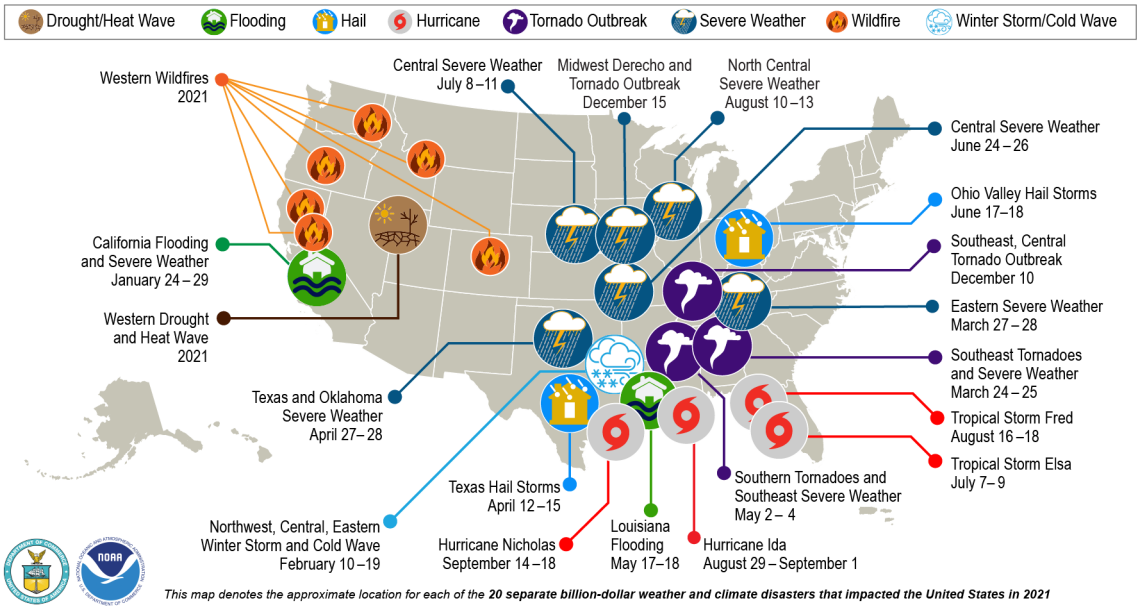

Fig. 7.5. Map depicting date, approximate location, and type of the 20 weather and climate disasters in the United States in 2021, with losses for each exceeding $1 billion (U.S. dollars). (Source: NOAA/NCEI.)

Preliminary reports indicate that there were 1376 tornadoes across the CONUS during 2021, above the 1991–2010 annual average of 1251 tornadoes. A tornado event on 10–11 December in the Mid-Mississippi River Valley spawned two EF-4 (on the Enhanced Fujita Scale) tornadoes, including the longest-track December tornado on record (nearly 266 km across Tennessee and Kentucky) and the deadliest December outbreak on record with at least 90 fatalities reported. Another significant outbreak occurred on 15 December and produced 94 tornadoes from Nebraska to Wisconsin—the most tornadoes confirmed on any day during 2021.

3) MEXICO—R. Pascual Ramírez and A. E. Martínez

The year 2021 was Mexico's fourth-warmest year on record and marked the nation's 11th consecutive year with above-normal temperatures. The 2021 annual precipitation was slightly above normal for the nation; however, precipitation varied across the region, with several regions across the southwest experiencing above-normal conditions, while northern states had below-normal annual precipitation.

(i) Temperature

The 2021 national mean temperature was 0.8°C above the 1991–2020 average (Fig. 7.6a) and the fourth highest on record. Only the years of 2017, 2019, and 2020 were warmer. Every month in 2021, with the exception of January, was warmer than average. December 2021 was Mexico's warmest December on record. While no state reported their warmest year on record in 2021, 12 states (of 32) observed an annual average temperature that ranked among their five highest.

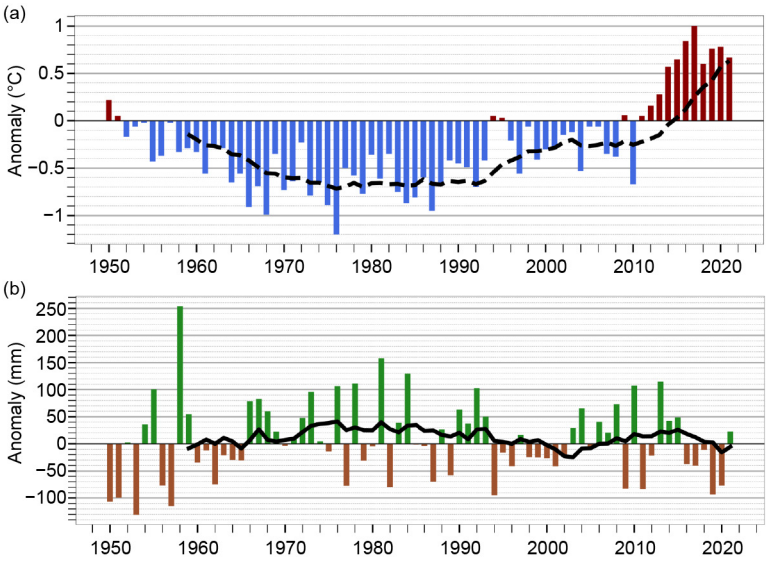

Fig. 7.6. Annual (a) temperature (°C) and (b) precipitation (mm) anomalies for Mexico for the period 1950–2021 (1991–2020 base period). Black solid lines represent a 10-year running mean. (Source: National Meteorological Service of Mexico.)

Regionally, above-normal annual temperatures were observed across the north-central region, along the Pacific coast, and over the Yucatan Peninsula, with the largest positive anomalies (> +2°C) in Coahuila in northern Mexico. Only small regions in the south and along the Sierra Madre Occidental had below-normal annual temperatures, while near-normal temperatures were present across the northwest and parts of states along the Gulf of Mexico (Fig. 7.7a).

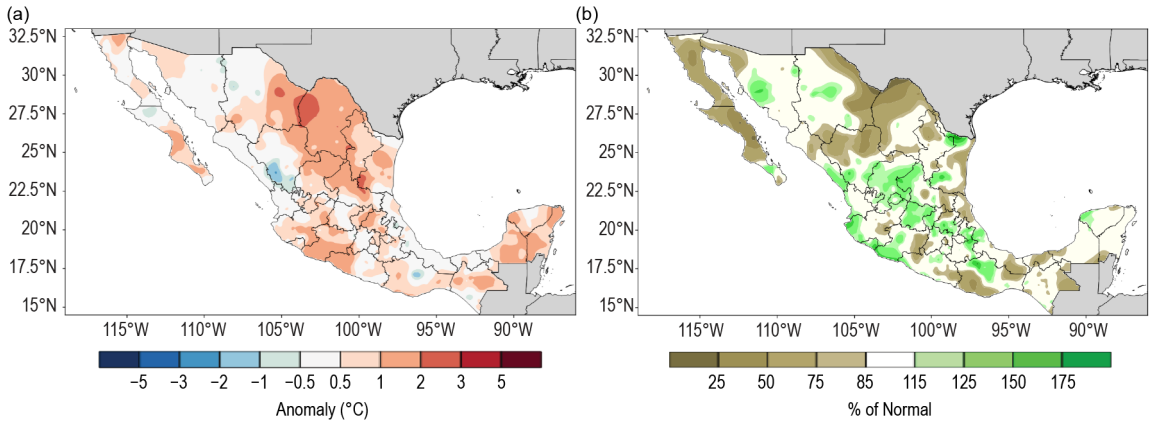

Fig. 7.7. 2021 annual mean (a) temperature (°C) and (b) precipitation (% of average) anomalies over Mexico (1991–2020 base period). (Source: National Meteorological Service of Mexico.)

(ii) Precipitation

Precipitation in 2021 varied across the country (Fig. 7.7b). Below-normal annual precipitation was observed across parts of northern and northwestern Mexico, while above-normal conditions were present across central Mexico. Averaged as a whole, Mexico had its wettest year since 2015 with 769.5 mm, which is 103.7% of normal. On a state basis, Colima, located in southwestern Mexico, had its wettest year on record, while five other states in the same region (Morelos, Aguascalientes, Jalisco, Nayarit, and Sinaloa) had an annual precipitation total that ranked among their 10 highest on record. Meanwhile, several states (San Luis Potosí, Tabasco, and Baja California) reported annual rainfall totals that ranked among their nine driest years on record. This year marked the second consecutive year with below-average rainfall across the northern states.

The hurricane season typically provides a considerable amount of precipitation for Mexico; however, despite an active 2021 hurricane season in the Atlantic, only two tropical cyclones (Grace and Nicholas) in this basin were close to or made landfall in Mexico from the Caribbean or Gulf of Mexico coast (1991–2020 average is 2.7), and thus brought significant localized precipitation. In the Pacific basin, five hurricanes (Enrique, Nora, Olaf, Pamela, and Rick) and one tropical storm (Dolores) brought significant rainfall to the west coast of the country, promoting an above-average rainfall pattern (Fig. 7.7b).

Climatologically, September is Mexico's rainiest month, typically contributing the largest amount of precipitation to the country; however, in 2021, August was the rainiest month, mainly due to Hurricanes Nora and Grace, which brought significant precipitation over the Pacific coast and into eastern Mexico. September had below-normal precipitation, mainly due to the lack of cyclonic activity during the month. Climatologically, March is the driest month of the year with an average of 13.1 mm, just 1.8% of annual precipitation; however, in 2021, February was Mexico's driest month with only 7.9 mm or 1% of the annual precipitation for 2021.

(iii) Notable events and impacts

During the first few months of 2021, the effects of winter storms were felt mainly in northern Mexico. The interaction of a frontal system and a winter storm on 14–15 February brought snowfall to the states of Sonora, Chihuahua, and Coahuila. Snowfall and colder-than-normal conditions caused power outages and blackouts in Chihuahua, Coahuila, Nuevo Leon, and Tamaulipas. The lowest temperatures (–7°C to –14°C) were recorded between 15 and 20 February in northeastern Mexico. This event was part of a cold wave that also affected eastern Canada and the southeastern United States.

During the first half of the year, severe to extreme drought, and in some cases, exceptional drought conditions dominated some areas of northwest Mexico, according to Mexico's Drought Monitor. Over 7330 fires were reported during 2021, with 7161 of them occurring in the first six months; a wet second half of the year helped alleviate the fire activity. Overall, 2021 had the third-highest surface area burned, behind 2011 and 2017, according to data since 2011.

c. Central America and the Caribbean— A. Sánchez-Lugo, Ed.

1) CENTRAL AMERICA—J. A. Amador, H. G. Hidalgo, E. J. Alfaro, B. Calderón, and N. Mora

For this region, nine stations from five countries were analyzed (see Fig. 7.8 for data and station list). The station distribution is representative of the relevant seasonal and intraseasonal regimes of precipitation (Amador 1998; Magaña et al. 1999; Amador et al. 2016a,b), wind (Amador 2008), and temperature (Hidalgo et al. 2019) on the Caribbean and Pacific slopes of Central America (CA). Precipitation and temperature records for the stations analyzed and regional winds were provided either by CA National Weather Services (CA-NWS), NOAA, or the University of Costa Rica. Anomalies are reported using a 1991–2020 base period and were calculated from CA-NWS data. The methodologies used for all variables can be found in Amador et al. (2011).

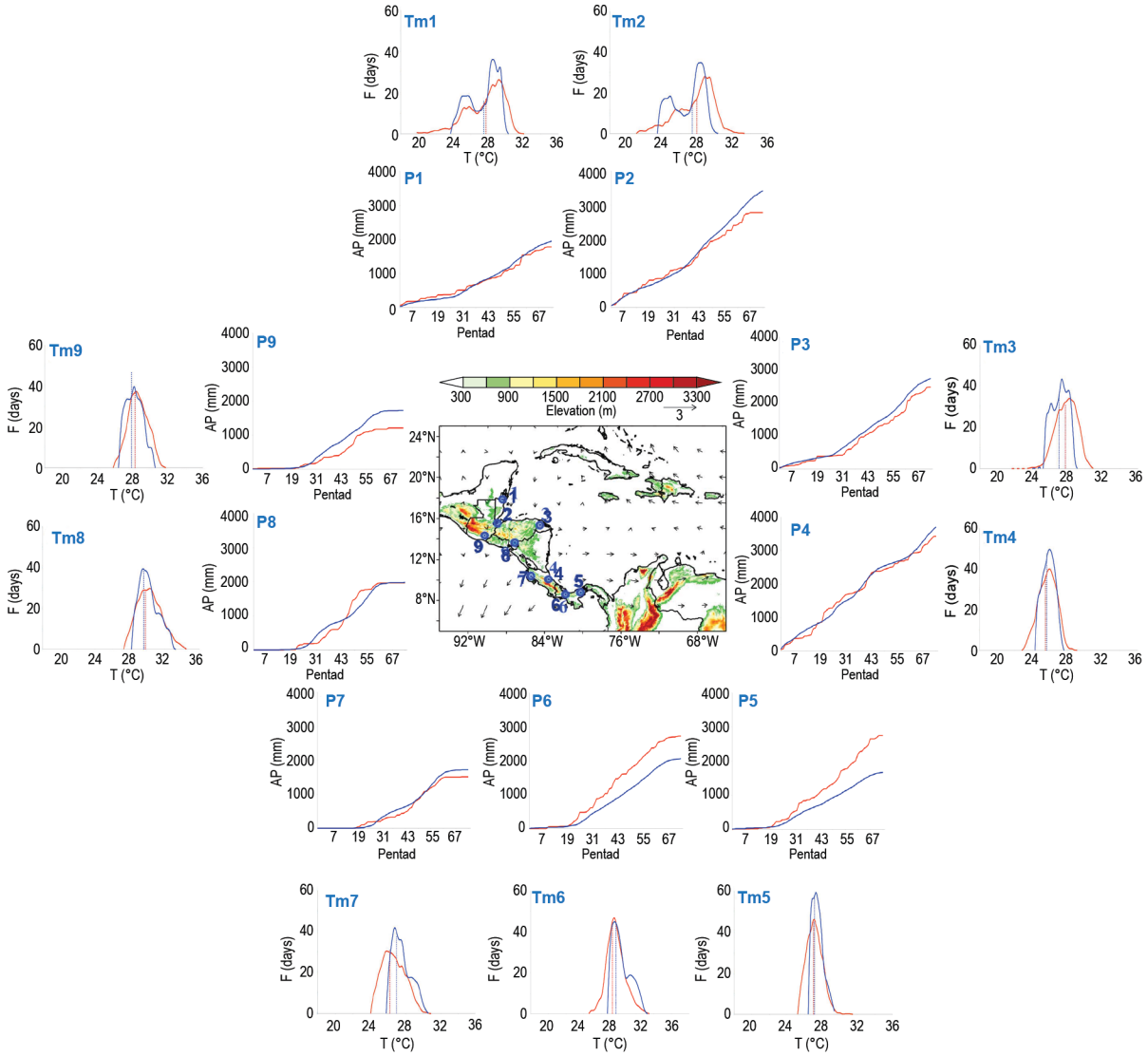

Fig. 7.8. Mean surface temperature (Tm; °C) frequency (F; days) and accumulated pentad precipitation (P; mm) time series are presented for nine stations (blue dots) in Central America: (1) Philip Goldson International Airport, Belize; (2) Puerto Barrios, Guatemala; (3) Puerto Lempira, Honduras; (4) Puerto Limón, Costa Rica; (5) Tocumen International Airport, Panamá; (6) David, Panamá; (7) Liberia, Costa Rica; (8) Choluteca, Honduras; and (9) Puerto San José, Guatemala. The blue solid line represents the 1991–2020 average values and the red solid line shows 2021 values. Vertical dashed lines show the mean temperature for 2021 (red) and the 1991–2020 period (blue). Vectors indicate July wind anomalies at 925 hPa (1991–2020 base period). Shading depicts regional elevation (m). (Sources: NOAA/NCEI and CA-NWS.)

(i) Temperature

The mean temperature (Tm, °C) pentad frequency distributions in 2021, as well as the climatology, for all stations analyzed are shown in Fig. 7.8. Most stations across Central America had near- to above-normal annual temperatures. Only the stations of David, Panamá (Tm6), Tocumen International Airport, Panamá (Tm5), and Liberia, Costa Rica (Tm7), had significant below-normal annual temperature anomalies: −0.6°C, −0.2°C and −0.9°C, respectively. Philip Goldson International Airport, Belize (Tm1), Puerto Limón, Costa Rica (Tm4), and Choluteca, Honduras (Tm8), had near-normal annual temperatures. Meanwhile, Puerto Barrios, Guatemala (Tm2), San Jose, Guatemala (Tm9), and Lempira, Honduras (Tm3), had above-normal annual temperature anomalies, ranging between +0.4°C and +0.8°C. The two northernmost stations, Philip Goldson International Airport, Belize (Tm1), and Puerto Barrios, Guatemala (Tm2), exhibited a bimodal temperature distribution over the course of the seasonal cycle during 1991–2020. An explanation of that distribution is beyond the scope of this report, but it is suggestive of a different climate when compared with the previous base period 1981–2010, as in last year´s climate report. The two-peak

distribution in Tm is also visible in both stations in 2021, a feature observed for the first time at those stations in 2017 (Amador et al. 2018). A comparison between the climatology and the 2021 pentad distributions show that five of the nine stations presented different distributions, except Limón (Tm4), Tocumen (Tm5), Choluteca (Tm8), and San Jose (Tm9), indicating that the Tm for around half the stations was distributed significantly differently from the climatology in 2021.

(ii) Precipitation

The accumulated pentad precipitation (P, mm) time series for the nine stations in Central America are presented in Fig. 7.8. Most stations had a drier-than-normal year, with the exceptions of Tocumen International Airport (P5) and David (P6), both located in Panama, which had wetter-than-normal conditions throughout most of the year. Choluteca, Honduras, had a near-normal annual precipitation total (P8). Belize (P1), Puerto Barrios (P2), Limon (P4), David (P6), Liberia (P7), Choluteca (P8), and San Jose (P9) showed different 2021 distributions from that of the base period, while the remainder of the stations showed no significant differences from climatology. San Jose (P9) was drier-than-normal for the year, while the rest of the stations showed no significant change in the annual average. Note that Liberia (P7) and San José (P9) had a relatively prolonged mid-summer drought-like period (Magaña et al. 1999), a regional precipitation characteristic that was also observed, but to a lesser extent, in Choluteca (P8).

Despite 2021 being a prevailing La Niña year (see section 4b), low-level circulation anomalies in the westernmost Caribbean Sea and Pacific regions showed opposite signs (positive and negative deviations, respectively) from the 1991–2020 average winds related to the trade system during July (vectors in Fig. 7.8). This wind pattern that has been associated with the precipitation distribution during boreal summer did not follow the normal behavior (Amador 2008). During a typical La Niña event, below-normal winds dominate both basins, implying below-normal precipitation along the Caribbean slopes as in Puerto Barrios, Puerto Lempira, and Limón, and above-normal precipitation on the Pacific slopes, a feature not observed in Liberia and San José. This is the second consecutive year with an anomalously active hurricane season in both basins, which may be responsible for those anomalies.

(iii) Notable events and impacts

Tropical cyclone activity during 2021 was considered near-normal in the Caribbean basin, where there were four named systems: Hurricane Elsa (2–5 July), Tropical Storm Fred (11–13 August), Hurricane Grace (15–19 August), and Hurricane Ida (26–27 August). The strongest storm in the basin was Hurricane Elsa (Category 1), and no storms made landfall in Central America. In 2021, no systems formed in the eastern tropical Pacific that impacted Central America. During the rainy season, 59 fatalities were reported due to hydro-meteorological events and 19 deaths by lightning strikes.

2) CARIBBEAN—T. S. Stephenson, M. A. Taylor, A. R. Trotman, C. Charlton, T. Allen, L. A. Clarke, J. M. Spence, J. D. Campbell, K. Kerr, and C. J. Van Meerbeeck

The year 2021 was generally characterized by above-normal mean temperatures and below-normal rainfall. The annual average temperature was 0.34°C above the 1991–2020 average, marking the fifth-warmest year since the start of the record in 1891 (Fig. 7.9a). Every year since 2014 (except 2018) ranks among the 10 warmest years on record. The annual temperatures since 1891 have been increasing at an average rate of 0.11°C decade^{-1} (0.22°C decade^{-1} since 1970). Positive anomalies were highest over the northwestern Caribbean (Jamaica, Cuba, and the Bahamas) and over Trinidad, Barbados, and the Windward Islands (Fig. 7.10a). The San Juan Metro Area in Puerto Rico observed its ninth warmest year (0.4°C above average) since its records commenced in 1899. The average annual rainfall anomaly for the Caribbean was −0.27 mm day^{-1}, marking the 18th-driest year since the record began in 1921 (Figure 7.9b). Annual rainfall total is decreasing at

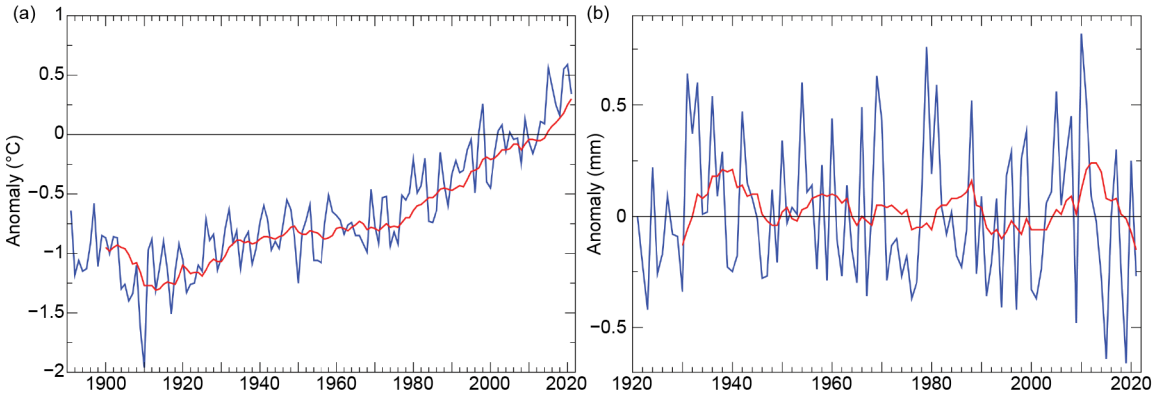

Fig. 7.9. Annual average (a) 2-m temperature anomalies (°C) and (b) rainfall anomalies (mm day^{-1}) for the Caribbean (9°–27°N, 58°–90°W) for the periods 1891–2021 and 1921–2021, respectively, relative to the 1991–2020 average. The red line is the 10-year running mean. (Sources: NCDC v3 and GPCC v2020 from the KNMI Climate Explorer.)

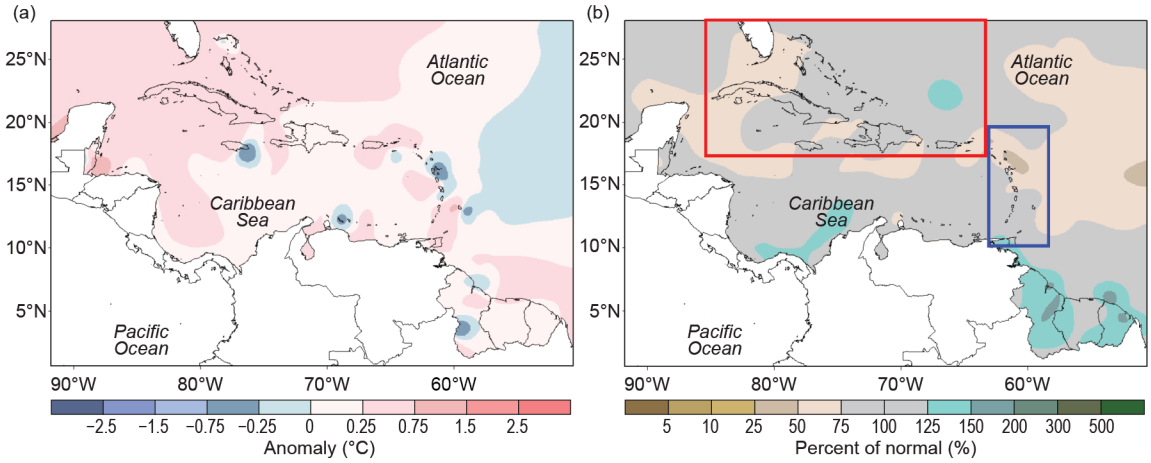

Fig. 7.10. Annual (a) mean temperature anomalies (°C) and (b) total precipitation anomalies (% of normal) relative to 1991–2020. (Source: Caribbean Climate Outlook Forum [CariCOF] and the Caribbean Institute for Meteorology and Hydrology.)

a rate of approximately –1.9 mm decade^{-1} (–1.1 mm decade^{-1} since 1970), even as strong multi-year and year-to-year variations are observed.

(i) Temperature

The December–February temperatures were above normal over much of the region, with negative anomalies in the northwest. The season's 2m-average temperature anomaly was 0.32°C above normal and was the fifth highest since records began in 1881 (Fig. 7.9a); this follows 2020, which was the warmest December–February period on record (0.59°C above normal). Each year since 2014 ranks among the 10 highest December–February average temperatures. Crown Point, Tobago, recorded its highest mean maximum temperature (0.7°C above average) and mean temperature (also 0.7°C above average) for the December–February period since its record began in 1973.

During spring (March–May) and summer (June–August), the region-wide temperature anomalies changed to positive over the north (Cuba, The Bahamas, Jamaica, and Haiti) and negative over the south. In summer, above-normal temperatures occurred over eastern Cuba, eastern Jamaica, and the northern Bahamas. The below-average temperatures in the south were interspersed with some above-normal temperatures over the eastern Caribbean. Anomalies for March–May were 0.18°C above average, while June–August temperatures were 0.11°C above normal. Positive anomalies covered most of the region in September–November.

(ii) Precipitation

In 2021, below-normal rainfall was observed over most of the Caribbean (Fig. 7.10b). Exceptionally dry conditions were observed in Martinique, Antigua, southeastern Dominican Republic, eastern Jamaica, western Cuba, and the northern Bahamas. Four stations recorded their driest year in the last 51 years: VC Bird Airport, Antigua (47% of normal); La Derisade, Guadeloupe (47% of normal); La Trinité, Martinique (50%); and Le Vauclin, Martinique (52%). Henry Rohlsen Airport, St. Croix, recorded its driest year since the start of its record in 1964 (60% of normal). Cyril King Airport, St. Thomas had its sixth driest year in its 50-year record (70% of normal).

The region generally experienced below-normal rainfall for December–February. In spring, some locations observed normal to above-normal rainfall, likely due to La Niña conditions that facilitate wetter conditions in the southeastern Caribbean during the dry season of November–April (Taylor et al. 2002). Very dry conditions were recorded for Antigua, parts of the Bahamas, northern Cuba, and eastern Guadeloupe while very wet conditions were observed for Grenada and Trinidad. Cabrera in the Dominican Republic recorded its lowest rainfall (40% of normal) for December–February since 1971. In March–May, Caroni, Trinidad, recorded its highest spring rainfall total (279% of normal) since 1971. The expansion of normal to above-normal rainfall conditions was notable in the northern Caribbean during summer when the El Niño-Southern Oscillation (ENSO) was neutral (see section 4b for details). Piarco, Trinidad, recorded its second highest summer rainfall (891.1 mm) since 1998. Overall, the annual rainfall at Piarco was 124% of normal and was the fourth wettest year since 1946. Below-normal rainfall returned over the region in September–November. Tobago experienced its driest November (23% of normal) since 1969.

(iii) Notable events and impacts

Hurricane Elsa impacted St. Lucia, Barbados, St. Vincent and the Grenadines, Haiti, and Jamaica during 2–6 July. In St. Lucia, strong winds damaged buildings and telecommunications along with water infrastructure. Agriculture and fisheries were also impacted. Elsa was the first hurricane to impact Barbados in 66 years, since Hurricane Janet. Impacts to Barbados, Haiti, and Jamaica included power outages, displaced roofs, fallen trees, flooding, and damage to agriculture.

Trinidad was impacted by two tropical waves and the Intertropical Convergence Zone, which produced intense rainfall and thunderstorm activity primarily during 17–20 August. The adverse weather resulted in overflowing riverbanks, impassable roads, and wide-scale flooding. Other significant rain events were recorded on 8, 12, 14, and 15 August, which together yielded the seventh-wettest August (386.8 mm, 151% of average) in the 76-year record.

Hurricane Grace impacted Haiti on 16–17 August, causing flooding in more than 600 houses. Grace also impacted Jamaica on 17–18 August as a tropical storm, causing silt and debris to impact several communities and about 200 roads. Initial damage estimates were $1.1 million (U.S. dollars). Jamaica and Cuba were impacted by Tropical Storm Ida on 26–28 August. Impacts included flooding, landslides and fallen trees affecting roads and infrastructure.

Sidebar 7.2: **Rainfall extremes across Central America**—S. Fuhrman, C. Recalde, and W. M. Thiaw

In Guatemala, flooding and landslides affected many departments at various times in 2021. During mid-January, floods were reported in the municipalities of Las Cruces, Sayaxché, and San Luis in Guatemala's Petén Department. Severe weather during 21–24 May affected more than 10,000 people in the departments of Baja Verapaz, Izabal, Petén, Quetzaltenango, San Marcos, Santa Rosa, Suchitepéquez, and Sololá. Flash floods, landslides, coastal flooding, and high winds all contributed to damage of more than 200 homes. In mid-June, flash floods caused three fatalities when the Quibá River overflowed in Sololá and severely damaged 30 homes. Heavy downpours during the week of 25 July triggered flooding and landslides, resulting in many people affected in the departments of Alta Verapaz, Izabal, and Zacapa. According to Crisis24, a global risk management organization, as of 26 July, more than 632,000 people were affected by the floods; eight people died, and at least 5600 people were evacuated. The eruption of the Pacaya Volcano near Guatemala City on 4 August sent steam and gas plumes into the atmosphere as high as 1 km above the summit and drifted as far as 3 km in multiple directions during 5–10 August, according to the Smithsonian/US Geological Survey Weekly Volcanic Activity Report, and exacerbated the disaster in this region. Heavy rains also caused problems in Guatemala in mid-September, when floods and landslides were reported in areas of San Marcos, Sololá, Guatemala, and Santa Rosa. The floods destroyed two bridges in Tajumulco, San Marcos, and other roads in San Antonio Palopó, San Lucas Tolimán, and Santa Catarina Palopó municipalities in Sololá and also damaged over 70 homes in Barberena, Santa Rosa. Landslides damaged four roads and at least four homes in various areas. In December, despite general drying conditions, localized heavy rain caused flash floods in some parts of Guatemala that included Izabal Department during the week of 16–22 December. Floods were also reported in the Petén department within the municipalities of Dolores and Sayaxché during the final week of the month.

Early in the year, the northern Honduran coast was plagued by flooding during the weekend of 16–17 January. Rainfall in excess of 100 mm led to rising rivers, including Lancetilla, Ruth García, and Highland Creek, in Atlántida and Tela Departments. During the summer, heavy rainfall from 22 to 29 July caused destructive and deadly flooding in Costa Rica and Panama. Several rivers in Costa Rica overflowed their banks. According to Costa Rica's emergency management department, Comisión Nacional de Emergencias, over 2700 incidents, including floods, landslides, and road collapses, were reported in 36 of the country's 82 cantons, along with at least two fatalities. In Panama, rivers, including the Sixaola and its tributaries, also overflowed their banks. Twenty people had to be rescued, and over 5000 homes were damaged, according to news sources. Five landslides were also reported. Panama also reported heavy rains on 21 November, which triggered flash floods in Las Cuevas de Bayano, located 50 km east of Panama City. According to Panama's Sistema Nacional de Protección, there were at least two fatalities and 13 injuries.

Dry conditions were also observed during 2021 across different countries in Central America. Rainfall deficits in the region were observed since May; in Nicaragua and Honduras, deficits of more than 100 mm degraded vegetation health and impacted Primera season (April–June) cropping activities. Low Standardized Precipitation Index (SPI) values for the 2-month period May–June indicate a significant moisture deficit in these areas (Fig. SB7.3). Following already dry conditions in September, very low monthly rainfall in October caused abnormal dryness to rapidly expand through the area and drought conditions emerged.

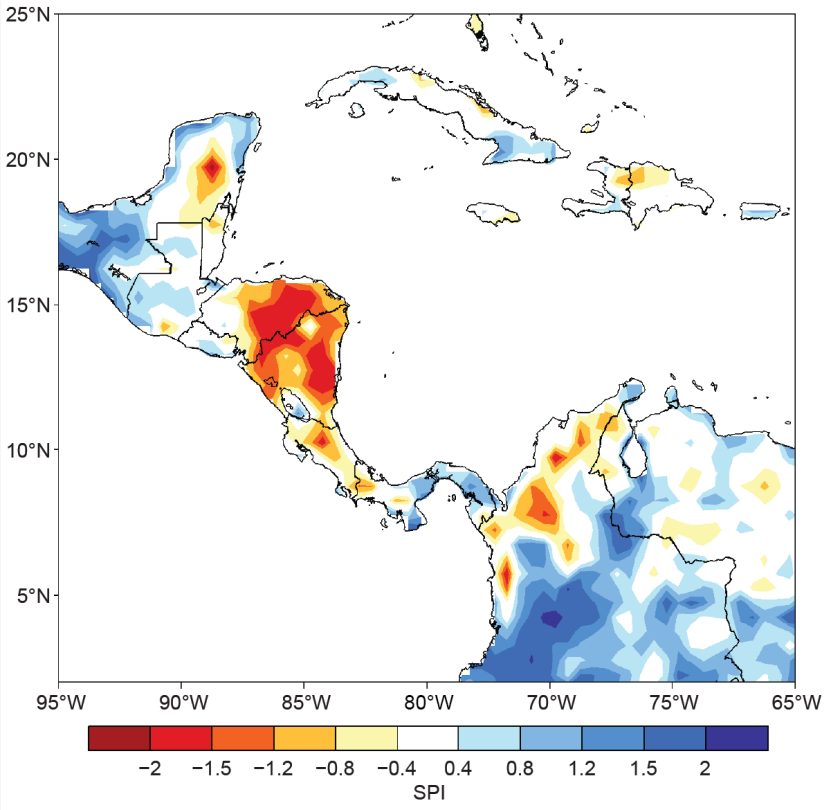

Fig. SB7.3. Standardized Precipitation Index (SPI) for May–June 2021 (1999–2020 base period). (Source: CMORPH, NCEP.)

Rainfall deficits during the September–October period increased substantially through Honduras, Nicaragua, Guatemala, and Belize. Deficits widely exceeded 100 mm and locally were more than 300 mm. Moisture deficits combined with periods of heat negatively impacted growing conditions. In December, wildfires were of particular concern. The onset of the dry season after a largely failed Postrera rainfall season (August–December) created ground conditions that were highly favorable for fire activity. Many fires were reported throughout 10 departments in Guatemala. Over 39 hectares were consumed, according to the country's government. Maps of 'hot spots' registered by MODIS-VIRS satellite-based infrared sensor show that fire activity was not only observed in Guatemala over the course of December, but also across other Central American countries with abnormally dry ground conditions, including El Salvador, Honduras, northern Belize, and northern Nicaragua.

d. South America—A. Sánchez-Lugo, Ed.

La Niña was present in the tropical Pacific Ocean throughout much of 2021, strengthening southerly winds, which were present in the Pacific coastal region of northern South America throughout the year. Additionally, the positive pressure pattern, as measured by the Southern Oscillation Index (SOI), which had high values (+20) at the start of the year, helped keep the Intertropical Convergence Zone (ITCZ) farther north than normal during the first three months of the year. Between April and June, the SOI returned to near-normal values; however, by June it again reached thresholds characteristic of a La Niña event and remained throughout most of the year, which added to the strengthening of the trade winds and the negative sea surface temperature anomalies (SSTA) in the southeast Pacific, decreasing the convective activity of the ITCZ.

Meanwhile, via meridional winds from the north, humidity from the Caribbean entered the region, advancing through northeastern South America and contributing to increased rainfall in some countries, as well as in part of the Andean region. This led to the development of some extreme events across the region.

1) NORTHERN SOUTH AMERICA—J. Nieto and F. Costa

The northern South America region includes Colombia, Ecuador, French Guiana, Guyana, Suriname, and Venezuela.

(i) Temperature

The 2021 mean temperature for northern South America was 0.30°C above normal and the sixth-highest on record. Venezuela had the highest annual national temperature anomaly for the region at +0.45°C, while Ecuador had the lowest at +0.03°C. The highest temperature anomaly observed throughout the year was recorded in November in the Caribbean region of Colombia with a temperature departure of +4.70°C, while the lowest was observed at Margarita Island in Venezuela, which had an anomaly of –3.74°C in September.

Minimum annual temperatures for 2021 were below normal across much of central and northern regions of Venezuela (up to –0.75°C) and across much of Ecuador, predominantly in the south (up to –1°C). Above-normal minimum annual temperatures were observed in French Guiana, Suriname, and the southern half of Guyana (up to +1°C; Fig. 7.11a), as well as in southern Venezuela and southern and Caribbean regions of Colombia. The below-normal minimum temperature anomalies in Ecuador during the year may be associated with the influence of the La Niña in the tropical Pacific Ocean throughout most of the year.

The 2021 maximum annual temperatures were near- to above normal across the region, with the highest temperature departures in Venezuela, especially in the northern region (up to +1.5°C).

Mean annual temperatures were slightly above normal across much of Venezuela, French Guiana, Suriname, and Guyana (+0.50°C). Above-normal temperatures were also observed in the Caribbean (up to +0.75°C), east-central region of Colombia, and eastern Ecuador (+0.50°C; Fig. 7.11b).

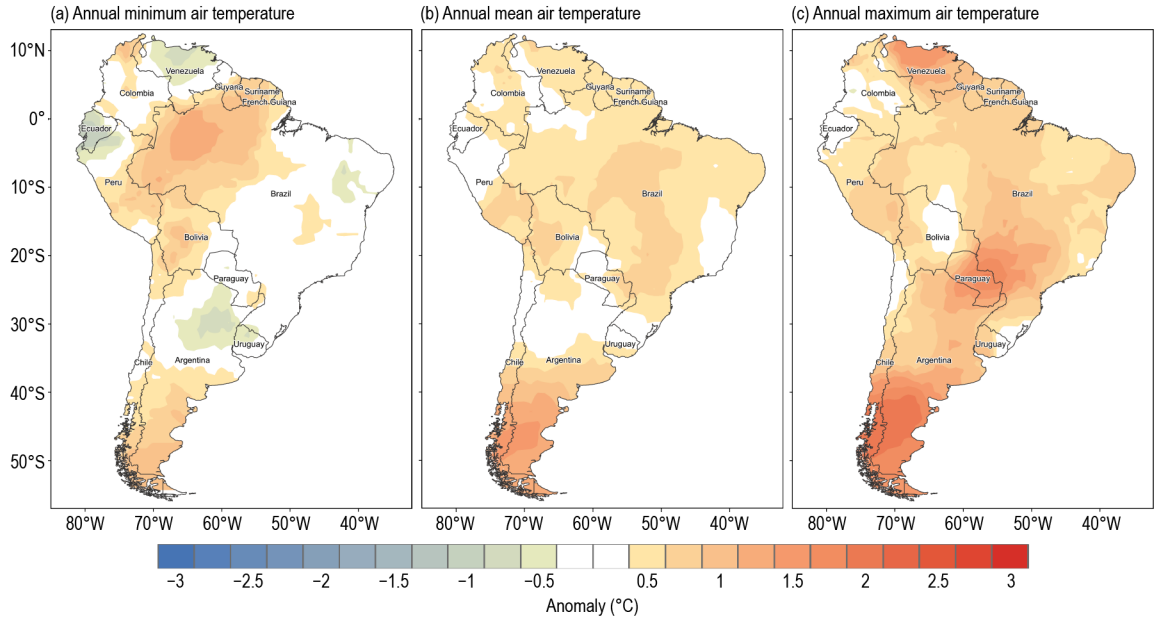

Fig. 7.11. The 2021 (a) annual minimum, (b) mean, and (c) maximum temperature anomalies (°C; 1981–2010 base period). (Source: Data from NMHSs of Argentina, Bolivia, Brazil, Chile, Colombia, Ecuador, Paraguay, Peru, Uruguay, and Venezuela; processed by CIIFEN.)

(ii) Precipitation

In 2021, northern South America had predominantly near- to above-normal precipitation. Below-normal precipitation was only observed in a small area in central Colombia and the Colombian Caribbean region (up to −40%) and in a small area along the central coast of Ecuador (–20%). Above-normal precipitation was observed across much of French Guiana, Suriname, and Guyana (up to +30%), in southeastern Venezuela (up to +30%), most of the Pacific and east-central region of Colombia (up to +50%), in the northern Andes (up to +30%), and northern and southern parts of Ecuador (up to +50%; Fig. 7.12). The average precipitation total for the region was 3.9% above normal.

(iii) Notable events and impacts

During 2021, the most notable hydrometeorological events across northern South America were related to intense rainfall. In Guayaquil, in the southern coastal region of Ecuador, the first accumulated rain of 2021 was 41% above average for January. Thunderstorms brought moderate to heavy rainfall to the region, prompting floods that damaged many vehicles.

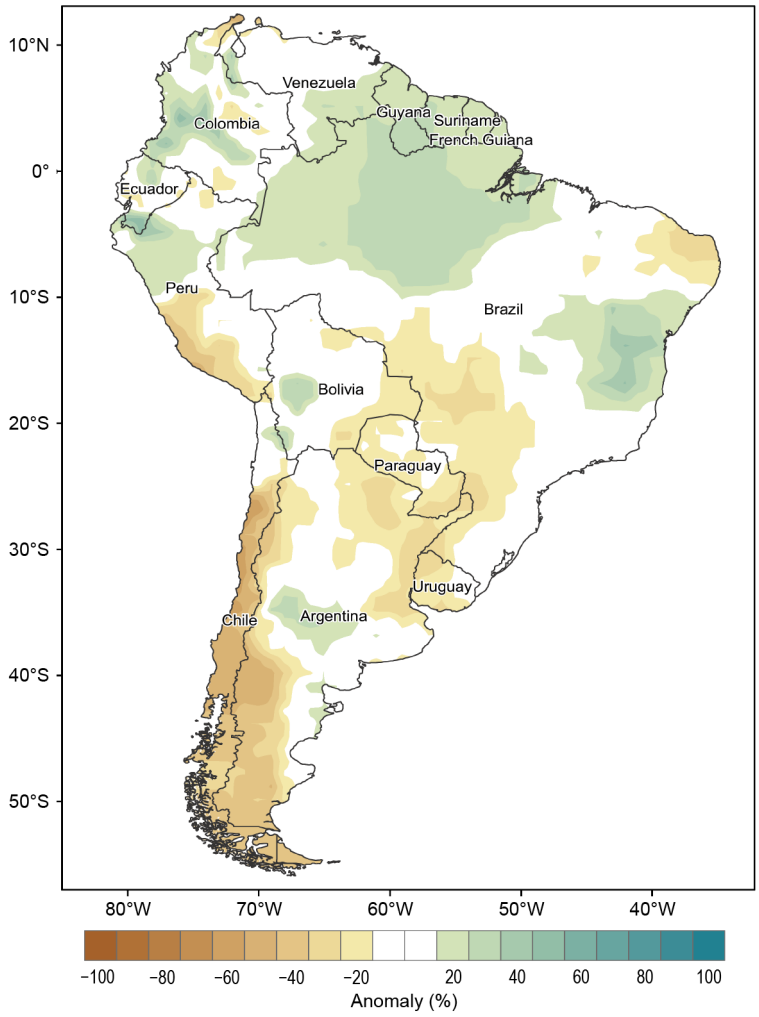

Fig. 7.12. The 2021 annual precipitation anomalies (%; 1981–2010 base period). (Source: Data from NMHSs of Argentina, Bolivia, Brazil, Chile, Colombia, Ecuador, Paraguay, Peru, Uruguay, and Venezuela; processed by CIIFEN.)

Torrential rain fell across Suriname during April, causing floods across the nation's 10 districts. Roads were flooded in several locations, making these areas inaccessible. The flood situation worsened between the Nickerie River and Wageningen when the dam located in this region broke. Gas stations, supermarkets, and houses were flooded with water up to one meter, and in some regions access to electricity was limited. Heavy rains were also recorded in May, causing floods to last for weeks in regions and isolating some communities.

Also, in May, intense rainfall caused rivers to overflow in the city of Cuenca, in the southern Andean region of Ecuador, causing widespread damage. The Tarqui River observed its worst flood in the last 11 years. Sixty homes were affected, as well as pastures and pedestrian bridges, and water system pipes were damaged. In July, heavy rains were also observed in the provinces of Pastaza, Napo, and Tungurahua in the central and southern highlands and in the Amazon region of Ecuador. Some regions of the Amazon, which typically receive close to 300 mm of precipitation during July, observed 77 mm of rain during one 24-hour period.

During 24 May to 10 June, heavy rain fell across Guyana, with precipitation totals reaching 510 mm in some regions. The intense rainfall resulted in the overflow of rivers and triggered severe floods across Region Nine in southern Guyana, affecting over 15,000 people. The floods wreaked havoc across the region, damaging roads, infrastructure, and about 16,000 hectares of crops. About 30,000 families were affected by the floods.

On 12 July in the city of Guayana, in Venezuela, there was a 3-hour episode of intense rains with strong winds, which caused widespread damage to the region. More than 60 trees collapsed, there was an extended interruption of electricity, internet, and water services, as well as collapsed roofs and damage to other infrastructure.

In August, intense rain events were again recorded in some regions of Venezuela, including the Mérida region, where floods and landslides killed 20 people and led the government to declare a state of emergency in this and other states. During this event, close to 55,000 people were affected throughout the country.

Colombia's department of Putumayo, bordering Ecuador, had intense rains during July that affected more than 10,000 families in 12 municipalities, including Mocoa, Putumayo's capital. This rain event destroyed crops, domestic animals disappeared, primary and secondary roads were blocked, municipalities were left without aqueduct service, bridges were obstructed, and areas were isolated. Overall, total rainfall for the month in Putumayo was 40% above normal.

According to the National Unit for Disaster Risk Management between 15 September and 27 October, there were 72 floods, 15 flash floods, 61 landslides, 45 gales, 27 storms, 8 hailstorms, and thunderstorms in 27 of the 32 departments of Colombia. At the beginning of November, intense rainfall occurred in the department of Nariño and triggered a landslide in Mallama, where at least 12 people died and another 10 were injured. Overall, Mallama received November precipitation 60% above its average.

2) CENTRAL SOUTH AMERICA—J. A. Marengo, J. C. Espinoza, L. M. Alves, J. Ronchail, A. P Cunha, A. M. Ramos, J. Molina-Carpio, K. Correa, G. Avalos, W. Lavado-Casimiro, J. Baez, and R. Salinas

This region includes Brazil, Peru, Paraguay, and Bolivia.

(i) Temperature

The 2021 mean temperature for central South America was 0.4°C above normal, resulting in its seventh-warmest year since records began in 1961 (Fig. 7.13). The year was characterized with near- to above-normal mean temperatures across the region. Parts of central and southern Brazil had the largest mean annual temperature departures, ranging between 0.5° and 1.0°C above normal (Fig. 7.11b). During the year, the highest monthly mean temperature departures (2–5°C above normal) occurred during August–September across the region east of the Andes (15°–25°S). Below-normal minimum annual temperatures were observed across much of Peru and a small

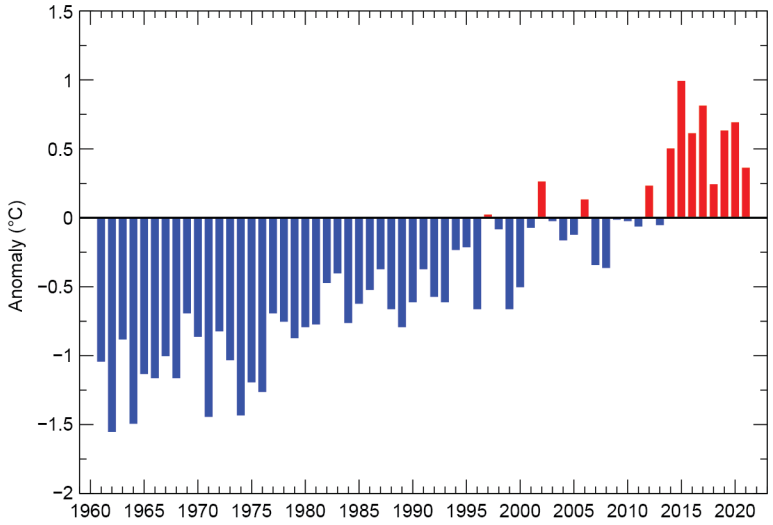

Fig. 7.13. Time series of mean annual regional air temperature anomalies (°C; 1991–2020 base period) for the period 1961–2021 for central South America (Brazil, Bolivia, Paraguay, and Peru). (Source: NOAA/NCEP GHCN CAMS data.)

area in northeastern Brazil, while the rest of the region had near- to above-normal minimum annual temperatures (Fig. 7.11a). Maximum annual temperatures were above-normal across the region (Fig. 7.11c).

Several significant heat waves were also observed across the region. Of note, temperatures were above 30°C in the Peruvian Amazon during 13–15 April, reaching an all-time historical maximum record of 34.2°C in the city of Jelacio, San Martin State. Conversely, between the end of June and the first week of July, two powerful cold spells impacted the region (see *Notable events and impacts* section).

(ii) Precipitation

Above-normal annual precipitation was observed across much of northern Brazil and across parts of northwestern Peru, eastern Brazil, and western Bolivia (Fig 7.12). Below-normal annual precipitation was present across parts of southwestern Peru, northeastern and western Brazil, eastern Bolivia, and across Paraguay.

During January–October, precipitation was below normal across most of the region, including the coast of Peru, the southern Amazon, and southeast Brazil, and from August to October in the Bolivian Andes. Rainfall was above normal during December 2020–May 2021 in the northern Amazonia (north of 5°S) and, by 1 June, the Rio Negro at Manaus reached its highest water level in 102 years of record, resulting in significant floods (see *Notable events and impacts* section).

(iii) Notable events and impacts

Several significant weather and climate extreme events occurred across central South America in 2021 (see Fig. 7.14).

After several months of above-normal rainfall, the water level of the Rio Negro in Manaus (central Brazilian Amazon) was above 29.00 m (the emergency threshold) by early June 2021 and remained above that threshold for a total of 91 days. It reached a record high level of 30.02 m on 16 June, surpassing the previous record of 29.97 m set in June 2012. The overflow of the river caused damaging floods that surpassed the "once-in-a-century" Amazon flood in 2012 (Espinoza et al. 2021; see Sidebar 7.3 for more information). Over 800 houses, educational centers, bridges, and road sections were reported damaged. By the end of June, according to IDAM (2021), the flood in the Brazilian Amazonia generated economic losses of $40 million (U.S. dollars) for the rural sector and affected more than 450,000 people.

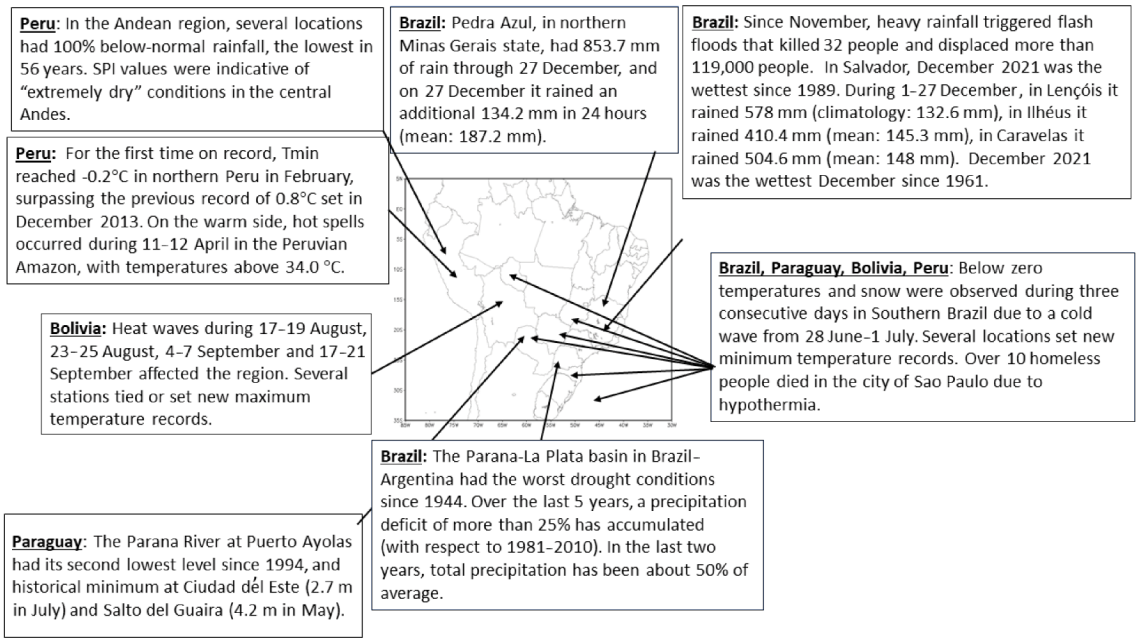

Fig. 7.14. Extreme and notable events across central South America in 2021. (Sources of information: Peru: SENAMHI; Bolivia: SENAMHI, Paraguay: DMH; Brazil: INMET, CEMADEN, Climatempo, INPE; International: UN OCHA, Web Relief, UNDRR). The historic flood in Amazonia is discussed Sidebar 7.3.

A multi-year drought affected central-southern Brazil (Minas Gerais, São Paulo, Paraná, Mato Grosso do Sul) and parts of Paraguay and Bolivia throughout the year. Due to its prolonged duration and severity, the drought impacted many socio-economic and ecological systems, increased risk of wildfires, decreased river transport, reduced hydroelectric energy production, and impacted crops and livestock in these highly agricultural regions. By May 2021, more than half of the municipalities in Upper Parana had about 40% of their crops damaged by the drought (Naumann et al. 2021). The government declared a water crisis in September, as reservoirs in southeastern and central-western Brazil were operating at 23%, the lowest level in 20 years, and these regions were at high risk of water and energy shortages and rising water and electricity prices.

Drought spanned the Paraguayan Chaco, Brazilian Pantanal, and southeastern, central, and southern Brazil, and the southwestern Bolivian Amazon during the austral summer and autumn, as shown by the IDI (Cunha et al. 2019; Figs. 7.15a–d. The Paraguay River shrank to its lowest levels in half a century, resulting in potable water accessibility issues and limited river traffic, March–May soil moisture deficits, delayed planting operations and wheat germination, and brake on cereal production in Paraguay. Parts of the Chiquitania dry forest region in Bolivia were also affected by drought and warm weather in August–October, favoring fires that had burned 3.4 million hectares by 15 October (Rodriguez and Ibarnegaray 2021), about 94% in the Santa Cruz and Beni provinces.

The effects of the 2020–21 drought in the Paraná basin on ecosystems were particularly severe in the Pantanal, one of the largest wetlands in the Americas (Libonati et al. 2021; Marengo et al. 2021). Authorities were concerned about the cumulative effects of fires in 2020 and 2021, and the area affected by fire in the Brazilian Pantanal at the end of September 2021 (1,089,975 ha) was well above the historical average of 616,125 ha. However, differently from 2020, when fires reached the northern part of Pantanal, the most critical region affected in 2021 was the southern part.

In November and December 2021, rainfall was more than 300% above normal in northeastern Brazil, triggering the worst flash floods in recent decades in the states of Bahia and Minas Gerais. On 7 December, storms caused by instabilities associated with a subtropical cyclone over the Atlantic Ocean affected several cities in the southern part of Bahia, which impacted about 220,000

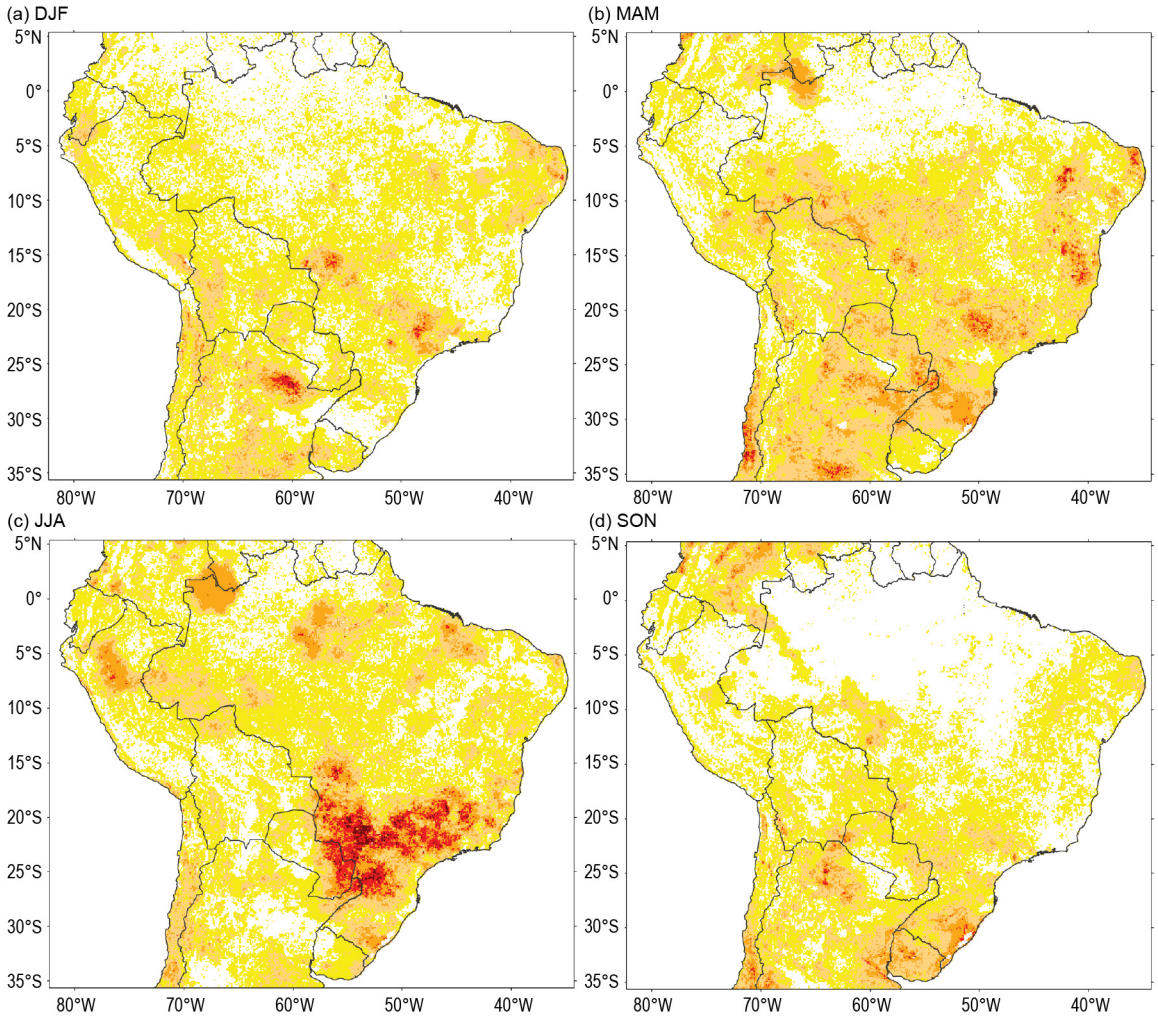

Fig. 7.15. Integrated Drought Index (IDI) maps for central South America during (a) DJF 2020/21, (b) MAM 2021, (c) JJA 2021, and (d) SON 2021. (Source: CEMADEN.)

people and caused 12 fatalities and over 260 injuries. In the same region, flooding on 23 December destroyed and damaged houses, schools, hospitals, and other infrastructure, affecting over 810,000 people and caused over 30 fatalities and 500 injuries. According to INMET and CEMADEN, the rain total for December 2021 was almost 400–500 mm above normal. Daily values surpassed 150 mm and accumulated values in some locations reached 500 mm during 23–27 December, and up to 800 mm during the month of December (climatology between 150–200 mm).

Three significant cold waves affected central South America during 20 June, 26 June–2 July, and 27 July–1 August, where some locations reported minimum temperatures that were 11–29°C below average and set new minimum temperature records. Of note, the Campo Belo station in the National Park Itaiaia, in the highlands of the state of Rio de Janeiro, recorded a minimum temperature of –14.8°C (climatology: 14.4°C) on 1 July, and, if verified, could be the lowest minimum temperature on record. Thirteen fatalities were attributed to these cold waves, and frost affected coffee, vegetables, fruit, and wine production in southern and southeastern Brazil, reducing the production by 30% and contributing to increased prices of food and commodities. The cold waves also affected western Amazonia, where minimum temperatures were 8–11°C below average. Some locations across Paraguay observed close to freezing temperatures, and several locations across eastern Bolivia set new record low minimum temperatures. Frost was recorded for the first time on record in some areas (FAN 2021).

Sidebar 7.3: **Major floods in the Amazon**—G. Koren

The Amazon forest has experienced several extreme events in the last decade, including large-scale floods and droughts. In 2021, with La Niña conditions present most of the year, the Amazon experienced higher-than-normal precipitation, leading to anomalously high river discharge and floods in downstream regions. Here, a quantification of the severity and extent of these anomalies are reported, including an assessment of the societal impacts of these extreme events, which coincided with the ongoing COVID pandemic.

Earlier major floods occurred in 2009, following extreme rainfall that progressed from the western to eastern part of the Amazon during the first months of that year (Filizola et al. 2014). A few years later, in 2012, record-high water levels were reached in the Manaus Port, as a result of excess atmospheric moisture supply in the preceding months, focused mostly on the western part of the Amazon basin (Satyamurty et al. 2013). There were also major floods in 2014, but these were located primarily in the southwestern region of the Amazon basin (Espinoza et al. 2014).

Precipitation anomalies

An overview of precipitation estimated by CHIRPS (Funk et al. 2015) over the Amazon forest and surrounding regions is presented in Fig. SB7.4. The map shows the accumulated precipitation anomalies over the first four months of 2021. These anomalies were calculated with respect to the 1991–2020 baseline, which includes the aforementioned wet years, but also

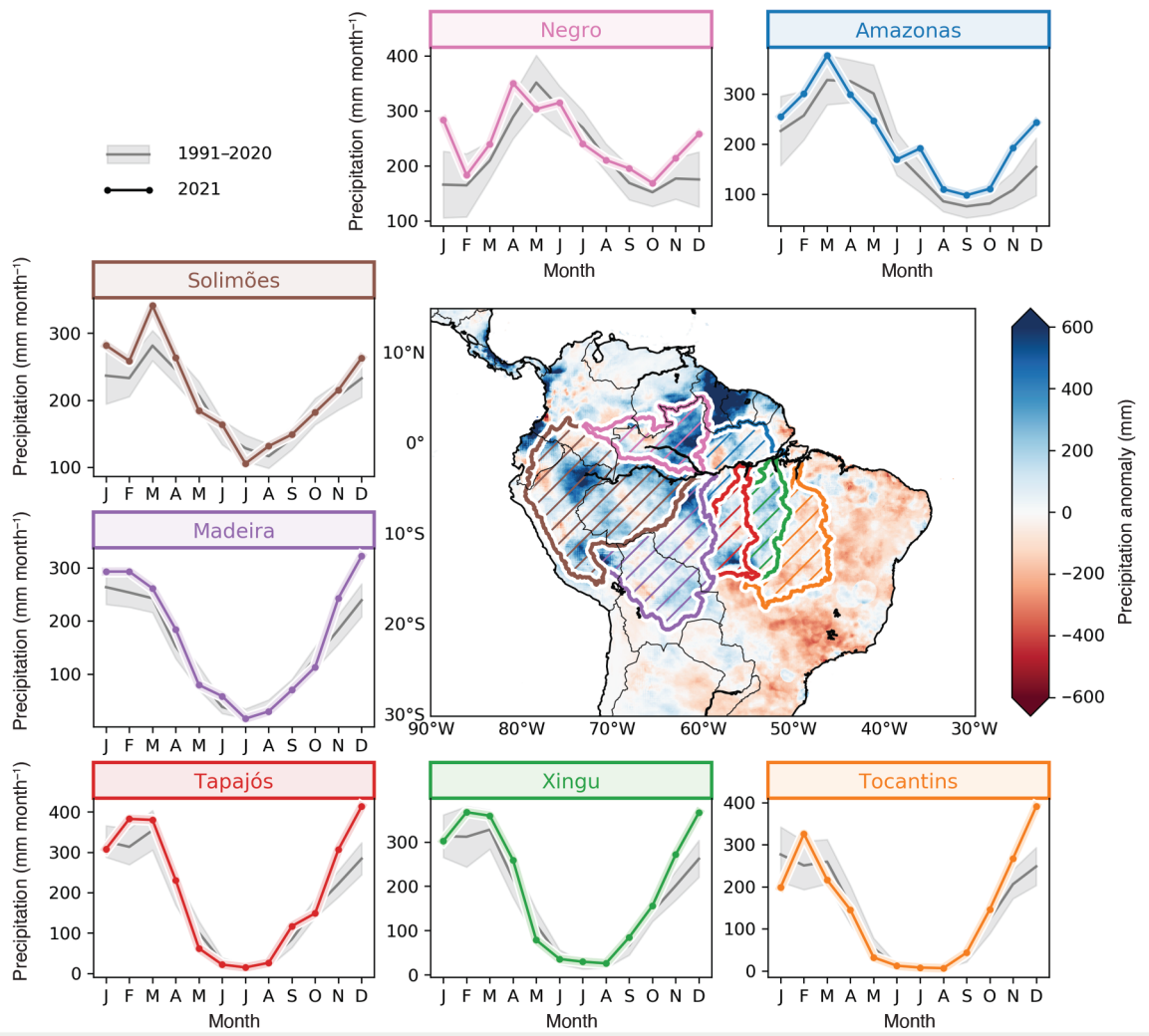

Fig. SB7.4. Precipitation (mm month^{-1}) over the Amazon forest and surrounding areas. The map shows the accumulated precipitation anomalies over Jan–Apr 2021, relative to the baseline 1991–2020. The time series plots show the mean precipitation (gray line) and its standard deviation (gray shading) with the 2021 precipitation averaged over the Tocantins basin (orange) and sub-basins of the Amazon (other colors). The location of these (sub-)basins follows the HydroBASIN definition (Lehner and Grill 2013) and is illustrated by the corresponding color in the map. (Source: CHIRPS [Funk et al. 2015].)

the dry years 2010 (Lewis et al. 2011) and 2015–16 (Koren et al. 2018). Across the Amazon basin, above-average precipitation anomalies were dominant, and are linked to strengthening of the Walker circulation (Espinoza et al. 2022). High rainfall totals are also apparent north of the Brazilian Amazon, in Guyana and Suriname, whereas drier-than-usual conditions were found to the east of the Amazon, in the Caatinga and Cerrado regions.

The temporal variation of precipitation averaged over the Tocantins basin and several sub-basins of the Amazon basin was calculated using the HydroBASIN definitions from Lerner and Grill (2013) and is included in Fig. SB7.4. The climatologies (gray lines and shading) reveal a substantial difference between the dry season minima for the northwestern sub-basins (e.g., always exceeding 100 mm month^{-1} for the Negro sub-basin), whereas precipitation over the Xingu sub-basin remained for a period of roughly five months below the 100 mm month^{-1} threshold. Focusing on the 2021 precipitation (colored lines), it is clear that both the start and end of the year 2021 were anomalously wet, whereas the drier period in the middle of the year was not exceptional. There is also a spatial dependency in the anomalies: the western sub-basins (e.g., Solimões) experienced high anomalies in the early part of 2021, whereas for the southeastern (sub-)basins (e.g., Xingu, Tocantins), the wet anomalies at the end of 2021 are most pronounced.

River discharge and floods

The anomalous rainfall in 2021 resulted in extreme discharge in the Amazon basin. Discharge measurements from the Óbidos station, which is situated along the Amazon River and drains an area of approximately 4.7 million km2 (van Schaik et al. 2018), show positive anomalies throughout the year, even exceeding 2-σ standard deviation (Fig. SB7.5). To verify that this is not simply resulting from the intensification of the hydrological cycle in the Amazon (Barichivich et al. 2018), the effect of removing the long-term linear trend is also included.

Figure. SB7.5 also contains a map of discharge anomalies from the GloFAS-ERA5 reanalysis product v3.1 (Harrigan et al. 2020) integrated over the period March–June (the integration period was delayed by two months relative to the map in Fig. SB7.4, as the discharge peaks for Óbidos were delayed by roughly two months relative to the peaks in rainfall). Spatial patterns in the discharge anomalies resemble the precipitation anomalies in Fig. SB7.4, with positive anomalies in the Amazon basin and the Guyanas, whereas the Cerrado and Caatinga areas to the southeast of the Amazon show negative anomalies.

Impacts

The floods during May and June affected several villages and cities around the Amazon River, including the Amazonas state capital Manaus. The town Anamã with its ~13,000 inhabitants, which is situated alongside the Amazon river in the Solimões region, was completely flooded. Unfortunately, the floods coincided with high infection rates of COVID-19 in this region, complicating evacuations and other means to manage the flood impact.

Several months later, at the end of 2021, regions outside the Amazon forest also experienced heavy rainfall, culminating in major floods in the northeastern state of Bahia. Two dams in the region collapsed, leading to major floods that resulted in severe damage and casualties in the city of Itabuna with its ~200,000 inhabitants. The impacts of these extreme events extend into 2022.

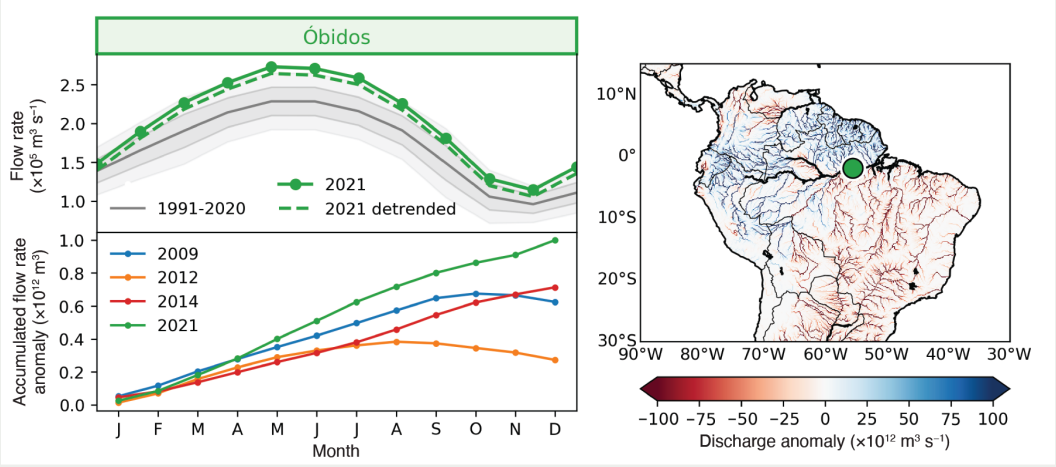

Fig. SB7.5. River discharge (m^3 s^{-1}) from in situ observations. The time series plot (top panel) shows the mean climatology (gray solid line) and the 1 std. dev. (dark gray shading) and 2 std. dev. (light gray shading) areas are indicated, alongside the discharge for 2021 (green line) for the Óbidos station. The bottom panel shows the accumulation of the discharge anomaly over time for four recent wet years (2009, 2012, 2014, and 2021). The map shows GloFAS discharge anomalies for Mar–Jun 2021, and the location of the Óbidos station is indicated (green circle). (Source: National Water Agency of Brazil (ANA 2021) and the GloFAS-ERA5 reanalysis product v3.1 [Harrigan et al. 2020].)

1) SOUTHERN SOUTH AMERICA—L. S. Aldeco, C. R. Cortés Salazar, D. A. Domínguez, N. Misevicius, and A. J. Reyes Kohler

This region includes Argentina, Chile, and Uruguay.

(i) Temperature

Above-normal temperatures were observed across most parts of southern South America (SSA) during 2021 (Fig. 7.11b). The highest temperature departures were observed south of 35°S. Below-normal temperatures were limited to northern parts of Uruguay and Chile and across parts of central and northern Argentina. The national mean temperature anomalies for Argentina, Chile, and Uruguay were +0.52°C, +0.51°C and +0.1°C, respectively (Fig. 7.16). These anomalies placed 2021 as the fifth-warmest year on record for Argentina and Chile and the 13th-warmest year on record for Uruguay, all in the 1961–2021 period. Near- to below-normal annual minimum temperatures during 2021 were observed across northern parts of Argentina and Uruguay, while above-average conditions were present across much of southern Argentina and northern and southern Chile (Fig. 7.11a). Annual maximum temperatures were above normal across the region (Fig. 7.11c).

Summer (December–February) 2020/21 had near-normal temperatures, on average, in most parts of the region. Some parts of northern and western Argentina, northern Uruguay, and central and northern Chile recorded below-normal temperatures. Above-normal temperatures were recorded in western Patagonia, Argentina, and Chile. Heat waves affected Uruguay, Chile, and central and northern Patagonia in Argentina, leading to several locations setting new historical maximum temperature records in Patagonia of Chile and Argentina: Cipolletti (Argentina) recorded a maximum temperature of 43.8°C on 22 January, its highest value since 1961, and Puerto Williams (Chile) recorded 26.1°C on 27 February, its highest since 1968.

During austral autumn (March–May) temperatures were near-normal in most parts of the region and higher temperatures were recorded at central and southern Argentina.

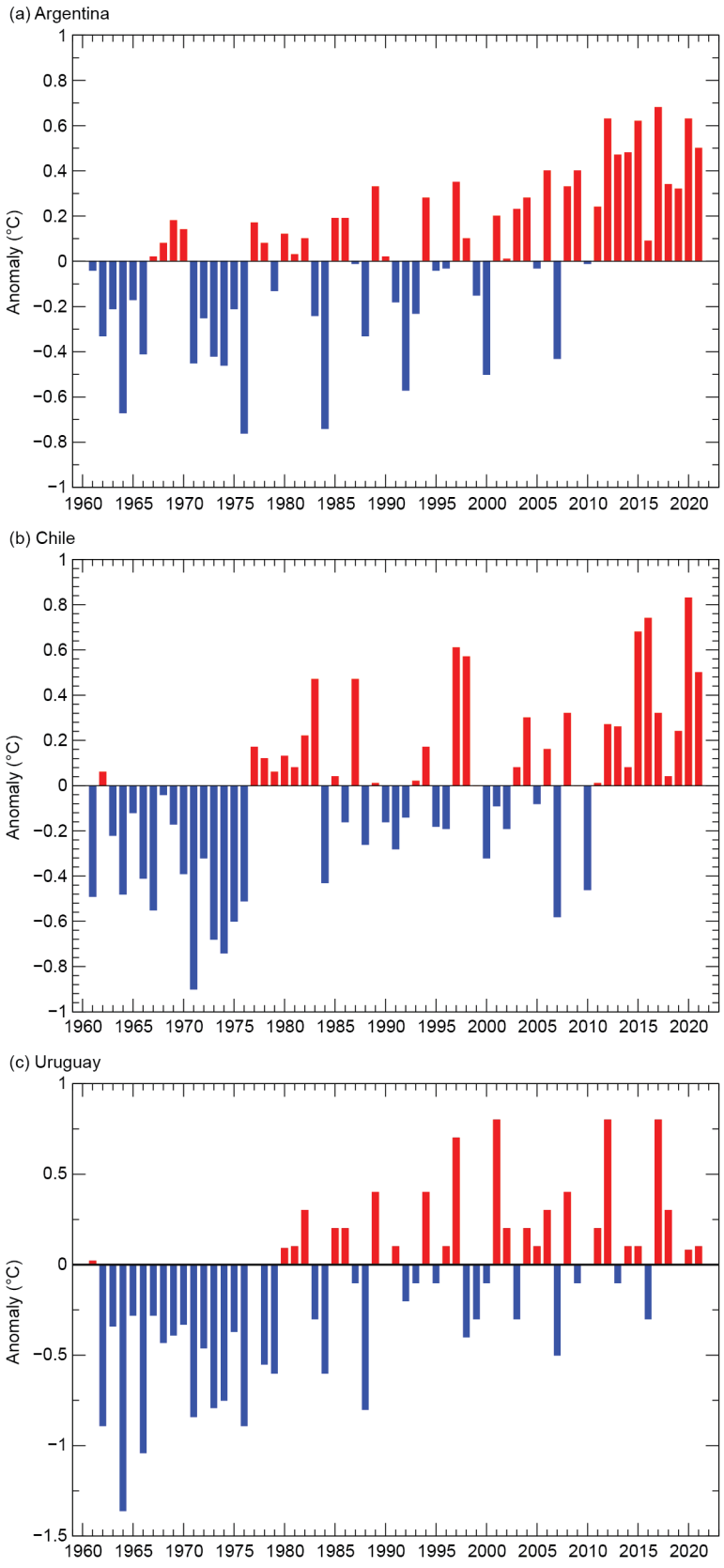

Fig. 7.16. National annual temperature anomalies (°C) for (a) Argentina, (b) Chile, and (c) Uruguay for the period 1961 to 2021.

March temperatures were above average during the first half of the month in northwestern Patagonia in Argentina, leading to the warmest March for the city of Bariloche since 1961. Some locations across Uruguay had their highest mean temperature for April since 1981 (Carrasco, Prado, Colonia, and Mercedes).

Winter (June–August) was warmer than normal in the southern regions of Chile and Argentina. Most of Chile, Uruguay, and northern Argentina had below- to near-normal temperatures. Cold air outbreaks occurred in Uruguay and central and northern Argentina during the last two weeks of June. In Argentina, new minimum and maximum temperature records were set. Of note, Villa María del Río Seco recorded its lowest minimum temperature (–9°C on 30 June) and Laboulaye its lowest maximum temperature (5.8°C on 16 June), both since 1961. Colonia and Salto in Uruguay recorded maximum temperatures of 9.8°C and 7.2°C, respectively, on 28 June. By the end of July, another cold irruption favored colder temperatures in the northern regions of Argentina and Uruguay, and a new record for minimum temperature in Argentina was set in Presidencia Roque Saénz Peña with –7.4°C on 29 July, its lowest since 1961.

Spring (September–November) was characterized by a period of high temperatures that were recorded during the last week of October. This warm period affected central and southern parts of Argentina and Uruguay, resulting in 22 stations in Argentina setting new daily maximum temperature records for October. In Uruguay, several records were set for the highest mean, maximum, and minimum temperature for the season at several stations since records began in 1981.

(ii) Precipitation

Most of southern SSA had below-average annual rainfall during 2021 (Fig. 7.12). The most affected region was south-central Chile and northeastern Argentina. Within that area, the annual rainfall was 30–60% below average. Since 2010, south-central Chile has been under a rainfall deficit period that has been called the "Mega Drought", and 2021 added to this period. The city of Santiago de Chile recorded its fifth driest year since 1914, and Junín in Argentina had its driest year since 1961. Also, from La Araucanía region to the Lakes region in Chile, 2021 was the driest year since 1961 with a deficit of –42%. Meanwhile, local regions in central and northwest Argentina had above-average annual rainfall, with the highest anomalies ranging between 20–40% above normal.

During austral summer 2020/21, La Niña conditions were present, and most of the SSA region had below-normal rainfall. Typically, La Niña favors less precipitation than normal in Uruguay and central and northeast Argentina, especially during spring and summer, while northern Chile tends to have above-normal precipitation during summer. During summer 2020/21, above-normal rainfall was recorded in eastern Uruguay, northeastern and central-western Argentina, and central Chile, mainly due to sub-seasonal variability that favored some precipitation events. In Argentina, rainfall was about double its normal in San Rafael, and other stations, including Dolores, Puerto Deseado, and Iguazú, recorded rainfall between 50–75% above normal. Dolores recorded its highest daily rainfall since 1961 (276 mm on 5 January). In Chile, Curicó recorded 59.6 mm on 30 January—its highest daily and monthly precipitation for January since 1950.

During austral autumn, frontal activity favored above-normal rainfall in central and northwestern Argentina, Chile, and Uruguay. During this season, Marcos Juárez and General Pico, in central Argentina, recorded rainfall 97% and 85% above normal, respectively. In Chile, Juan Fernandez station recorded 121 mm on 19 April—its second highest daily rainfall since 1963. In Uruguay, the highest daily rainfall of the year was recorded in Treinta y Tres Orientales with 230 mm on 10 April. Nevertheless, drier conditions continued affecting Uruguay, central and southern Chile, and southern and northeastern Argentina, reinforcing drought. In northeastern Argentina, the Iguazú station recorded precipitation that was 71% below its normal.

Typically, during spring, La Niña favors below-normal precipitation in central and southern Chile. Winter and spring 2021 had below-normal precipitation over most parts of SSA. La Niña was present at the time, and the most affected regions with precipitation deficits were south-central

Chile and central, western, and northern Argentina. Some stations in Argentina reported rainfall totals that were 80%–90% below normal for winter. Argentina had its fourth-driest October since 1961. Above-normal rainfall was only recorded in localized parts of northern Argentina and southeastern Uruguay.

(iii) Notable events and impacts

Argentina, parts of Uruguay, and Chile were under severe drought conditions during 2021 (Fig. 7.17). Drought was extreme or exceptional across parts of the region, according to the Drought Monitor. In addition, these conditions, combined with high temperatures, favored the development of fires and bushfires in different parts of central, southwestern, and northern Argentina during the summer. The city of El Bolsón, western Patagonia, was one of the most affected regions, with great damages and human loss during February and March.

Polar air irruptions led not only to below-normal temperatures in most of the SSA region, but also to unusual snow events in central Argentina during June and in Uruguay during July. Of note, the city of Pilar, Argentina recorded a snow event for the first time for the month of June.

During austral autumn and spring, some convective precipitation events affected central and northern Argentina and Uruguay, leading to flooding in some regions and forcing the evacuation of residents. Santiago del Estero city (Argentina) recorded 108.6 mm on 3 March, San Rafael recorded 81 mm on 20 April, and Marcos Juárez recorded 225 mm on 8 April. All set a new record for their highest daily value since 1961. The heavy rain prompted floods in San Rafael and Marcos Juárez.

During the last week in October strong wind events affected parts of the Argentinian Patagonia, with major damage reported in Comodoro, Rivadavia, and Esquel Cities. Gusts of more than 150 km h^{-1} were recorded during that period.

Fig. 7.17. Extreme and notable events in southern South America during 2021 (Argentina, Chile, and Uruguay).

e. Africa—A. Mekonnen, Ed.

This 2021 report for Africa is based on observational records from meteorological and hydrological services across the region, rainfall from the Global Precipitation Climatology Project (GPCP), and reanalysis products from the National Centers for Environmental Prediction/National Center for Atmospheric Research (NCEP/NCAR). Notable events in 2021 across the continent were compiled based on reports and information from government agencies, regional and international organizations, and research/Early Warning organizations. The climatological base period is 1991–2020. Terms "normal" and "average" are interchangeably used to refer to as the 1991–2020 climatology.

In 2021, temperatures over much of Africa were above normal. Annual temperatures ranging from 1.5° to 2°C above normal were observed over most of Algeria, Sudan, southern South Sudan, and adjoining southwest Ethiopia and northern Uganda, while areas across the boundaries of Niger-Nigeria-Chad had below normal temperatures (Fig. 7.18). Below-normal temperatures were also evident over most of South Africa, Botswana, and southern Namibia.

The mean annual rainfall over much of the continent was within normal ranges (±0.5 mm day^{-1} around normal). However, rainfall over most of southern Nigeria, southwest Ethiopia, Uganda, southeastern Kenya, most of Zambia, Malawi, northeastern areas of Democratic Republic of Congo, and eastern Angola was below normal (Fig. 7.19).

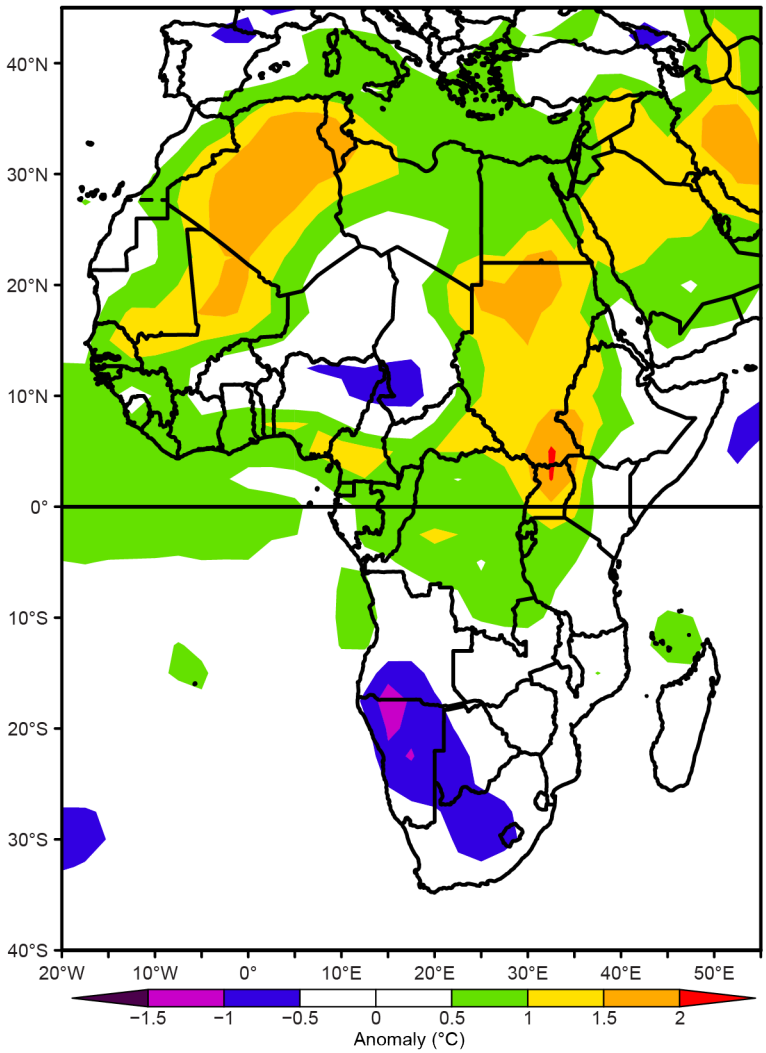

Fig. 7.18. The 2021 annual temperature anomalies for Africa (°C; base period 1991–2020). (Source: NCEP/NCAR.)

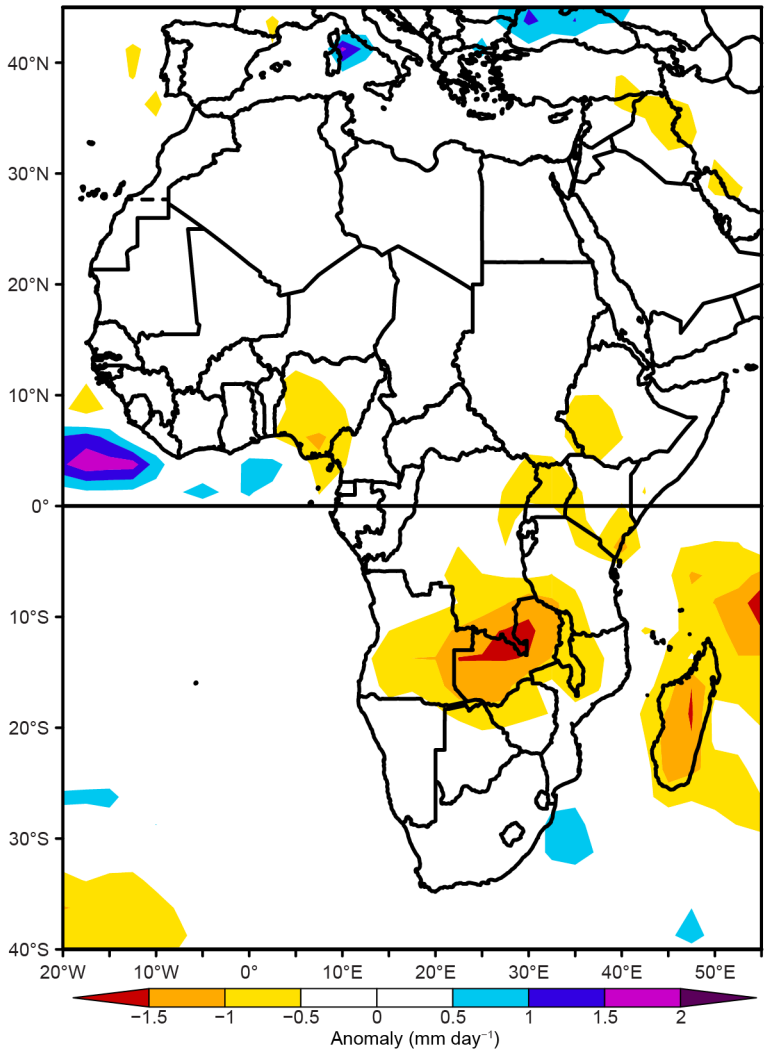

Fig. 7.19. The 2021 annual rainfall anomalies for Africa (mm day^{-1}; base period 1991–2020). (Source: NCEP/NCAR.)

Extreme weather events and high climate variabilities were also reported from several countries. Cold snaps, heat waves, and forest fires that affected extensive areas were reported from Morocco and Algeria. Record maximum temperatures, heavy rains resulting in extreme flooding and river overflows, and windstorms were observed in Central and West Africa. Heavy downpours over the Blue Nile catchment that affected downstream countries were reported from the Horn of Africa. In contrast, annual rainfall in equatorial East Africa was much below normal. Extremely heavy rainfall was reported in parts of southern Africa. An active tropical cyclone season was observed over the southwest Indian Ocean. The details of these and other extreme events are compiled by region below.

1) NORTH AFRICA—K. Kabidi, A. Sayouri, M. ElKharrim, and A. E. Mostafa

North Africa comprises Mauritania, Morocco, Algeria, Tunisia, Libya, and Egypt. Much of this region is characterized by arid and semi-arid climate, while northern parts exhibit Mediterranean climates. Precipitation over the region is highly variable both in space and time. Rainfall over western North Africa is generally of short duration but at times intense. Overall, station records from Morocco show below-average (19% below normal) rainfall during 2021. Egyptian stations reported below-average rainfall in the south, while above-average rainfall was reported in the north. The 2021 mean temperatures over the region were above average.

(i) Temperature

The winter (DJF; December 2020–February 2021) mean temperature over the region was above average. Morocco observed temperatures about 0.4°C above normal (Fig. 7.20a); however, in January, temperatures of 0.9°C below normal were reported from mountain regions of the country, while February temperatures were 1–3°C above normal over eastern parts. Most Algerian and Tunisian meteorological stations reported temperatures up to 3°C above normal in February. Winter temperatures over much of Egypt were 1–2°C above average.

Spring (March–May) temperatures were above average (+0.5°C) over Morocco, Mauritania, and much of Egypt. Most of Algeria and Tunisia were about 1–2°C above normal (Fig. 7.20b). In March, near-normal temperatures were reported from Algeria, Tunisia, and northern Libya. In May, mean maximum temperatures ranging from 1.5° to 2°C above normal were observed over northern and Saharan regions and 3°C above normal was reported over central regions in Morocco. During April and May, temperatures were about 2–4°C above normal over central Algeria, southern Tunisia, and western Libya.

Summer (June–August) temperatures were 0.6°C above normal over the region. Northern and northeastern Algeria and Tunisia exhibited temperatures 2° to > 3°C above normal (Fig. 7.20c). Summer temperatures more than 1°C above normal were also observed in Mauritania, Libya, and parts of Egypt. In July, temperatures exceeding 40°C were reported from several areas of Morocco (> 60% of stations reported heat waves). Generally, maximum temperatures of 1.1°C above normal were observed over Morocco, with anomalies of +1.5° to +3°C in central and southern regions of Morocco and parts of Egypt. A new record of 49.6°C was reported from Sidi-Slimane station in Morocco on 10 July. A maximum temperature of 48°C was reported at El-Wadi Al-Gadid station in Egypt on 12 June and again on 3 July. Anomalies of +4°C were reported from central Algeria and southern Tunisia in June and +2.5°C during July in Algeria, Tunisia, and Libya. In August, temperature anomalies reached +3.5°C in northeast Algeria and Tunisia. Tunisia had its hottest summer on record since 1950.

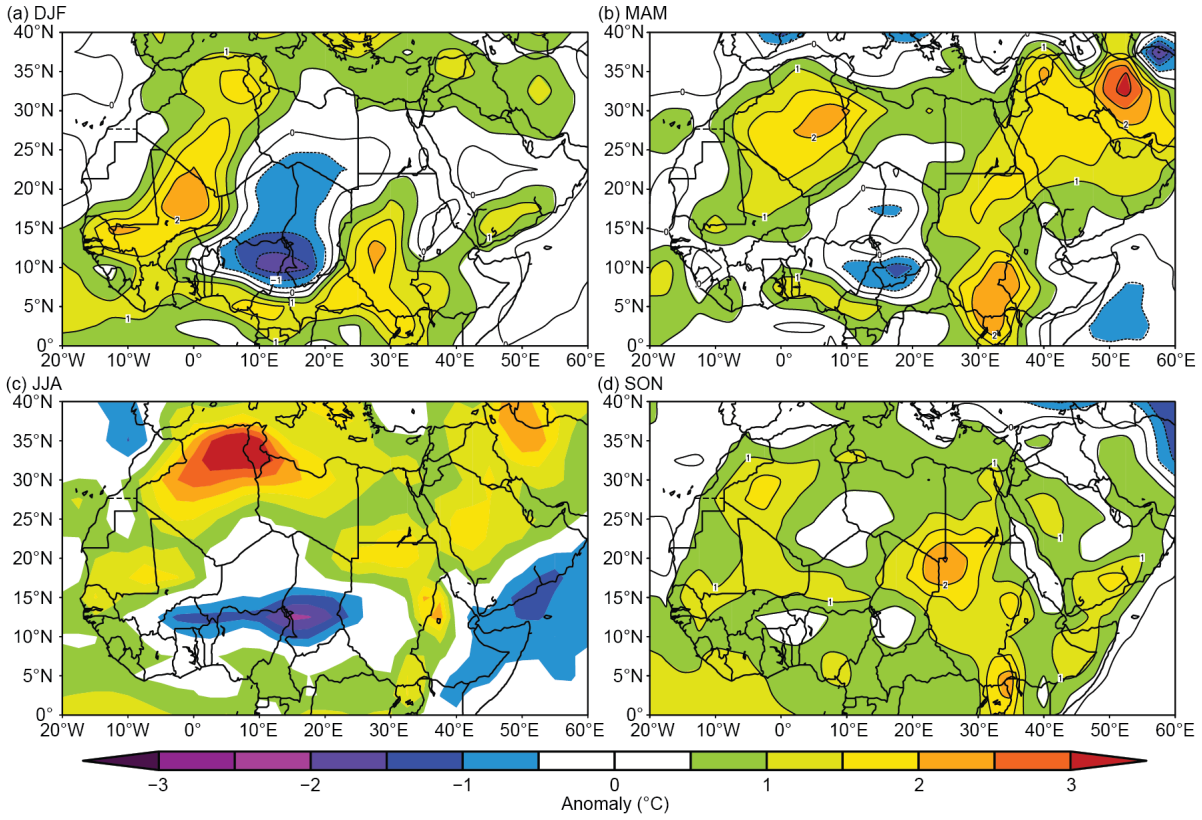

Fig. 7.20. North Africa seasonally averaged mean temperature anomalies (°C; 1991–2020 base period) for (a) DJF 2020/21, (b) MAM 2021, (c) JJA 2021, and (d) SON 2021. (Source: NOAA/NCEP.)

During autumn (September–November), temperature anomalies of about +1° to +2°C were observed over southern Algeria, northeastern Mauritania, southern Egypt, and southeastern Libya (Fig. 7.20d). Autumn temperatures were near normal to slightly above normal over much of Morocco. However, average minimum temperature anomalies of more than –1.4°C (range of –0.5° to –2.7°C) were reported across all Moroccan stations. In September, temperatures were above normal in central Algeria, and in October near-normal temperatures were reported in Algeria, Tunisia, and Libya. November temperatures were 2–3.5°C below normal in Libya. Additionally, a minimum temperature of –1°C was reported on 1 November at Saint Catherine in Egypt.

(ii) Precipitation

Winter precipitation was near-normal over most of central and southern Morocco and southern Algeria, Egypt, and Libya (Fig. 7.21a). Precipitation ranging from 50% to 126% above average was reported during January over northern Morocco. Reports also indicate more than 100% of normal precipitation over southern Morocco.

Spring rains were below to near-normal over much of the region (Fig. 7.21b). Seasonal precipitation totals were 55% below normal over Morocco; however, in March, heavy rainfall (47% to 349% above normal) was observed. Spring rains were below to near-normal in Algeria, Tunisia, and Libya. The summer season was mostly dry over North Africa.

Autumn rains were below normal over most parts of the region (Fig. 7.21c); however, above-normal precipitation was reported from northern Algeria in November. The seasonal deficit reached 49% in Morocco and about 36% in Tunisia.

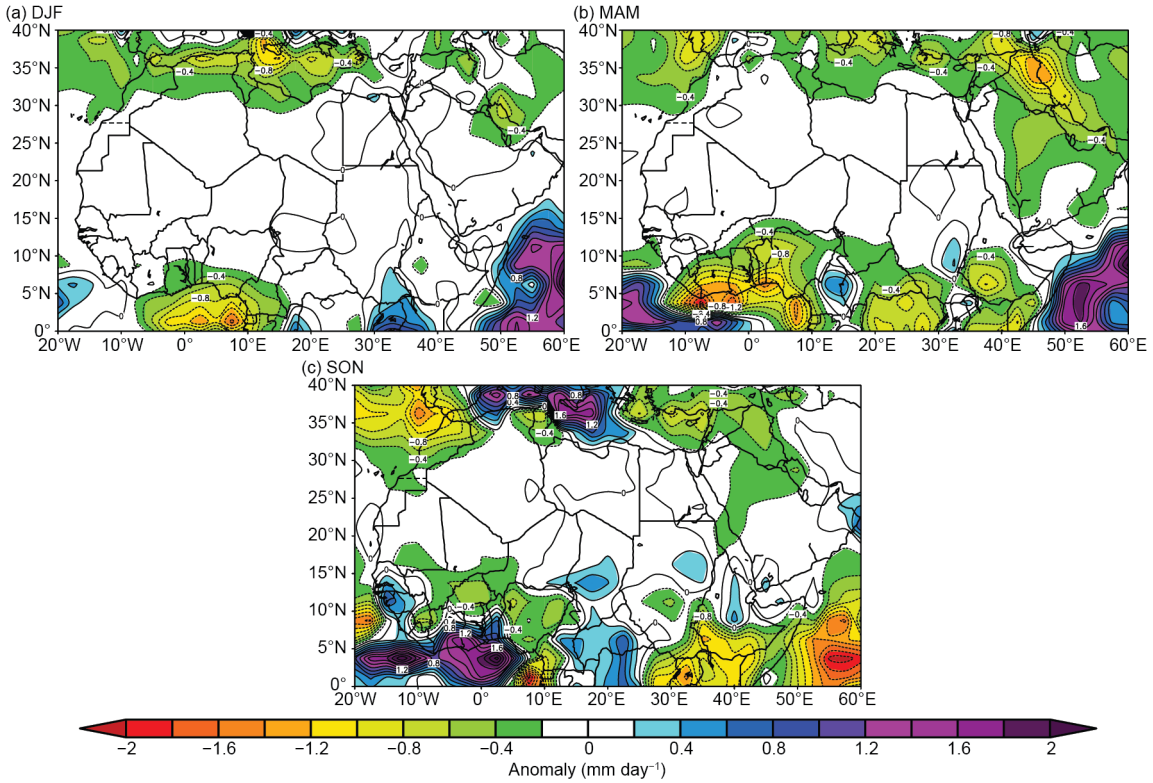

Fig. 7.21. North Africa seasonally averaged rainfall anomalies (mm day–1; 1991–2020 base period) for (a) DJF 2020/21, (b) MAM 2021, and (c) SON 2021. (Source: GPCP NOAA/NCEP.).

(iii) Notable events and impacts

Severe storms, heat and cold waves, strong winds exceeding 140 km h^{-1} in the Saharan region and 100 km h^{-1} in the extreme north region, and forest fires were all reported in Morocco and Algeria in 2021. Additional information is given below.

Meteorological and hydrological services of Morocco reported heat waves during February, July, October, and December. Similar heat waves were reported from Algeria in July, August, and September. Additionally, 285 forest fires that affected 2782 hectares were reported between January and September in northern Morocco and Algeria. The fires damaged more than 89,000 hectares and caused at least 90 deaths.

In January and March, Morocco experienced several storm events that led to flooding. Flash floods caused by convective precipitation occurred in March in extreme northern areas of Morocco, where extensive property damage was reported. Heavy rains affected northwestern Algeria during March, October, and November, causing 11 fatalities in total and significant property damage. Heavy rainfall also occurred in northwestern Tunisia during September and October, causing three deaths and extensive property damage.

2) WEST AFRICA—W. M. Thiaw, W. Agyakwah, S. Hagos, F. Zeng, I. A. Ijampy, F. Sima, and O. Ndiaye

West Africa extends from the Guinea coast to about 20°N and from the eastern Atlantic coast to Niger. Climatologically, it consists of two distinct but inherently linked sub-regions: (1) The Sahel to the north from about 12° to 17°N, spanning countries from Senegal and The Gambia in the west to Niger in the east and (2) the Gulf of Guinea region to the south from about 4° to 10°N encompassing the Guineas to the west along the east Atlantic coast and Nigeria and Cameroon to the east. The rain season over the Sahel runs from June to September and its interannual variability is controlled by the adjacent (Atlantic Ocean) and remote (central and eastern Pacific and the Indian Ocean) sea surface temperatures, including variabilities of the middle tropospheric easterly jet, Saharan heat low, and north–south movement of the deep convective zone.

(i) Temperature

The highest mean annual temperatures, between 28° and 30°C, were observed across the western and central Sahel, encompassing eastern, southern Mauritania, and central Mali (Fig. 7.22a). Mean annual temperatures were between 22° and 28°C in the eastern and southern Sahel and the Gulf of Guinea Region (GGR), with the lowest temperatures of 22–24°C registered over western GGR. Mean annual temperatures were above normal over the western region and along

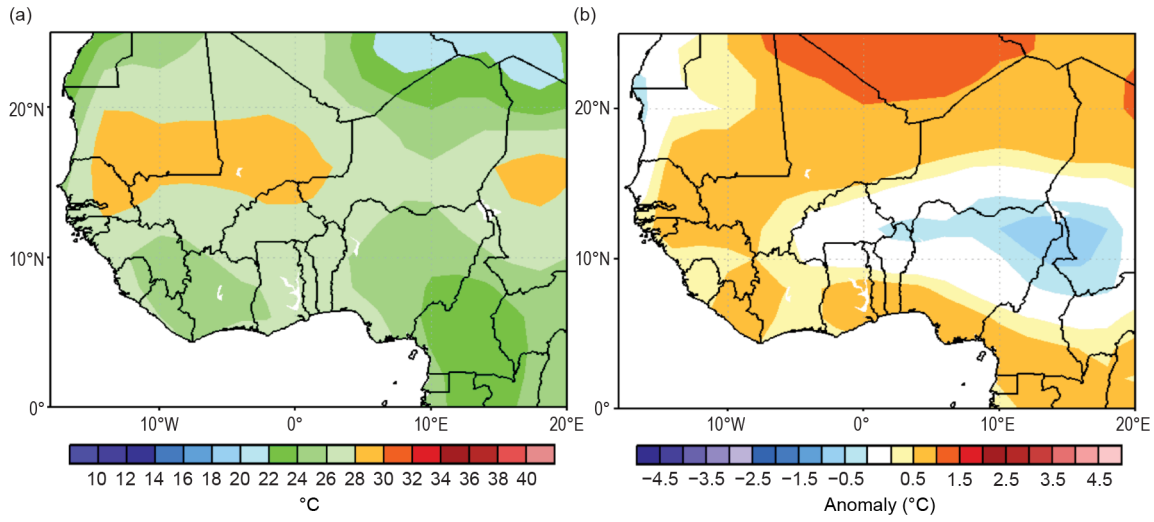

Fig. 7.22. Annual (a) mean temperature and (b) mean temperature anomaly (°C; base period 1991–2020) for West Africa. (Source: NOAA/NCEP.)

the Guinean coast, with departures from the mean of about +0.5° to +1°C (Fig. 7.22b), placing 2021 among the 3% of warmest years in this area. Temperatures were 0.5° to 1°C below the mean over northern Nigeria. Annual maximum temperatures (Tmax) exceeded 36°C in central Mali (1° to 1.5°C above the mean) and ranged between 34° and 36°C across most areas from eastern Senegal to Niger. These were average values in the western Sahel but 1° to 2°C below the mean in the area encompassing Burkina Faso to northern Nigeria. Tmax was 28–32°C (1.5–2.5°C above the mean) over the southern Nigeria. The highest Tmax values were observed during March–May season, averaging 40° to 46°C across the Sahel from eastern Senegal to Niger, with peak values extending from southeastern Mali and northwestern Burkina Faso to southern Niger. These were 1–1.5°C above the mean in this sector, but 1–2°C below the mean in the western Sahel. Annual minimum temperatures (Tmin) exceeded 24°C along the Sahel and Guinea coasts, about 1.5–2.5°C above the mean and ranking in the 90th percentile in the western Sahel.

(ii) Precipitation

Annual rainfall ranged between 1000 and 2000 mm over the Gulf of Guinea region with areas of maximum rainfall over 2000 mm along the western Guinea coast over Sierra Leone and western Liberia (Fig. 7.23a). Rainfall decreased northward from 2000 mm in the Guinean Highlands to 300 mm at about 15°N in the Sahel. The climatologically dry areas of the northern Sahel near 20°N registered rainfall between 50 and 300 mm. Overall, annual rainfall was average over much of the Sahel and the Gulf of Guinea region, except for areas in western Mali, which observed cumulative totals between 1000 and 1500 mm (only 50 to 100 mm above the mean), and along the Guinean coast from Liberia to Ghana, where totals ranged between 1250 and 1500 mm (also 50 to 150 mm above the mean). Rainfall was below average over Nigeria with the largest deficits at least 200 mm below the mean in the central and southeastern areas.

In the Sahel, rainfall totals during the period July–September account for much of the annual cumulative rainfall. Totals ranged from 100 mm at about 20°N to 500 mm at 15°N, between 500 mm and 1000 mm in the central areas (12°–15°N), to over 1200 mm in the areas of maximum precipitation, including the western Guinean coast (Fig.7.23b). These corresponded to above-average rainfall in the western Sahel with moisture surpluses between 20 and 100 mm in Senegal and western Mali. Above-average rainfall was also observed during the 2019 and 2020 seasons in the Sahel. However, rainfall was off to a slow start in the western Sahel in June and July 2021, with deficits more than 100 mm below the mean in southeastern Senegal and western Mali. Mali quickly recovered in July with surpluses more than 50 mm above the mean in some locations,

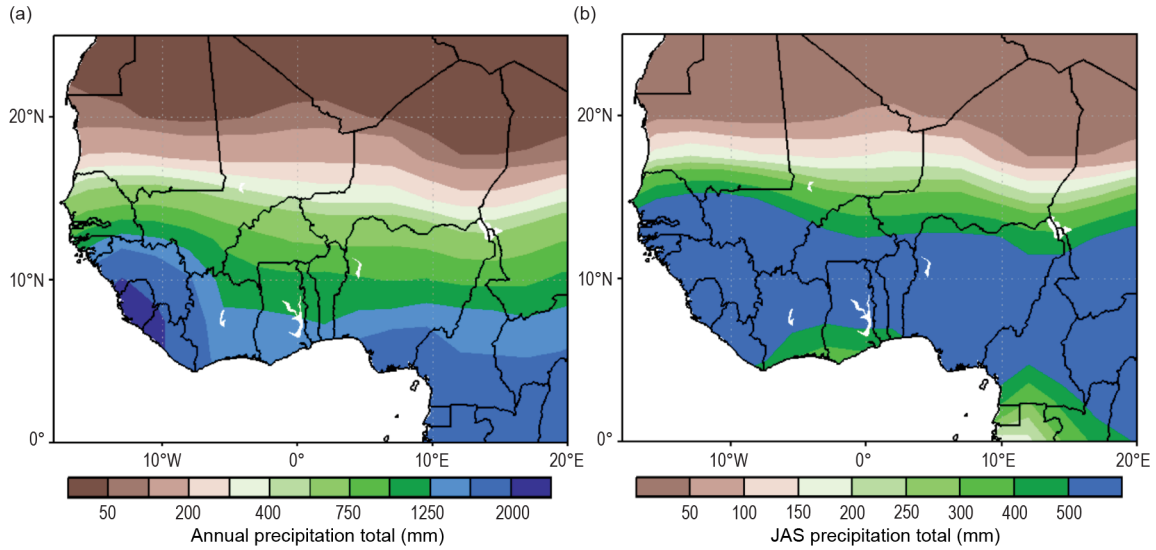

Fig. 7.23. Annual (a) rainfall total (mm) and (b) July–September rainfall total (mm) for West Africa. (Source: NOAA/NCEP.)

while deficits about 50 mm below the mean persisted over Senegal. Heavy downpours in August of about 300 mm (100 mm above the mean and ranking in the 90th percentile) in Senegal contributed to the overall wetter-than-normal rainfall season in this western sub-region of the Sahel. The rainfall period over West Africa runs from June to September. Figure 7.24 shows the June–September (JJAS) rainfall anomaly over the region. Consistent with the warm SST conditions over the Gulf of Guinea, the precipitation was mainly concentrated along the coastal regions with interior West Africa being comparatively dry. Below-normal rainfall over much of Nigeria and western Cameroon was observed.

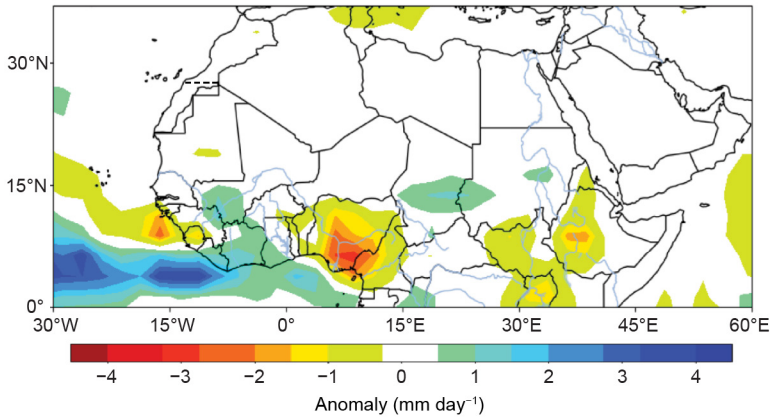

Fig. 7.24. Rainfall anomalies for June–September (mm day–1; base period 1991–2020) for West Africa. (Source: GPCP via NOAA/NCEP.)

Along the Guinean coast, much of the annual rains fall during the spring during April–June and in the autumn during September–November following the seasonal north–south displacement of the area of maximum convergence in West Africa. However, in the area extending from Sierra Leone to Ghana, the July–September rains surpassed 700 mm (100–150 mm above the mean). The performance of the seasonal rainfall in the GGR during April–June was poor as totals ranged between 300 and 500 mm, except for southeastern Nigeria which received amounts in excess of 500 mm. Rainfall deficits across the area encompassing southwestern Nigeria to Sierra Leone exceeded 100 mm below the mean, with the highest deficits reported in May, which was among the 3% of driest months in the recent 30-year period. The months of September and November brought rainfall surpluses more than 100 mm above the mean along the coast from Ghana to Sierra Leone in September and in southern Nigeria in November.

(iii) Notable events and impacts

Reports show September 2021 was the warmest September on record for the region, while July and August were the seventh and third warmest for their respective months. In Nigeria, before the start of the rainy season, the average maximum daily temperature surpassed 40°C on more than 50 days at several stations (Dutse, Maiduguri, Nguru, Potiskum, Sokoto, Yola, Zaria stations), according to the Nigerian Meteorological Agency.

Most of the extreme precipitation and associated costly flooding events occurred near the end of the rainy season. In Douala, Cameroon, extreme flooding affected several neighborhoods after 186 mm of rain fell over 24 hours during 11–12 August. Hundreds of homes were flooded. Later that month, Ouémé River overflow in southern Benin led to severe flooding in the town of Zagnanado, according to local media. Similarly, in Niger, 60 people were reported to have died either from drowning in flood water or from collapsing buildings, according to the nation's Civil Protection Authorities. In northeastern Ghana, five people died while attempting to cross a swollen river and due to lightning strikes. During 30–31 August, heavy rains in Guinea led to five fatalities, and

the resulting flood affected about 70,000 people in total, according to Guinea Red Cross Society. According to Nigeria's Emergency Management Agency, flooding due to heavy rains that fell on 12 September in Abuja and surrounding areas led to four fatalities.

In Chad, the UN Office for the Coordination of Humanitarian Affairs (OCHA) reported that flooding affected nearly 247,000 people across 400 villages. Fifteen people lost their lives, 17 were reported missing, and a total of 329 people were injured over the rainy season. In early October, the meteorological agency of Côte d'Ivoire reported that 105 mm of rain fell in Yopougon and 106 mm in Attécoubé in a 12-hour period.

Flood events were recorded in many parts of Nigeria between June and November. The resultant floods from heavy rainfall destroyed homes, valuable properties, farms, roads, and bridges. As a result, thousands of people were displaced and several lives were lost. These events also contributed to the spread of vector borne diseases and exacerbated the cholera outbreak in many states of the country. Kano was one of the most affected states, with a rainfall total of 98.8 mm on 24 July following a torrential downpour that lasted several hours. This led to 19 fatalities in the Doguwa Local Government Area after a vehicle was washed away in a flood. During the same period, several homes were submerged and property damage was estimated at over 100 million naira ($240,000 U.S. dollars), according to Kano State Emergency Management Agency (SEMA).

In July, The Gambia experienced a windstorm surge that affected almost 17,000 people in more than 100 communities across all seven regions, causing internal displacement and homelessness. More than 100 people were severely injured as a result of fallen walls and trees. 10 deaths were confirmed as a result of collapsed buildings. According to the Meteorological Department, on 7 July, winds reached 85 km h–1 and was the highest wind speed recorded in the last five years. 12 people died and more than 109,000 people were affected.

3) CENTRAL AFRICA—W. M. Thiaw and W. Agyakwa

Central Africa features a unique climate system marked by a strong annual cycle as it spans a wide area of Africa across both the Northern and Southern Hemispheres (SH). It extends from the southern tip of the Democratic Republic of Congo (DRC) northward into the central areas of Chad. Longitudinally, the region extends from about 5°E to ~35°E. Given the overlap with areas in West Africa and East Africa, this analysis focuses strictly on the sub-region encompassing Cameroon, Chad, Central Africa Republic (CAR), DRC, Congo, Gabon, Equatorial Guinea, and Sao Tome & Principe.

(i) Temperature

The mean annual temperature was between 22° and 28°C across much of the region, except for the western and southern ends of DRC, where it was 22–24°C. Temperatures were 0.5–1°C above the mean across the region, except for southwestern Chad and northern Cameroon, where they were 1°C below the mean. Much of DRC westward to Gabon and southern Cameroon reported annual temperatures above the 90th percentile (Fig. 7.25a). The months of September through December had the highest anomalies in mean temperature, reaching 28°C in western DRC, and overall exceeding the 95th percentile across much of the region. Below-normal temperature anomalies in excess of –3°C prevailed over northern Cameroon and southwestern Chad in February, making this month the coldest in the 30-year base period.

Annual maximum temperatures were around 30–34°C, above the 95th percentile across much of the region (Fig. 7.25b). Though Tmax reached or exceeded 40°C in southern Chad and northern Cameroon, the temperatures were 2°C below the mean and in the 3% lowest temperatures in the base period, with the period April–August accounting for much of the low Tmax values. Southern DRC reported record-breaking Tmax exceeding 38°C, with the highest elevated values of more than 5°C above the mean in July through September; with the warmest August in the 30-year period. Annual minimum temperature (Tmin) was above normal in the northern areas

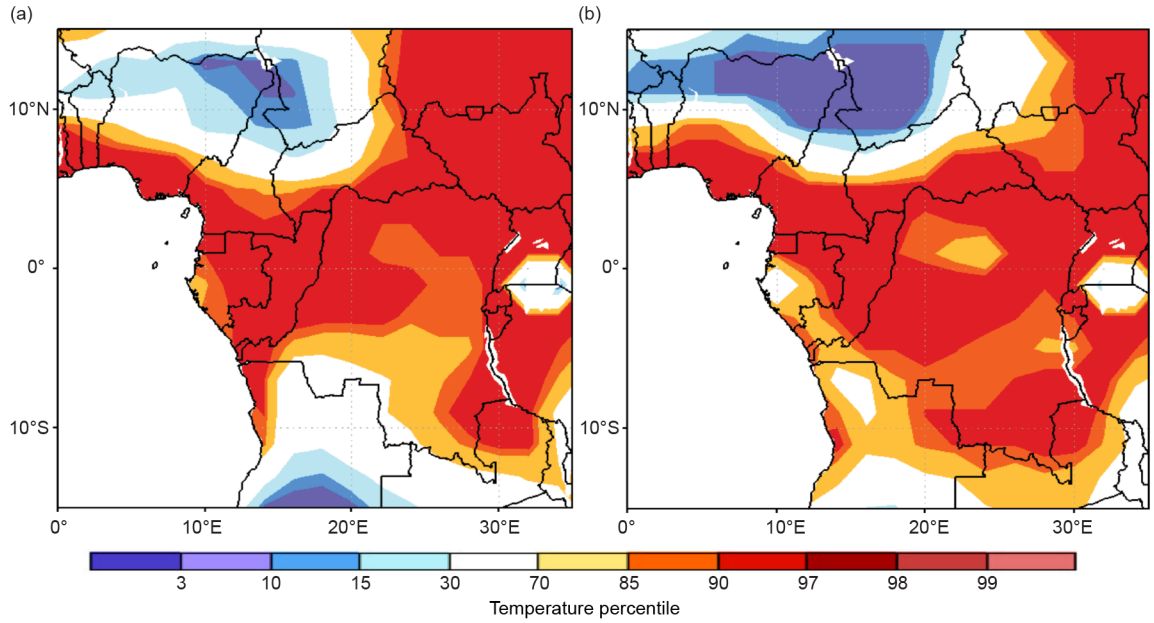

Fig. 7.25. Annual (a) average temperature percentile rank and (b) maximum temperature percentile rank for Central Africa. (Source: NOAA/NCEP.)

of the region with the highest positive anomalies (about 2°C above the mean) observed during January–March and November–December.

(ii) Precipitation

As stated earlier, the climate of Central Africa (CA) exhibits seasonality at both the north and south ends of the region. The rainfall pattern is closely related to the north–south movement of the maximum deep convective zone and wind flow pattern. Rainfall is unimodal in the northern areas of the region and marked with dry conditions during the NH autumn through spring and a return of the rains in the summer. The southern areas of the region are dry during the NH summer and wet during autumn through early spring seasons. The central areas of the region around the equator receive rainfall year-round. The area of maximum annual rainfall is located along coastal Cameroon with annual totals exceeding 2000 mm. On average, rainfall amounts range between 1200 mm over the southern tip of DRC and the southern areas of CAR and Cameroon to 2000 mm across much of DRC, Congo, Gabon, and southern Cameroon (Fig. 7.26a). Annual rainfall totals are generally less over southern Chad with a steep north–south gradient indicated by about 200 mm in the central areas of Chad to about 1000 mm in the southern tip.

During 2021, an area of maximum annual rainfall over east central DRC, with totals exceeding 2000 mm (Fig. 7.26a). A rain band in the 2000 mm covering most of the northern half of DRC narrowed and extended to the west to cover the area from central Congo to coastal Cameroon. Annual rains totaled 500 mm in the southern tip of DRC, with a northward gradient reaching 1750 mm in the southern areas bordering Angola and in the east. A similar pattern is observed in the northern areas of CA, with lower rainfall totals about 500 mm in central Chad increasing southward to northern DRC. Rainfall was above average over the western half of DRC, Congo, and southern CAR, with surpluses ranging between 50 and 150 mm (Fig. 7.26b) and totals ranking in the 85th percentile. Western Cameroon and southeastern DRC observed rainfall deficits of 200 mm below the mean, ranking in the 10th and 3rd percentiles, respectively.

Examination of the evolution of rainfall throughout the year suggested deficits reaching 100 mm below the mean (15th percentile) in February in the area encompassing Congo northward to Cameroon. Rainfall was significantly below average over the southern tip of DRC during January–March as totals averaged less than 300 mm, bringing rainfall deficits to more 150 mm (3rd

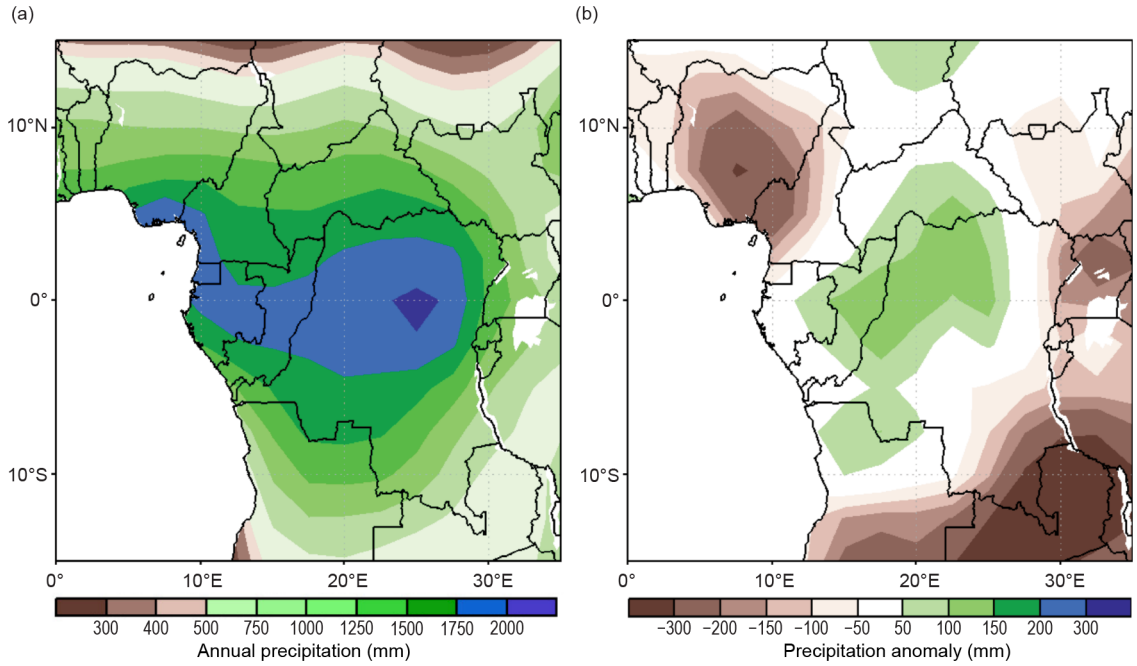

Fig. 7.26. Annual (a) total rainfall and (b) rainfall anomaly (mm; base period 1991–2020) for Central Africa. (Source: GPCP via NOAA/NCEP.)

percentile), indicative of extremely dry conditions. Rainfall was much above average in the western two-thirds of DRC during August–October, with departures from the mean exceeding 150 mm; much of the surplus was due to heavy downpours in October, with excess rains more than 300 mm (above the 95th percentile). A similar pattern with rainfall surpluses about 100 mm above the mean was observed in December.

(iii) Notable events and impacts

Heavy rainfall in Bangui (CAR) during 19–23 July flooded several districts in the city, affecting more than 70 families and 300 people. Stagnant water and mud remained for days in some areas, increasing risk of waterborne diseases, according to the International Organization for Migration (IOM). About two weeks following the floods, torrential rain fell over Bangui on 7 August, damaging or destroying more than 400 households in over a dozen districts and affecting 4000 people who needed shelter, according to the International Federation of Red Cross (IFRC).

Heavy rains triggered flash flooding in Bukavu in DRC on 19 August, causing widespread damage, while the neighboring province of North Kivu was pounded by heavy rain on 20 August, causing the Nyakariba River to overflow its banks in Rutshuru Territory. Flood water, debris, and mud swamped homes and crops, affecting 200 households, according to OCHA. Several neighborhoods in the cities of Pointe-Noire and Brazzaville were affected by a heavy rainfall event on 29 November. This rainfall on top of already saturated soils, from an early start to the rainfall season in September, caused the water level of the river to rise 2.4 m above the riverbed, leading to the flooding of several villages. This situation forced thousands of people to leave their homes and lose their livelihoods, and the government declared a state of emergency, according to the IFRC.

4) EAST AFRICA—E. Bekele and W. M. Thiaw

East Africa, or the Greater Horn of Africa (GHA), spans the equator and extends 10°S–20°N and 20°–50°E. Its northern sector comprises Sudan, South Sudan, Ethiopia, Eritrea, Djibouti, and the northern two-thirds of Somalia. Southern Somalia, Kenya, northern Tanzania, Uganda, Rwanda, and Burundi are in its equatorial sector, while the southern sector encompasses central

and southern Tanzania. The region has a complex terrain, with elevation ranging from about 160 m below sea level at Ethiopia's northern exit of the Rift Valley to more than 5000 m above sea level at glaciated Mount Kilimanjaro. This complex topography is further typified by the presence of large lakes and is reflective of multi-faceted climate zones modulated by local and large-scale forcing such as the deep convective and moisture convergence zone, ENSO (El Niño-Southern Oscillation), the Indian Ocean dipole, the Madden Julian Oscillation, and tropical-extratropical interactions. Rainfall is bimodal in the equatorial sub-region, with two distinct rainfall seasons in March–May (MAM) and October–December (OND). Seasonal rainfall is unimodal in the northern and southern sectors, spanning November–April in the south and June–September in the north. The June–September rainfall over Ethiopia-Eritrea is locally known as "Kiremt" rains.

(i) Temperature

Annual mean temperatures exceeded 26°C over much of Sudan, Somalia, Djibouti, Eritrea, far eastern Ethiopia, and Kenya (Fig. 7.27a). Annual mean temperatures were less than 22°C in most of central Ethiopia. However, anomalously high annual temperatures (1.5–2°C above the mean) were observed across southwestern Ethiopia, southeastern South Sudan, northwestern Kenya, northern Uganda, and northern Sudan (Fig. 7.27b). Annual mean maximum temperatures exceeded 40°C locally in eastern Sudan and ranged between 34° and 40°C in other parts of the country. Eastern Kenya and much of Somalia, Djibouti, and Eritrea observed maximum temperatures between 34° and 38°C, while temperatures were less than 30°C in central and southern Ethiopia and in the Lake Victoria region.

Anomalously elevated temperatures, most prominent in central and southern Sudan, prevailed across much of the region between March and December 2021. Between December–February (DJF) 2020/21 and October–December (OND) 2021, mean temperatures were above normal over much of Sudan and South Sudan. Above-normal temperatures were also observed across much

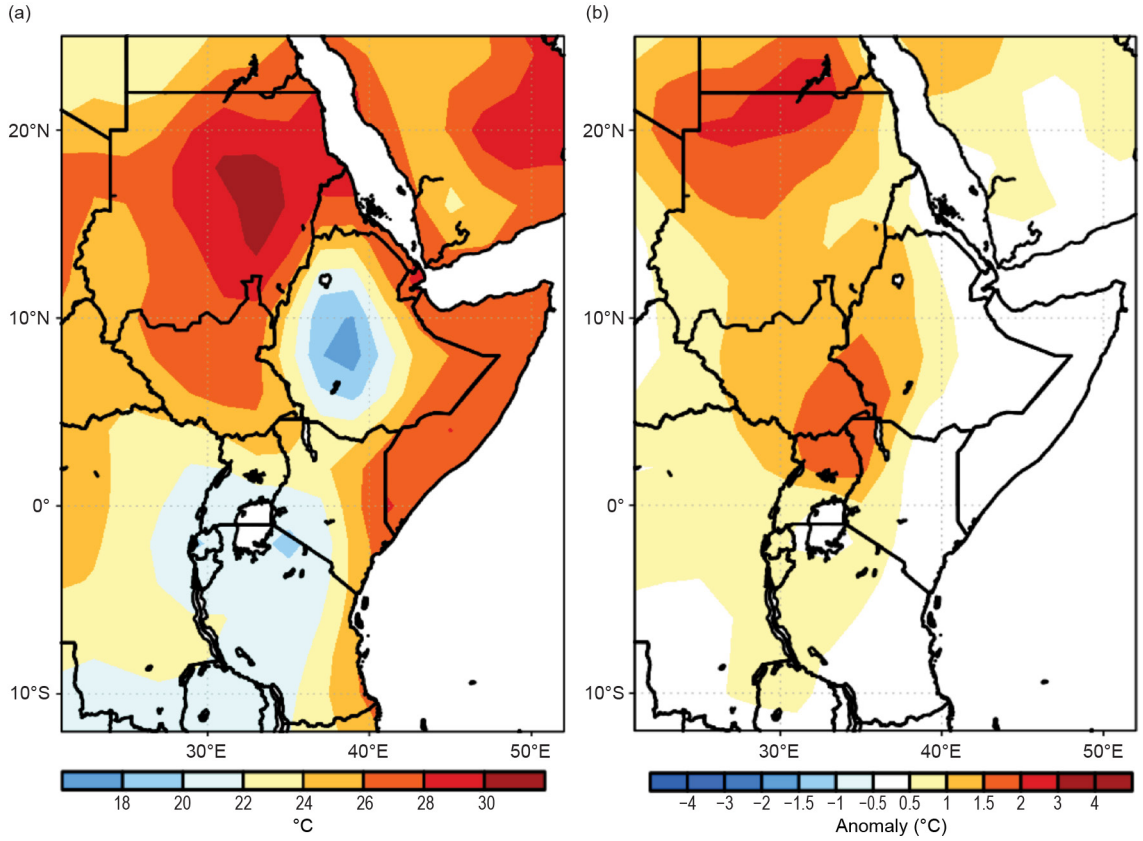

Fig. 7.27. Annual (a) mean temperature and (b) mean temperature anomalies (°C; base period 1991–2020) for East Africa in 2021. (Source: NOAA/NCEP.)

of Uganda, Rwanda, Burundi, western Kenya, western Tanzania, and parts of southeastern Ethiopia. Maximum temperatures were above normal over much of the region during OND, with the highest anomalies located over eastern Sudan, western areas of Ethiopia, eastern South Sudan, Uganda, and western Tanzania. The highlands of central Ethiopia exhibited the lowest annual minimum temperatures (Tmin), less than 12°C. Tmin ranged between 12° and 18°C across the rest of Ethiopia, southern Uganda and Kenya, and much of Tanzania, except for the coastline, and were 20–25°C over much of eastern Sudan, South Sudan, and Somalia.

(ii) Precipitation

Annual rainfall surpassed 1000 mm across western Ethiopia, portions of South Sudan, Uganda, Rwanda, Burundi, and northwestern Tanzania (Fig. 7.28a). Western Kenya, central Ethiopia, eastern South Sudan, northeastern Uganda, and much of Tanzania received rainfall between 600 mm and 1000 mm. Totals were less over northern Sudan, Eritrea, Djibouti, and northern Somalia, with rainfall amounts ranging between 50 mm and 600 mm. Overall, rainfall was below normal over much of equatorial East Africa (Fig. 7.28b). Rainfall deficits exceeded 250 mm over parts of southern Ethiopia, coastal Kenya, and southern Tanzania. Rainfall totals averaging 150–250 mm below the mean were recorded over parts of central and southeastern Ethiopia, southern Somalia, much of Kenya, Uganda, Rwanda, Burundi, and Tanzania. Kiremt rains (June–September) were 1–2 mm day^{-1} (~120–240 mm total) below normal over southwestern Ethiopia. The seasonal rains were generally below normal over northern and central Ethiopia, most of South Sudan, and Uganda (see Fig. 7.24).

Annual rainfall was below the 10th percentile over southern Ethiopia, southern Somalia, and portions of Kenya, northern Uganda and southern Tanzania. The most significant rainfall deficits, below the 3rd percentile, were observed over portions of southern Ethiopia, localized areas of southern Somalia, northern Uganda, and southern Tanzania. Most of equatorial East Africa received below-average rainfall during all seasons, with deficits most pronounced during OND over southern Ethiopia, southern Somalia, much of Kenya, and Tanzania. Rainfall was also below average over southwestern Ethiopia, South Sudan, Uganda, Rwanda, and Sudan.

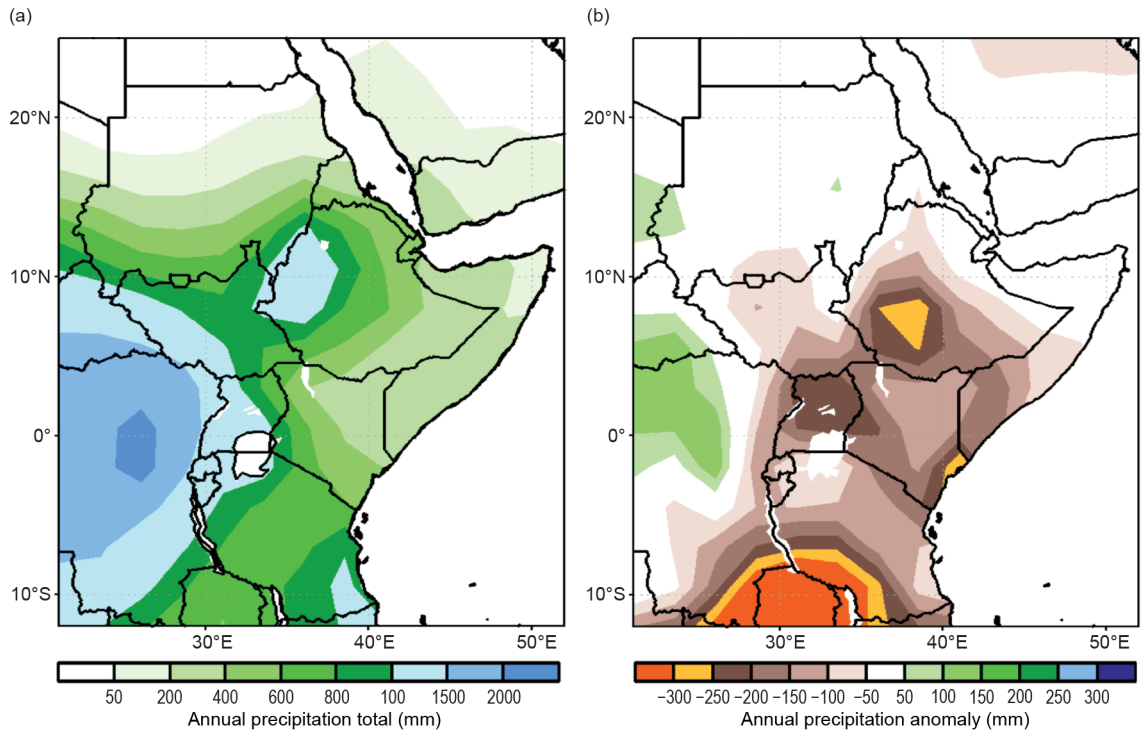

Fig. 7.28. Annual (a) total rainfall and (b) total rainfall anomaly (mm; base period 1991–2020) for East Africa. (Source: GPCP via NOAA/NCEP.)

(iii) Notable events and impacts

The annual total rainfall was the lowest on record in portions of equatorial East Africa (> 2 std. dev.), leading to three consecutive failed rainy seasons that resulted in one of the worst threats to food security in 35 years for more than 20 million people in eastern Africa, according to the U.S. Agency for International Development Famine Early Warning Systems Network (FEWS NET).

NOAA's satellite rainfall estimates (RFE2) indicated heavy downpours upstream of the Blue Nile and Baro–Akoba River basin in Ethiopia, with June–September accumulation exceeding 1000 mm, contributing to major inundations downstream in Sudan and South Sudan. The heavy rains resulted in significant increases in river levels that submerged low lying lands with significant impacts on livelihoods, food production, and drinking supplies. According to the United Nations, the flooding affected more than 835,000 people in 33 of South Sudan's 78 counties. The states of Jonglei, Unity, and Upper Niles suffered the worst impacts with 80% of the flood victims, including 305,000 in Jonglei State, 220,000 in Unity, and 141,000 in Upper Nile.

5) SOUTHERN AFRICA—A. C. Kruger, C. McBride, M. Robjhon, and W. M. Thiaw

Southern Africa covers the southern part of the African continent extending from about 5° to 35°S. It comprises Angola, Namibia, Zambia, Botswana, Zimbabwe, Malawi, South Africa, Lesotho, Eswatini, and Mozambique. The region is characterized by two main seasons. While the wet season spans from November of the predecessor year to April, the dry season lasts from May to October.

(i) Temperature

During 2021, annual mean temperatures averaged between 12° and 26°C in the region, with higher values exceeding 20°C across northern Namibia, Angola, northern Botswana, Zambia, northern Zimbabwe, Malawi, and Mozambique (Fig. 7.29a). The warmer regions included northwestern Angola and coastal Mozambique, where annual mean temperatures averaged 24–26°C. In contrast, the colder regions included much of Namibia, southern Botswana, central Zimbabwe, South Africa, Lesotho, and Eswatini, where annual mean temperatures averaged between 12°

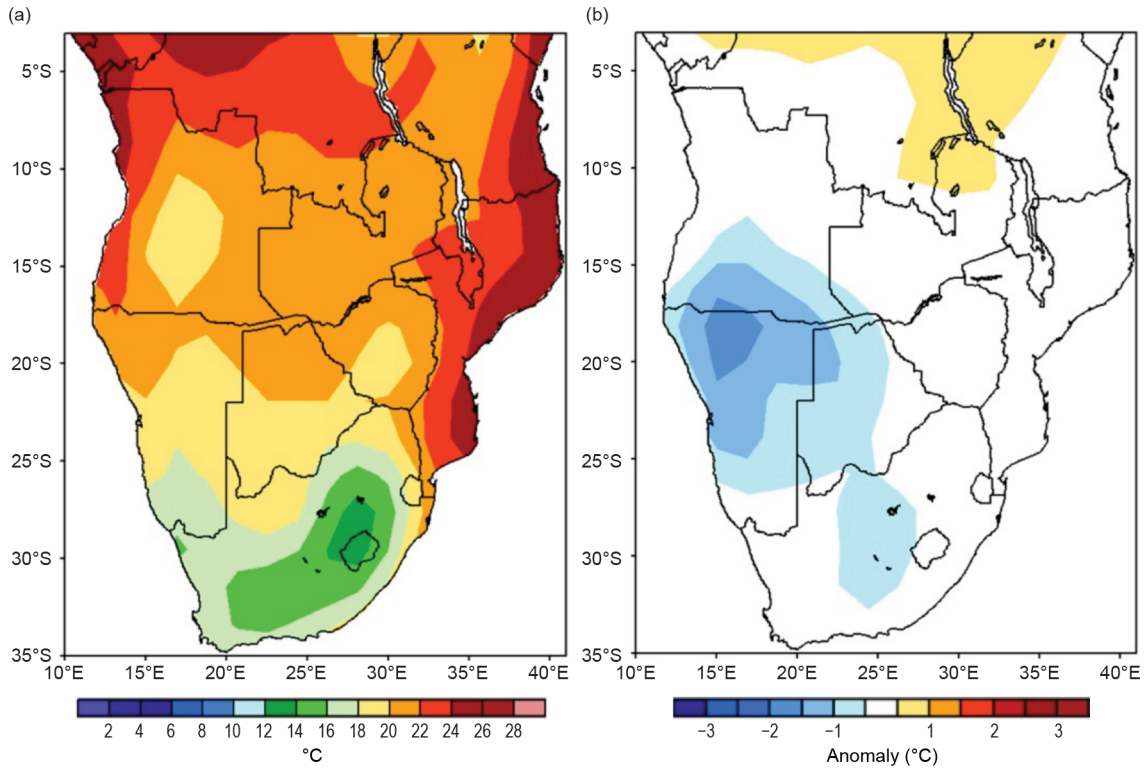

Fig. 7.29. Annual (a) mean temperature and (b) mean temperature anomaly (°C; base period 1991–2020) for southern Africa. (Source: NOAA/NCEP.)

and 20°C. The lowest annual mean temperatures registered over the interior of South Africa and Lesotho, and averaged between 12° and 16°C.

Annual mean temperatures were well below normal, with departures from the long-term average up to –2°C, over southern Angola, Namibia, and northwestern Botswana (Fig. 7.29b), ranking 2021 among the top 5% of the coldest years on record in these areas. Annual mean temperatures were near-normal elsewhere. An analysis of mean temperatures throughout the year show that below-normal mean temperatures persisted over southern Angola, Namibia, and parts of Botswana during all months, except for April, when near to above-normal mean temperatures were observed over the region. The coldest month was July, when well below-normal mean temperatures were observed over the region, with the largest departures from normal temperature, up to –3.5°C over parts of Angola, northeastern Namibia, and northwestern Botswana. On the seasonal time scale, mean temperatures remained below normal during DJF 2020/21, JJA, and SON over southern Angola and Namibia. Mean temperatures were above normal across central Angola, Zambia, Zimbabwe, Malawi, and northern Mozambique during SON.

South Africa experienced a somewhat warm year, which was quite mild compared to previous years. The warm year can be attributed, at least in part, to well-above normal rainfall over most of the country. The annual mean temperature anomalies for 2021, based on the data of 26 climate stations, was above average, making it approximately the 13th-hottest year on record since 1951 (Fig. 7.30). A warming trend of 0.16°C decade^{-1} is indicated for the country, statistically significant at the 5% level.

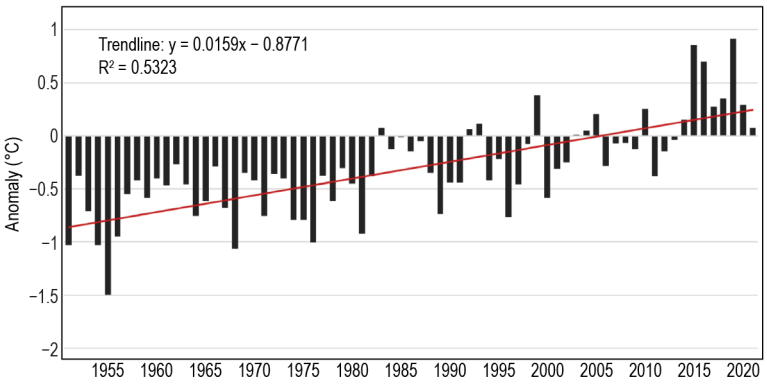

Fig. 7.30. Annual average surface temperature anomalies (°C; base period: 1991–2020) over South Africa based on 26 climate stations for the period 1951–2021. The linear trend is indicated by the red line. (Source: South African Weather Service.)

Annual maximum temperature (Tmax) averaged 20–34°C in the region. While Tmax ranged between 30° and 34°C in southern Angola, Namibia, southwestern Zambia, Botswana, western Zimbabwe, southern Malawi, and northern Mozambique, lower values averaging between 20° and 26°C were reported across much of South Africa, Lesotho, and Eswatini. Tmax was 0.5–1.5°C below normal over southern Angola, Namibia, southern Botswana, central South Africa, and Lesotho. Tmax was 0.5–1.5°C above normal farther north across northeastern Angola, Zambia, northern Zimbabwe, Malawi, and northern Mozambique.

Annual minimum temperature (Tmin) ranged from 4° to 24°C throughout the region, with values of less than 10°C in southern Namibia, South Africa, and Lesotho. Tmin was once again 0.5–2.5°C below normal over western portions of the region, including southern Angola, western Zambia, Namibia, and Botswana and near-normal elsewhere. Tmin ranked in the 3rd percentile over Namibia.

(ii) Precipitation

During 2021, annual rainfall was unevenly distributed across the region. While northern Angola and the eastern sector encompassing southern Malawi, Mozambique, Eswatini, and eastern South Africa had totals in excess of 800 mm, the central areas, including southern Angola, northeastern Namibia, Zambia, Botswana, central South Africa, Lesotho, and Zimbabwe received 400–800 mm. Limited accumulation of less than 400 mm was observed in the west across southwestern Angola, western Namibia, and northwestern South Africa (Fig. 7.31a).

Annual moisture deficits exceeded 250 mm across southern Angola, northern Namibia, Zambia, Malawi, and northern Mozambique, placing 2021 in the 3rd percentile in most areas. Annual rainfall was above normal over northern Angola, southwestern Botswana, central and northeastern South Africa, Eswatini, and southern Mozambique, with the largest surpluses of 150–200 mm over local areas in northern Angola and central South Africa (Fig. 7.31b).

An examination of the seasonal rainfall anomalies revealed an early onset of the rainfall season over eastern Angola and western Zambia in SON with departures 25 mm to 150 mm above the mean and ranking in the 90th percentile, while southwestern Angola and Mozambique experienced a slow start to the rainfall season. The peak of the rainfall season (DJF 2021/22) was extremely dry over southern Angola, Zambia, and northern Mozambique, with totals 150–250 mm below the mean and ranking in the lowest 3rd percentile. In contrast, eastern Namibia, Botswana, much of South Africa, Lesotho, Eswatini, Zimbabwe, and the southern two-thirds of Mozambique exhibited positive departures from the mean in the 50–350 mm range. Southern Mozambique had the highest moisture surpluses, up to +350 mm. Rainfall deficits (50–150 mm below the mean)

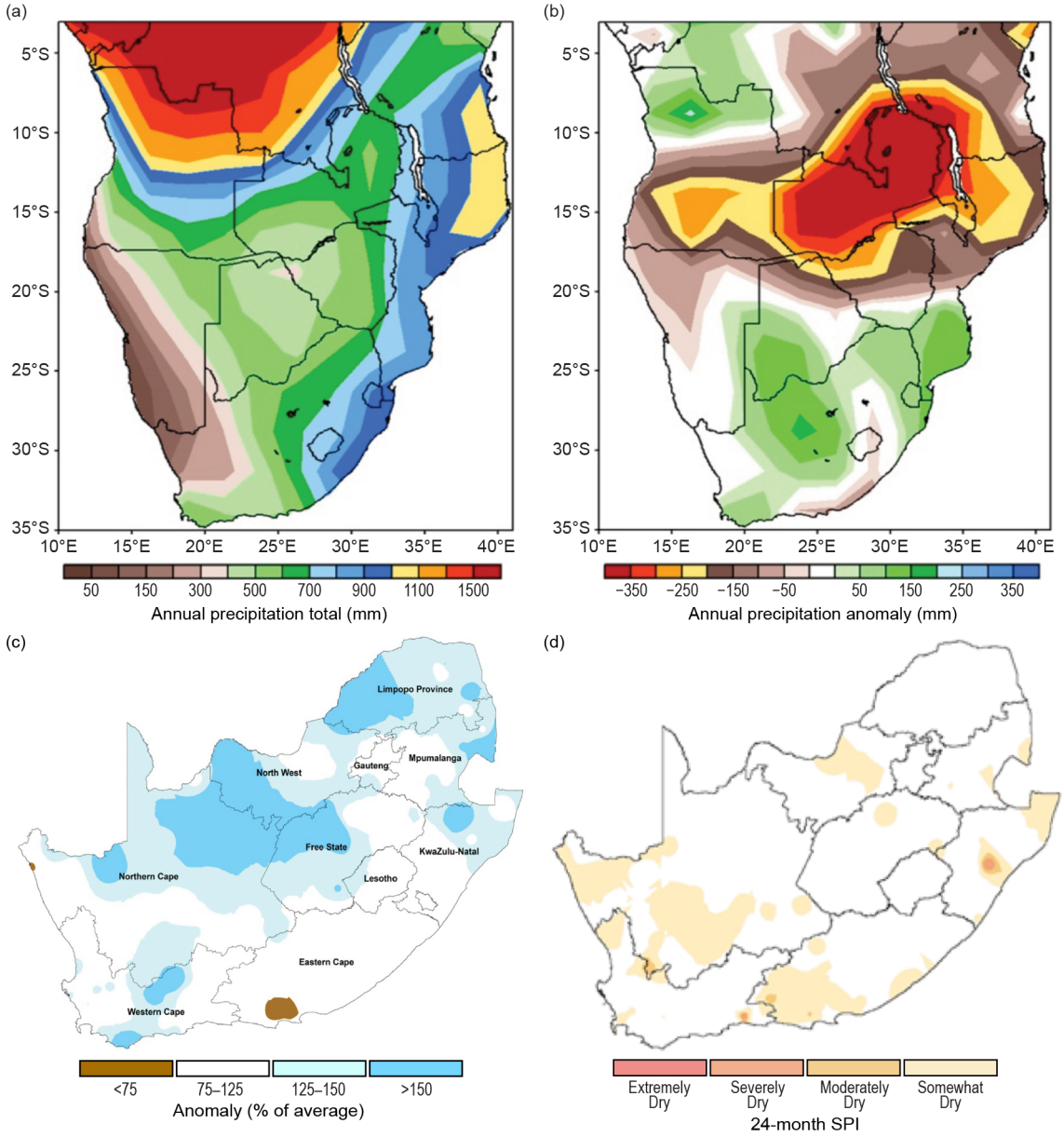

Fig. 7.31. Annual (a) rainfall totals and (b) rainfall anomaly (mm) for southern Africa. (c) Annual rainfall anomalies (% of average) for South Africa for 2021. (d) 24-month SPI map for South Africa ending December 2021. Base period for (a–c) is 1991–2020. (Sources: (a, b) GPCP via NOAA/NCEP and (c, d) South African Weather Service.)

prevailed toward the end of the rainfall season in MAM over much of the eastern sector from Zambia to eastern South Africa.

Figure 7.31c shows rainfall anomalies (expressed as percent of base period) for South Africa. The most significant feature of the rainfall during 2021 was the well-above normal rainfall received over extensive parts of South Africa. During 2021, ENSO was in a La Niña phase, which is associated with above-normal rainfall over most of the summer rainfall regions. The section of South Africa experiencing drought further decreased over the past year, due to the good rains in the early austral summer rainfall season of 2021/22, especially from November onwards. Figure 7.31d shows the 24-month SPI ending December 2021, which indicates that there were still some areas in the western and southern interior that could be considered somewhat dry, which shows persistence of the long-term drought this region has been experiencing (for almost a decade in some places).

The austral winter season (July–August) had unseasonal significant rainfall in the central and northwestern interior of South Africa, which persisted into spring. The early austral summer, starting in October, had well above-normal rainfall over especially the drought-stricken western interior, and spread to the south in November. In December, all of South Africa received above-normal rainfall. In many places, the monthly rainfall received were multiples of the normal rainfall totals. The early-summer rainfall season was, as a whole, characterized as above normal, except for some areas in the east and southeast of South Africa.

(iii) Notable events and impacts

Tropical Cyclone Eloise, with winds of around 140 km h^{-1} and gusts of up to 160 km h^{-1}, made landfall over the Sofala Province in Mozambique on 23 January and soaked several areas in the Sofala, Zambezia, Inhambane, and Manica provinces, with rainfall amounts up to 135 mm, according to the NOAA satellite rainfall estimates version 2 (RFE2). The resulting flooding affected 314,000 people, including 11 fatalities, according to United Nations Office for the Coordination of Humanitarian Affairs (OCHA). An estimated 600 classrooms and over 80 health centers needed repairs. In the aftermath of the storm, a low-pressure system brought heavy rains of about 135 mm during 14–15 February, according to the RFE2, and caused flooding over southern Mozambique, including the Maputo and Gaza provinces on 15 February. About 3000 homes were damaged or destroyed according to OCHA.

Extremely heavy rains of up to 105 mm drenched the Luanda area of Angola on 18–19 April, according the NOAA's CPC rainfall estimates by morphing technique (CMORPH), and triggered flash floods that affected more than 8000 people, including 14 reported fatalities and 12 injuries, and damaged over 1600 homes, according to the government of Angola.

In February northern parts of South Africa received substantial rain, but this was accompanied by much damage to infrastructure, mainly due to flash floods. In March, while it was hot in the eastern parts, with accompanying heat waves and record high temperatures, the Western Cape received high unseasonal rainfall, accompanied by flooding in places in the Cape Town metropole. The dry conditions in the western and southern interior were exacerbated in April with very low rainfall and abnormally high maximum temperatures. These conditions extended into May.

A winter storm brought extremely heavy rains (about 90 mm) over Cape Agulhas in the Western Cape Province of South Africa on 5 May and caused severe local flooding that damaged several homes and roads, and affected many people, according to local authorities in the province.

The high December rainfall totals were associated with a number of negative impacts. Of particular note, hundreds of families in Piet Retief, Mpumalanga, were left homeless after flash floods left a trail of damage and destruction on the 1st. The rain was accompanied by strong winds that blew roofs off houses and significant structural damages. Roads were also affected. At least two fatalities were reported on the 4th and 5th and at least two cars were swept away by floods on the 7th. Six people were killed and 44 injured after heavy rain affected Mthatha in the Eastern Cape

on the 9th. Seventy-seven families in the King Sabata Dalindyebo (KSD) Local Municipality lost their homes and 15 other families saw their houses collapse during heavy rain. Livestock were killed, and a preschool was damaged, along with power lines and other infrastructure.

6) WESTERN INDIAN OCEAN ISLAND COUNTRIES—G. Jumaux, K. R. Dhurmea, A. Abida, B. Andrade, M. Robjhon, and W. M. Thiaw

The Western Indian Ocean island countries consist of Madagascar, Seychelles, Comoros, Mayotte (France), Réunion (France), Mauritius, and Rodrigues (Mauritius). Overall, 2021 was warmer than normal (Fig. 7.32). Annual rainfall was below normal in Seychelles and Comoros and close to normal over the rest of the island countries (Fig. 7.32). There are two distinct main seasons: a warm and wet period spanning from November of the antecedent year to April, and a cold and dry season lasting from May to October.

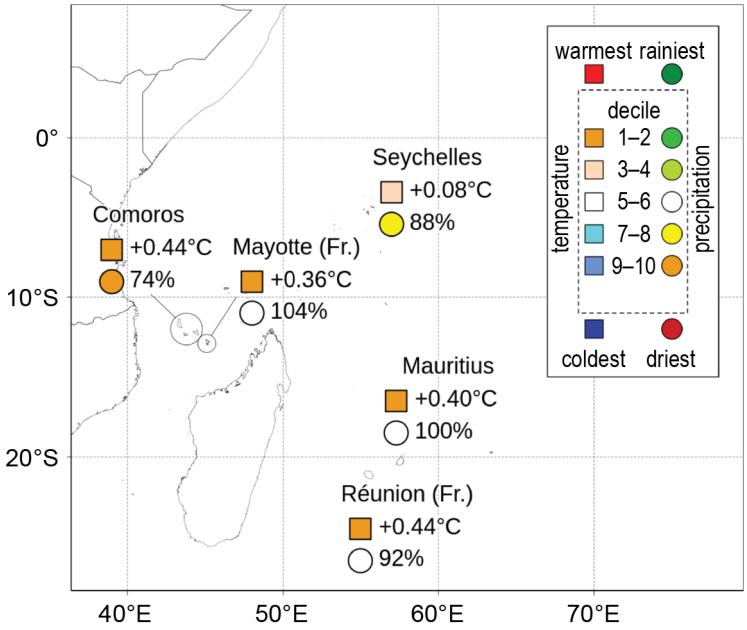

Fig. 7.32. Mean annual temperature anomalies (°C, squares), annual rainfall ratio to normal (%, circles), and their respective deciles for the western Indian Ocean island countries in 2021 (1991–2020 base period). (Sources: Météo France; and Meteorological Services of Mauritius, Seychelles, and Comoros.)

(i) Temperature

The annual mean temperature over Réunion Island (based on three stations) was 0.44°C above normal, the fifth highest since record keeping began in 1968 (Fig. 7.33). April and November, 0.9° and 0.8°C above normal respectively, were among the three warmest for their respective months. The annual minimum temperature anomaly was the second highest on record (+0.63°C), but 0.40°C below the record set in 2019. Maximum temperatures were near-normal during the cold season, but the annual average was still above normal (+0.26°C).

Over Mauritius, the annual mean temperatures (based on two stations at Vacoas and Plaisance) were above normal by 0.40°C, marking the eighth-warmest year since 1960. Both the maximum and minimum temperatures were above normal by 0.40°C. Mean temperatures were near-normal for most months (anomaly < +0.5°C), except for April, March, November, and December, where the anomaly exceeded +0.5°C. At Rodrigues, the mean temperature was near normal (+0.10°C). The maximum temperature was 0.30°C below normal, while the minimum was 0.50°C above normal.

In Comoros, the annual mean temperature for 2021 (based on four stations) was 27.1°C, which was 0.44°C above normal and the fourth-warmest year since 1991. The annual minimum

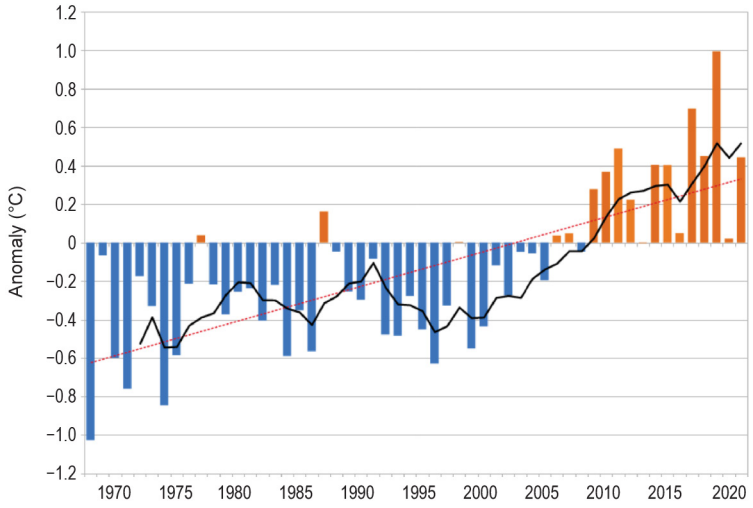

Fig. 7.33. Time series of Réunion Island annual mean temperature anomalies (°C; 1991–2020 base period) for the period 1968–2021. The black line is the 5-yr running mean and the red line represents the linear trend. (Source: Météo-France.)

temperature was 23.4°C, and the maximum temperature was 30.9°C. The absolute minimum temperature recorded was 17.4°C at Hahaya on 4 August. The absolute maximum temperature of 34.8°C was recorded at Hahaya on 28 December.

In Mayotte (Pamandzi Airport), the annual mean temperature was the seventh highest in the 61-year record, with at 27.41°C (0.36°C above normal). Five consecutive months from August to December were each among their five warmest on record.

At Seychelles International Airport, the annual mean temperature anomaly for 2021 was 0.08°C above normal, the 11th highest since 1972. Nearly all months were near-normal except March and October to December were above normal, and May was below normal.

Over Madagascar, annual mean temperatures averaged 20–26°C, with higher temperatures over the low-lying areas along the western and northern coasts and lower temperatures over the central highlands (Fig. 7.34a). Annual temperatures were slightly above normal with positive departures from the long-term mean ranging from +0.25° to +0.5°C across the western and central portions of the island (Fig. 7.34b). The annual mean temperature ranked between the 70th and 85th percentile over much of Madagascar, except for the mid-western sector, which had temperatures ranking in the 85th to 90th percentile.

An analysis of the temperatures throughout the year indicated that warmer-than-normal conditions dominated much of Madagascar during January–March and October–December when many areas experienced temperatures 1–2°C above normal, placing these months in the 90th to 97th percentiles. In contrast, the austral autumn season and latter part of the winter brought colder-than-normal conditions over the island.

On the seasonal time scale, DJF 2020/21 temperatures were well above normal throughout Madagascar, with the largest positive anomalies ranging from +1.25° to +1.5°C over the southern areas. March–May (MAM) brought changes with colder weather in the southern sector, near-normal conditions in the central areas, and elevated temperatures in the northeast. Warmer weather extended over central and northern Madagascar during September–November (SON) with the largest positive departures of +0.5° to +0.75°C observed in the Midwest.

Maximum temperatures (Tmax) ranged from 22° to 32°C over Madagascar with a steep east–west temperature gradient marked by values higher than 28°C in the west and lower than 26°C in the east. Tmax was 0.5–1°C above normal in the west-central and northwestern parts of the island. Tmin averaged 14–26°C over Madagascar and exceeded 20°C along the western and northern coasts and was above-normal across the northern two-thirds of the country, with departures from normal in the 0.25–0.75°C range. The largest positive anomalies (+0.5° to +0.75°C) were observed over western Madagascar ranked in the 90th to 97th percentiles.

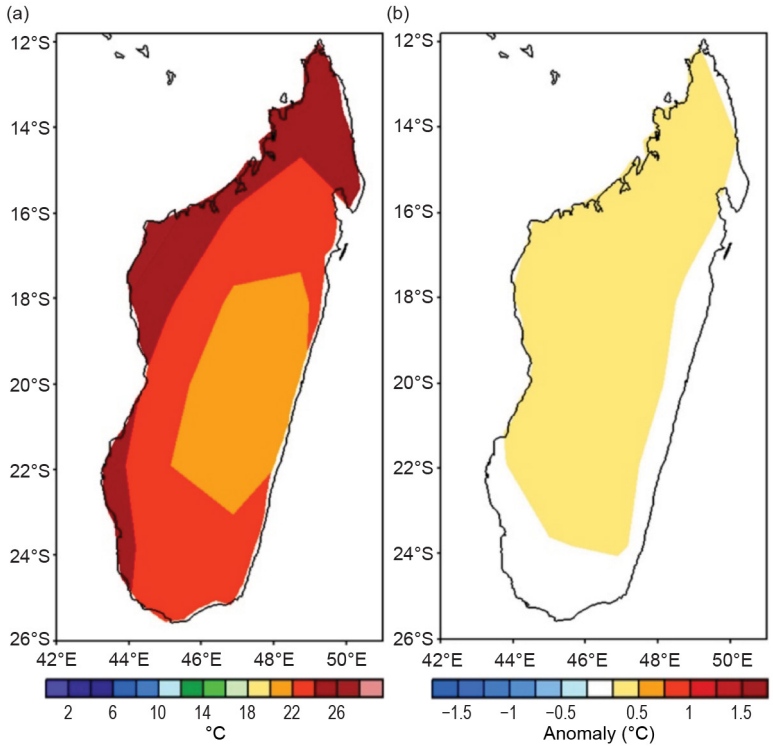

Fig. 7.34. Annual (a) mean temperature and (b) Annual mean temperature anomaly (°C; base period 1991–2020) for Madagascar. (Source: NOAA/NCEP.)

(ii) Precipitation

The annual rainfall total over Réunion Island was 92% of normal. Highlands and North Réunion Island experienced deficits during the rainy season (December–April), while the rainfall over East Réunion Island was close to normal. April was the wettest month of the year, reducing deficits just before the dry season (May–November) which was close to normal. April and August were among the wettest for their respective months over 50 years, at 220% and 200% of normal, respectively. Conversely, February and May were among the driest for their respective months, at 32% and 38% of normal. Remarkable rainfall intensities were recorded on the volcano and its southern flank (132 mm in 1 hour at La Crête station and 700 mm in 24 hours at Bellecombe-Jacob) on 28 August, which was quite unusual during the dry season.

In Mauritius, the mean annual rainfall total (based on 23 stations) was about 2025 mm, which was normal (average is 2018 mm); however, a marked seasonal variability was observed (Fig. 7.35a). The summer months January–March, which are the rain-bearing months, were all deficient in rainfall. February 2021 was the ninth driest on record and the driest in the last 19 years. November, another summer month, was the driest on record (since 1904), with only 11% of its normal rainfall recorded. Dry conditions prevailed until the first two weeks of April. The second half of April was exceptionally wet, recording most of the rainfall for the month with frequent floods and flash floods. Overall, April 2021 was the fifth wettest on record (since 1904) and the wettest in the last 19 years. A marked seasonal variability was observed at Rodrigues, with a wet winter and a dry summer. Most winter months had above-normal rainfall, except October. August was the wettest on record since 1954. All summer months had below-normal rainfall, except December, which was the third wettest in the last 35 years. March was the driest in the last 35 years and the second driest on record since 1954.

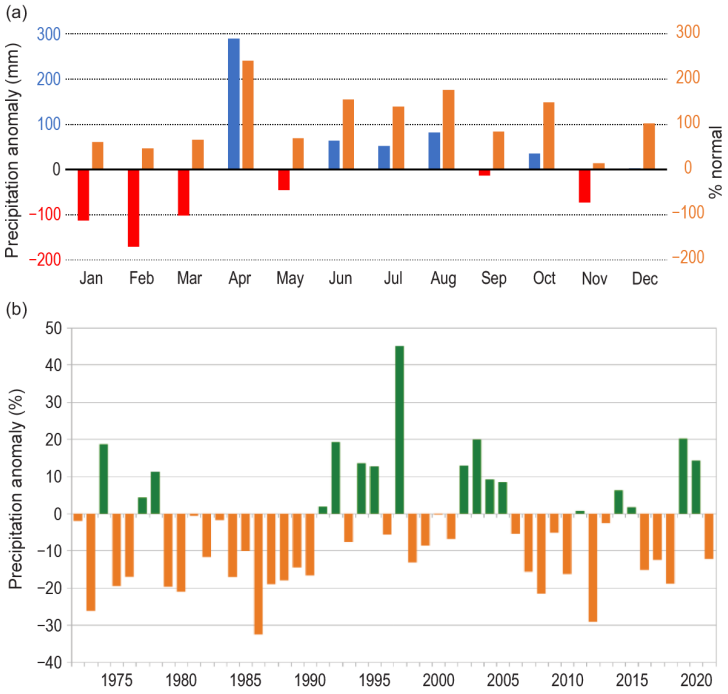

Fig. 7.35. (a) Monthly rainfall anomalies (mm; 1991–2020 base period) and percent of normal in Mauritius in 2021 (Source: Meteorological Services of Mauritius). (b) Annual rainfall anomaly time series (%; 1991–2020 base period) in Seychelles for the period 1972–2021. (Source: Seychelles Meteorological Authority.)

In Comoros, the total annual rainfall (average of three stations) was 1253 mm, which was 74% of normal and the fifth driest since 1991. The highest annual amount of rainfall compared to normal was recorded at the Moroni station at 112%. All months were below normal, except April and October.

In Mayotte, the total annual rainfall (average of two stations) was 1548 mm, which was 104% of normal. The total rainfall during the wet season was close to normal, but five consecutive months from May to September, during the dry season, were each below normal, leading to a 48% deficit in this period; this was the fifth driest such period in the 61-year record.

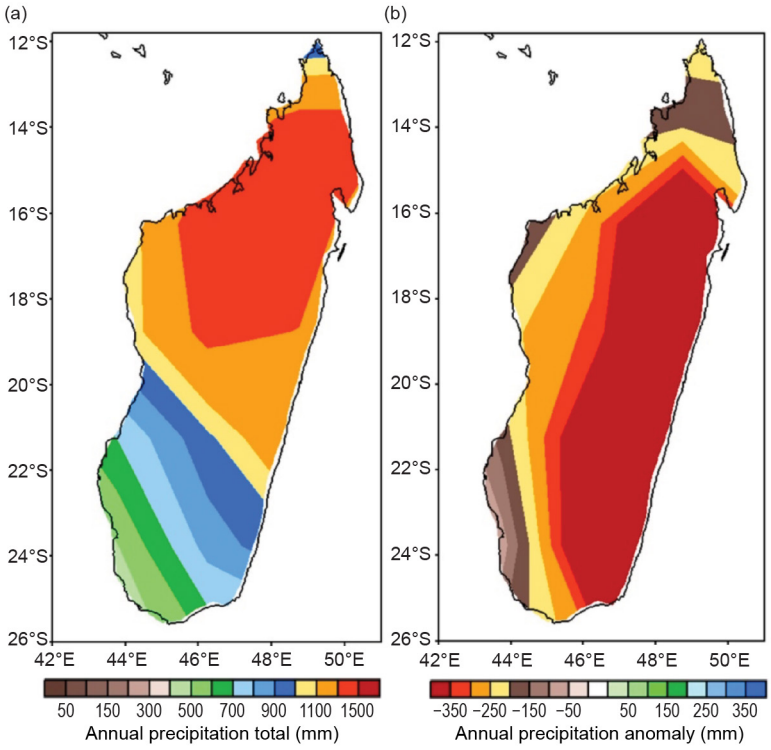

Fig. 7.36. Annual (a) rainfall total and (b) rainfall anomaly (mm; base period 1991–2020) for Madagascar. (Source: GPCP via NOAA/NCEP.)

In Seychelles, the total annual rainfall (2152 mm) was 88% of average, making 2021 the 20th-driest year on record since 1972 (Fig. 7.35b). Mainly related to the negative Indian Ocean dipole, all months between June and December had below-normal precipitation, except September.

In Madagascar, annual rainfall totals showed a north–south gradient, with a higher accumulation in excess of 1000 mm over the center and northern portions of the country and gradually decreasing amounts to about 400 mm in the southern areas (Fig. 7.36a). Annual rainfall was well below average, with departures varying from 50 mm to over 350 mm below the mean. The largest rainfall deficits surpassed 350 mm

over the eastern half of the interior of the island (Fig. 7.36b). The drier-than-normal conditions over central and eastern Madagascar placed 2021 among the top 3% driest over the past 30 years.

Examination of rainfall throughout the year indicated that drier-than-normal conditions persisted over Madagascar from January to May and October to December. The driest month was January, with deficits of 200–250 mm over eastern Madagascar.

Seasonal rainfall was well below average, with deficits between 25 and 350 mm across Madagascar during DJF 2020/21. The eastern half of the country was the driest region, with rainfall more than 100 mm below the mean, ranking in the 3rd percentile in coastal areas. The moisture deficits persisted and extended over the southern two-thirds of the island during MAM, while the northern and northeastern sectors registered rainfall surpluses. Rainfall deficits were observed over much of Madagascar during September–November, with the highest deficits of 50–150 mm, placing this season in the top 3% driest among such seasons.

(iii) Notable events and impacts

Tropical cyclones are the main natural hazard that can cause high impact flooding over the western Indian Ocean countries. With 12 named tropical storms and seven tropical cyclones, the November 2020–April 2021 tropical cyclone season was the fourth most active since 1998/99 (see section 4g6 for details).

Tropical storm Chalane, the first in the season made landfall in Fenoarivo Atsinanana in eastern Madagascar on 27 December 2020, causing flooding, infrastructure damage, and affected people in Toamasina, where rainfall accumulation totaled 351 mm during 26–27 December.

Tropical Cyclone Eloise made landfall as a tropical storm over Antalaha in northeastern Madagascar on 19 January, dumping 115 mm of rainfall, causing flooding with one fatality, destroying houses, and affecting ~1000 people in Antalaha, Maroantsetra, Vavatenina, and Toamasina, according to the United Nations Office for the Coordination of Humanitarian Affairs (UN OCHA). Eloise re-intensified into a tropical cyclone after crossing Madagascar and made landfall over central Mozambique four days later.

Extremely heavy rains (about 135 mm) fell during 11–17 February, triggering flooding and landslides, with one fatality reported and damaging many houses across several regions in central and western Madagascar, including the Alaotra Mangoro, Analamanga, Melaky, and Menabe. Nearly 1400 people were affected, according to the National Bureau of Risk and Disaster Management (BNGRC) in Madagascar.

The 2020/21 below-average rainfall season prolonged an unprecedented 6-year drought over southern and southwestern Madagascar, resulting in widespread food insecurity and malnutrition for over 1.14 million people over the Grand Sud, Great South, in Madagascar, according to the United Nations Fund for Population Activities.

f. Europe and the Middle East—P. Bissolli, Ed.

The region "Europe and the Middle East" in this context is defined by the so-called RA VI Region of WMO, which comprises 51 countries. The names of the countries are listed on the WMO website https://public.wmo.int/en/about-us/members. Throughout this section, 1991–2020 is the base period used for both temperature anomalies and precipitation percentages, unless otherwise specified. European countries conform to different standards applied by their individual national weather services. All seasons mentioned in this section refer to the Northern Hemisphere. More detailed information can be found in the *Monthly and Annual Bulletin on the Climate in RA VI – Europe and the Middle East*, provided by WMO RA VI Regional Climate Centre on Climate Monitoring (RCC-CM; http://www.dwd.de/rcc-cm). Anomaly information has been taken from Figs. 7.38–7.41 and aggregations of CLIMAT station data when national reports are not available. Appendix Table A7.1, at the end of this chapter, provides a list of included countries and the record lengths for both temperature and precipitation, along with their respective annual anomalies where available.

1) OVERVIEW

Based on the Global Historical Climate Network (GHCN) v4.0.1 dataset (Menne et al. 2018), Europe (36°–72°N, 23°W–60°E) experienced a slightly warmer-than-normal year with an anomaly of +0.2°C (Fig. 7.37) above the 1991–2020 average. This reflects the continuation of the long-term warming trend in Europe. Most of Europe had anomalies of close to normal, between −0.3°C and +0.5°C (Fig. 7.38). Only parts of southern Greece, most of Türkiye, west Kazakhstan, and Italy, and the Caucasus region were well above average with anomalies around +1.0°C. Türkiye reported its fourth-warmest year on record and west Kazakhstan its fifth warmest.

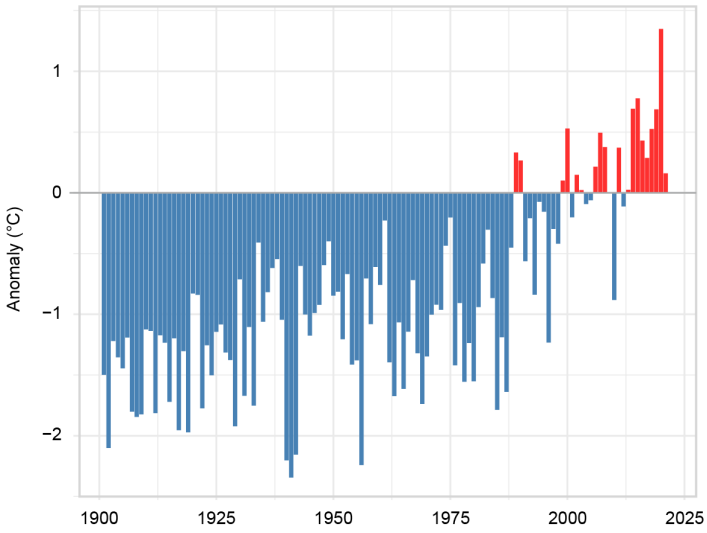

Fig. 7.37. Annual average land surface air temperature anomalies for the period 1900–2021 for Europe (36°–72°N, 10°W–60°E) relative to the 1991–2020 base period. (Source: GHCN version 4.0.1 dataset [Menne et al. 2018].)

Precipitation was also close to normal for many countries in Europe. For the southeastern part of Türkiye, the Middle East, west Kazakhstan, and areas around Caspian Sea, the year was characterized by a large precipitation deficit, as low as 40–60% of normal across wide regions (Fig. 7.39).

During winter 2020/21 (DJF), temperatures were above average or close to normal over most of the RA VI domain, except for European Russia, the United Kingdom, and Ireland (Fig. 7.40). Well-above-normal temperatures occurred over the southeast of RA VI and the western European Arctic with anomalies ranging from 1.0°C to 3.0°C above normal. The year started with a mild January (up to 4.0°C above normal) in southeastern Europe and the western European Arctic, and a generally colder January in Western Europe; a change of the prevailing atmospheric circulation with a significant weakening of the polar vortex took place in February, and a sharp air mass border developed over Europe with very cold air in the northern half and warm air in the southern half. Later, the cold air also moved to the southeast, which caused considerable variation in temperatures during February. Precipitation anomalies during winter (Fig. 7.41) were scattered; many parts of Europe were near normal, with local dry spots (as low as 40% of normal) in southern Spain, the west coast of Norway, the Baltic states, and the Middle East. Due to westerly weather conditions and cut-off lows, many parts of the Mediterranean and Eastern Europe, as well as south Caucasus received above normal precipitation—up to 160% of normal or more.

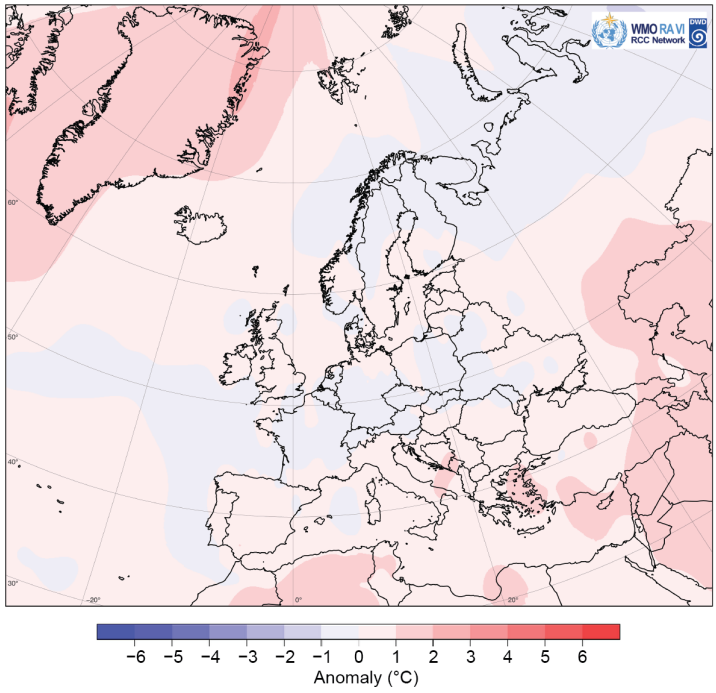

Fig. 7.38. Annual mean air temperature anomalies (°C; 1991–2020 base period) in 2021. (Source: interpolated climate station data over land and ship data over oceans; Deutscher Wetterdienst [DWD].) Since 1991–2020 normals were still not available for all stations, the 1991–2020 anomalies were computed from gridded 1981–2010 anomalies as a preliminary solution.

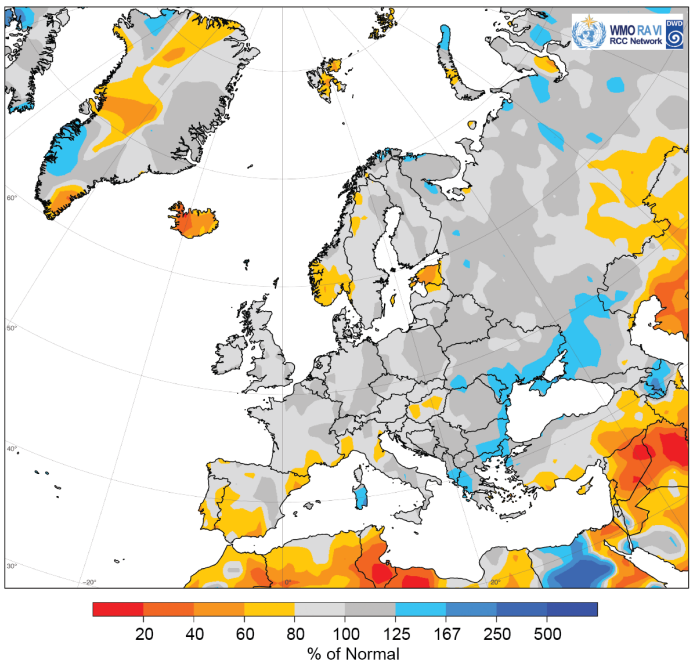

Fig. 7.39. European precipitation totals (% of 1991–2020 average) for 2021. Please note that data over Iceland should be interpreted with caution because it appears to be low compared with recent national data from the Icelandic Meteorological Service, which are not yet included in this analysis. A data check has been in progress at the time of publication of this report. Annual precipitation totals in Iceland were about 85–100% of normal in 2021. (Source: GPCC, created by DWD.)

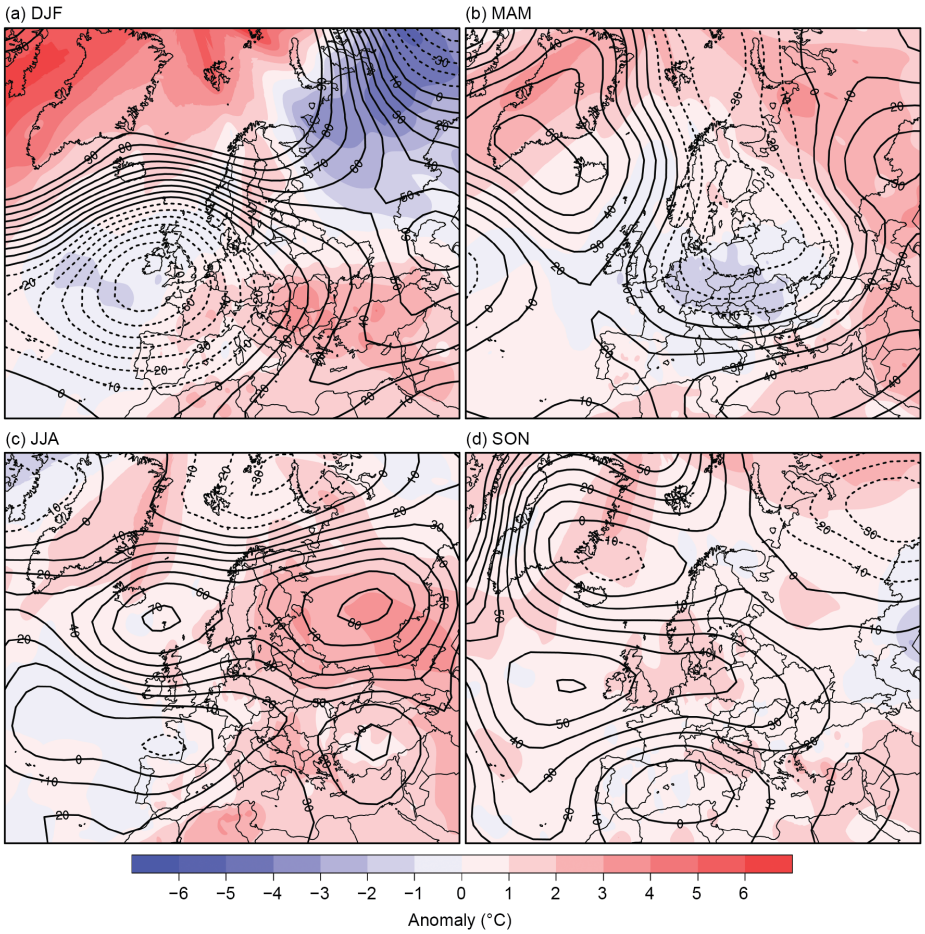

Fig. 7.40. Seasonal anomalies (1991–2020 base period) of 500-hPa geopotential height (contour; m) and surface air temperature (shading; °C) using data from the NCEP/NCAR reanalysis and DWD, respectively, for (a) DJF 2020/21, (b) MAM 2021, (c) JJA 2021, and (d) SON 2021.

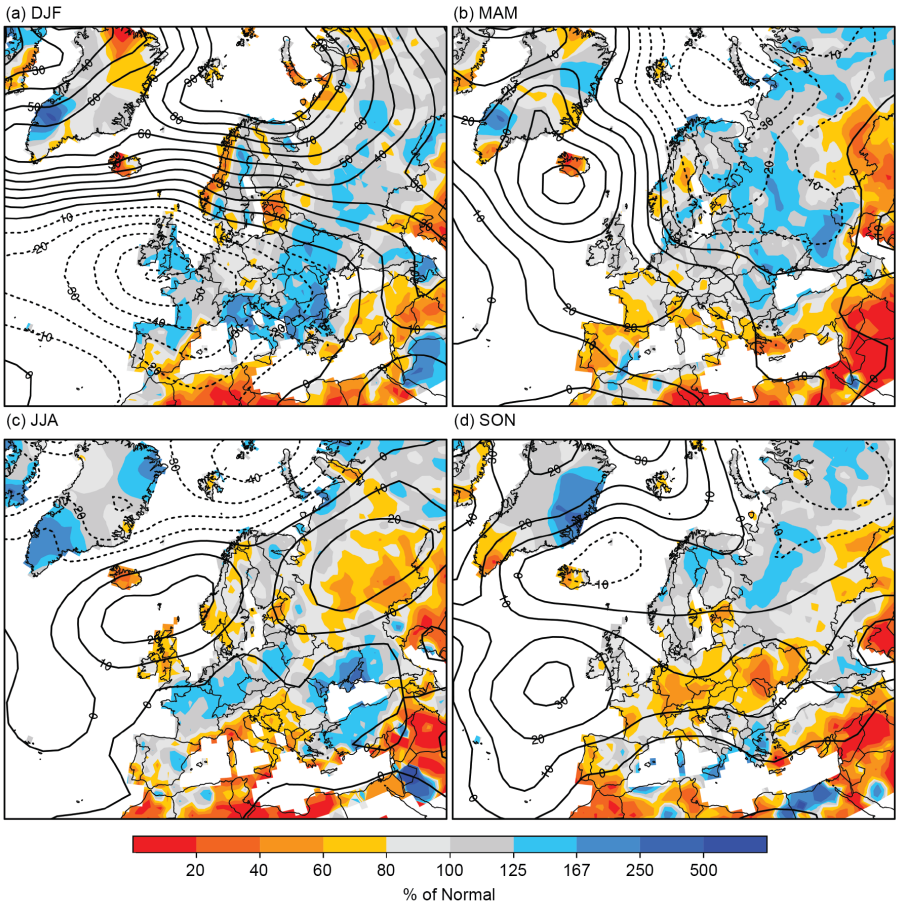

Fig. 7.41. Seasonal anomalies for 2021 (1991–2020 base period) of sea level pressure (hPa) from NCAR/NCEP reanalysis (contours) for (a) DJF 2020/21, (b) MAM 2021, (c) JJA 2021, and (d) SON 2021. Colored shading represents the percentage of seasonal mean precipitation for 2021 compared with the 1991–2020 mean from GPCC (Schneider et al. 2018). Please note that data over Iceland should be interpreted with caution because it appears to be low compared with recent national data from the Icelandic Meteorological Service, which are not yet included in this analysis. A data check has been in progress at the time of publication of this report.

Spring was dominated by below-normal air temperatures across most European areas, with anomalies exceeding –2.0°C or –3.0°C in Western and Central Europe. A strong area of high pressure was present over the North Atlantic and Greenland, and winds became more northerly than usual over northwestern Europe, bringing a persistent flow of cold polar air down to most of the continent, while also keeping the western part of Europe mostly dry. Spain, Portugal, Italy, and Greece received precipitation mostly around 60% of normal, while the Middle East had much higher precipitation deficits, as less than 20% of the normal rain fell in some areas. The situation was reversed northeast over western European Russia and Scandinavia, with southerly winds bringing warm air to the region. In May, low pressures and associated frontal weather systems prevailed over northwestern Europe, bringing much wetter conditions. Farther east, western European Russia saw a similar pressure pattern at the beginning of May, with strong and warm southerly winds bringing record warmth to the region (4.8°C above average), including to the fringes of the Arctic and west Kazakhstan.

Due to extended high-pressure influence, summer 2021 was the second-warmest summer on record (after 2010) for the RA VI region (+0.7°C anomaly) and for a number of countries, including Latvia (+2.6°C), Greece (+1.6°C), and Malta (+2.0°C). June was the second-warmest June on record for the RA VI region at 1.5°C above normal; particularly high anomalies were observed in Finland (+3.7°C) and western European Russia. The hottest temperatures were observed at the end of the season over the Mediterranean, the Balkan Peninsula, and Türkiye, exceeding 40°C

at times. During this hot spell, a new (provisional) European maximum temperature record was set in Sicily, Italy, where temperatures reached 48.8°C due to anticyclonic weather conditions. Characteristically for the blocking high pressure situation over Europe, summer in Italy and the Balkan states was dry, with precipitation totals as low as 60–80% of normal, while parts of Central Europe, Western Europe and Eastern Europe recorded close to normal or precipitation totals up to 167% of normal (locally even more) mainly due to higher low-pressure influence than usual and enhanced convective activity.

Autumn was warmer than average for most European countries, especially in the United Kingdom, Ireland, Denmark, and Mediterranean regions, where temperature anomalies exceeded +1.0°C (Fig. 7.40). In the Middle East, temperature anomalies also reached +1.0°C, while South Caucasus and West Kazakhstan reported a colder-than-normal autumn. Autumn precipitation was slightly below normal for Western Europe, parts of Scandinavia, and most of the Mediterranean countries, with local wet spots. Central Europe and the Iberian Peninsula received precipitation of around 60% of normal. Ukraine, Moldova, Türkiye, and the Middle East, where high-pressure influence was strong, were even drier for the season, with precipitation mostly 20–60% of normal.

December 2021 was again a warm month across most of Europe, except for Scandinavia and the Baltic Countries and northern Russia. It was wetter than normal during the month across much of Eastern Europe and the Balkan countries, but very dry for the season in eastern Iberia, Scandinavia, and the Middle East.

2) WESTERN EUROPE

This region includes Ireland (1981–2010 base period), the United Kingdom (1981–2010), Belgium, the Netherlands, Luxembourg, and France (1981–2010).

(i) Temperature

Ireland and France reported a slightly warmer year than normal, with anomalies of +0.5°C and +0.4°C, respectively, while it was slightly colder than normal for Belgium (–0.4°C) and Luxembourg (–0.4°C). A near-normal year was reported from the Netherlands and United Kingdom.

Except for the United Kingdom and Ireland (–0.2°C anomaly), all western European countries reported a warmer winter season than normal (France: +1.2°C, Belgium: +0.6°C, Luxembourg: +1.0°C, Netherlands: +0.5°C).

Spring started with near-average temperatures, but became cooler than average in April and May. Monthly temperature anomalies in April were around –3.0°C in Belgium, the Netherlands, and Luxembourg, setting new April records. Belgium had its coldest April since 1986 and its eighth coolest overall. The United Kingdom reported its coldest May since 1989 with an anomaly of –1.3°C, while Luxembourg reported its coolest spring since 2013, with an anomaly of –2.1°C.

At the beginning of summer, rapid warming occurred across Western Europe, where temperatures 2.0°C above normal were reported. The Netherlands had its warmest June on record (+2.0°C anomaly), France its fifth warmest (+2.0°C), and Belgium its third warmest (+1.9°C). July was the fifth warmest for the United Kingdom since the start of its record in 1884, at 1.5°C above normal.

Warm conditions continued across the region into autumn. September was warmer than normal for all countries: second warmest on record for the United Kingdom (+2.1°C anomaly) and third warmest for France in the past 50 years (+2.0°C). The seasonal mean was reduced, however, by a cool November. Overall, autumn ended with temperature anomalies of +0.3°C for Belgium, +0.4°C for France, +0.7°C for the Netherlands, –0.1°C for Luxembourg, +1.45°C for Ireland, and + 1.4°C for the United Kingdom. December 2021 was mild across the western European countries, with temperatures around +1.0°C above normal.

(ii) Precipitation

Annual precipitation totals were close to normal in the region, except for Belgium, which reported its third wettest year since 1991 (124% of normal).

The winter season was slightly wetter than normal for all countries, with 102–124% of normal precipitation. Only southeastern France received slightly below-normal precipitation. January was wetter than normal, with up to 140% of normal precipitation in France and 133% of normal in the United Kingdom.

Spring was near-normal in most places, except for France (80% of normal). Summer brought strong and persistent rainfall to France, Belgium, Luxembourg, and the Netherlands. Ireland and the United Kingdom reported below-average summer precipitation of around 75% of normal. In July, moist air flowed into Western Europe. Following extremely heavy precipitation, several severe weather events with flooding were reported from France, Belgium, Luxembourg, and the Netherlands. Belgium registered its highest July precipitation since 1991 (216% of normal), France reported its third-wettest July since 1955 (150% of normal), and Luxembourg reported its second-wettest July (264% of normal). In southern France, dry conditions set in with August, and the country received 60% of its normal precipitation for the month, marking its sixth-driest August on record.

This situation persisted into autumn; dry conditions extended into the Benelux countries, with precipitation totals between 52% and 86% of normal. Ireland and the United Kingdom each reported a slightly drier autumn than normal, with 86% and 96% of normal precipitation, respectively.

(iii) Notable events and impacts

During 18–21 January, Storm Christoph passed over northwestern Europe; minimum pressure fell to 950 hPa and wind gusts up to 190 km h^{-1} were recorded on exposed locations in the United Kingdom. Three-day precipitation totals reached 50% of the average January monthly rainfall in some areas, leading to record high river levels and flooding. This caused damage to bridges, roads, and power lines. On 21 January, the Dee River in North Wales reached its highest water level on record since the water gauge was installed in 1996. Approximately 2300 homes were evacuated. Following this storm, the United Kingdom experienced a rare thundersnow event, receiving up to 17 cm fresh snow on 24 January. Roads were closed and vehicles stranded.

During February, several Atlantic low-pressure systems brought heavy precipitation to France, the United Kingdom, and the Netherlands, leading to extensive traffic disruptions. Since soil was already saturated by rainfall, brought by Storm Christoph, the heavy rain in early February caused near-record river levels and widespread flooding. Southwestern France reported flooding, landslides, blocked roads, and damage to roads, bridges, and houses. During 12–13 February, cold air from the east caused extreme freezing rain in all of northern France. Ice layers reached a thickness up to 1 cm, making roads impassable for several hours.

On 31 March, Western Europe experienced unusually high maximum temperatures. France, Belgium, the Netherlands, and Luxembourg recorded local national record daily maximum temperatures around 25–30°C.

Conversely, during 6–8 April, many local cold records were set in France and Belgium as cold air flowed in from the North Sea due to a low-pressure area with central pressure 963.7 hPa in Överkalix-Svartbyn in northern Sweden. In southern France, frost caused considerable damage to agriculture.

During June, intense thunderstorms were observed across Belgium, the Netherlands, Luxembourg, the United Kingdom, and France. Heavy rain, tornados, tennis ball-sized hail, strong wind, and frequent lightning led to local flooding, roads blockages, and damage to agriculture and infrastructure.

From 12 to 15 July, Storm Bernd brought exceptionally high precipitation, leading to flooding, heavy damage to property, and casualties in the Netherlands, Belgium, Luxembourg, and France.

On 14–15 July, a total of more than 150 mm rain was measured in Limburg (southern Netherlands), which is more than double its normal precipitation total for July. Several stations in the provinces of Namur and Liège (southeastern Belgium) measured up to 271.5 mm rainfall in 48 hours. Liège City was completely flooded after the water level of the Meuse River rose. Approximately 2000 people were displaced, and at least 36 were killed. At the end of July, the Netherlands, Luxembourg, and the United Kingdom also experienced significant flooding.

During a heat wave in mid-August in southern France, local monthly record temperatures were set at multiple stations; for example, Valensole (located on a high plain in the Provence region in southern France) reported a maximum temperature of 37.5°C and La Chippa in Corsica reported 40.7°C.

During 2–3 October, northwestern France experienced extreme precipitation and strong winds. In the city of Nantes, a new daily record was set with a 24-hour total rainfall above 100 mm. Wind gusts up to 126 km h^{-1} caused power outages and blocked rail traffic.

At the end of December, above-normal temperatures were reported due to a high-pressure area in Western Europe. Local temperature records for December were set in Nimes (20.9°C) on 29 December and Marseille-Marignane (20.7°C) on 30 December in France.

3) CENTRAL EUROPE

This region includes Germany, Switzerland, Liechtenstein, Austria, Poland, Czechia, Slovakia (1981–2010), and Hungary.

(i) Temperature

Overall, Central Europe was around normal, with annual temperature anomalies ranging from −0.1°C to +0.4°C in 2021.

Winter 2020/21 was mostly mild. Switzerland reported a winter that ranked among its 10 warmest in some places (e.g., Geneva and Berne), at 0.5°C above normal on national average, while Slovakia reported an anomaly of +2.1°C. In February, several Atlantic low-pressure systems followed increasingly southerly tracks and brought warm air masses to southern parts of Central Europe, leading to temperature departures of +1.9°C in Austria, +2.1°C in Hungary, and +2.8°C in Switzerland. With Germany and Poland still under the influence of cold arctic air at the beginning of the month, their overall February temperatures were close to normal.

During spring, temperature anomalies were more than –1.0°C across the entire region. Switzerland reported its coolest spring in more than 30 years, at 1.6°C below normal. Hungary, Slovakia, Czechia, and Germany reported spring temperature departures ranging from –2.1°C to –1.7°C, while Poland and Austria observed departures near –1.0°C.

Summer was warmer than normal, with anomalies of +0.4°C to +2.0°C. Poland reported its fourth-warmest summer on record, at 1.0°C above normal. June was the warmest month of the season. Austria reported its third-warmest June since 1767, Poland its second warmest (+2.5°C), and Hungary reported its third-warmest June since 1901, with an anomaly of +2.2°C, and its warmest July, with an anomaly of +2.3°C. August was colder than normal everywhere, with anomalies ranging from –0.7°C to –1.6°C; Austria reported its coldest August since 2014 at 1.3°C below normal.

With a high-pressure system in place over Central Europe, autumn began with a warm September: anomalies of +1.7°C in Switzerland and +1.3°C in Austria, Germany, and Czechia. October was slightly colder than usual in the southern countries of the region, with anomalies between −0.5°C and –1.3°C, while Germany and Poland were slightly warmer than normal. The season ended with temperatures near-normal in November, but again warmer in the north and colder in the south. Overall, autumn was near-normal for many countries in Central Europe.

(ii) Precipitation

Precipitation was close to normal (90–116%) in the region for the year.

January was wetter than normal, with multiple storms passing over Europe; Switzerland and Germany received 202% and 130% of their normal precipitation, respectively. Austria reported 166% of normal, with the western part of the country measuring record high precipitation (Bregenz received as much as 500% of normal) and the northeastern part near-normal. In February, most countries reported near-normal precipitation, except Slovakia, which reported a slightly wetter February (130% of normal), and Austria and Switzerland reported a drier February (65% and 72% of normal, respectively). Overall, winter 2020/21 was near-normal for Czechia, Hungary, Poland, and Germany, while Austria, Switzerland, and Slovakia reported a slightly wetter winter season, up to 130% of normal.

During March, below-average precipitation was observed across much of Central Europe. Hungary reported a dry month, with 35% of its normal precipitation (locally even less than 10%). Austria and Slovakia also reported less than 50% of their normal precipitation. The season ended with a wetter-than-normal May, due to a trough over Central Europe. Czechia, Germany, Switzerland, Poland, and Slovakia received up to 140% of their normal precipitation, and Hungary and Austria received up to 120%. On average, spring precipitation was slightly below normal for many countries in the region.

Summer started with a drier-than-average June across many parts of Hungary, Slovakia, Poland, and Austria, while Germany received up to 130% of its normal precipitation. Switzerland received 108% of its normal June precipitation; however, there was a sharp contrast between northern and southern Switzerland, at 152% and 28% of average, respectfully. Precipitation did not exceed 40% of normal anywhere in Hungary, Austria, or Slovakia. Hungary reported 21% of its normal precipitation on average, making it the second-driest June since 1917. In July, due to multiple low-pressure systems bringing heavy convective precipitation to the region, Germany, Austria, Czechia, and Poland received up to 120% of their normal rainfall on average. Switzerland received 195% of its normal precipitation, which resulted in its wettest July on record since 1864. Wet conditions continued into August; Poland received up to 173% of normal precipitation, making this its second-wettest August in history. Overall, summer was wetter than normal for all countries, except Hungary (65% of normal).

The wet summer was followed by a drier-than-normal (widespread 58–70% of normal) autumn for most of Central Europe. In particular, September and October were very dry across Germany and the southeast of the region. Austria reported its driest September since 1975, with 52% of its normal precipitation. Czechia reported just 38% and 39% of its normal precipitation in September and October, respectively. Similarly, Slovakia reported just 38% of its normal precipitation in October.

(iii) Notable events and impacts

During 9–14 February, an extreme cold spell with snowstorms was reported in Germany, Switzerland, Austria, and Czechia. New monthly local records were set in central Germany (Thuringia region), with temperatures as low as –26.7°C. New all-time snow depth records were measured at several lowland stations in Germany, with snow depths of 60–70 cm, on 8–9 February. Southwesterly winds brought warm air to several parts of Central Europe, which caused considerable variation in temperatures. A new record February maximum temperature of 21.9°C was reached in Vaduz (Liechtenstein). On 26 February, several new high daily maximum temperatures for February were set at multiple stations: 22.1°C in Maków Podhalański (Poland), 20.8°C in Hurbanovo (Slovakia), and a new national February record of 22.4°C was set in Kiskunfélegyháza (Hungary). Additionally, a record-breaking temperature rise of 41.9°C within one week was reported in Göttingen (northern Germany), from –23.8°C on 14 February to 18.1°C on 21 February.

The ongoing warm airflow from the southwest caused record high temperatures in late March. On 31 March, a new national March record of 27.7°C in Rheinau-Memprechtshofen was set in Germany.

During 19–22 June, Switzerland and Germany experienced thunderstorms accompanied by sometimes heavy precipitation and exceptionally large hail events. Station Wädenswil in Switzerland received a 24-hour daily precipitation total of 62.6 mm. Station Root in Luzern County (Switzerland) reported 36.5 mm in 10 minutes. An F4 tornado struck several villages in southern Moravia (Czechia) on 24 June, with major damage and six deaths reported. This was the strongest tornado on record in the Czech Republic.

While a wet summer helped to replenish water resources after the preceding relatively dry years in many parts of Central Europe, Hungary continued to be affected by water scarcity in soils. The top 50 cm of soil dried out and soil moisture fell below the critical 40% level across almost the whole country due to the long-lasting drought situation.

Between 12 and 15 July, Storm Bernd (same as noted for Western Europe) brought heavy rainfall to Central Europe, which led to extreme flooding, particularly in western Germany where several towns were completely flooded. Water levels in rivers far exceeded historical records, locally 7–8 m above normal. The flooding caused heavy damage to property and infrastructure. Additionally, 179 people were killed in Germany, which was one of the deadliest weather events on record for the country. Several districts in western Germany declared a state of emergency, and hundreds of troops from the German army were deployed to help. Local precipitation records were exceeded in many places. More than double of the monthly normal rainfall was received within a few hours or days over entire river catchment areas.

In August, a new national daily wind gust record was set for Austria. The Tiszavasvar station in northeastern Hungary measured 121 km h^{-1}, the highest wind gust in a series dating from 1977. During 20 and 21 October, Storm Aurore brought severe weather to Central Europe, including wind gusts that surpassed 150 km h^{-1}.

4) THE NORDIC AND BALTIC COUNTRIES

This section includes Iceland, Norway, Denmark, Sweden, Finland, Estonia, Latvia, and Lithuania.

(i) Temperature

Temperatures across the Nordic and Baltic region in 2021 were mostly close to normal, with anomalies ranging from −0.4°C to +0.9°C.

Winter 2020/21 was near-normal, with anomalies between +1.1°C in Finland and −0.7°C in Norway. Temperatures varied considerably during February due to a change in the prevailing atmospheric circulation pattern mid-month. Sweden observed a new national February record for daily maximum temperature, but nevertheless monthly average temperatures for February were below normal across almost the entire country, similar to the other Nordic and Baltic Countries, with –3.2°C in Lithuania, –2.0°C in Norway, and –1.4°C in Denmark.

Spring was slightly warmer than normal, with anomalies up to +1.0°C in the Fenno-Scandinavian countries, while Denmark, Iceland, and the Baltic countries reported near- to slightly below-normal temperatures for the season.

In June, the northeastern part of the region experienced a heat wave that led to several record and near-record monthly anomalies in Estonia (+4.0°C, highest since 1961), Latvia (+3.6°C, highest since 1924), Finland (+ 3.7°C, highest since 1900), Lithuania (second highest since 1961), and Sweden (+3.4°C, second highest since 1860). Norway was also affected, with an anomaly of +2.3°C. July followed as the warmest on record for Latvia (+3.7°C) and Lithuania (+3.8°C), which resulted in the warmest summer on record for Latvia, with an average anomaly of +2.1°C, and second warmest summer for Finland, at +1.8°C. The summer season ended with temperatures slightly

below normal for August, ranging from near-normal to 1.2°C below normal in Denmark. Summer as a whole was the warmest on record at several locations in northeastern Iceland.

During autumn, temperatures were slightly above normal (around +1°C anomaly) in all Nordic and Baltic countries. Denmark reported its fifth-warmest autumn.

With temperature anomalies of –3.3°C in Estonia, –3.0°C in Latvia, –1.8°C in Norway, –3.6°C in Finland, and –2.2°C in Lithuania in December, 2021 ended rather cold in the region.

(ii) Precipitation

Annual total precipitation was mostly near-normal across the region, with considerable short-term variability. Winter 2020/21 brought a deficit of precipitation to most of the Nordic and Baltic countries, except Sweden where precipitation was near-normal on average, but distributed inhomogeneously. Due to a blocking high-pressure area expanding from Central Europe in February, especially dry conditions prevailed over southern Sweden and the Baltic countries. Latvia received less than 30% of its normal precipitation, resulting in its fifth-driest February in the record dating to 1924.

Dry conditions continued into spring. Sweden and the Baltic states reported a drier-than-normal March and April, while the season ended wetter than normal for most of the Nordic countries. In May, Latvia and Estonia each received nearly double their normal precipitation, while the national average in Finland, Sweden, and Denmark was around 125% of normal. For the other countries in the region, May was drier than normal.

During summer, overall precipitation was near to slightly below normal for all countries of the region, except Estonia and Iceland where the dry spring continued into summer. August was wetter than normal in Finland, Estonia, and Sweden, with around 150% of normal precipitation or higher. Denmark, Norway, and Iceland each reported a drier-than-normal August, though with high spatial variability of anomalies.

For autumn, Denmark and the Baltic states reported 90–95% of their normal precipitation while Fenno-Scandinavian countries received around 110% of normal. October was the third wettest for Finland, with 166% of its normal precipitation.

In December 2021, precipitation was below normal for all of the Nordic and Baltic States.

(iii) Notable events and impacts

In early February, cold arctic air moved into northern Europe. On 12 February, Denmark's coldest night in nine years was reported: –20.7°C in Horsens, on the eastern coast of Denmark. At the end of February warm air moved from southern to northern Europe, with new February records set in Sweden and Denmark. The station at Kalmar in southern Sweden reported a new national February record of 17.0°C. In Denmark, the temperature rose by 35.7°C in 11 days: from –20.7°C to 15.0°C on 22 February in Jyndevad. On 29 March, a new local record of 19.7°C was set at station Harstena (southeastern Sweden) where measurement started in 1942.

During 5–6 April, extreme snowfall was observed in Norway, with an April record of 25–41 cm of fresh snow in 24 hours (measurements commenced in 1896).

In June, Scandinavia and the Baltic countries experienced a heat wave, with high temperatures exceeding 30°C and reported tropical nights. Finland recorded the hot-weather threshold of 25°C on 25 days somewhere in Finland. Tampere (southern Finland) reported its highest temperature on record (33.2°C) on 22 June. New national June maximum records were also set for Estonia (34.6°C) and Latvia with a high minimum nighttime temperature (23.7°C), both on 23 June. The warmth continued in July; Liepaja in Latvia observed a new local record of 30.4°C on 2 July. Stations in northern Sweden, Norway, and Finland measured new local records above 30°C. Temperatures in northeastern Europe were high in the following 11 days. In Lithuania, temperatures above 30°C for more than 11 days had not been measured since 1961.

Later in summer, unusual warmth also reached Iceland. On 24 August, a station in Hallormsstadur (eastern Iceland) measured 29.4°C, which was the highest temperature ever recorded in August.

Temperatures remained high in autumn. On 8 September, Drammen (Norway) reached 28.6°C, 0.1°C above the previous September national record that was first set in 1906 in Austad, and later equaled in Meråker in 1958 and Drammen in 1991. On 4 October, a temperature of 16.2°C was measured in Abisko in northern Sweden, which was the highest October temperature in the station's history for more than 100 years.

During 18–19 November, Denmark observed a nighttime minimum temperature of 10°C, the highest night temperature ever recorded in the country that late in the year.

5) IBERIAN PENINSULA

This region includes Spain (1981–2010 base period), Portugal (1971–2000), and Andorra.

(i) Temperature

Spain and Portugal reported annual temperatures 0.5°C and 0.4°C above normal, respectively. Winter 2020/21 was slightly warmer than normal but with variations between months. While, January was cold overall, with an average temperature of 0.6°C below normal in Spain and 0.8°C below normal in Portugal, the season ended with a very warm February, the third warmest for Spain (2.5°C above normal) and fifth warmest for Portugal (1.7°C above normal).

Spring also was warmer than normal, as anomalies were up to +0.4°C for Spain and +1.0°C for Portugal. The season began with temperatures near-normal for March in Spain, while Portugal reported an anomaly of +0.7°C. While April was also normal in Spain, Portugal reported an anomaly of +1.9°C. May concluded the season with slightly above-normal temperatures on the Iberian Peninsula.

Summer was normal for both Spain and Portugal. During August, temperatures were above normal, but only Spain reported monthly anomalies close to +1.0°C, which marked its ninth-warmest August.

Autumn was also near-normal but with variation between months. October was warmer than average, with temperatures 1.0°C above normal in Spain and 1.5°C above normal in Portugal, while November was colder than average, with anomalies of –1.2°C for both countries.

The year ended with a warmer than normal December. Spain reported an anomaly of +1.9°C, while Portugal reported +1.7°C above normal, making this its fourth-warmest December on record.

(ii) Precipitation

Annual precipitation totals in Portugal and Spain were near-normal, with small deficits in the southern Andalusian region and in northeastern Spain. The main rainfalls occurred in winter, while autumn precipitation was below normal. Summer is climatologically a dry season anyway and spring was extremely dry.

February brought abundant rainfall but mainly in the northwest of the Peninsula where the mean precipitation was around 160% of normal in Portugal (third highest since 2000).

Spring set in with a strong precipitation deficit for the region, at 62% and 67% of normal for Portugal and Spain, respectively. This marked the fourth-driest spring on record for Spain.

Summer precipitation was near-normal for Spain (101% of normal) and below normal for Portugal (64%), with variations between months. Overall, June was wetter than normal, and July and August were drier than normal. Portugal received only 28% of its normal precipitation for the month, making it the fifth-driest August since 2000.

While autumn started with above-normal precipitation in September—160% of normal for Portugal and 133% for Spain—the season concluded with below-normal rainfall across most of

the region, except for northeastern Spain. Portugal reported its third-driest November on record with just 17% of its normal rainfall in November.

(iii) Notable events and impacts

A severe winter storm affected the Iberian Peninsula in early January. Storm Filomena brought abundant cooling, high precipitation totals with flooding, and large amounts of snow to Spain and Portugal. Central and northern areas of Spain came to a standstill following record snowfall up to 50 cm. On 6 January, Spain registered its national all-time lowest temperature in Catalan Pyrenees at –34.1°C. Some locations in the center of Spain also reported their lowest local temperature on record, including Toledo (–13.4°C) and Teruel (–21.0°C). Madrid Barajas International Airport was forced to suspend all flights on 9 January. Areas of the southern Andalusian region recorded heavy rainfall, with more than 200 mm total on 8 January. Flash flooding and damaged roads and homes were reported due to overflowing rivers. At least seven fatalities were reported from storm Filomena.

During summer, there were several significant warm episodes observed in mainland Spain. An intensive heat wave occurred from 11 to 16 August, with temperatures exceeding 40°C across much of southern Spain. A new national all-time maximum temperature record was set in Montoro on 14 August at 47.4°C. Additionally, a local all-time maximum temperature record was set in the capital of Spain, Madrid, at 42.7°C on 14 August.

Several heavy rain events with flash flooding occurred in eastern and southern Spain during autumn. The region around Montsia and Baix Ebre in eastern Spain recorded a 24-hour total of 233.5 mm of rain on 1 September. A 1-hour total of 112.4 mm was recorded in Huelva in southern Spain on 23 September. Eastern parts of Spain and the Balearic Islands were also affected by floods and heavy rainfall on 21 September (e.g., 24-hour total of 124 mm in Mura/Mallorca). Several roads were cut off or closed. On 22 October, a quasi-stationary low that developed over the central Mediterranean led to intense heavy rainfall up to 102 mm and subsequent flooding in Alicante (near the eastern coast of Spain). On 6 November, a low-pressure area developed over the western Mediterranean, which brought heavy precipitation and thunderstorms, particularly notable on the Balearic Islands, with 113 mm of rainfall reported in a 12-hour period on 11 November in Mallorca. Further heavy rainfall of over 150 mm in 24 hours caused severe flooding in northern Spain during 23–29 November.

6) CENTRAL MEDITERRANEAN REGION

This region includes Italy (1961–90 base period), Monaco (1981–2010), Malta (1981–2010), Slovenia (1981–2010), Croatia (1981–2010), Serbia (1981–2010), Montenegro (1981–2010), Bosnia and Herzegovina (1981–2010), Albania (1981–2010), North Macedonia (1981–2010), Greece (1981–2010), and Bulgaria.

(i) Temperature

Temperatures in the Mediterranean and Balkan States were well above normal for 2021, but were not as high as the record-breaking year of 2020. For Italy (+1.3°C anomaly), Serbia (+0.8°C), North Macedonia (+0.7°C), Albania (+0.4°C), Slovenia (+0.7°C), Greece (+1.2°C, fourth warmest on record), and Malta (+0.8°C, second warmest on record), 2021 was warm throughout the year.

An exceptionally warm winter, with widespread above-normal temperatures up to +3.0°C, was reported from the Mediterranean and Balkan States. Bulgaria and Greece each observed their second-warmest winter on record, with anomalies of +2.6°C and +2.1°C, respectively. Serbia reported its third-warmest winter, with an anomaly of +3.0°C. Both January and February were exceptionally warm, with above-average temperatures throughout the region. Anomalies up to +3.5°C in Bosnia and Herzegovina and +2.3°C in Italy were reported in February.

Except for Greece, Italy, and Malta (near-normal), spring was colder than average for the rest of the region. Bulgaria, Slovenia, and Serbia reported anomalies of –1.2°C or below, while Albania, Croatia, and North Macedonia reported slightly below-normal temperatures. Similar to Central and Eastern Europe, the lowest temperature anomalies occurred in April, up to –2.0°C.

During summer, the entire area experienced above-average temperatures. Greece and Malta each reported their second-warmest summer on record, at +1.6°C and +2.0°C, respectively, while North Macedonia reported its third warmest (+1.7°C) and Serbia, Italy, and Bulgaria their fifth warmest. June was the warmest month for the northwest part of the region, with many countries reporting anomalies close to or above +2.0°C; Italy reported its fourth-hottest June on record (+3.2°C). Conversely, July was the warmest month for the southeastern part of the region: second-warmest July on record for Serbia (+2.8°C) and Greece (+1.8°C), third warmest for Bulgaria (+2.2°C) and Malta (+1.7°C), and fourth warmest for Italy (+2.3°C). The season ended with a warmer-than-normal August for the whole region, except the northernmost areas. Greece and North Macedonia reported their hottest August on record, at 2.3°C above normal, while Malta reported its second-warmest August (+2.1°C).

Autumn temperatures were near-normal for the season across the region, but with variation in months. While the warmth continued in September, with anomalies of +2.1°C in Italy (fourth highest on record) and +1.6°C in Malta (second highest), October was colder than normal in the region, for example, 2.5°C below average in North Macedonia. November was warmer than normal, with anomalies between +0.5°C and +2.2°C in the central Mediterranean region.

(ii) Precipitation

Annual precipitation totals for 2021 were near or slightly above normal for the Mediterranean and Balkan countries. Elevated anomalies were observed around the Aegean Sea, southern Bulgaria, and Albania, where totals were around 160% of normal, which was mainly attributed to intense convective events that occurred during winter 2020/21. Drier-than-normal conditions were observed in northern Italy.

Winter was wet, especially in the Balkans and Italy. Serbia and Bulgaria each reported their fourth-wettest winter, with precipitation 160% and 175% of normal, respectively. January was the wettest winter month in the region. North Macedonia reported its wettest January on record, with 321% of normal precipitation. Bulgaria, Serbia, Albania, and northern Greece also observed totals up to 300% of normal. Additionally, localized precipitation totals of 500% were reported.

Due to developing strong high-pressure systems over the North Atlantic and Greenland in April, expanding to southeastern Europe, spring precipitation was mostly near- or drier than normal, except for Bulgaria (118% of normal) and Serbia (110%). Slovenia reported a wetter-than-normal May, with 214% of its normal precipitation due to low pressure over the North Sea progressing farther to southeastern Europe.

Summer continued with drier-than-normal conditions in the Mediterranean and Balkan regions. Italy received 50% of its normal rainfall and Slovenia, Croatia, Bosnia and Herzegovina, Albania, and North Macedonia reported 60–75% of their normal totals, while precipitation in Greece was near-normal. The season started wetter than normal for Greece and Bulgaria, while drought conditions—severe in some places—prevailed in most of Croatia, Sicily, and Malta, where precipitation totals were just 20–40% of normal in June. In July and August, the distribution of precipitation was scattered, with many regions reporting dry conditions. Northern Italy, Slovenia, and Serbia reported local wet spots.

During autumn, precipitation was near-normal for large parts of the region, with slightly wetter conditions reported for the southern parts of Italy and Greece; however, the season began with a drier-than-normal September throughout the region, with 30–40% of normal precipitation. October was wetter than normal, with precipitation 200–300% of normal in Greece, North Macedonia, and Bulgaria (fourth wettest on record), while Slovenia and Italy had below-normal

precipitation. The season ended with around 160% of normal precipitation for Italy, Croatia, and Bosnia and Herzegovina in November. For Macedonia, Greece, and Bulgaria, autumn ended with slightly below-normal precipitation.

(iii) Notable events and impacts

Several winter storms affected the western Mediterranean and the Balkan countries, followed by cold and warm extremes during winter. During 6–10 January, heavy rains caused landslide damage in southwest Italy and Albania. In mid-January, a storm low developed over the North Atlantic, causing heavy precipitation (over 200 mm in 24 hours on the Balkan Peninsula), followed by flooding in Albania, Montenegro, Serbia, Bulgaria, and northern Greece due to overflowing rivers. A state of emergency was declared in some municipalities in Serbia.

During February, many new temperature records were set in the Balkans and Mediterranean as a sharp air mass boundary developed over Europe with very warm air in the Mediterranean. Later, cold air flowed south from the northern half of Europe. On 4–6 February, Calabria in southern Italy reported 26°C and Sicily 29°C. Bilije in Slovenia reported 25.3°C and Knin in Croatia reported 26.4°C. In mid-February, Florina in northwestern Greece measured –25.1°C, its lowest temperature in the last 15 years for this time period. The Veneto Region in Italy recorded –28°C. Many other stations in the Mediterranean also recorded low temperatures. On 15 February, heavy snowfall with gale-force winds was reported in Greece, resulting in suspended transport and power outages. At least three people were killed.

Abnormally cold spring temperatures affected Balkan regions in early April. On 7 April, a record amount of snow was reported in the capital of Serbia (Belgrade), with 10 cm snow depth. A national April low temperature record of –20.6°C was set for Slovenia at station Nova vas Bloka.

Later in spring and summer, there were several significant warm episodes, with heat waves observed in Italy and the Balkan regions. At the end of March, new local March maximum temperature records were set: in the capital of Slovenia, Ljubljana reached 25.1°C, and Florence, Italy, reached 29.4°C. On 30 April, temperatures reached near-record levels, exceeding 30°C in Italy, Greece, Serbia, Albania, and North Macedonia. On the same day, a new April record for the warmest night in Europe was measured near Chania on the island of Crete (Greece). The temperature did not drop below 30°C.

A major heat wave occurred from 8 June, with temperatures exceeding 40°C across many Balkan cities, including Mostar (Bosnia), Shkoder (Albania), and Danilovgrad (Montenegro). A second heat wave followed on 11 August, with temperatures reaching 48.8°C in Sicily, Italy, and 47.1°C in Lagada, Greece. Large forest fires occurred in areas affected by the strong heat. On 13 August, more than 500 wildfires were burning across Italy. During these heatwaves, Greece also lost more than 56,000 hectares to fires. A state of emergency was declared.

On 4 October, record-breaking rainfall was measured in Liguria and Piedmont Regions in northern Italy. The Liguria environmental agency reported a national 1-hour record of 181 mm in Vicoromasso. The weather station in Cairo Montenotte reported 496 mm in 6 hours, which tied the previous Italian 6-hour rainfall record set in 2011. A new European 12-hour rainfall record was set in Rossiglione (northwest Italy), with a total of 740.6 mm, which is more than 50% of its annual average of 1270 mm. Roads and public places were closed as a consequence of flash floods and landslides.

Between 5 and 15 November, Medistorm Heli impacted the region, bringing abundant precipitation with thunderstorms, particularly notable on the western Mediterranean islands and the Mediterranean coasts. Sardinia received a 4-hour total of 100 mm, while a station on Sicily measured a 12-hour total of 271 mm. The storm caused flooding in Bosnia and Herzegovina, due to a heavy 24-hour rainfall of more than 100 mm. Several areas were left without electricity and homes were flooded.

7) EASTERN EUROPE

This region includes the European part of Russia (1981–2010), Belarus, Ukraine (1981–2010), Moldova, Romania (1981–2010), and western Kazakhstan (west of 50°E, 1981–2010).

(i) Temperature

The year was near-normal for eastern Europe, with temperature anomalies between −0.2°C and +0.9°C of average for most countries. West Kazakhstan, however, observed its fifth-warmest year on record, at 1.5°C above normal.

During winter, anomalies were above normal for Moldova, Romania, and Ukraine; Romania reported its second-warmest winter on record at 3.2°C above normal, equaling the record set in 2020. European Russia and West Kazakhstan reported a slightly colder winter than usual, at 1.6°C and 0.4°C below normal, respectively.

During spring, only European Russia (+1.5°C) and West Kazakhstan (+3.2°C; third-warmest spring) reported above-normal temperatures, while the other countries reported temperatures ranging from 1.6°C below normal in Moldova to near-normal in Belarus. April contained the largest negative anomalies of the season for Belarus (–2.2°C), Moldova (–2.5°C), Ukraine (–1.3°C), and Romania (–1.9°C). European Russia and West Kazakhstan, in contrast, reported a warmer-than-normal April, with anomalies of +2.3°C and +3.3°C, respectively. The season closed with a colder-than-normal May for most of the region, except for Kazakhstan (up to +6.6°C anomaly in the Atyrau region; warmest May on record) and European Russia (+2.3°C). Anomalies in Belarus and Moldova were more than –1.0°C, while Romania reported a closer-to-normal May (–0.7°C).

During summer, the entire region experienced temperatures 1.4–3.2°C above normal, except for Moldova, which was near-normal. Belarus and European Russia each reported their second-warmest summer on record, at 2.6°C and 2.5°C above normal, respectively. The season started with the warmest June on record for European Russia (+3.9°C anomaly) and the third-warmest June for West Kazakhstan (+4.0°C) and Belarus (+3.5°C). July was also a near-record warm month for Belarus (second warmest, +4.1°C), Romania (second warmest, +2.5°C), and Ukraine (fourth warmest, +3.1°C). August concluded the season with near-normal temperatures for Belarus, Moldova, and Romania. Temperature anomalies up to +2.0°C and above were reported from Ukraine, European Russia, and West Kazakhstan.

Autumn was near-normal, with anomalies between −0.3°C and +0.5°C throughout the region. September was colder than usual, and temperatures ranged from around 1.3°C below normal in Belarus to around 0.5°C below normal in West Kazakhstan. In October, only European Russia and Belarus reported slightly above-normal temperatures, while Moldova, Romania, Ukraine, and West Kazakhstan were slightly colder than normal. The season ended with a warmer-than-normal November across the entire region. Belarus reported its fifth-warmest November on record, with an anomaly of +2.4°C.

(ii) Precipitation

The year was near-normal across the region, with 98–111% of normal precipitation; western Kazakhstan reported a lower total of 47% of normal, which resulted in its third-driest year on record. The areas around the Caspian Sea received the least precipitation for the region.

During winter, European Russia and eastern Ukraine received near-normal precipitation. Moldova, Romania, and western Ukraine each reported around 150% of normal. Except for western Kazakhstan, which reported below-average precipitation, January was wetter than normal. Belarus, Ukraine, Moldova, and Romania received up to 180% of their normal precipitation, while European Russia reported near-normal precipitation. For Ukraine, European Russia, and western Kazakhstan, February was the wettest month of the season, with 150%, 180%, and 188% of their normal precipitation, respectively. Belarus, Moldova, and Romania reported a slightly wetter-than-normal February.

Spring was slightly wetter than normal for European Russia, Moldova, and Romania and was near-normal for Belarus and Ukraine. West Kazakhstan received only 35% of its normal precipitation, which resulted in its third-driest spring on record. During March, the areas near the Black Sea in Romania, European Russia, and Ukraine received above-normal precipitation, while Belarus and western Kazakhstan reported around 70% of normal precipitation. For Belarus, Ukraine, Moldova, European Russia, and Romania, May was the wettest month of the season, with nationally averaged precipitation around 150% of normal. West Kazakhstan, however, reported a very dry May, with average precipitation less than 15% of normal and even less in localized areas. Romania reported its driest April on record.

Summer was drier than normal for western Kazakhstan and slightly drier than normal for European Russia, at 27% and 82% of normal precipitation, respectively. Areas around the Caspian Sea received only 20% of their normal precipitation; however, precipitation was near- or slightly above normal for Belarus, Romania, and Ukraine. In Moldova, around 60% of the country received 100–170% of its normal precipitation, while the remaining 40% received 180–240% of normal. Although some areas, especially around the Black Sea received above-normal precipitation, June and July were drier than normal for most countries in the region. July rainfall was near-normal for Romania and Ukraine, but above normal for Moldova, with 100–250% of normal precipitation. Summer ended with above-normal precipitation in Belarus (around 180% of normal), Moldova (around 160%), and Romania and Ukraine (around 120%). Meanwhile, western Kazakhstan reported below 20% of its normal precipitation.

Belarus and European Russia reported near-normal rainfall for autumn. Moldova received only 15–35% of its normal precipitation; such a low total is observed on average once every 15–30 years. Romania and Ukraine received around 60% of its normal precipitation. The season started with above-normal precipitation in September for Belarus and southern European Russia, while Ukraine, Moldova, and Romania received around 60% of their normal totals. October was drier than normal throughout the region: Belarus, Ukraine, and Romania received 30–60% of normal precipitation on country average, while it was especially dry in south Belarus, Ukraine, Moldova, and southern European Russia where large areas received less than 20% of normal precipitation. In western Kazakhstan, rainfall was also very low—around 40% of normal. The season concluded with above-normal rainfall across Belarus and northern European Russia, with nationally averaged precipitation of 120% and 150% of normal in November, respectively, while the rest of the region received slightly less precipitation than normal. December saw well above-normal precipitation (125–250% of normal), particularly west and north of the Black Sea (Romania, Moldova, Ukraine).

(iii) Notable events and impacts

Early spring was characterized by unusually cold temperatures in Ukraine and Romania due to an Arctic air inflow over all of Europe, as reported earlier. Many stations in northern European Russia reported new daily low temperature records as minima fell below –30°C (e.g., in region Murmansk), and some minimum temperatures even dropped below –40°C in late March. Following this cold period, an extreme warm spell was observed over European Russia. On 13 April, a temperature of 22.6°C was measured in the capital of Russia (Moscow). This was the highest temperature for that day of the year since 1881. On 17 and 18 May, two more new daily high temperature records were broken in Moscow, at 30.6° and 30.8°C, respectively. Many other stations in Russia set new daily heat records of 30–35°C. On 22 May, a record temperature of 39.7°C was measured in Khasavyurt (southwestern Russia), which was a new national spring record. An additional new monthly record of 40.5°C was recorded in Novyj Ushtogan, West Kazakhstan, on the same day.

During 22–23 June, extremely high temperatures were again measured in European Russia. Many stations reported temperatures up to 35°C. On 22 June, Petrozavodsk (northwestern Russia) measured a maximum temperature of 34.3°C, which tied the previous station record set in 2010.

Moscow reported a maximum temperature of 34.8°C, which was the highest in June for the last 120 years.

Following heavy rain in July, overflowing rivers damaged roads, bridges, and power lines in the Krasnodar region (Russia) and Crimea. Approximately 177 people were displaced, and at least two people were killed.

8) MIDDLE EAST

This region includes Israel, Cyprus (1981–2010), Jordan, Lebanon (1981–2010), and Syria (1981–2010).

(i) Temperature

Overall, the year was warmer than usual across the Middle East, with temperatures 0.8–1.9°C above normal. It was the second-warmest year on record for Jordan (+1.3°C anomaly), third-warmest year for Cyprus (+1.3°C) and Syria (+1.9°C), and fourth warmest for Israel (+0.8°C).

Winter was warmer than normal for the region. Syria reported its second-warmest winter on record, with an anomaly of +2.5°C. Israel and Jordan each observed their third-warmest winter, at 1.7°C and 1.9°C above normal, respectively. January was the warmest month of the season, with anomalies +2.0°C or above. Syria reported its second warmest January, with an anomaly of +2.6°C. Cyprus (+2.0°C), Israel (+1.9°C), and Jordan (+1.9°C) reported their second-, fifth-, and fourth-warmest January on record, respectively. The season ended with ongoing above-normal temperatures (up to +2.0°C) in February.

Spring started with a near-normal March, except for Syria and Lebanon, which reported anomalies up to +1.5°C. April was warm throughout the region, with anomalies above +1.0°C. Jordan reported its third-warmest April on record, with an anomaly of +2.5°C. Above-normal temperatures continued into May: Israel and Cyprus each reported their third-warmest May (+2.0°C and +2.6°C, respectively), Jordan its second warmest (+2.9°C), while Syria had its warmest May on record (+3.5°C). Altogether, spring 2021 was the third warmest for Syria and second warmest for Jordan.

Summer temperatures ranged from 0.6°C above average in Israel to 1.7°C above average in Lebanon. June was near- to below normal across most of the region, as Cyprus reported its fourth coldest June. August was the warmest month of the season; anomalies for Cyprus, Syria, and Jordan were +2.0°C, which was the second highest for August for each country. Israel reported its third-warmest August, with an anomaly of +1.4°C. For Syria and Jordan, it was the fifth-warmest summer, at 1.5°C and 1.0°C above normal, respectively.

Autumn was warm for the entire Middle East; most countries observed temperatures around 1.0°C above normal. Cyprus reported its third-warmest November on record, with an anomaly of +2.6°C, while Israel, Lebanon, and Jordan reported also temperature anomalies above +2.0°C. During December, anomalies were mostly not quite as high but still well above +0.5°C. Syria observed an anomaly of +2.7°C, which tied its previous December record.

(ii) Precipitation

Annual precipitation totals were mostly below average across the Middle East (20–80% of normal (Fig. 7.39).

Winter was drier than normal; many areas received precipitation less than 80% of normal and less than 60% of normal in localized areas. During January, the northern and western parts of the region were wetter than normal. In February, many parts of Jordan were wetter than normal, while much of Syria and Lebanon received only 20–60% of their normal precipitation (even less in central Syria).

Spring was especially dry. Large parts of Israel and Jordan received below-normal precipitation, even beyond their dry season. Central and northern Israel received 50–80 mm in March and April combined. In Cyprus, precipitation was around 40% of normal. Lebanon and northwestern

Syria received little precipitation. All spring months were drier than normal for the Middle East, with precipitation totals mostly 0–30% of normal. As is typical, May was the driest month of the season, with no precipitation at all measured in Jordan, Cyprus, or Israel.

At the beginning of summer, only localized areas observed some precipitation in northern Jordan and Lebanon; otherwise the Middle East received precipitation well below 40% of normal or none at all. In July, it was dry as usual in Jordan, while some unseasonal precipitation fell across most of Israel and Lebanon. August, too, had some precipitation in the region, ranging from 125–250% of normal (except for northwestern Syria and Lebanon).

Autumn was drier than normal, with overall precipitation distributed inhomogeneously over the months. After a wetter-than-normal start in September, localized areas in Israel, Lebanon, and Jordan received about 10 mm of precipitation (monthly normal for September at most stations is 1–3 mm), large areas of the Middle East received well below 20% of their normal precipitation in October. For the most western parts of Syria, Lebanon, and Israel, precipitation was around 20–60% of normal in November, while the eastern parts of Jordan and Northern Cyprus received slightly above-normal precipitation.

(iii) Notable events and impacts

After a winter storm accompanied by heavy rain, northwestern Syria experienced flooding on 18 January. The floods made living conditions for over 120,000 displaced people living in tents difficult. At least one child was killed, and more than 22,000 tents were damaged or destroyed.

On 16 February, heavy snow and storms led to disrupted traffic and closed schools in the Middle East. A daily total of 15 cm snow was measured in Damascus (Syria) and 10–15 cm in Jerusalem (Israel), and gale force winds up to 100 km h^{-1} were reported in Lebanon.

During a spring heat wave, many countries in the Middle East reached near-record temperatures for that time of year. On 19 April, 42.7°C was measured at Besor Station in southern Israel, 35.6°C in Jerusalem, 38.0°C in Damascus (Syria), and 36.5°C in Jordan. On 3 May, Cyprus measured 39.1°C, and 44.6°C was reported from Israel and Jordan on 5 May. Significant rainfall occurred in northwestern Israel on 24 July with amounts of 10–30 mm, very unusual for this month.

Following a November with warm spells—high maximum temperatures for Cyprus (33.4°C), Lebanon (29°C), and Israel (33°C)—an exceptionally intense winter storm occurred in Israel in December. On 21 December, a daily total of 147 mm was measured in Mikve Yisrael, along the central coast of the country (third on record of more than 100 years of measurements at this station; the station record was set in 1938 with 199 mm). During 21–24 December, average total rainfall of 170–221 mm was reported at the area between Tel Aviv and Ben Gurion Airport, Israel.

9) TÜRKIYE AND SOUTH CAUCASUS

This region includes Türkiye, Armenia (1961–90), Georgia, and Azerbaijan.

(i) Temperature

Overall, the year was warmer than normal for the region, with annual temperatures 1.4–2.1°C above normal. Türkiye observed its fourth-warmest year on record, while Armenia observed its third warmest. The year started with a warmer-than-normal winter. Türkiye saw temperatures that were 1.3°C above normal, while anomalies for Armenia, Georgia, and Azerbaijan were around +2.0°C. Türkiye reported its second-warmest January on record with an anomaly of +2.7°C, while February was the warmest month in the period: +3.4°C in Armenia, +2.3°C in Georgia, and +1.5°C in Türkiye and Azerbaijan.

Spring started with a near-normal March. After a warmer-than-normal April for South Caucasus (anomalies +2.3°C to +4.0°C) and Türkiye (+1.3°C), May was also warmer than normal: the warmest May in the past 50 years in Türkiye (+2.6°C) and the warmest May on record for Armenia (+2.9°C).

Overall, spring was warmer than usual by up to 2.0°C in Armenia and Azerbaijan, while Türkiye reported temperature anomalies up to +1.5°C and Georgia a slightly warm anomaly of +0.6°C.

The above-normal temperatures in summer were dominated by a hot June in the South Caucasus region. In Armenia and Azerbaijan, anomalies were as high as +4.0°C and around +1.5°C in Georgia. For Türkiye, July was the hottest month in the season and the second-warmest July on record (+1.8°C anomaly). The season ended with temperatures well above normal in August across the region; anomalies were still above +2.0°C in large parts. Armenia observed its hottest summer on record, an average temperature anomaly of +2.5°C.

Autumn started with slightly below-normal temperatures in Türkiye and South Caucasus. For Türkiye, September temperatures were normal, while Armenia and Azerbaijan reported slightly above-normal temperatures (+0.5°C anomaly) and Georgia reported a below-normal anomaly of −0.5°C. October was colder than normal in northeastern Türkiye and South Caucasus. Anomalies were slightly below −1.0°C. The season ended with a warmer-than-normal November in the region, with anomalies up to +2.0°C.

(ii) Precipitation

With average precipitation totals 95% of normal, the year was near-normal for Türkiye and Georgia, while precipitation totals up to 80% of normal were reported in Armenia and 130% of normal in Azerbaijan. Distribution of precipitation was inhomogeneous in both time and space.

Winter was very wet in Azerbaijan, with precipitation up to 162% of normal. Winter was near-normal for Türkiye and Georgia and slightly below normal in Armenia (90%).

March was wetter than normal across the region. The Black Sea area received precipitation totals as high as 250–260% of normal, 150% of normal in Armenia. Overall, spring was wetter than normal for Azerbaijan (165% of normal), while Georgia reported a normal spring. Türkiye was drier than normal (75%), Armenia slightly drier than normal (90%).

Summer was drier than normal for Armenia, Azerbaijan, and Georgia with 70–95% of normal precipitation Türkiye received 123% of its normal precipitation. While some eastern regions in Türkiye were drier than normal, the national average was above normal due to wetter parts in the west. June was exceptionally dry in Armenia with the average precipitation total only 27 % of normal. Severe droughts were observed in the last week of June.

Autumn was wetter than normal for Georgia, with 115–155% of normal precipitation. Azerbaijan reported a near-normal autumn, while Türkiye observed a drier autumn than normal, with 86% of its normal precipitation, Armenia 75%. September was the wettest month in the season for Armenia in terms of anomalies, with 98% of normal precipitation, while October had 86% of normal. For Azerbaijan, October was the wettest month in the season, with 178% of normal precipitation. Georgia, Armenia, and Azerbaijan each reported a drier November than usual, with only about 50% of normal precipitation.

Overall, Türkiye and the South Caucasus reported an increase in extreme precipitation events over the year but with short duration and rather localized.

(iii) Notable events and impacts

During January and February, Türkiye experienced several winter storms with heavy rain and winds. During 6–10 January, the western Turkish province of Izmir Türkiye reported flash flooding that inundated streets, houses, and shops. The southern province of Antalya received around 98 mm of precipitation in 24 hours, causing severe flooding. On 2 February, Güzelyali station in Izmir Province reported a 6-hour rainfall total of 113 mm (February average is 102.3 mm). Subsequent flooding caused traffic disruption, heavy damage to residences, and at least two fatalities.

On 21 May, South Caucasus and Türkiye reported unusually high maximum temperatures. In Ambrolauria (Georgia) a maximum of 36.6°C was measured. Armenia reported a new local monthly May record of 36.1°C in the capital Yerevan. In Urfa, southeastern Türkiye, 40.4°C was

reported, which tied the previous May local record. Many other stations in southeastern Türkiye reported maximum temperatures around 40°C that day.

During summer, there were several significant warm episodes, with three heat waves exceeding 40°C observed in Türkiye and South Caucasus. A major heat wave occurred at the end of June, with new monthly temperature records set in Yerevan (Armenia), 41.1°C on 24 June, and in Baku (Azerbaijan), 40.4°C on 26 June. New monthly records were also set in Georgia and Türkiye. On 20 July, Tbilisi (Georgia) reported 40.6°C, which tied the previous July record set in 2018. Cizre (Türkiye) measured 49.1°C on the same day.

On 20 July, Cizre in southeastern Türkiye measured 49.1°C. This value sets a new national maximum temperature record for Türkiye.

During 28 July–3 August, wildfires broke out in southern Türkiye (especially notable in the provinces of Antalya and Mugla). More than 130 fires scorched at least 118,790 hectares, displaced more than 10,000 people, and killed at least eight people. On 3 August, a new local maximum temperature record of 45.1°C was reported at Aydin (also southern Türkiye). Meanwhile, due to a medistorm in the Black Sea region, heavy rainfall and flooding caused severe damage to infrastructure and houses in Türkiye, and at least 77 deaths were reported on 10 August.

On 1 December, Azerbaijan observed its hottest December day on record: 29.1°C at Lankaran.

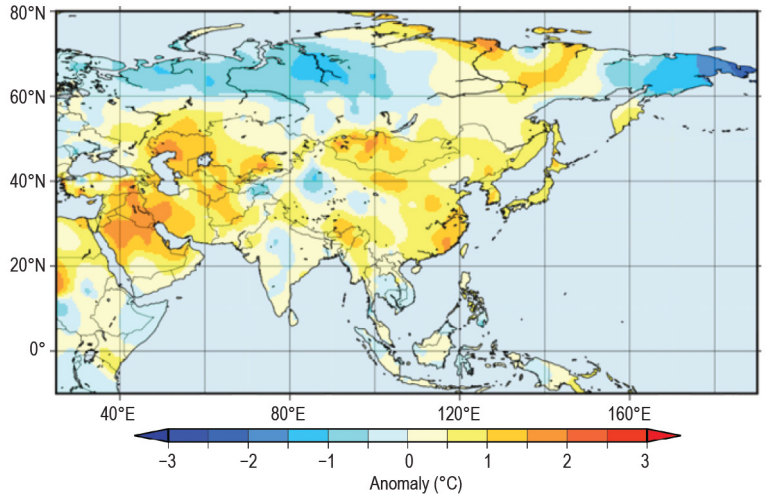

Fig. 7.42. Annual mean surface temperature anomalies (°C; 1991–2020 base period) over Asia in 2021. (Source: Japan Meteorological Agency.)

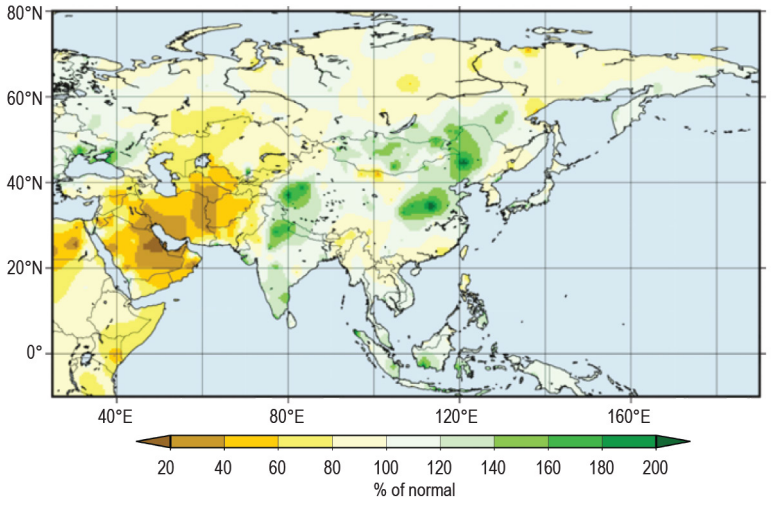

Fig. 7.43. Annual precipitation (% of normal; 1991–2020 base period) over Asia in 2021. (Source: Japan Meteorological Agency.)

g. Asia—Z. Zhu, Ed.

Throughout this section, the base periods for climatological normals and anomalies vary by region. The standard base period is 1991–2020, but earlier base periods are still in use in several countries and regions, and are noted as such in the analyses. All seasons in this section refer to the Northern Hemisphere, with winter referring to December–February 2020/21, unless otherwise noted.

1) OVERVIEW—Z. Zhu, P. Zhang, T.-C. Lee, A.-M. Setiawan, M. Hanafusa, Hir. Sato, Hit. Sato, S. Wakamatsu, K. Takahashi, G.-S. Im, D. Dulamsuren, M.-V. Khiem, and H.-P. Lam

Annual mean surface air temperatures during 2021 were above normal across most of Asia, with anomalies more than +1.0°C in southeastern China, part of western Mongolia, and Central and Southwest Asia (Fig. 7.42). Annual precipitation totals were above normal (> 120% of normal) in the northern part of eastern China and the Tibetan Plateau, Mongolia, parts of Indonesia, and northern and southern India, and below normal (< 80%) in Central and Southwest Asia (Fig. 7.43).

In winter, below-average temperatures dominated Siberia (Fig. 7.44a), while

temperatures were above normal in eastern China, the Tibetan Plateau, and northern Mongolia. Seasonal precipitation was below normal from eastern India to Myanmar (Fig. 7.44b) and much above normal in southwestern India, the Philippines, and in and around southern central Siberia. In spring, temperatures were above normal in western and southwestern Asia and from the southeast coast of China to northeast Asia (Fig. 7.44c). Much-above-normal precipitation prevailed from western China to India (Fig. 7.44d). In summer, above-average temperatures were observed from central Siberia to northern Japan and in western central Asia (Fig. 7.44e), and central China and

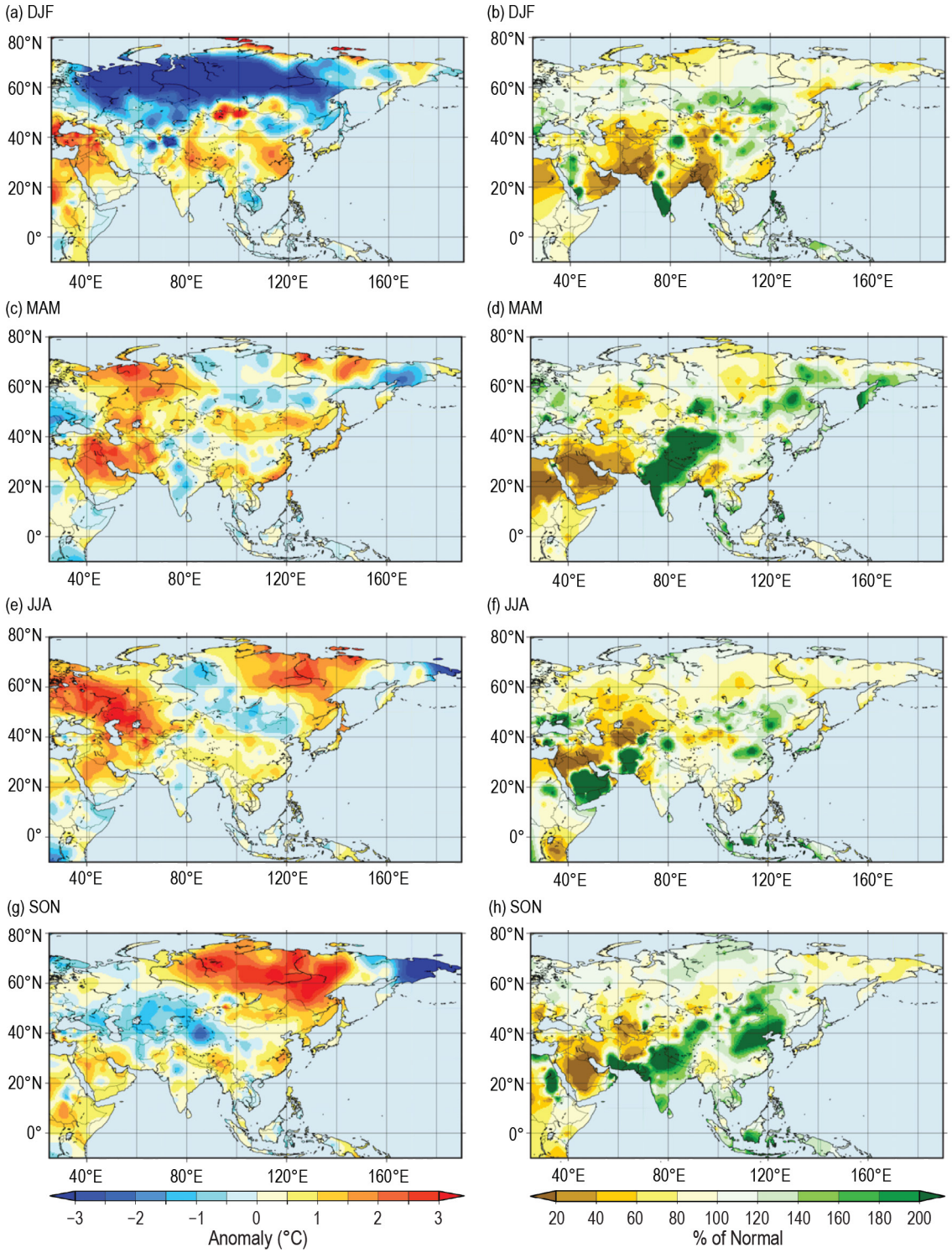

Fig. 7.44. Seasonal mean surface temperature anomalies (°C, left column) and seasonal precipitation ratios (% of normal, right column) over Asia in 2021 for (a), (b) winter, DJF; (c), (d) spring, MAM; (e), (f) summer, JJA; and (g), (h) autumn, SON. Anomalies and ratios are relative to 1991–2020. (Source: Japan Meteorological Agency.)

southern Japan experienced much-above-normal precipitation (Fig. 7.44f, see details in Sidebar 7.4). In autumn, above-average temperatures dominated Siberia, except for the easternmost region (Fig. 7.44g). Seasonal precipitation totals were much above normal in and around India and Tibet, and across Indonesia, eastern Mongolia, and northern China (Fig. 7.44h).

In winter, negative anomalies of 500-hPa geopotential height and 850-hPa temperature prevailed over Siberia (Fig. 7.45a). In spring, anti-cyclonic anomalies were dominant to the south of the Aleutian Islands at the 500-hPa and 850-hPa levels (Figs. 7.45c,d), accompanying positive 850-hPa temperature anomalies in Northeast Asia (Fig. 7.45c). In summer, significantly positive anomalies of 500-hPa geopotential height and 850-hPa temperature were observed from central Siberia to northern Japan (Fig. 7.45e). Convective activity was enhanced over the subtropical western North Pacific (Fig. 7.45f). In autumn, convective activity was enhanced from the northern Arabian Sea to the southern Indochina Peninsula and from the eastern tropical South Indian Ocean to the west of New Guinea, associated with a pair of 850-hPa cyclonic circulation anomalies straddling the equator in the tropical Indian Ocean (Fig. 7.45h).

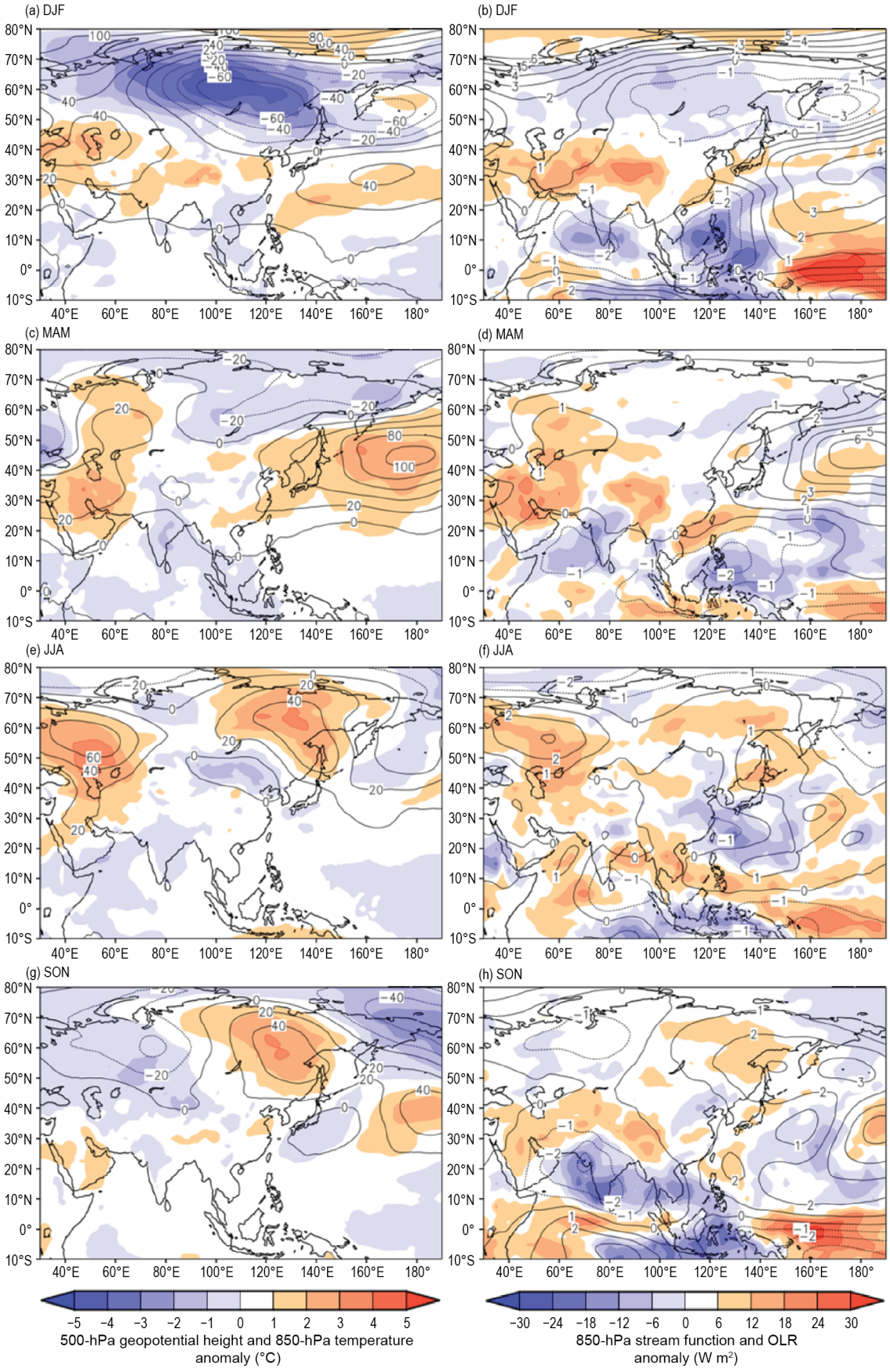

Fig. 7.45. Seasonal mean anomalies of atmospheric circulation variables in 2021 for (a), (b) winter, DJF; (c), (d) spring, MAM; (e), (f) summer, JJA; and (g), (h) autumn, SON. Left column: 500-hPa geopotential height (contour, gpm) and 850-hPa temperature (shading, °C). Right column: 850-hPa stream function (contour, 1 × 10^6 m^2 s^{-1}) using data from the JRA-55 reanalysis and OLR (shading, W m^{-2}) using data originally provided by NOAA. Anomalies are relative to 1991–2020. (Source: Japan Meteorological Agency.)

2) RUSSIA—M. Yu. Bardin and N. N. Korshunova

Estimates of climate features for Russia are obtained from hydrometeorological observations of the Roshydromet Observation Network. Anomalies are relative to the 1961–90 base period, and national rankings and percentiles are based on the 1936–2021 period of record. Note that the temperature database was extended significantly, which in some cases changed previous ranking. The boundary between Asian Russia and European Russia is considered to be 60°E.

(i) Temperature

The year 2021 in Russia was almost 2°C colder than the record warmest year of 2020, ranking 14th highest with annual mean temperature 1.3°C above normal (Fig. 7.46). Warm areas with anomalies above the 95th percentile were located in the Far East (Kamchatka, Sakhalin, lower Amur region) and the Lower Volga–Caspian region. The only small region with below-normal temperatures was in Chukotka.

Russia as a whole observed its record warmest summer with a temperature 2.0°C above normal; the previous two warmest summers occurred in 2016 and 2010. By region, Asian Russia was record warmest (1.66°C above normal), while European Russia was second warmest (2.92°C

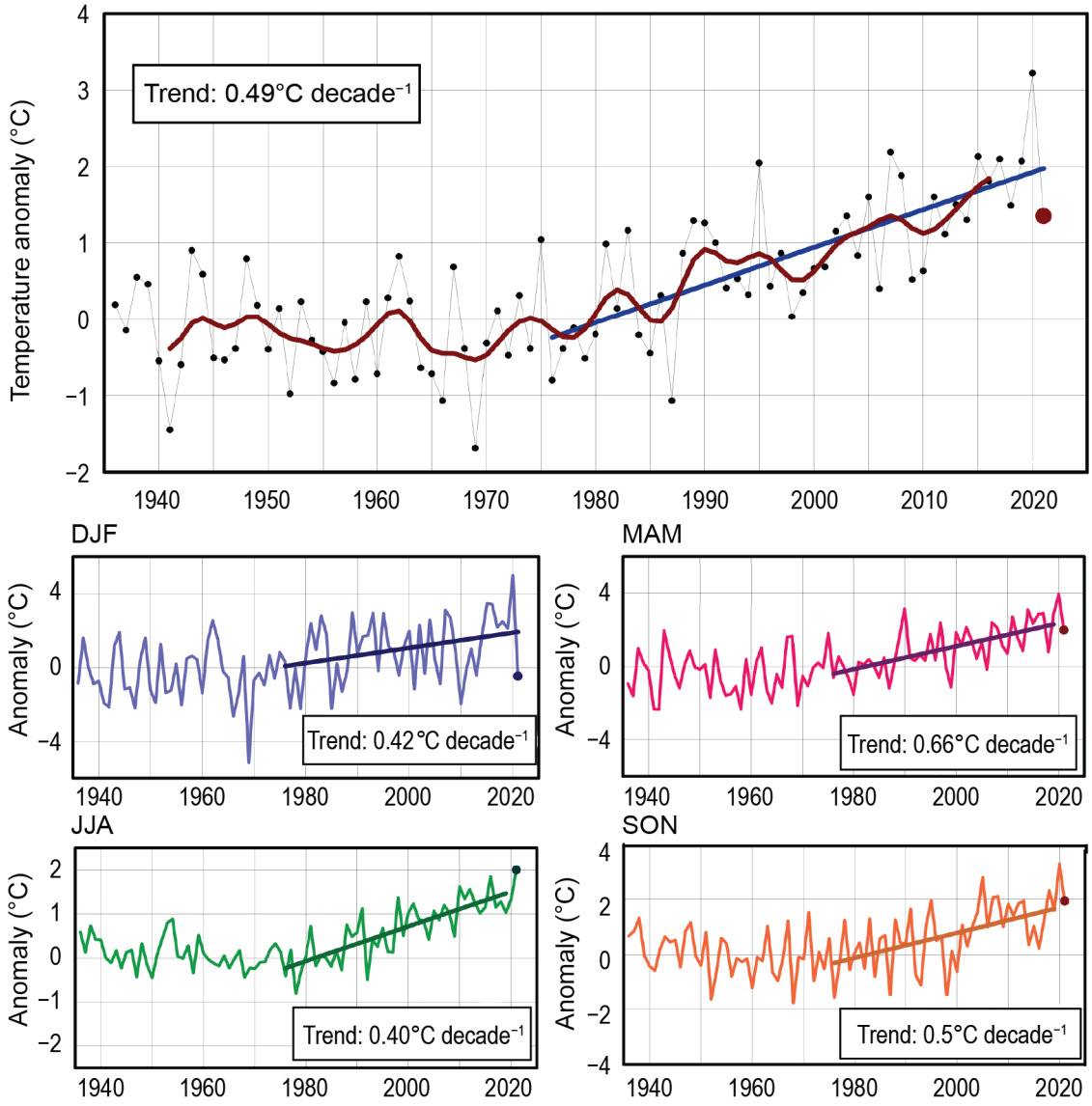

Fig. 7.46. Annual and seasonal mean temperature anomalies (°C; 1961–90 base period) averaged over the Russia territory for the period 1936–2021. The bold red line on the annual mean time series in (a) is an 11–point binomial filter. Linear trend b (°C decade^{-1}) is calculated for the period 1976–2021 for each panel.

above normal). This anomalous temperature pattern was mostly due to persistent anticyclonic circulation regimes observed simultaneously in European Russia and its eastern Asian part in the second half of June and first three weeks of August (Fig. 7.45e).

Abnormal summer warmth was compensated by a colder-than-normal winter: 0.46°C below normal, among the coldest 30% of all winters since 1936. Seasonal temperatures of 4–5°C below normal were observed in Siberia in the area of 60°–65°N, 60°–100°E (Fig. 7.45a). Above-average temperatures were reported only within narrow strips along the Arctic coast of Asian Russia, the Baikal and Amur regions along the southern borders of Russia, and in western European Russia. January was colder than normal in Asian Russia (2.6°C below normal), while February was colder than normal in European Russia (3.2°C below normal). The cold was especially noteworthy in the Northwestern Federal District, at 5.7°C below normal, ranking among its five coldest Februarys on record; at many stations, anomalies were below their fifth percentile (Fig. 7.46).

Spring was warmer than average (2.0°C above normal; 13th warmest on record) for Russia as a whole. Notably, May was abnormally warm over the vast areas encompassing eastern European Russia, the Urals, and western parts of Siberia, with temperature anomalies up to +6°C and temperatures above the 95th percentile at most stations. Autumn was also warmer than average for Russia as a whole (1.94°C above normal, seventh warmest on record), especially in eastern Asian Russia: up to 5°C above normal.

All of the seasons in Russia have warmed since the mid-1970s. Annual and seasonal trends were statistically significant at the 99% confidence level, except winter. Winters strongly warmed from the 1970s to the mid-1990s, and mostly leveled off or cooled thereafter (Fig. 7.46). However, the record warm winter of 2020 made the trend estimate for 1976–2021 formally statistically significant; this estimate should be treated with caution.

(ii) Precipitation

Across Russia as a whole, 2021 was among its 10-wettest years on record, with total precipitation about 107% of normal (Fig. 7.47). European Russia observed its sixth-wettest year, with 110% of normal precipitation. Asian Russia had 106% of normal precipitation, its 13th wettest. Spring was the third wettest on record, at 122% of normal, while summer was third driest, at 93% of normal. Winter and autumn were moderately wetter than average (11th and 12th-highest seasonal precipitation totals, respectively).

In winter, February was the second wettest on record (157% of normal precipitation); Asian Russia received 154% of average precipitation (second wettest on record) and European Russia received 159% of average (fifth wettest). February was wet across the southern latitudes of Russia, especially in the Baikal and Amur regions (≥ 260% of average), while polar regions were dry. Abnormal warmth in the Volga and the Southern Urals in May was accompanied by precipitation deficits that were 40–60% of normal.

In all summer months, precipitation deficits were observed across most of Russia. July (89% of average) and August (91% of average) were both among their five driest on record. Similar to May, anomalous warmth and rainfall deficit were observed simultaneously in the Volga and the Southern Urals. Strongly excessive precipitation was observed in southern European Russia, where a persistent cyclone caused heavy rains during 8–16 August (Fig. 7.48). Previous monthly and daily records were surpassed at many

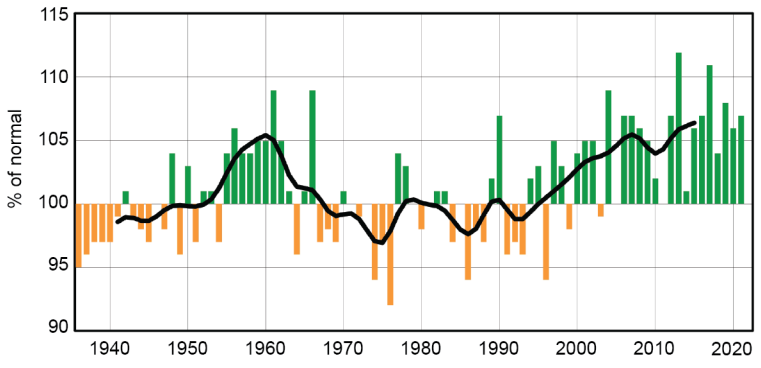

Fig. 7.47. Annual precipitation (% of normal; 1961–90 base period) averaged over the Russian territory for 1936–2021. The smoothed time series (11-point binomial filter) is shown as a bold black line.

stations. The heaviest rain was observed on 16 August in Temryuk (Krasnodar region): 355 mm (eight times its monthly normal), and monthly precipitation here totaled 596 mm (more than 13 times its normal). In Novorossiysk, maximum precipitation (110 mm) was recorded on 16 August.

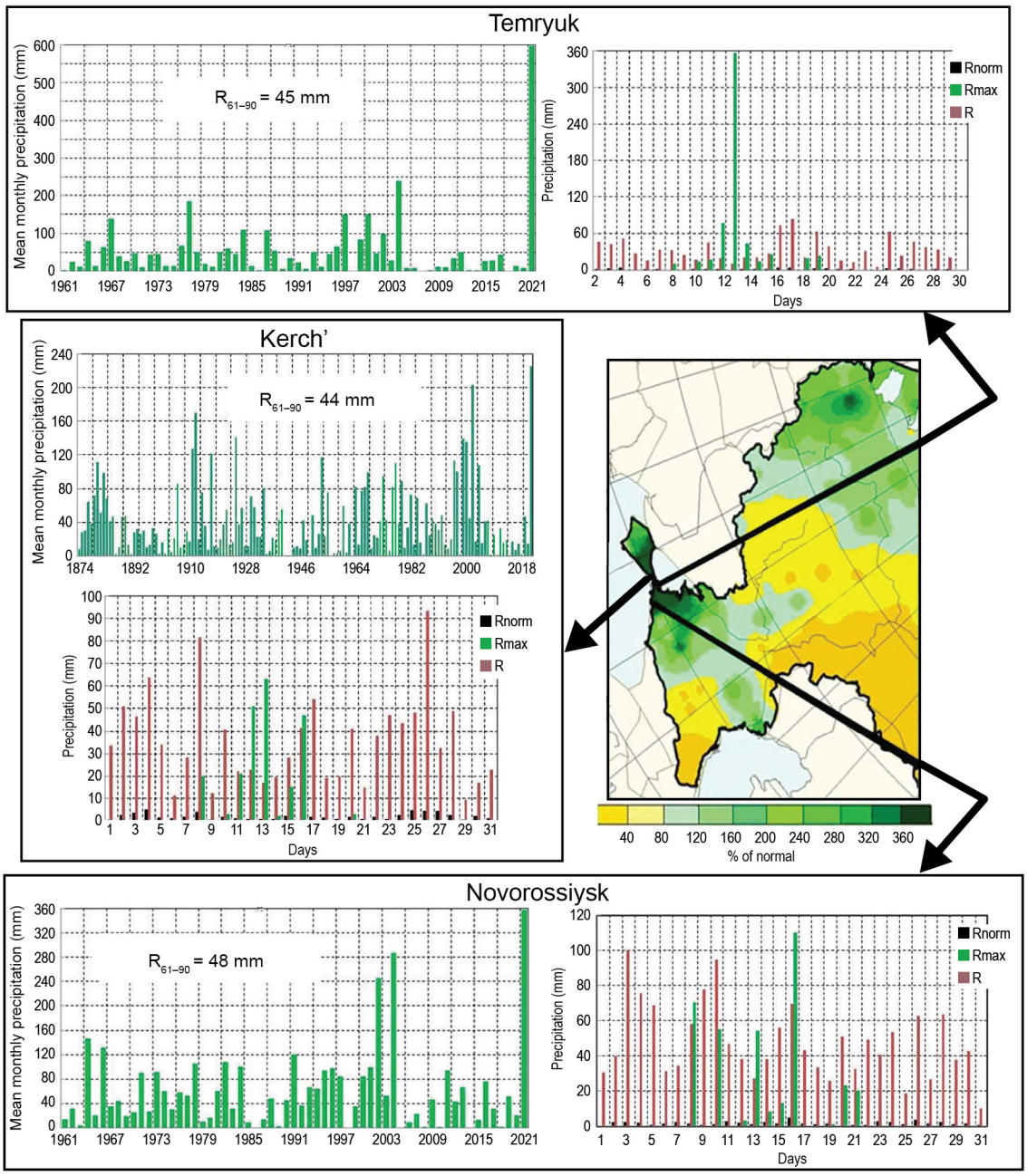

Fig. 7.48. Precipitation in Aug 2021 over southern regions of European Russia. The map shows the monthly precipitation (% of normal) and the insets provide the mean monthly precipitation (mm) in Kerch' (1874–2021) and Temryuk and Novorossiysk (1961–2021), and daily precipitation (mm): observed (R: green), along with the climatological normal (Rnorm, black) and the absolute maximum (Rmax, brick red) at these stations. R61–90 (mm) is the 1961–1990 normal precipitation for the month.

(iii) Notable events and impacts

On 8–9 April, easterly winds reached 33–38 m s^{-1} in the far eastern region of Petropavlovsk–Kamchatsky and up to 40–47 m s^{-1} along the nearby coastal regions, causing significant damage estimated at 7.1 million rubles to the city infrastructure.

On 12 May, wind speeds in Moscow and the Moscow region reached 20–24 m s^{-1}; leading to one fatality, four injuries, uprooting of 147 trees, and damage to dozens of cars.

On 17–18 June, heavy rain in Yalta, a city on the southern coast of the Crimean Peninsula, persisted for 16 hours, resulting in 133 mm rainfall accumulation. Pedestrian underpasses were inundated and many streets were completely flooded.

On 18 July, mudflow 100 m wide and up to 2.5 m thick descended along the bed of the Derekoika River. Traffic in the center of Yalta and the entrance to the city were completely diverted. A state of emergency was declared, and direct damage was about 15 billion rubles.

On 23 July, Khosta, part of Great Sochi, received 154 mm of precipitation in six hours. Runoff and river overflows in the Khosta region inundated roads, adjacent territories, a hospital, and ambulance substations. Mudflows affected the urban infrastructure in Kudepst, Matsesta, and Khosta.

From 5 August to 20 September, excessive rainfall led to flooding on the Amur River, impacting the Amur Region, Jewish Autonomous Region, and Khabarovsk Territory. Water levels in the river rose to 0.3–1.0 meters above the hazardous mark. A state of emergency was declared, as roads, communication lines, bridges, and houses were flooded.

On 17 October, heavy wet-snow precipitation (3–6 cm) was recorded on Sakhalin, accompanied by winds as high as 33–36 m s^{-1}. Dozens of villages lost power and heating. Rooftops were damaged in Aleksandrovsk–Sakhalinski, killing two people. Traffic was restricted and flights were delayed.

3) EAST AND SOUTHEAST ASIA—P. Zhang, T. C. Lee, A. M. Setiawan, M. Aurel, M. Hanafusa, Hir. Sato, S. Wakamatsu, G. S. Im, D. Dulamsuren, M.-V. Khiem, and H.-P. Lam

Countries/places considered in this section include China, Hong Kong (China), Indonesia, Japan, Korea, Mongolia, Singapore, and Vietnam. Unless otherwise noted, anomalies refer to the 1991–2020 base period.

(i) Temperature

Annual mean temperatures for 2021 across East and Southeast Asia are shown in Fig. 7.42. The annual mean air temperature for China was 10.5°C, 0.64°C above the 1991–2020 normal, the highest since the start of the record in 1951. It was also the warmest year in Hong Kong since its records began in 1884, with an annual mean temperature of 24.6°C which was 1.1°C above normal.

Annual mean temperatures were significantly above normal in northern and western Japan and above normal in eastern Japan and in Okinawa/Amami. The annual mean temperature over South Korea was 13.3°C (0.8°C above normal), which was the second highest since records began in 1973. Spring and autumn, in particular, were significantly warmer than normal.

The annual mean temperature over Mongolia was 1.7°C (2.3°C above average; also the second highest since 1940), The second-warmest February and third-warmest March on record contributed to this annual warmth.

Annual mean temperatures were above normal across Indonesia (0.4°C above the 1991–2020 normal), based on the record of 89 weather stations, marking the eighth-warmest year since start of the record in 1981. The highest temperature recorded in 2021 was 37.9°C on 22 October in Surabaya (East Java).

The annual mean temperature for Singapore was 27.9°C, which is 0.1°C above normal and marked the 10th warmest year on record. In January and August, below-average temperatures were associated with significantly above-average rainfall. Notably, January 2021 was the coolest January in the past 30 years, while August 2021 was the second coolest August in the past 20 years.

The monthly mean temperature was above normal across Vietnam for most months in 2021. Some stations in North and South Vietnam recorded historically high monthly mean temperatures, including: Dong Van (Ha Giang): 17.4°C (surpassing 17.1°C in 2015); Cao Lanh (Dong Thap): 28.7°C (28.3°C in 2015); Soc Trang: 28.6°C (28.2°C in 2017); Rach Gia (Kien Giang): 29.5°C (29.3°C in 2017).

(ii) Precipitation

Annual precipitation for 2021 as a percentage of normal over East and Southeast Asia is shown in Fig. 7.43. For China, the average annual precipitation total was 672.1 mm, 105.4% of its 1991–2020 normal. The annual precipitation total was highest in the 61-year record in both North China (154% of normal) and the Haihe River basin (174%). The precipitation in spring, summer, and autumn in total was also record high with 133% of its normal. The total annual rainfall for Hong Kong in 2021 was 2307.1 mm, 95% of its normal.

In Japan, annual precipitation totals were significantly above normal on the Pacific side of eastern Japan, and above normal on the Pacific side of northern Japan, the Sea of Japan side of eastern Japan, and in western Japan. The annual precipitation total in South Korea was 1244.5 mm, which was 93.7% of its normal of 1331.7 mm. Low-pressure systems, typhoons, and the Meiyu/Baiu/Changma fronts mainly affected the southern region; precipitation totals across the central region were below normal. Annual precipitation for Mongolia was 261.7 mm above normal, its fifth highest total since 1940.

The spatially averaged annual rainfall total for Indonesia was 2910 mm, placing 2021 as the second-wettest year since the start of the record in 1981. 2010 and 1998 were the wettest and the third wettest years, respectively, both of which experienced strong La Niñas in the second half of the years. The highest rainfall anomaly in 2021 was recorded at Sultan Iskandar Muda station, Banda Aceh, at about 249% of its 1991–2020 normal.

The annual total rainfall for Singapore in 2021 was well above average, resulting in the country's second wettest year since 1981. Average rainfall totals in January (480.5 mm) and August (426.2 mm) were at least twice their respective long-term monthly averages. The annual total rainfall at the Changi climate station of 2809.6 mm and the average total of 3167.7 mm across island-wide stations with long-term records was 133% and 125% of their respective long-term annual averages of 2113.3 mm and 2534.4 mm, respectively.

(iii) Notable events and impacts

In China, the Meiyu/Baiu/Changma season, which started later and ended earlier than the 1991–2020 normal, was eight days shorter overall, with 267.2 mm rainfall (78% of normal). However, the rainy season in North China in 2021 lasted 59 days, the second longest since the start of the record in 1961, with average total rainfall of 276.4 mm (203% of normal, the third highest on record). From 15 to 22 July, heavy precipitation fell in central and southern North China, the middle reaches of the Yellow River, and the upper reaches of the Huai River basins, with maximum cumulative precipitation records observed at 26 stations, including Zhengzhou in Henan (851 mm). During this period, Zhengzhou observed a maximum daily precipitation total of 624.1 mm, close to its 1981–2010 annual normal of 641 mm (see Sidebar 7.4). During September and October, the Weihe River, a tributary of the Yellow River, experienced its largest flood for this time of year since 1935. In 2021, under the control of the strong subtropical high, daily maximum temperatures exceeded 40°C at Toxon (46.5°C on 25 July) in Xinjiang, Fushun (41.5°C on 3 August) in Sichuan, and Mizhi and Yichuan (40.6°C on 31 July) in Shaanxi, breaking or equaling the historical record since 1961. From early November 2020 to early February 2021, due to scarce precipitation (20% to 50% of normal in most areas) and well-above-normal temperatures, moderate to severe meteorological drought developed rapidly in Jiangnan and South China, leading to less water storage in lakes and reservoirs and severe impacts on water resources and agricultural production in the concerned areas.

Hong Kong, China, experienced record-breaking monthly mean temperatures of 22.0°C in March, 29.0°C in May, and 29.7°C in September. Sixty-one hot nights (daily minimum temperature ≥ 28.0°C) and 54 very hot days (daily maximum temperature ≥ 33.0°C) were reported in 2021, both of which were the highest annual totals on record. Hong Kong was exceptionally dry during the first five months of 2021 with only 163.1 mm of rainfall, the second lowest amount on record for

this period. Tropical Cyclone Lionrock brought 329.7 mm of rainfall to Hong Kong on 8 October, the highest daily rainfall on record for that month. Tropical Cyclone Rai was the first super typhoon to occur in the South China Sea in December since 1961.

In central Vietnam, during 22–23 October, a new 24-hour record rainfall total of 488 mm in Tam Ky station (Quang Nam) was set, breaking the previous record of 381 mm on 20 October 2001. Additionally, Quang Ngai, Tra Khuc, and Chau O stations (Quang Ngai) observed record high totals of 532 mm, 576 mm, and 641 mm, respectively, compared to their previous records of 525 mm, 518 mm, and 439 mm on 29 September 2009.

In August, active stationary fronts formed between the Okhotsk High and the North Pacific Subtropical High, and moist air along these fronts brought record-breaking monthly precipitation amounts to western Japan.

South Korea observed its highest March monthly mean temperature (8.7°C; +2.6°C above normal) since the start of the record in 1973. As a result, the cherry blossoms bloomed 5–16 days earlier than normal across the country.

In Mongolia, 129 weather disasters/extreme events (strong winds, flash floods, heavy precipitation, etc.) were reported around the country in 2021. The most devastating of these was the strong winds and dust storms that spread across Mongolia on 13–15 March, which led to 10 fatalities, and more than 700 people were injured.

Tropical cyclone Seroja brought extremely heavy rainfall to Indonesia on 5 April, with daily rainfall totals of more than 200 mm recorded at many point observations. The heaviest rainfall was 460 mm, recorded in Tilong Dam, east of Kupang (East Nusa Tenggara provinces capital city).

In December, Typhoon Rai passed over Song Tu Tay station in Vietnam where maximum winds of 45.6 m s^{-1} (gusts of 56.8 m s^{-1}) were recorded. This was the highest wind speed observed in the Vietnam observation system in the last 40 years.

Sidebar 7.4: Unprecedented extreme rainfall over East Asia in July and August 2021—

Z. Zhu, X. Liu, R. Lu, S. Wakamatsu, and K. Takahashi

During July 2021, heavy rainstorms caused devastating floods across a wide range of areas in North China. On 20 July, a 1-hour precipitation total in Zhengzhou—the capital of Henan province in central China and home to more than 10 million people—reached 201.9 mm, breaking the record for the largest hourly precipitation in mainland China. The disastrous rainstorms inundated the city, leading to 380 fatalities or missing people.

The July mean precipitation anomalies (Fig. SB7.6a) showed two maximum centers > 8 mm day^{-1}: one in North China (red box) and one in the Yangtze River Delta. Steered by the dominant large-scale anomalous circulation, Typhoon In-fa (shown in Fig. SB7.6b) retained its status as a Category 2 storm, churning north of Taiwan and landing in the Yangtze River Delta; this led to the maximum center in the region. Meanwhile, a moist onshore flow from the East China Sea was induced by the dominant easterlies over the northern flank of Typhoon In-fa and southern flank of the westward-extended western North Pacific Subtropical High (WNPSH; Fig. SB7.6b). The easterly moisture belt formed an atmospheric river spanning thousands of miles, which continuously transported water vapor to North China. With the help of the unique terrain over North China, the windward upslope moisture flow contributed to the unprecedented extreme rainfall over North China (Figs. SB7.6c,d).

Large-scale rainfall anomalies were often directly linked with the anomalous atmospheric circulation, which was further induced by boundary layer forcing (e.g., sea surface temperatures [SST] and sea ice cover). Notably, positive SST anomalies were observed over the tropical Atlantic during July (Fig. SB7.6e), which was highest since the start of the record in 1979, and the topical Atlantic SST was historically correlated with North China rainfall (Fig. SB7.6d), suggesting its potential role in driving the abnormal North China rainfall. Associated with the tropical Atlantic SST is a circumglobal teleconnection (Branstator and Teng 2017) emanating from the North Atlantic to East Asia (Fig. SB7.6e). At the end of the teleconnection was an anticyclonic anomaly, leading to the westward-extended WNPSH, which was conducive to the transportation of water vapor into North China (Fig. SB7.6b).

In addition to the Atlantic SST anomaly, sea ice cover in the Laptev and East Siberian Seas was significantly below average in July 2021 (Fig. SB7.6f). Historically, sea ice cover in the Laptev and East Siberian Seas is negatively correlated with North China rainfall. The Arctic sea ice cover in July 2021 was the lowest since the start of the record in 1979 (see section 5d for details), which may have contributed to the positive North China rainfall anomaly (Fig. SB7.6d). The reduced sea ice cover could shift the polar vortex to southward and further enhance WNPSH over Northeast Asia and the moist onshore flow from the East China Sea, leading to the unprecedented North China rainfall in July (Fig. SB7.6f).

Monthly precipitation in August was above normal from central China to eastern Japan and in and around Mongolia. In particular, areas from western to eastern Japan experienced record-high rainfall, totaling as much as 1400 mm from mid-to-late August in association with a highly active stationary front over the region.

The widespread heavy rainfall in western and eastern Japan was partially attributed to the unusual formation of a stationary front during midsummer, which was related to a significant north–south temperature gradient in the lower troposphere between the Okhotsk High to the north of Japan and a southward-shifted WNPSH expanding to the south of Japan. The southward shift of the WNPSH that caused a large amount of water vapor flow into western and eastern Japan was related to the southward shift of the subtropical jet stream (STJ) over East Asia in the upper troposphere. Furthermore, significant southward meandering of the jet stream to the west of Japan was considered to have produced favorable conditions for updraft occurrence and persistent rainfall from western to eastern Japan. The southward shift of the STJ was likely affected by SST anomalies accompanying a negative phase of the Indian Ocean Dipole (Saji and Yamagata 2003) conditions (see section 4f) and related suppressed convection over the Asian summer monsoon region.

In conclusion, the simultaneous boundary forcings from different regions (both tropical and polar regions) led to unprecedented extreme rainfall in East Asia during the summer of 2021. Given that the Atlantic warming and Arctic Sea ice loss may be partly a manifestation of global warming, more extreme rainfall events are expected in the near future.

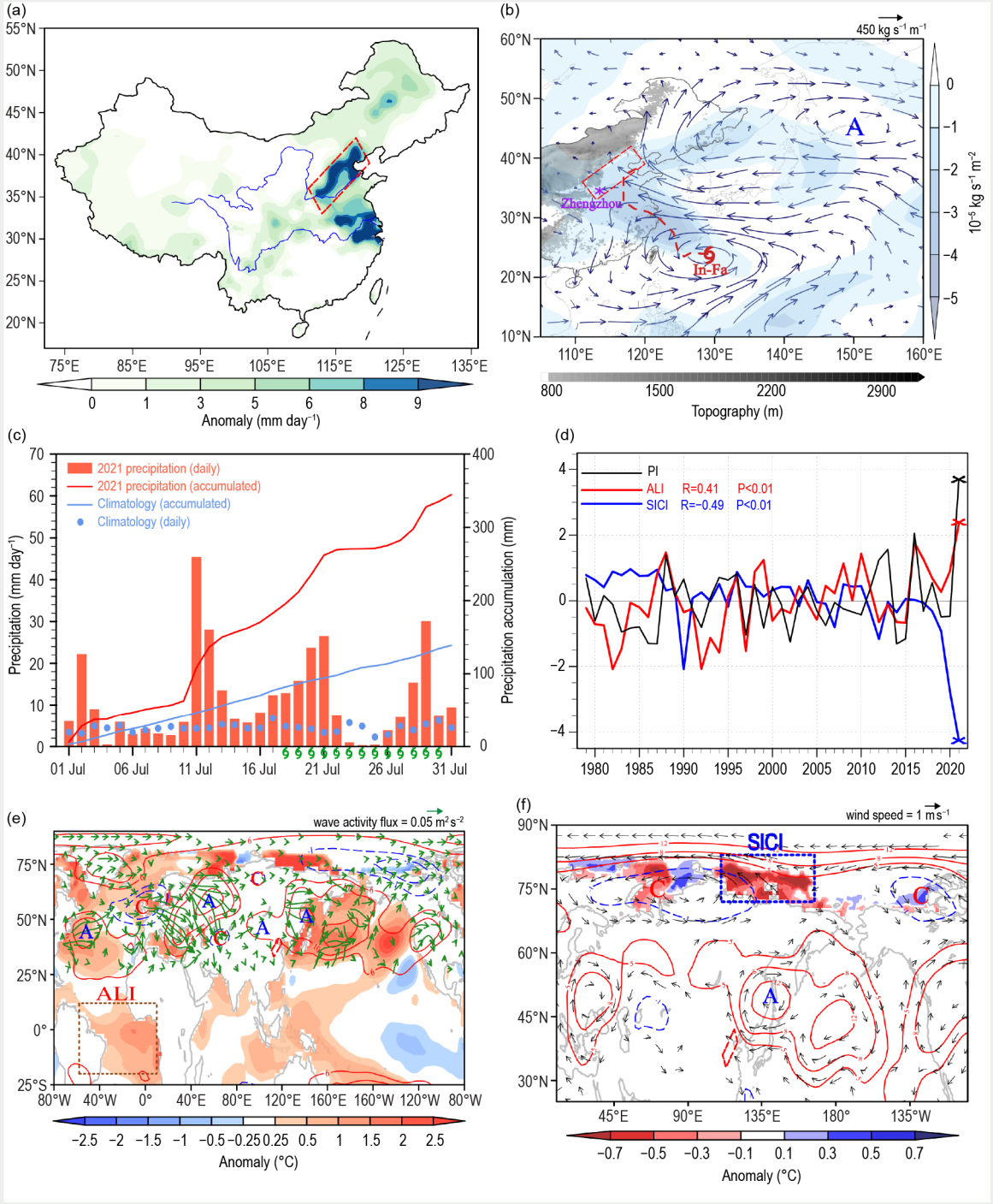

Fig. SB7.6. (a) Rainfall anomaly (shading, mm day^{-1}) in China for Jul 2021. (b) The 1000–700-hPa integrated moisture flux anomaly (vector, kg s^{-1} m^{-1}) and convergence (shading, × 10^{-5} kg s^{-1} m^{-2}) in July 2021; gray shading is topography (m), the dashed curve denotes the moving track of Typhoon In-fa, and the purple asterisk marks the city of Zhengzhou. (c) Evolution of the daily precipitation (mm day^{-1}) and accumulated precipitation (mm) averaged in Jul over North China. The green typhoon sign marks the duration of Typhoon In-fa. (d) The standardized time series of the North China precipitation index (PI, black, for averaged mean precipitation over North China), the tropical Atlantic sea surface temperature index (ALI, red, averaged mean SST over brown box in [e]), and the Arctic sea ice cover index (SICI, blue, averaged mean sea ice cover over black box in [f]) in July. The correlation coefficient between the PI and ALI (SICI) is shown in red (blue). (e) SST anomalies in Jul 2021 (shading, °C), and the regressed 500-hPa geopotential height (contour, gpm), wave activity flux (vector, m^2 s^{-2}) onto ALI. (f) Sea ice cover anomalies in Jul 2021 (shading, °C), and the regressed 500-hPa geopotential height (contour, gpm) and wind (vector, m s^{-1}) onto SICI. The letters A and C denote the centers of the anticyclonic and cyclonic anomalies, respectively. The dashed box in (a), (b), (e), and (f) outlines North China.

4) SOUTH ASIA—O. P. Sreejith, A. K. Srivastava, and M. Rajeevan

Countries in this section include Bangladesh, India, Pakistan, and Sri Lanka. Unless otherwise noted, climate anomalies are relative to the 1981–2010 base period.

(i) Temperature

In 2021, South Asia generally experienced above-normal temperatures. The annual mean land surface air temperature averaged over India was 0.44°C above normal, making 2021 the fifth-warmest year on record since nationwide records commenced in 1901 (Fig. 7.49). Seasonal mean temperatures were above normal for all seasons. The winter season (January–February, 0.78°C above average) and post-monsoon season (October–December, +0.42°C) mainly accounted for the above-normal annual temperature. The five-warmest years on record in order are: 2016 (+0.71°C), 2009 (+0.55°C), 2017 (+0.54°C), 2010 (+0.54°C), and 2021 (+0.44°C).

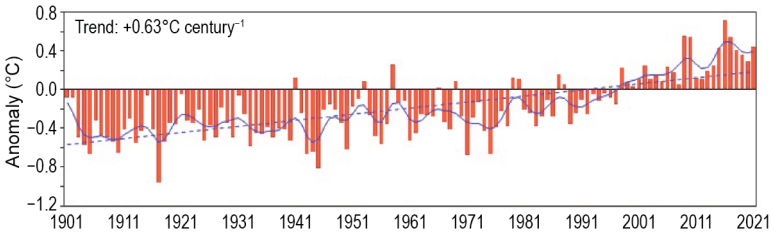

Fig. 7.49. Annual mean temperature anomalies (°C; 1981–2010 base period) averaged over India for the period 1901–2021. The smoothed time series (9-point binomial filter) is shown as a continuous blue line. The dotted blue line depicts the linear trend (°C century^{-1}).

(ii) Precipitation

The summer monsoon season (June–September) contributes about 75% of the annual precipitation over South Asia. In 2021, the summer monsoon set in over Kerala (southwestern parts of Indian peninsula) on 3 June (climatological normal is 1 June). The monsoon covered the entire country on 13 July (climatological normal is 8 July).

For India, the long-term average (LTA) of the summer monsoon rainfall, calculated using all data from 1961 to 2010, is 880 mm with a standard deviation of about 10%. However, over smaller regions, the standard deviation is much larger (around 19%). During 2021, the Indian summer monsoon rainfall (ISMR) averaged over India as a whole was 99% of its LTA value. Rainfall was fairly well distributed over the country, except for the eastern and northeastern regions. Seasonal rainfall was 96%, 104%, 111%, and 88% of LTA, respectively, over the homogeneous regions of Northwest India, Central India, South Peninsula, and East and Northeast India. On the monthly scale, rainfall for the country as a whole was above normal during June and September (110% and 135% of LTA, respectively) and below normal during July and August (93% and 76% of LTA, respectively). For the country as a whole, spatially-averaged rainfall was above or near-normal both at the beginning and end of the season (Figs.7.50, 7.51).

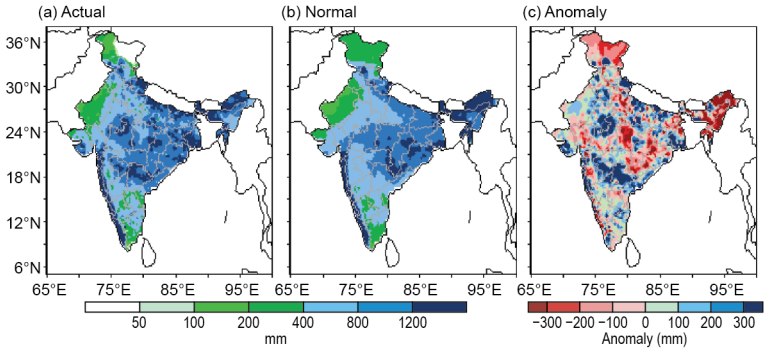

Fig. 7.50. Spatial distribution of (a) actual, (b) normal, and (c) anomalous monsoon seasonal (Jun–Sep) rainfall (mm) over India in 2021.

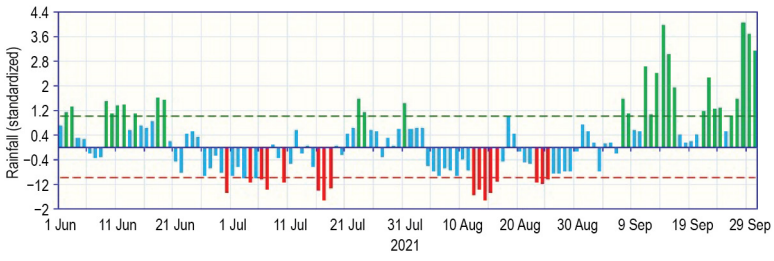

Fig. 7.51. Daily standardized rainfall time series averaged over the core monsoon zone of India for the period 1 Jun–30 Sep 2021.

Rainfall over India was below normal (68% of its LTA) during the winter season (January–February) and was above normal (118% and 144% of LTA) during the pre-monsoon season (March–May) and the post-monsoon season (October–December).

Pakistan, which is at the western edge of the pluvial region of the South Asian monsoon, received 60–70% of its annual rainfall during the summer monsoon season (July–September). The summer monsoon typically sets over eastern parts of Pakistan around 1 July, with a standard deviation of five days. In 2021, summer monsoon rainfall over Pakistan was normal (89% of LTA). Pakistan observed normal rainfall during July (104% of LTA), significantly below-normal rainfall during August (38%), and significantly above-normal rainfall during September (160%). During September, the monthly rainfall totals were generally above average throughout the country and significantly above average over South Pakistan and areas of Punjab province. The post-monsoonal rainfall (October–December) in 2021 was 89% of the LTA. However, in October, Pakistan as a whole received exceptionally above-normal rainfall (234.3% of its LTA), making it the fifth-wettest month on record since the start of the record in 1961. The unusually high rainfall totals during October were mainly associated with Severe Cyclonic Storm Shaheen, which formed at the beginning of the month, as well as subsequent passages of frequent westerly waves, with troughs affecting the region.

Bangladesh received normal rainfall (104% of its LTA) during its summer monsoon season in 2021 (May–September), while Sri Lanka received above-normal rainfall during its summer monsoon season.

Toward the end of the year, the northeast monsoon (NEM) set in over the southern Indian peninsula on 25 October and over Sri Lanka in late November. The NEM contributed 30–50% of the annual rainfall over the southern Indian peninsula and Sri Lanka as a whole. Seasonal rainfall over this region was exceptionally above normal (171% of LTA) and was the highest (579.1 mm) since the start of the record in 1901. The exceptionally above-normal rainfall during the season was mainly due to the frequent formation of many low-pressure systems. Northeast monsoon rainfall activity over Sri Lanka during October–December, however, was normal.

(iii) Notable events and impacts

In 2021, thunderstorms and lightning claimed around 800 lives across different parts of India. On 12 July, at least 74 people were killed by lightning strikes in Rajasthan, Uttar Pradesh, and Madhya Pradesh. At least 41 people—mostly women and children—were reportedly killed in Uttar Pradesh state. The highest death toll of 14 was recorded in the city of Allahabad. In Rajasthan, 11 people were killed when they were struck by lightning at Amer Fort near Jaipur.

Heavy rainfall and flood-related incidents claimed over 750 lives across different parts of India during the year. Of those lives lost, 215 were from Maharashtra, 143 from Uttarakhand, 55 from Himachal Pradesh, 53 from Kerala, and 46 from Andhra Pradesh.

In Bangladesh, continuous heavy rains from late July to early August caused severe floods, which claimed 21 lives. More than 2.6 million people were affected, and there was widespread loss of crops and houses.

During the monsoon season in June, 46 people died on the 16th and 17th due to severe floods in Nepal, and 10 people died in Bhutan. In another incident, during the first week of July, floods and landslides associated with heavy rains claimed 74 lives in Nepal. During 16–22 October, more than 100 people died due to floods and landslides resulting from heavy rains. In Sri Lanka, 26 people died due to floods associated with intense rainfall on 6–7 October.

During 2021, five tropical cyclones formed over the North Indian Ocean. Extremely Severe Cyclonic Storm Tauktae, which formed during the pre-monsoon season over the Arabian Sea, crossed the Saurashtra coast on 17 May. The storm claimed 144 lives, mainly from western India, stretching from Kerala in the far southern part of the country to Gujarat in the northwest. Severe Cyclonic Storm Yaas (23–28 May), which formed during the pre-monsoon season over the Bay of Bengal, crossed the north Odisha coast on 26 May, and caused nine fatalities. Over 1.3 million people in total were affected by the floods. Cyclonic Storm Gulab (24–28 September) crossed the north Andhra Pradesh/south Odisha coasts on 26 September, claiming 19 lives in the coastal

districts. See section 4g5 and Fig. 4.36 in The Tropics chapter for more details about the 2021 North Indian Ocean cyclone season. The tracks of these cyclonic storms are shown in Fig. 7.52.

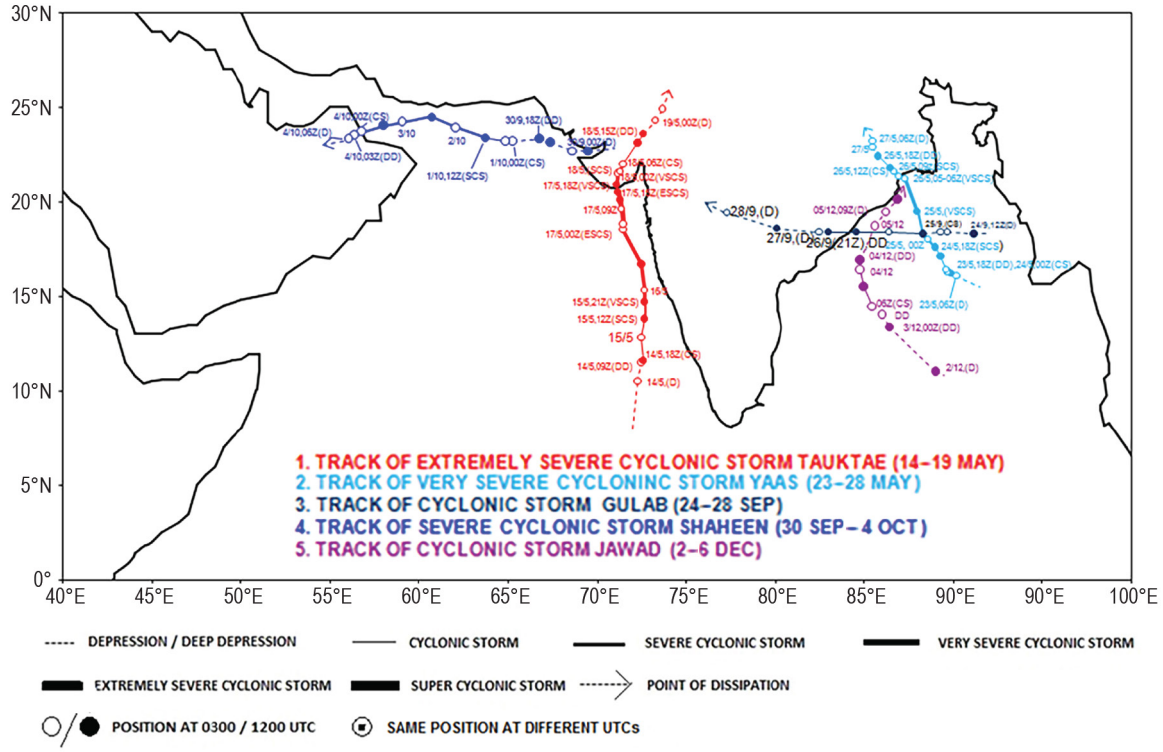

Fig. 7.52. Storm tracks of all cyclones that formed in the North Indian Ocean basin in 2021.

5) SOUTHWEST ASIA—A. Vazifeh, A. Fazl–Kazem, P. Asgarzadeh, and M. Mohammadi

This section only covers Iran. Climate anomalies are relative to a 1981–2010 base period for temperature and precipitation.

(i) Temperature

Based on synoptic station data analysis (around 500 stations), the annual average temperature for Iran in 2021 was 19.4°C, 1.9°C above normal. The annual maximum average temperature was 26.6°C, 2.2°C above normal, and the annual minimum average temperature was 12.2°C, 1.6°C above normal. West of the country, temperatures over the Zagros Mountains and plains in northern parts of the Persian Gulf were 1.6–2.5°C above normal, and all provinces were warmer than normal (Fig. 7.53).

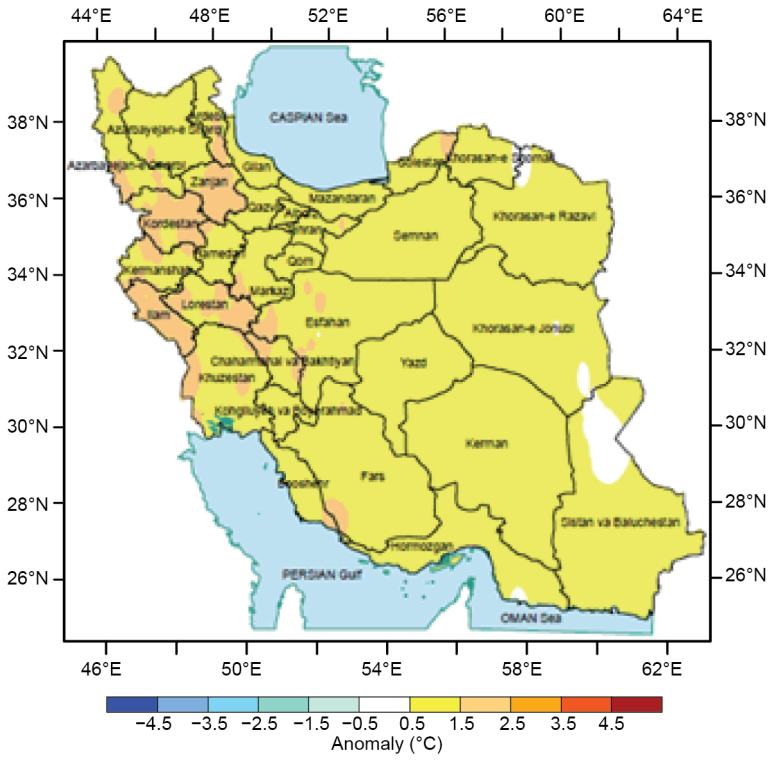

Fig. 7.53. Annual average temperature anomalies (°C; 1981–2010 base period) in Iran for 2021.

(ii) Precipitation

The average annual accumulated precipitation for all provinces in Iran was below normal (53.7% of normal), the lowest since 1991. The greatest deficits occurred in

the central Zagros Mountains in western and southwestern Iran, in the domains of the Alborz extending north, in the southern Caspian Sea, and in the south in provinces along the Persian Gulf. The three greatest deficits were observed in: Bushehr (24.8% of normal), Sistan va Baluchestan (26.3%), and Hormozgan (29.2%) provinces, all in southern and southeastern Iran (Fig. 7.54).

Thus, exceptional below-normal annual precipitation, together with above-normal temperatures, made 2021 the driest year on record since 1991, as shown by the standard precipitation index (SPI, Fig. 7.55).

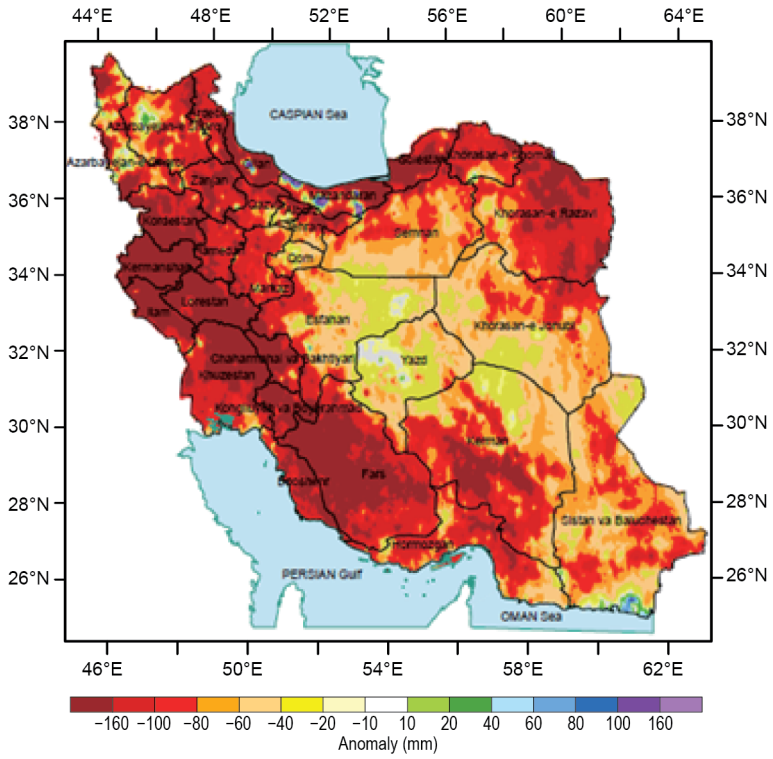

Fig. 7.54. Annual average precipitation anomalies (mm; 1981–2010 base period) in Iran for 2021.

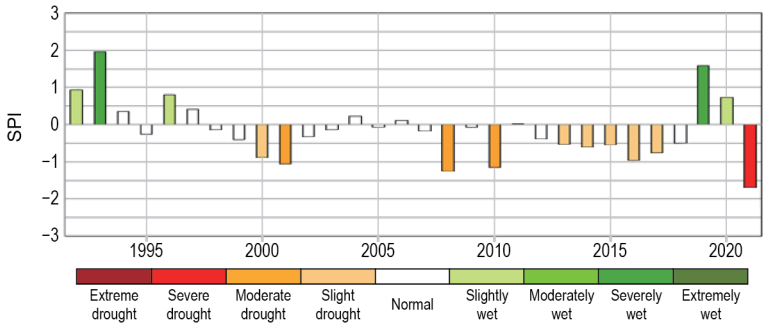

Fig. 7.55. Timeseries of the standard precipitation index (SPI) for Iran over the period 1992–2021.

6) CENTRAL ASIA—W. M. Thiaw, S. Fuhrman, and M. F. Zaheer

Central Asia is a landlocked, semi-arid region spanning a wide latitudinal area that extends from the northern temperate zone, with Russia at its northern border, to the southern subtropics. It exhibits a complex topography, ranging from vast plains to high mountains, with the Caspian Sea at its western edge. Its climate is diverse and is influenced by the strong inhomogeneity of the terrain. For the purpose of this analysis, Central Asia is defined as the region encompassing the countries of Afghanistan to the south; from east to west, Turkmenistan, Uzbekistan, Tajikistan, and Kyrgyzstan in the central part of the region; and Kazakhstan to the north. Unless otherwise specified, the climatological base period is 1991–2020 for both temperature and precipitation.

(i) Temperature

Climatologically, annual mean temperatures were lowest (0° to –10°C) over the central and southern areas of Tajikistan. The northern and east central areas encompassing northern Kazakhstan, Kyrgyzstan, western Tajikistan, and northeastern Afghanistan registered average temperatures (0° to 15°C). Mean temperatures were higher (15° to 25°C) over western Afghanistan, while they were (15° to 20°C) over eastern and western Turkmenistan.

During 2021, the annual mean temperature was between 15° and 25°C in western Afghanistan (Fig. 7.56a). Temperatures ranged between 15° and 20°C in eastern and western Turkmenistan, and between 0° and 15°C in the remainder of the region, except for the central and eastern areas of Tajikistan, where readings dipped to –20°C. Mean temperatures were 2–4°C below normal over the Afghanistan Panhandle extending into Tajikistan and eastern Kyrgyzstan (Fig. 7.56b), making 2021 one of the coldest years, in the 5th percentile based on the 1991–2020 period. Temperature departures from average ranged between –0.5° and –1.5°C in northeastern Kazakhstan, and northern Afghanistan, and westward to the border with Turkmenistan. In contrast, western Kazakhstan and southern Afghanistan registered 0.25° to 1°C above normal, with local areas observing mean annual temperatures in the 80th to 90th percentiles.

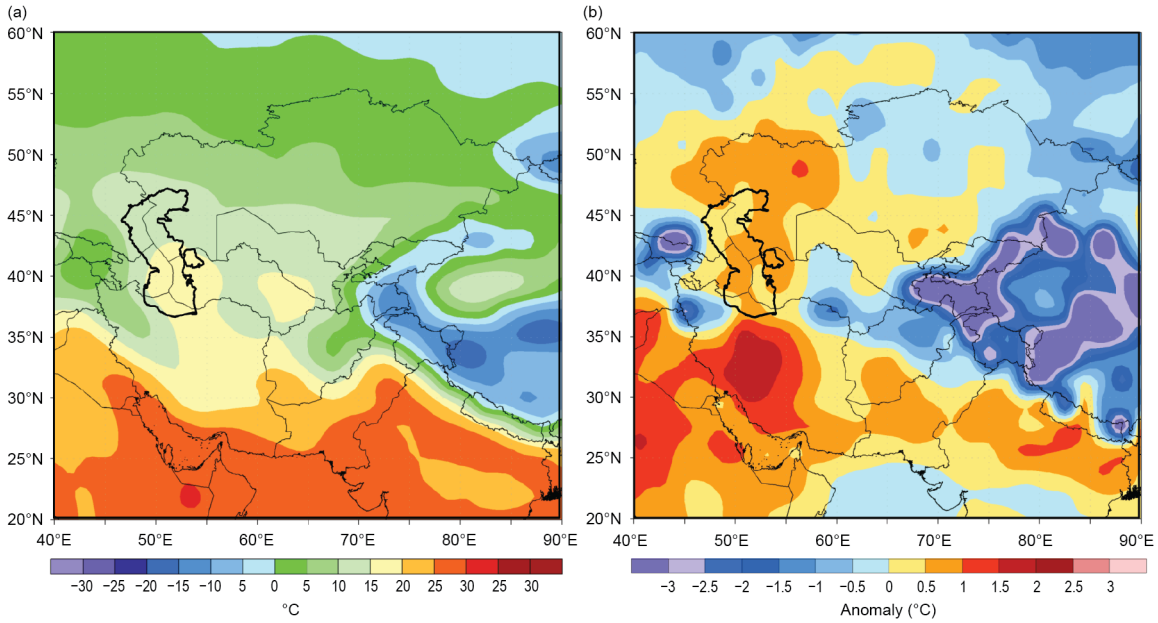

Fig. 7.56. Annual mean (a) climatological and (b) 2021 anomalous temperatures (°C) for Central Asia with respect to the 1991–2020 base period. (Source: NOAA/NCEP.)

An analysis of the evolution of temperature throughout the year shows that January was extremely cold in much of Central Asia, with temperatures hovering around –10°C in southern Kazakhstan and plunging to –20°C in the north, about 2–4°C below the mean over much of Kazakhstan. Mean temperatures were milder in February, ranging between –15°C in northern Kazakhstan to +15°C in the southern areas of the region. These were 0.5° to 3°C above the mean over much of the region, and in the 85th to 95th percentiles in southern Afghanistan.

During the spring and summer months, temperatures soared, and May was among the warmest months in the climatological period in the western two-thirds of Uzbekistan and much of Kazakhstan, with temperatures ranging between 15° and 30°C (4°C above the mean and in the 90th percentile) across this sub-region. Temperatures approached 40°C (≥ 2°C above the mean and exceeding the 85th percentile) in the southern tip of Afghanistan in July. Mean temperatures ranged between 30° and 35°C over much of the central and western sectors of the region from western Afghanistan northward into Turkmenistan, Uzbekistan, and southern Kazakhstan. These

were about 2–3°C above the mean and in the 90th percentile locally over eastern Turkmenistan and southeastern Kazakhstan. However, Tajikistan and Kyrgyzstan registered near-freezing temperatures as records indicated –5°C in eastern Tajikistan, while central Tajikistan and southern Kyrgyzstan registered 0° to +10°C. This was about 4°C below the mean and lower than the 5th percentile across Tajikistan.

Temperatures were more than 3°C below the mean across most of the mid-Central Asian countries from Kyrgyzstan and Tajikistan to Uzbekistan, including northern Afghanistan and southern Kazakhstan during October–December. This was below the 5th percentile in most areas in October and November. Freezing temperatures persisted in Tajikistan in December, falling to below –25°C (more than 3°C below the mean in far eastern Tajikistan).

The southern areas of Afghanistan and Kazakhstan, Turkmenistan, and Uzbekistan registered maximum temperatures (Tmax) between 40° and 45°C, but these were in the average range over most areas except for northwestern Kazakhstan where departures from normal ranged from +4° to +8°C. Tmax was lowest in Tajikistan, with departures ranging from 0° to –5°C (more than –8°C below the mean and less than the 3rd percentile) in August.

Annual minimum temperatures (Tmin) featured a steep east–west temperature gradient with the lowest temperatures between –20° and –30°C in eastern Tajikistan, more than 5°C below the mean, and less than the 3rd percentile. Tmin was average and hovered between 0° and 10°C in northern Kazakhstan. Tmin ranged from 0°C to 15°C from southern Kazakhstan southward to Uzbekistan and western Afghanistan. May exhibited the most elevated Tmin values (3–5°C above the mean) in the western half of Kazakhstan, while eastern Tajikistan registered Tmin values less than 5°C below the mean in November and December.

(ii) Precipitation

The climatological annual mean precipitation was variable across Central Asia and ranged from less than 200 mm over southwestern Afghanistan and central areas of Turkmenistan and Uzbekistan to 200–500 mm over central Afghanistan, far western Turkmenistan, extreme eastern Uzbekistan extending into Kyrgyzstan, and much of Kazakhstan. Precipitation was more than 500 mm over northeastern Afghanistan and Kazakhstan. Typically, winter and spring seasons accounted for the highest precipitation (rain and snow) amounts across the region, while the summer months tended to be drier.

Precipitation patterns in 2021 featured rainfall deficits across much of the region, except for a northeastern–central axis of Kazakhstan, where amounts ranged from 300 mm in the central areas to 750 mm in far northeastern sector (Fig. 7.57a), which was 25–50 mm above the mean across this sub-region (Fig. 7.57b). Deficits were highest over much of Afghanistan, the eastern areas of Turkmenistan and Uzbekistan, and western Tajikistan, where totals were as low as 10 mm to 50 mm (100–200 mm below the mean and in the 3rd percentile); in particular, totals were 300 mm below normal in southwestern Afghanistan. Totals averaged 50–150 mm (100–300 mm below the mean, below the 10th percentile) across the remainder of the sub-region. Examination of the evolution of precipitation throughout the year provided evidence of a dipole structure featuring above-average rainfall totals in northern Kazakhstan and below-average totals in the south in the areas encompassing the eastern sectors of Uzbekistan and Turkmenistan, along with Afghanistan, during winter. Precipitation totals in the north ranged from 100 mm to 300 mm (25–100 mm above the mean), and from less than 5 mm to 75 mm (50–200 mm below the mean, below 10th percentile) in the south. Much of the annual rainfall deficit was due to dryness in the winter through early spring. Precipitation was generally near-average across the region during the summer months through autumn.

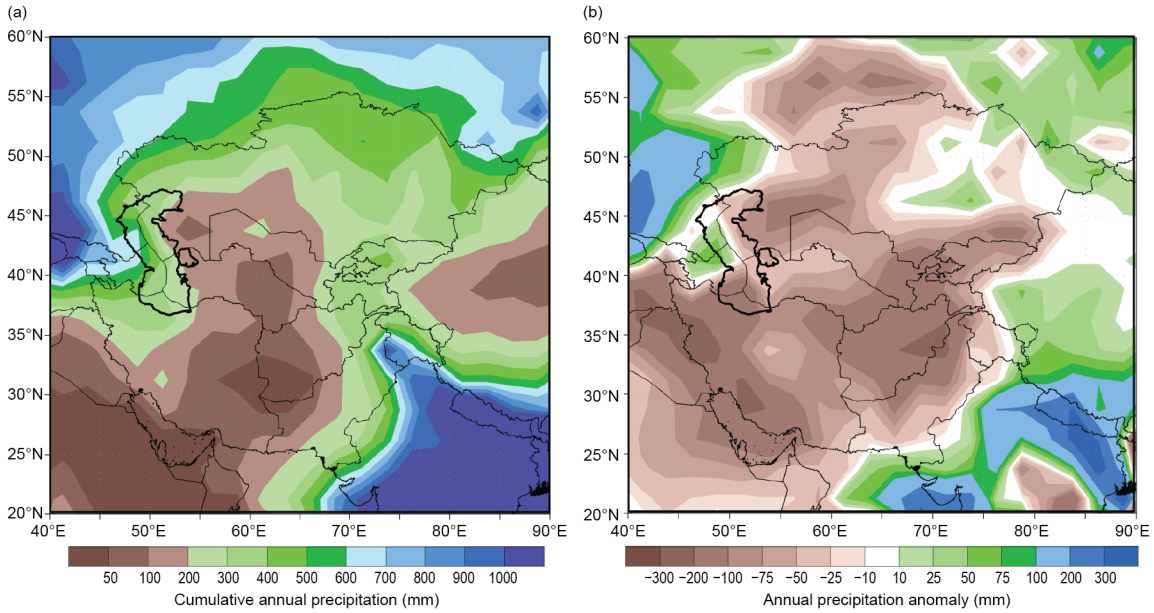

Fig. 7.57. Annual mean (a) climatological and (b) 2021 anomalous precipitation (mm) for Central Asia with respect to the 1991–2020 base period, GPCP data. (Source: NOAA/NCEP.)

(iii) Notable events and impacts

In central Afghanistan, 50–100 mm of rain fell during 27 April–3 May, according to NOAA's satellite rainfall estimates version 2 (RFE2), causing widespread flooding in the region. The Afghanistan National Disaster Management Authority reported 37 fatalities, along with the destruction of many homes that resulted in the displacement of more than 400 families.

The Aksy District in Jalal-Abad region of western Kyrgyzstan, close to the Uzbekistan border, experienced floods and landslides on 10 and 12 July due to heavy rains (~100 mm total). Kyrgyzstan's Ministry of Emergency reported that seven people were killed, and roads and four bridges were destroyed. Flood waters flowed downstream into the Namangan region of Uzbekistan, causing severe damage. The Ministry of Emergency Situations of the Republic of Uzbekistan reported eight fatalities and six injuries.

Large rainfall deficits were measured in Afghanistan during spring and autumn, with rainfall totals less than 50% of normal across the western two-thirds of the country and less than 30% of normal in the far southwest, according to data from the Global Precipitation Climatology Project (GPCP); these deficits led to a severe drought with significant impacts. The U.N. Food and Agriculture Organization estimated that wheat harvest in the region was about 20% less compared to the harvest in 2020. The U.S. Agency for International Development (USAID) projected that more than half of the country's population would be food insecure by winter 2021. In response to the humanitarian crisis, USAID disbursed more than $100 million (U.S. dollars) in food and nutrition assistance, essential healthcare, agriculture, and support to aid workers and access to critical relief supplies to care for more than 18.4 million vulnerable Afghans.

The spring drought in Afghanistan extended northward to Kazakhstan by the summer. Significant rainfall deficits were persistent here from April through August, especially in the western half of the country where totals were generally less than 50% of normal. A summer heat wave in the southern and western regions, with high record temperatures (including a reading on 7 July as high as 46.5°, which was 18° above the mean, according to the Kazakhstan Meteorological Service), exacerbated the situation. The drought, combined with the heat, resulted in the loss of thousands of livestock, depleted freshwater resources, and devastated crops. The Kazakhstan Ministry of Agriculture estimated crop yields were about 18% less compare to 2020. USAID provided Red Crescent of Kazakhstan with a grant in the amount of $100,000 (U.S. dollars) to support the population most affected by the drought.

h. Oceania—C. Ganter, Ed.

1) OVERVIEW

The region of Oceania (shown in Fig. 7.58) began 2021 with La Niña conditions in place. While regional assessments of La Niña differ slightly, conditions returned to a neutral El Niño–Southern Oscillation state in the middle of the year, with La Niña returning in the latter part of the year. La Niña typically leads to stark regional differences across the Oceania region, and 2021 reflected this, with drier conditions for some southwest Pacific Islands near the equator in the central and eastern part of the region and wetter conditions for eastern Australia. New Zealand experienced its typical warmer humid weather only during La Niña's return later in the year. The Micronesia region had a quiet year for typhoon activity, also typical of a La Niña influence. The negative Indian Ocean dipole, which was present through the middle of the year, was an additional factor contributing to Australia's wetter conditions, as was the positive Southern Annular Mode. New Zealand had its warmest year on record, with the climactic factors behind this discussed in Sidebar 7.5.

The BAMS *State of the Climate* editors and Micronesian co-authors would like to acknowledge the sad and sudden passing of Micronesian author Mark Lander in July 2022. Mark co-authored the Micronesian summary since its inclusion in the *State of the Climate* report in 2007, and he contributed immensely to the knowledge of how ENSO affects tropical storm, typhoon, and rainfall behavior in the North Pacific. Mark will be a huge loss to the tropical weather and climate community. Our thoughts and prayers are with his family during this solemn time.

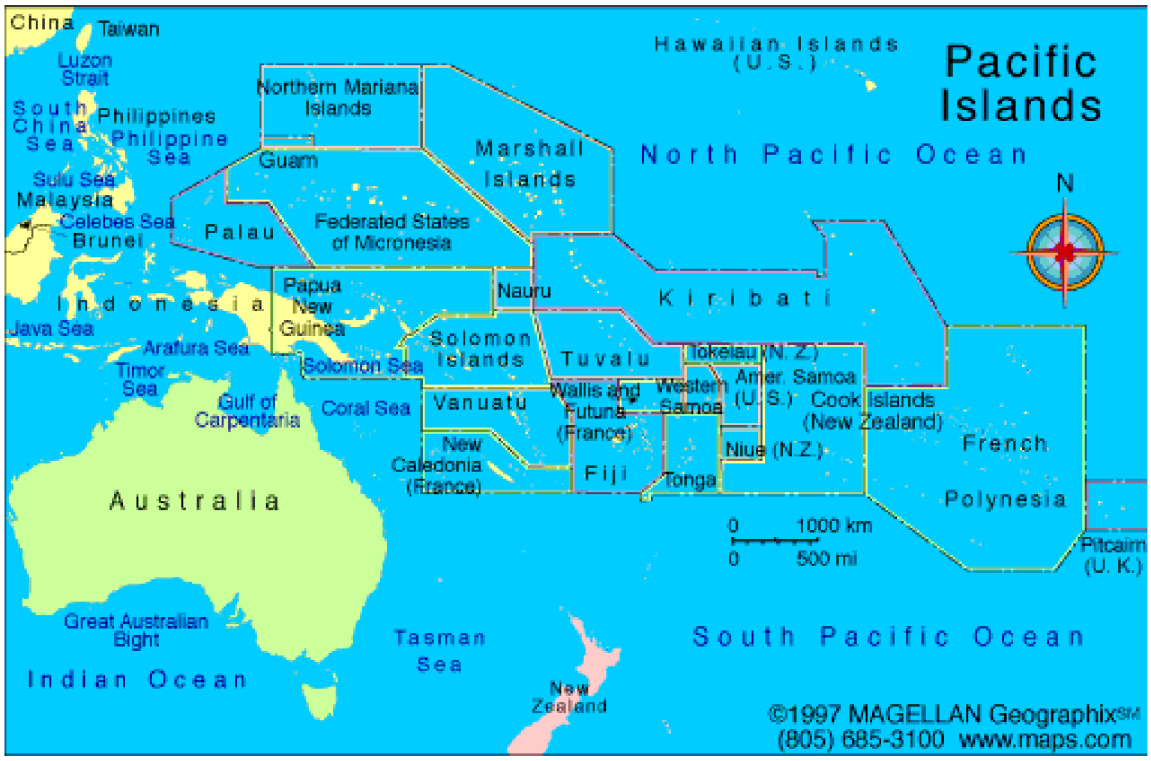

Fig. 7.58. The Oceania region as considered in this report includes the Pacific Islands from the Northern Mariana Islands in the western North Pacific to New Zealand in the south, Australia, Papua New Guinea, and Palau in the west, but excluding the islands of Indonesia, to French Polynesia in the east. (Source: https://www.infoplease.com/atlas/pacific-islands.)

2) NORTHWEST PACIFIC AND MICRONESIA—M. A. Lander, B. Bukunt, and C. P. Guard

This assessment covers the area from the date line west to 130°E, between the equator and 20°N. It includes the U.S.-Affiliated Islands of Micronesia, but excludes the western islands of Kiribati and nearby northeastern islands of Indonesia.

For much of Micronesia, the weather and climate of 2021 will be remembered for it being unusually quiet, with few extremes of wind, waves, or rainfall. There was a profound lack of tropical storms and typhoons in the western North Pacific basin, leading to quiet conditions throughout the region. Rainfall and temperature were near-average at most locations. Two La Niña characteristics stand out: (1) extreme dryness was confined to locations along the equator and (2) higher-than-normal sea levels exacerbated the magnitude of inundation from two high wave events in December.

(i) Temperature

Temperatures across Micronesia during 2021 varied regionally with both above- and below-average readings. The average 6-month maximum and minimum temperature anomalies are summarized in Table 7.1. Generally, warm daytime maximum temperatures are typically experienced in the Micronesian islands when skies are clear and winds are light; cooler temperatures occur when conditions are unusually cloudy, wet, and windy.

Table 7.1. Average 6-month temperature anomalies (Jan–Jun and Jul–Dec), and 6-month and annual rainfall totals and percent of average values for selected Micronesia locations during 2021. The average values are for the 1981–2010 base period. Latitudes and longitudes are approximate. "Kapinga" stands for Kapingamarangi Atoll in Pohnpei State, Federated States of Micronesia. The color fill of the boxes indicates: red for above average temperature and blue for below average; green for above average rainfall and yellow for below average rainfall. Note: extreme warmth at Saipan and at Yap are likely the result of ASOS sensor problems and a station relocation, respectively. The coolness at Palau may also be an effect of a relocation of the WSO Palau from the town of Koror to the international airport in Airai.

Location	Max Temp Min Temp		Rainfall (mm)							
	Jan–Jun	Jul–Dec	Jan–Jun	Jan–Jun	Jan–Jun	Jul–Dec	Jul–Dec	Jul–Dec	Jan–Dec	Jan–Dec
	°C	°C	AVG	2021	%	AVG	2021	%	2021	%
Saipan 15°N, 146°E	+1.87 +1.31	+0.69 +0.45	462.8	429.01	92.7	1306.1	1379.5	105.6	1808.5	102.2
Guam 13°N, 145°E	+0.06 +0.43	−0.04 +0.29	678.7	585.7	86.3	1813.6	1951.	107.6	2537.2	101.8
Yap 9°N, 138°E	−0.89 +1.24	−0.67 +1.40	1191.5	1662.8	139.5	1943.4	1689.4	86.9	3351.5	106.9
Palau 7°N, 134°E	−1.53 −0.35	−1.02 −0.67	1798.1	2170.4	120.7	2279.4	2525.3	110.8	4695.7	115.2
Chuuk 7°N, 152°E	−0.26 +0.68	−0.12 +0.75	1678.2	2102.9	125.3	1970.7	2122.7	110.7	4225.5	117.5
Pohnpei 7°N, 158°E	−0.70 +1.31	−0.49 +1.38	2361.2	3036.8	128.6	2308.4	2354.8	102.0	5391.6	115.5
Kapinga 1°N, 155°E	n/a	n/a	1880.6	1691.9	90.0	1485.1	1065.3	71.7	2757.2	81.9
Kosrae 5°N, 163°E	−0.19 −0.30	−0.23 +0.11	635.8	3941.3	149.5	2354.8	2686.0	114.1	6627.4	132.8
Majuro 7°N, 171°E	−0.14 +0.59	+0.23 +0.51	1459.0	2064.3	141.5	1875.0	1872.7	99.9	3937.0	118.1
Kwajalein 9°N, 168°E	+0.56 −0.05	+0.06 −0.04	898.4	831.9	92.6	1553.7	1319.8	84.9	2151.6	87.7

(ii) Precipitation

The average 6-month (January–June and July–December) and annual rainfall values for selected locations across Micronesia are summarized in Table 7.1. Three characteristics of the Micronesia regional precipitation during 2021 were particularly notable: (1) extreme dryness at Kapingamarangi; (2) a general tendency for wet conditions in central and western Micronesia, with drier conditions in the north (e.g., Saipan and Guam) and far east (e.g., Majuro and Kwajalein) for much of 2021; and (3) a record wet October at Guam.

Wet conditions across the average latitudes of the ITCZ (4°–8°N) are typical during La Niña. Also typical for La Niña is extreme dryness at Kapingamarangi and other locations along the equator. Dryness in eastern Micronesia (e.g., Majuro and Kwajalein) is often experienced during a prolonged La Niña event. Late in 2021, abundant rainfall returned to Kapingamarangi to help that island recover from the effects of long-term drought. On Guam, a large deficit of accumulated rainfall during a very dry 9-month period (January–September) was completely erased with record rainfall during October (Fig. 7.59).

Fig. 7.59. Guam accumulated rainfall deficit for 2021. Gray line denotes lowest point in 2021.

(iii) Notable events and impacts

The Pacific climate system entered La Niña in the second half of 2020, and these conditions were present through much of 2021. During La Niña, prolonged dryness with accompanying drought is typically experienced at islands near the equator (e.g., at Kapingamarangi). In keeping with a typical response to La Niña, conditions were very dry at Kapingamarangi (1.1°N, 154.8°E). Prolonged dry conditions there led to severe drought conditions that impacted potable water supplies, local vegetation, and food crops. A few islands away from the equator (e.g., the northern Marshall Islands) also experienced some periods of unusual dryness, but the dryness in these locations was not accompanied by severe impacts.

Persistent dryness at Guam during January–September abruptly ended with very wet conditions in October. The 677.7 mm of rainfall observed at the Guam Weather Forecast Office was a modern-day (post-World War II) record. Contributors to this high rainfall total included some passing tropical disturbances and slow-moving diurnal island thunderstorms in light-wind (i.e., 'doldrum') conditions.

The western North Pacific typhoon season of 2021 was quiet (Fig. 7.60), which is typical for the Micronesia region during La Niña. The Joint Typhoon Warning Center (JTWC) upgraded only 10 of the basin's tropical cyclones to typhoon status—the fourth lowest annual total in its 62-year historical record (the Japan Meteorological Center reported only 9 typhoons). Within Micronesia, only Palau experienced some moderate effects (gales and high surf) when Tropical Storm Rai passed close by in December. Several tropical

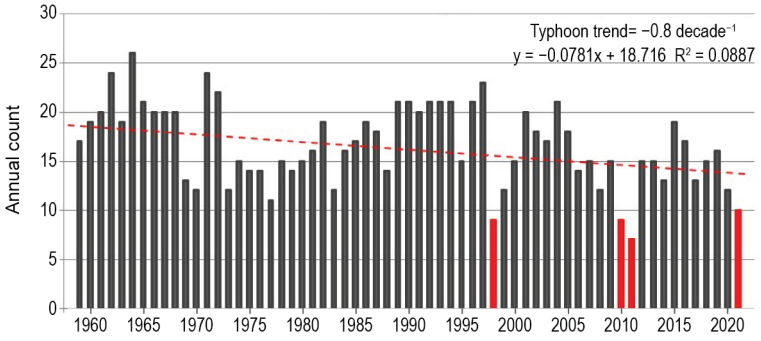

Fig. 7.60. JTWC annual count of typhoons in the western North Pacific Basin. The four lowest years are shaded red. The red dashed line indicates a general decreasing trend of typhoons occurrence over the six decades.

disturbances, including some that later became named tropical cyclones, made beneficial contributions to seasonal rainfall at islands across western Micronesia and at Guam. The island of Guam has not had a major typhoon (Category 3 or higher) since Typhoon Pongsona devastated the island in December 2002. See section 4g4 for more details on the 2021 western North Pacific tropical cyclone activity.

Much higher-than-average sea level across the tropical western Pacific is typical during La Niña. Indeed, sea level stands by the summer of 2021 were near their historical peaks throughout Micronesia. Time series of the sea level from two widely separated stations (Guam and Kwajalein) illustrate the strength of the coherence of the regional sea level, and the historical perspective of the very high stands during 2021 (Fig. 7.61). At Guam, the high stand reached during mid-2021 was the second highest in the historical record. Since 1998, the magnitude of sea level rise in the tropics of the western North Pacific has been among the highest in the world. The character of this rise was not gradual, but instead is best described as a step-function jump during 1998. The sea level increased by 30 cm from its low stand at the end of 1997 to a historically high stand at the end of 1998 (Fig. 7.61). Elevated sea levels then persisted to the present, with three major short-term dips during the 2002, 2015, and 2018 El Niño events. Very high sea level in the tropics of the western North Pacific is not a signal of climate change, but rather an artefact of a substantial increase in the strength of the Pacific trade-wind system (Merrifield et al. 2011). An abrupt increase in the strength of the trade winds in 1998 separates the recent historical climate of the western Pacific into two regimes: (1) weak trade winds, low sea level (1975–1998); and (2) strong trade winds, high sea level (1998–present).

During early December, two storm systems—Typhoon Nyatoh and an intense cut-off low to the northwest of Hawaii—churned up large waves that affected islands throughout the region. The large waves from these two concurrent storm events coincided with the monthly highest tides. In addition, due to La Niña conditions, the background sea level was 10–20 cm above average. Buoys in the region captured the long-period swell in real time. The following impacts were noted on the Kwajalein Atoll: flooding occurred on Roi Nemur and on Ebeye on 4–5 December; Yap Island and some of the outer islands received serious inundation, with water reported far inland; water inundation was reported up to 13 meters inland on some atolls of Chuuk State; and on Pohnpei, Nukuoro received inundation, and water penetrated 6 meters inland as far south as Kapingamarangi.

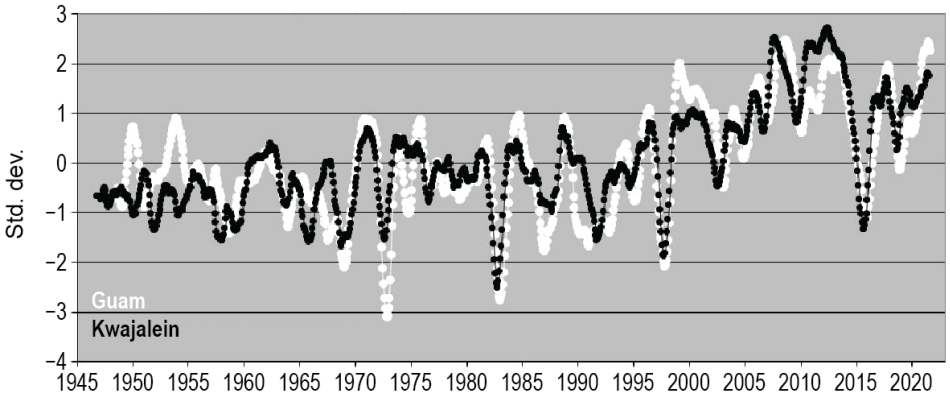

Fig. 7.61. Twelve-month moving average of the sea level anomaly at Guam (13.4°N, 144.8°E, white) and at Kwajalein (8.7°N, 167.7°E, black) during 1948 to present. Plotted values are normalized using their respective standard deviations. Note the continual high stands of the sea since 1998 at both stations. Note also the absolute historical high stands during 2010 through 2012 (a period of prolonged La Niña). At Guam, the high stand reached during mid-2021 was the second highest in the historical record. Strong El Niño events stand out as sharp dips. Note: y-axis is unitless due to normalization.

3) SOUTHWEST PACIFIC—E. Chandler

Countries considered in this section include American Samoa, Cook Islands, Fiji, French Polynesia, Kiribati, New Caledonia, Niue, Papua New Guinea (PNG), Samoa, Solomon Islands, Tonga, Tuvalu, Vanuatu, and Wallis and Futuna (Fig 7.58). The temperature analysis is based on the Climate Anomaly Monitoring System (CAMS) monthly surface air temperature anomalies. Anomalies are with respect to the 1991–2020 base period. The precipitation analysis is based on monthly analyses presented in the Climate and Oceans Support Program in the Pacific (COSPPac) Monthly Bulletin and COSPPac Online Climate Outlook Forum. The base period for precipitation is 1991–2020.

The year began with a mature La Niña event, with the tropical Pacific transitioning to a neutral ENSO state in the second quarter of the year. Sea surface temperatures were below average across the central and western equatorial Pacific during the first two months of 2021, before the cool regions retracted eastward and became patchy from March onwards as the equatorial water warmed. The tropical Pacific remained ENSO neutral during the middle months of the year before signs of La Niña re-emerged as the equatorial Pacific water again showed signs of cooling into the third quarter. Atmospheric indicators of the developing La Niña lagged the ocean cooling, although by October there was evidence of coupling, with trade winds strengthening and a reduction in cloud and rainfall near the date line.

Air temperatures and rainfall were both typical of a La Niña event at the beginning of 2021 and again as La Niña re-emerged toward the end of the year. Air temperatures began the year below normal along the equator, with warm anomalies in the far western Pacific. By March, air temperatures were near-normal in the equatorial Pacific and persisted until the last quarter of the year when above-normal temperatures became established to the east of the Maritime Continent and in a broad arc from PNG to French Polynesia. Rainfall was suppressed along the equator on and to the east of the dateline for most of the year, with the strongest anomalies in the western Pacific occurring at the start of 2021. In the off-equatorial South Pacific, positive rainfall anomalies were most evident along the South Pacific Convergence Zone (SPCZ) and at the beginning and end of the calendar year, coinciding with the southern wet season (approximately November to April). As expected, rainfall was more mixed for South Pacific countries during mid-year as ENSO-neutral conditions prevailed.

(i) Temperature

Air temperatures were below-normal along the equator at the start of 2021 and then warmed in this region during the first quarter of the year (Fig 7.62a). During January, a large region of temperatures 1–2°C below normal stretched from Nauru eastward past the Line Islands of Kiribati along the equator; however, by March this region had warmed to near-normal. A small region with air temperatures 1–2°C above normal was present in the far western Pacific near PNG during January, and a relatively large area covering the southern Cook Islands and southern French Polynesia had temperatures 1–3°C above normal. Both these regions returned to near-normal temperatures by March. The areas of above-normal temperatures during JFM were associated with above-normal SSTs in the same regions.

During April–June (AMJ), air temperatures across the equatorial Pacific remained close to normal. Small regions of air temperatures of 1–2°C below normal persisted in the far eastern Pacific near the coast of South America (Fig. 7.62b).

During July–September, the region covering the southern Cook Islands and southern French Polynesia warmed again, with temperature anomalies of +1° to +2°C (Fig. 7.62c). Warm anomalies of this magnitude were also present during August in a region around southern PNG. The region of warm air temperatures was associated with above-normal sea surface temperatures in the same area, with the highest anomalies near the southern Cook Islands and southern French

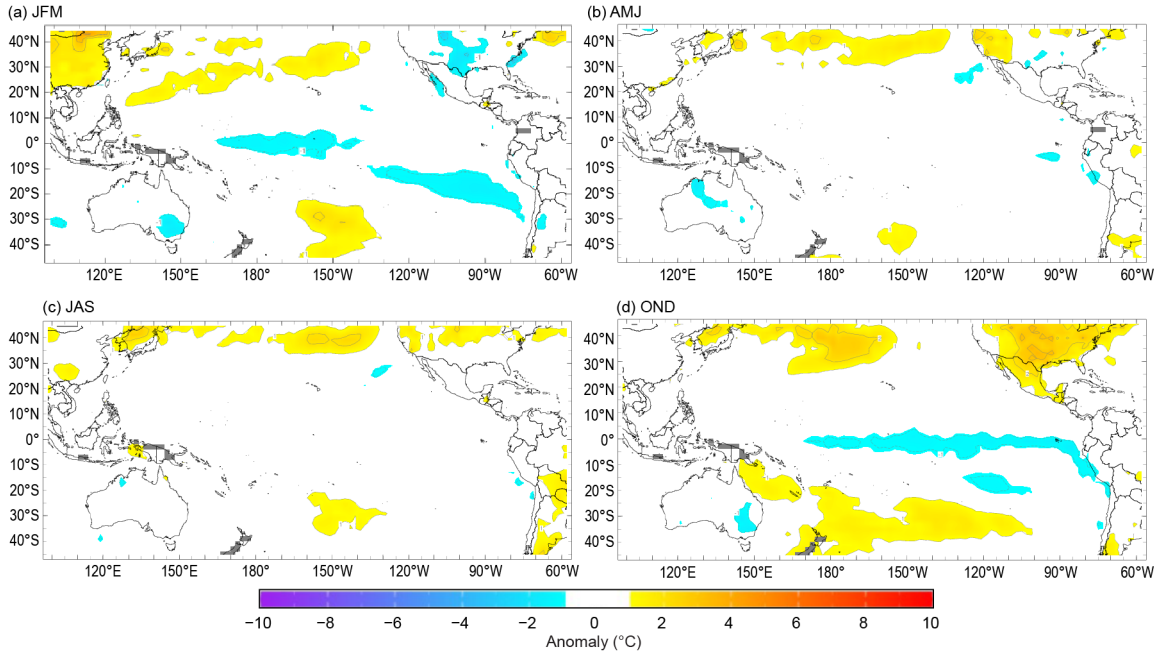

Fig. 7.62. Seasonal air temperature anomalies (°C) for (a) Jan–Mar, (b) Apr–Jun, (c) Jul–Sep, and (d) Oct–Dec. (Source: CAMS.)

Polynesia. Air temperatures across the equatorial Pacific were otherwise close to normal, with small areas of air temperatures 1–2°C below normal in the far eastern Pacific during September.

During the last quarter of the year, a region of positive anomalies (1–2°C above normal) in the South Pacific re-emerged near PNG and expanded southeastward in a narrow arc to encompass New Caledonia and as far south as New Zealand during November, although this weakened in spatial extent and strength by December. In contrast, the emerging La Niña contributed to regions of negative air temperature anomalies off the South American coast and extended along the eastern equatorial Pacific during October. The region of –1° to –2°C anomalies extended along the equator as far west as far as the date line by December, with a small region more than 3°C below normal observed in the far eastern Pacific (Fig. 7.62d).

(ii) Precipitation

Rainfall patterns at the start of the year reflected typical La Niña patterns across the tropical Pacific, including rainfall deficits along the equator in JFM and positive rainfall anomalies over most off-equatorial South Pacific Islands. The SPCZ was located to the south of its climatologically-normal position during JFM, bringing it closer to Vanuatu and Fiji (Figs. 7.63a–c). As a result of the SPCZ shifting south, a narrow band of positive rainfall anomalies was located between the Solomon Islands and Vanuatu, contributing to rainfall totals above the 90th percentile in Fiji, PNG, Tonga, and Vanuatu. Lemap (Vanuatu) recorded its third wettest JFM in its 61-year record (1294 mm). Conversely, the central and western equatorial regions from west of Nauru to eastern Kiribati experienced suppressed rainfall through the first quarter of 2021.

The SPCZ was close to its long-term average position during AMJ (Figs. 7.63d–f) as the tropical Pacific returned to ENSO neutral. The region experienced a mixed rainfall pattern during the second quarter of the year; during April there was a region of positive rainfall anomalies from PNG southeast through the Solomon Islands and New Caledonia, while negative rainfall anomalies were evident in a region straddling the date line during April and June. The southern Cook Islands, northwestern PNG, and Tonga all received rainfall above their 90th percentiles for the AMJ quarter. Rarotonga (Cook Islands) recorded its third wettest AMJ on record in its 123-year record (888 mm), as did Niuofo'ou (Tonga) in its 47 year-record (862 mm). Conversely, Samoa and the eastern Solomon Islands observed rainfall below their 10th percentiles during AMJ.

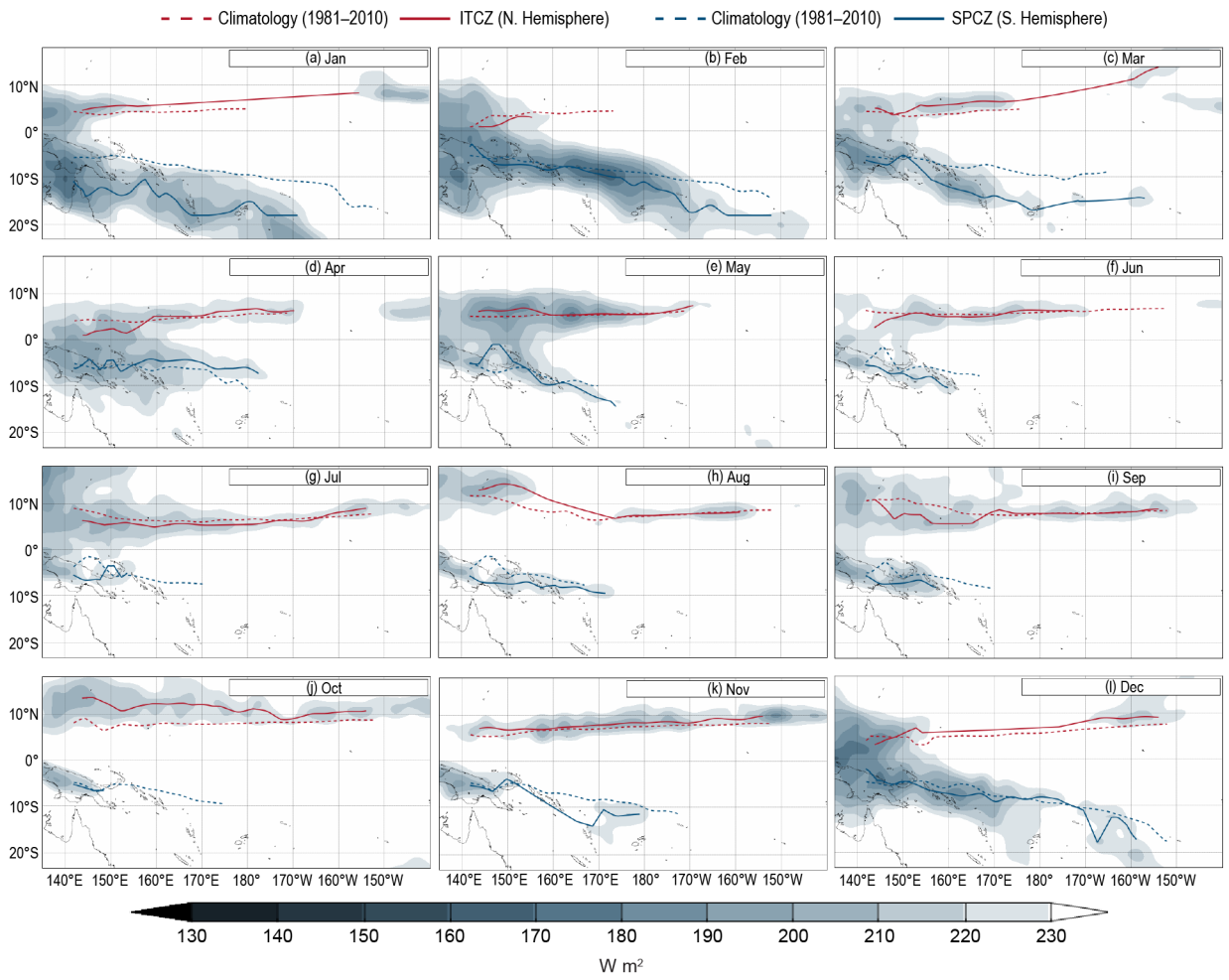

Fig. 7.63. South Pacific Convergence Zone (SPCZ) represented by 30-day average outgoing longwave radiation (OLR) monthly minimums for (a) Jan, (b) Feb, (c) Mar, (d) Apr, (e) May, (f) Jun, (g) Jul, (h) Aug, (i) Sep, (j) Oct, (k) Nov, and (l) Dec.

During JAS, the SPCZ was weak (Fig. 7.63g) before becoming more active and displaced to the south (compared to its usual position) during August and September (Figs. 7.63h,i) over the Solomon Islands, noting the SPCZ is not particularly active at this time of year during the South Pacific dry season. Weak cooling of the ocean surface occurred along the equator during this quarter as signs of another La Niña emerged. Notably, rainfall was suppressed in a large region around Nauru and Kiribati, which extended southward over Vanuatu and eastward over the northern Cook Islands by September. Niue recorded rainfall above its 90th percentile for the JAS quarter, and Faleolo (Samoa) recorded its third driest JAS on record in its 57-year record (86 mm).

Rainfall patterns during the last quarter of 2021 reflected the strengthening La Niña. Rainfall during October and November was suppressed along the equator, with the largest deficits occurring to the west of the date line. The SPCZ continued to be suppressed during October (Fig. 7.63j) before becoming increasingly active during November and December (Fig. 7.63k,l), as is typical for that time of the year. The active SPCZ near the date line in December was associated with enhanced rainfall and tropical cyclone activity in the South Pacific. The enhanced rainfall anomalies were highest in a broad region covering the PNG mainland, the northern Solomon Islands to Fiji and New Caledonia. Rainfall totals above the 90th percentile for OND were recorded in several areas, including Palau, PNG, and the Solomon Islands. Kirakira (Solomon Islands) recorded its wettest OND on record in its 53-year record (1417 mm). Conversely, Tarawa (Kiribati) recorded its second driest OND in its 74-year record (27 mm).

(iii) Notable events and impacts

Severe Tropical Cyclone Niran formed east of the Queensland coast of Australia and moved southeastward towards New Caledonia in early March. By 5 March, Niran had reached Category 5 tropical cyclone strength, with maximum 1-minute sustained winds of 260 km h^{-1} (140 kt) and a central pressure of 931 hPa. Niran was the second Category 5 storm of 2021 globally and the second Category 5 storm of the 2020/21 South Pacific cyclone season behind Tropical Cyclone Yasa which formed in December 2020. Despite not making landfall over New Caledonia, Niran passed close to its main island, Grande Terre, on 6 March; fortunately, the strongest winds remained offshore and, by this stage, it had weakened to a Category 3 storm. Niran continued to track to the southeast as it weakened and transitioned into an extratropical cyclone later that day. As Niran passed close to Grande Terre, gusts up to 150 km h^{-1} (81 kt) were recorded, with 69,000 households estimated to have lost electricity. There was damage to crops and, in the capital city Nouméa, many ships were forced aground along the coast. The damage caused by Niran was estimated at greater than $200 million (U.S. dollars), shared between Australia and New Caledonia (see section 4g7 for more details).

4) AUSTRALIA—S. Tobin and C. Ganter

For this section, monthly area-averaged temperatures are based on the ACORN-SAT dataset v2.2 (Trewin 2018), which begins in 1910. Daily temperatures and mapped temperature analyses are based on the Australian Water Availability Project (AWAP) dataset (Jones et al. 2009), which begins in 1910. Area-averaged rainfall values and mapped analyses use the Australian Gridded Climate Data (AGCD) dataset (Evans et al. 2020), which begins in 1900. Anomalies are based on the 1991–2020 average.

(i) Temperature

Due to the influence of La Niña, 2021 was Australia's coolest year since 2012 when the conclusion of the moderately strong 2011–12 La Niña brought cooler and wetter conditions for the first half of the year. The area-averaged annual mean temperature for 2021 was close to the 1991–2020 average (0.07°C below average), but overall was the 19th-highest in Australia's 112-year record. The annual nationwide mean maximum temperature (Fig. 7.64) was also 0.07°C below average, and the mean minimum temperature (Fig. 7.65) was 0.09°C below average.

In terms of annual anomalies, both mean annual maximum and minimum temperatures were above average for most of tropical northern Australia. Compared to the distribution across all 112 years of observations for 1910–2021, maximum temperatures were in the highest 10% of historical observations for most of the northern tropics, including the Kimberley in Western Australia, the Top End in the Northern Territory, and Queensland's Cape

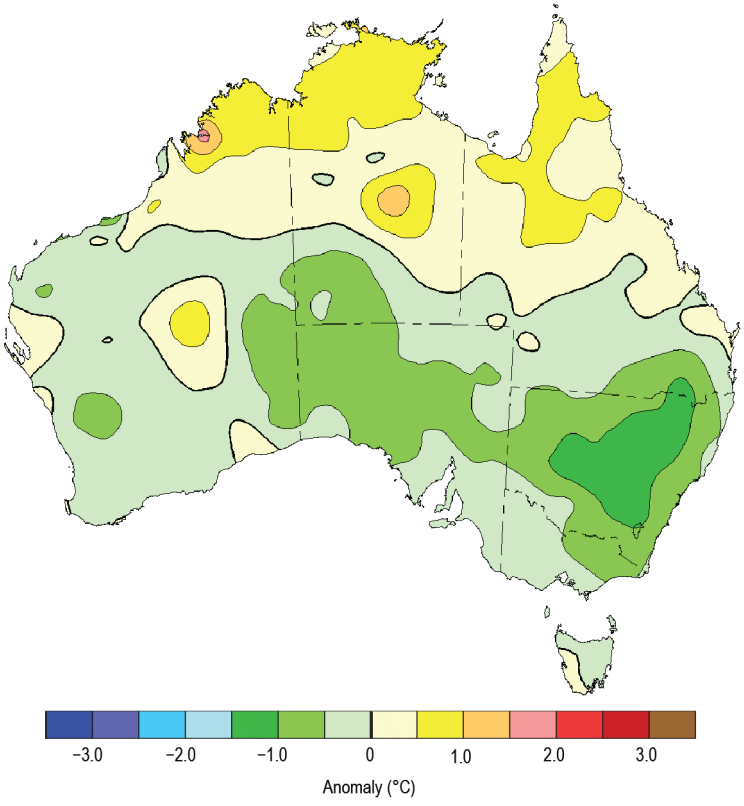

Fig. 7.64. Maximum temperature anomalies (°C; 1991–2020 base period) for Australia, averaged over 2021. Australian States/Territories are as follows, starting clockwise from the west: Western Australia, the Northern Territory, Queensland, New South Wales, Victoria, and South Australia, with the island of Tasmania in the southeast (Source: Australian Bureau of Meteorology.)

York Peninsula. However, much of central New South Wales west of the Great Dividing Range was in the bottom 30% of historical observations.

In terms of significant monthly anomalies, January brought heatwaves to the north of Western Australia and to southeast Australia. Mean temperatures were below average for much of the south and west in February. March and April were cooler than average across large parts of the mainland southeast, while much of the southern half of Western Australia was warmer than average during March, April, and May.

The northern tropics were warmer than average throughout the austral winter. July and August were particularly warm across much of the country, with the national mean temperature fourth and sixth highest on record for those months, respectively. Mean maximum temperatures were highest on record for large parts of northern Australia during July and for some areas along the northern coasts during August.

Warmth continued across the north into spring and early summer, with severe to extreme heatwave conditions in the Kimberley and Top End during October and parts of the north and west of Australia in November and December.

(ii) Precipitation

Averaged across Australia, rainfall for 2021 was 507.8 mm, 4.5% above the 1991–2020 average of 486.0 mm. Compared to the distribution across all 122 years of observations for 1900–2021, annual rainfall was above average for eastern Victoria, much of New South Wales, inland southeast Queensland, much of the west of Western Australia, and much of the far northern tropics, including the Top End of the Northern Territory and Cape York Peninsula in Queensland (Fig. 7.66). Annual rainfall was below average for a few areas, including around the border of South Australia and Victoria.

Very-much-above-average rainfall in eastern Australia was largely a result of an exceptionally wet March and November,

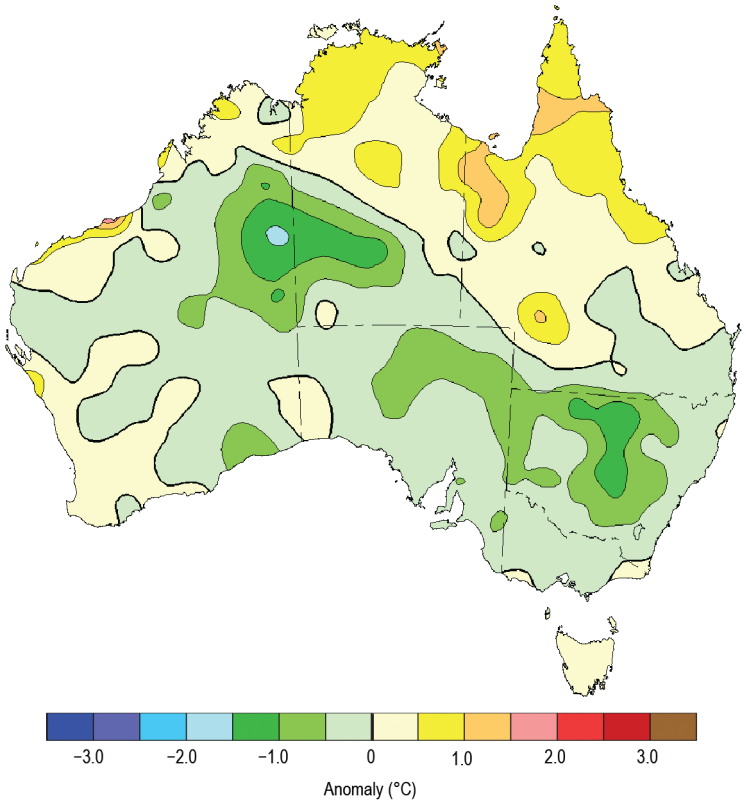

Fig. 7.65. Minimum temperature anomalies (°C; 1991–2020 base period) for Australia, averaged over 2021. (Source: Australian Bureau of Meteorology.)

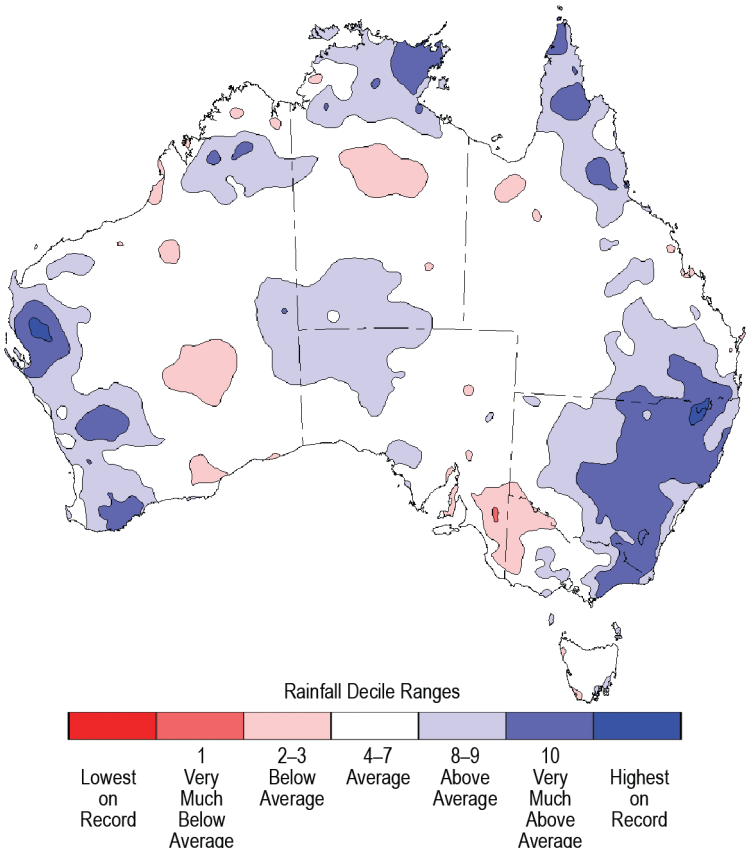

Fig. 7.66. Rainfall deciles for Australia for 2021, based on the 1900–2021 distribution. (Source: Australian Bureau of Meteorology.)

months both marked by flooding across large areas. Above-average rainfall in the west of Western Australia was a result of contributions spread across more of the year, mostly during February, March, May, and July.

La Niña was a dominant influence on Australia's climate during 2021, persisting through summer 2020/21, returning to neutral mid-year, and emerging again during austral spring. La Niña typically brings wetter conditions to much of northern and eastern Australia. A negative Indian Ocean dipole (IOD) during winter and spring also fueled above-average winter–spring rainfall over parts of southern Australia, as is typical of a negative IOD (Ashok et al. 2003). The third key influence for Australia was extended positive Southern Annular Mode conditions, with the strong positive value in June likely influencing drier conditions for southern Western Australia and western Tasmania. However, in Australia, the SAM influence varies strongly by season (Hendon et al. 2007). A positive SAM can also be promoted by La Niña in the spring and summer, which would have contributed to the extraordinarily persistent positive SAM during October–December 2021, a period during which the positive SAM likely contributed both to above-average rainfall across parts of eastern Australia and below-average rainfall over the west-facing coasts, such as southeast South Australia, western Victoria, and western Tasmania.

The year commenced with parts of southwest-to-central Western Australia and the southeastern quarter of Queensland affected by meteorological drought, with rainfall for the period commencing April 2020 in the lowest 10% of historical observations compared to all similar periods since 1900. Above-average rainfall during February resulted in a substantial lessening of deficiencies across much of Western Australia, with follow-up rain during March bringing further relief.

Rainfall during April 2021 was very low for the southeastern mainland. New South Wales observed its ninth-driest April on record and South Australia observed its seventh-driest.

The developing La Niña led to above-average rainfall becoming more widespread as the austral spring progressed. October rainfall was above or very much above average for large areas, and November rainfall was very much above average (highest 10% of historical observations for 1900 to 2021) for large areas of mainland Australia.

While deficiencies in Queensland contracted over the year across the Maranoa and Darling Downs in the inland south, closer to the coast serious or severe rainfall deficiencies persisted until November when very-much-above-average rainfall lifted totals across the Capricornia and Wide Bay and Burnett districts out of the lowest 10% of historical observations. Flooding occurred in numerous rivers in New South Wales and Queensland throughout November.

December rainfall was below average for most of Australia, and very much below average (lowest 10% of historical observations) for parts of the south coast and for most of Tasmania, which observed its sixth-driest December on record.

After commencing 2021 at 58% of capacity, water storages in the Murray–Darling Basin experienced significant filling over winter and spring, increasing to 90.7% by the end of the year, with some storages spilling or being operated to prevent spilling. However, storages in southeast Queensland remained low with the largest storage, Wivenhoe, only increasing from 39% to 47% during 2021. In northern Australia, the volume of water in Argyle Dam increased during 2021 but did not fill for the fourth consecutive year.

(iii) Notable events and impacts

Heatwave conditions affected most of mainland southeast Australia in the days leading up to 26 January. The hottest day was the 24th, with 45.3°C recorded at Port Augusta Aero in South Australia, 43.9°C at Ouyen in Victoria, and 43.6°C at Hay Airport in New South Wales. Sydney Observatory Hill recorded five consecutive days over 30°C from 22 to 26 January, only the ninth such instance since records began in 1859, but the third year in a row that this has occurred.

A major rain event affected many parts of eastern and central Australia in the second half of March. New South Wales observed its second-wettest March in the 122 year-record. Widespread

significant flooding resulted in coastal New South Wales, some adjacent parts of southeast Queensland and eastern Victoria, on some inland rivers in northern New South Wales and southern Queensland, and in eastern Tasmania. Data from the Insurance Council of Australia showed insured claims from this event reached more than $600 million AUD ($420 million US dollars) as of March 2022.

Severe tropical cyclone Seroja brought heavy rains and damaging winds to areas around Kalbarri and Geraldton in Western Australia during April. This was the farthest south a tropical cyclone has crossed the Western Australian coast since the 1950s (see section 4g7 for details).

Low temperatures, heavy rainfall, and damaging winds affected parts of Victoria on 7 and 8 June. The Victorian State Emergency Service received more than 9000 calls for assistance and power was cut to more than 200,000 homes. Repairs to the electrical supply and telecommunications networks took several weeks in some locations due to the severity of damage and large number of fallen trees. Many roads were closed due to flooding, particularly through Gippsland. Insured claims from this event approached $300 million AUD ($210 million US dollars) as of April 2022.

Australia's wettest November on record was due in part to record-high November rainfall at numerous sites in New South Wales and Queensland. Areas of flash flooding and riverine flooding affected eastern and southeast Australia, including large areas of Queensland and inland New South Wales.

The north of Western Australia experienced severe heatwave conditions several times during December, with parts of the northwest observing their hottest December on record, with respect to either mean maximum or mean minimum temperature. Marble Bar recorded a total of 16 days with maximum temperatures of 45°C or above, the highest count for December on record and the second-highest count for any month. Marble Bar also recorded 29 consecutive days of at least 42°C, exceeding the site's December record of 25 days in 1986. Slightly farther south, Geraldton Airport recorded six consecutive days with maximum temperatures at 40°C or above between 24 and 29 December, the longest such run in December and equal to the second-longest run for any month using composite site records that date 1941.

5) NEW ZEALAND—N. Fedaeff

In the following discussion, the base period is 1981–2010. The nationwide average temperature is based upon New Zealand's National Institute of Water and Atmospheric Research (NIWA) seven-station temperature series that began in 1909 (Mullan et al. 2010). All statistics are based on data available as of 12 January 2022.

(i) Temperature

According to NIWA's seven-station temperature series, 2021 was New Zealand's warmest year since records began in 1909. The annual nationwide average temperature was 13.56°C, 0.95°C above average. Mean annual temperatures were above average (+0.51°C to +1.20°C) across much of the country. Well-above-average temperatures (> 1.20°C) occurred in parts of Auckland, Bay of Plenty, Tasman, and Fiordland. Near-average (± 0.50°C of average) temperatures occurred in western Waikato, coastal Wairarapa, and parts of northern Canterbury and Otago (Fig. 7.67a, the named regions are shown in Fig. 7.68). There were several climate drivers that contributed to the record warm year, which are expanded upon in Sidebar 7.5.

The hottest spell of the year occurred over New Zealand from 25 to 28 January, with several locations observing record or near-record high daily maximum and daily minimum temperatures for January. The highest temperature of 2021 was 39.4°C and was recorded at Ashburton on 26 January. This became New Zealand's second-highest January temperature on record and equaled the country's 10th hottest temperature on record for any month. On 27 May, Dunedin airport recorded a minimum temperature of −8.8°C. This equaled the lowest temperature on record at

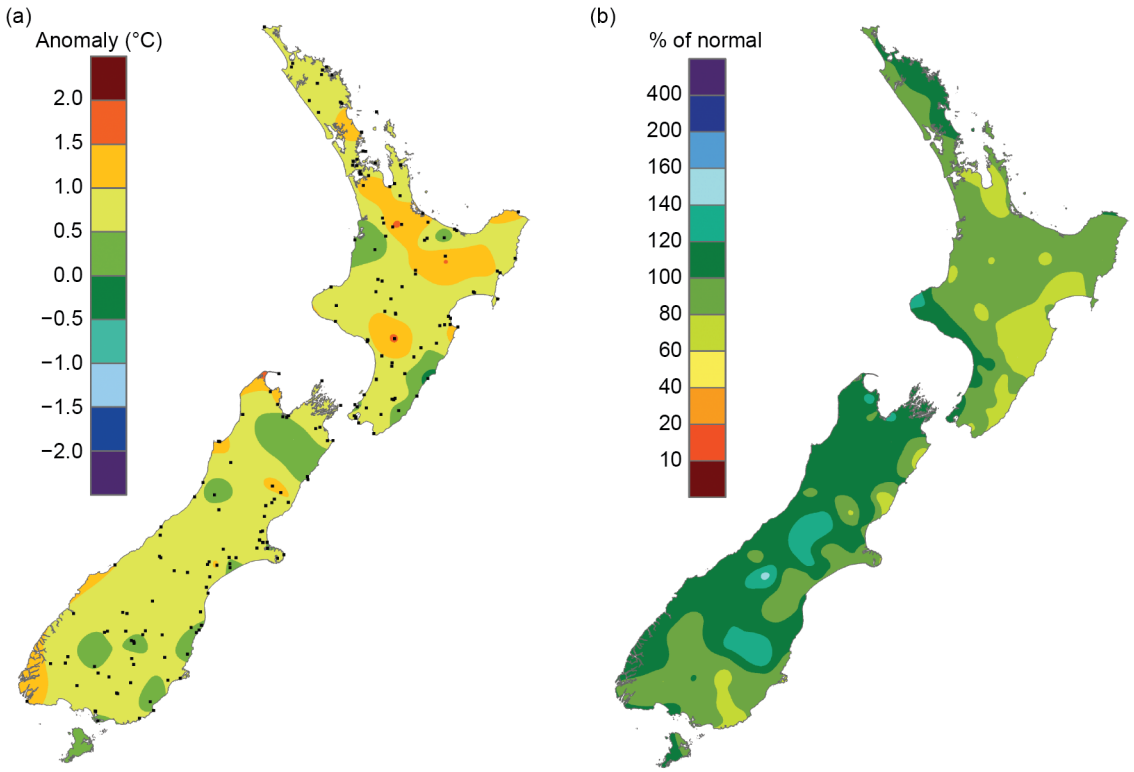

Fig. 7.67. 2021 annual (a) average temperature anomaly (°C) and (b) total rainfall (% of normal), relative to 1981–2010 base period. The dots on (a) represent the locations of climate stations used to create both the temperature and rainfall maps. (Source: NIWA.)

the site since records began in 1962. The lowest air temperature of the year was –10.8°C recorded at Tara Hills on 27 May.

(ii) Precipitation

In 2021, New Zealand rainfall was characterized by extended dry spells, under mainly anticyclonic conditions, interspersed with extreme rainfall events. Annual rainfall totals were near-normal (80–119% of normal) for most of the country. Above-normal rainfall (120–149%) occurred in the west of the lower North Island. Parts of Nelson, interior Canterbury, and Otago also experienced above-normal rainfall (Fig. 7.67b). Lake Tekapo experienced its third wettest year since records began in 1925, while Lauder and Greymouth experienced their fourth wettest (records began in 1924 and 1947, respectively). Conversely, Ohakune and Western Springs in Auckland experienced their third driest year on record (records began in 1948 and 1961, respectively). Of the regularly reporting rainfall gauges, the wettest location in 2021 was Cropp River, in the Hokitika River catchment (West Coast, South Island, 975 m above sea level), with an annual rainfall total of 14,090 mm. The driest of the regularly reporting rainfall sites in 2021 was Alexandra, which recorded 402 mm of rainfall for the year.

(iii) Notable events and impacts

See Fig. 7.68 for a schematic of notable events. The start of 2021 featured extended dry spells in the North Island. Meteorological drought (as defined by the NZ Drought Index [Mol et al. 2017]) developed in the Far North district during January and persisted through late February. Additionally, very dry to extremely dry conditions became widespread across large parts of the North Island, as well as Marlborough and northern Canterbury during February. Water restrictions were temporarily implemented in Northland, Auckland, Wairarapa, and the Hastings District.

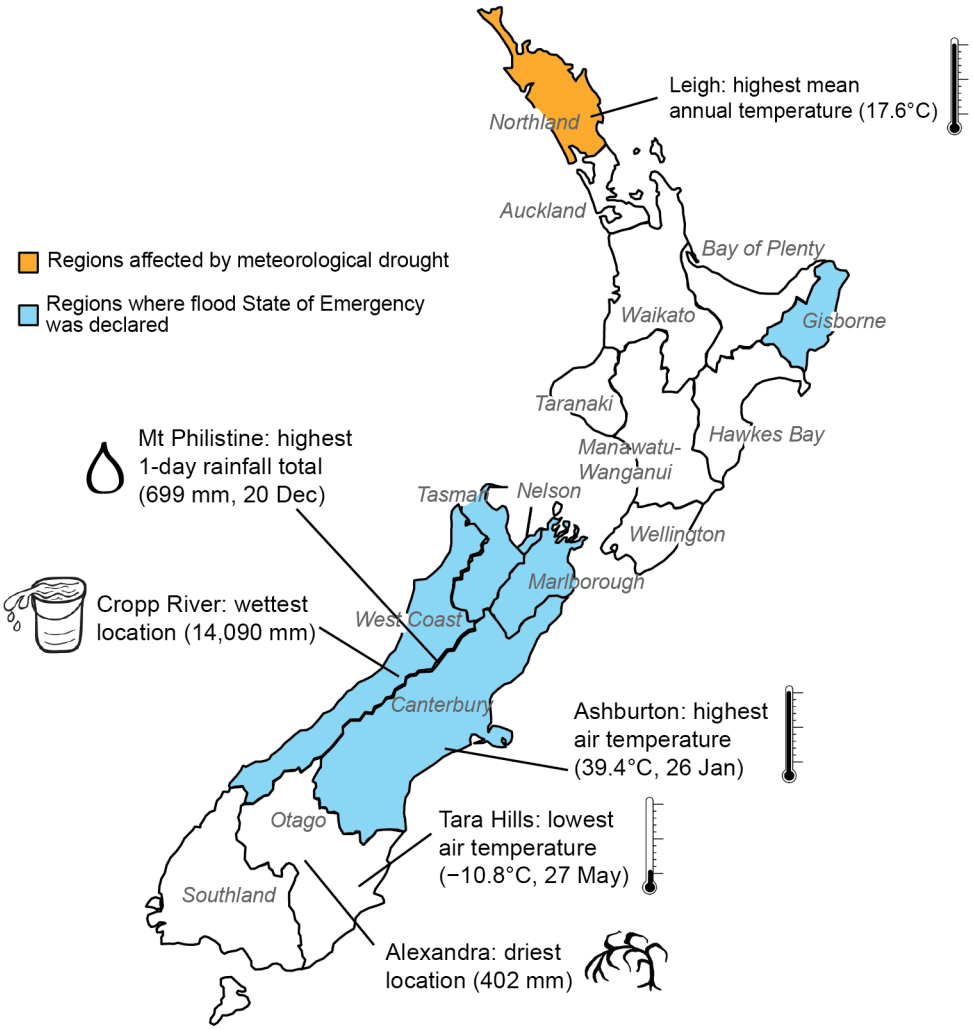

Fig. 7.68. Notable weather events and climate extremes for New Zealand in 2021. (Source: NIWA.)

Three flooding events during 2021 led to State of Emergency declarations. During 29–31 May, prolonged and heavy rain fell over Canterbury and set numerous 24-hour and 48-hour rainfall records for the month of May. Damage caused by the flooding was widespread, with many roads closed, bridges damaged and impassable, and farms suffering considerable impacts to infrastructure and livestock. The emergence of a negative Indian Ocean dipole event (see section 4f for details) and the presence of the active phase of the Madden Julian Oscillation in the Indian Ocean, Maritime Continent, and western Pacific during winter (see section 4c) were likely tropical sources of enhanced moisture supply available to the passing midlatitude cyclonic systems (Fauchereau et al. 2016; Ashok et al. 2007). The most notable flooding event occurred from 15 to 18 July, when an atmospheric river brought heavy rain to the West Coast, Tasman, Nelson, and Marlborough regions. This event led to the Buller River recording the highest flow rate for a New Zealand river. The flooding required evacuations and resulted in an estimated $132.4 million (New Zealand dollars; $91.8 million U.S. dollars) in privately insured damage according to the NZ Insurance Council. The third flooding event occurred during 3–5 November, when a slow-moving subtropical low caused persistent heavy rainfall that affected the eastern North Island and brought flooding and landslides to parts of Gisborne.

Sidebar 7.5: **New Zealand's hottest year on record**—N. Fedaeff

The year 2021 was New Zealand's warmest since records began in 1909. Separately, 12 locations across the country also observed their warmest year on record, and an additional 50 locations experienced an annual average temperature in their respective four highest on record (record lengths for each location are variable, ranging from 21 to 155 years).

Only three months (January, February, and September) had near-average temperatures (± 0.50°C of average), while nine months had above average temperatures (> 0.50°C). No months were cooler than average. Averaged daily data across the whole country based on NIWA's Virtual Climate Station Network shows that, for the country as a whole, 26% of days in 2021 featured below average temperatures, 19% of days had near-average temperatures, and 55% of days experienced above average temperatures.

There were several climate drivers that contributed to the record warm year. The Southern Annular Mode (SAM), an indicator of Southern Hemisphere climate variability, was positive 73% of the time during 2021. The positive SAM phase is associated with higher-than-normal air pressure around New Zealand, which tends to bring light winds, higher temperatures, and drier-than-usual weather to the country (Kidston et al. 2009). There have only been three other years (1993: 75%, 1998: 76%, and 2008: 74%) that have experienced a higher percentage of time in the positive SAM phase with the series extending back to 1979.

In line with the observations of the SAM index, annual mean sea level pressure for 2021 was higher than normal over the North Island and to the east of New Zealand. This was associated with more northerly quarter winds (winds from the northwest to northeast quadrant) than normal. The Trenberth M1 meridional index compares the mean sea level pressure between Hobart, Australia, and the Chatham Islands, New Zealand (Trenberth 1976; Salinger and Mullan 1999). Negative values are associated with northerly airflow. Based on this index, 2021 ranked 13th in terms of the strongest annual northerly airflow anomaly with records extending to 1909 (Fig. SB7.7).

During January and February, moderate La Niña conditions in the central Pacific (which began in October 2020) gradually eased. La Niña in New Zealand is often associated with northeasterly winds and warmer weather; however, the weather patterns at the start of 2021 were generally not consistent with those expected in La Niña. January featured more southwesterly winds than usual, and February featured more easterlies. Both months were some of New Zealand's coolest of the year (relative to the time of year). It is likely the atypical impacts can be attributed, in part, to a non-traditional central Pacific (CP) type of La Niña "modoki" (Capotondi et al. 2015), whereby the minimum sea surface temperature (SST) anomalies are located in the central Pacific rather than the east. Re-developing La Niña conditions during austral spring resulted in a transition from a westerly air flow, near-average temperatures, and widespread

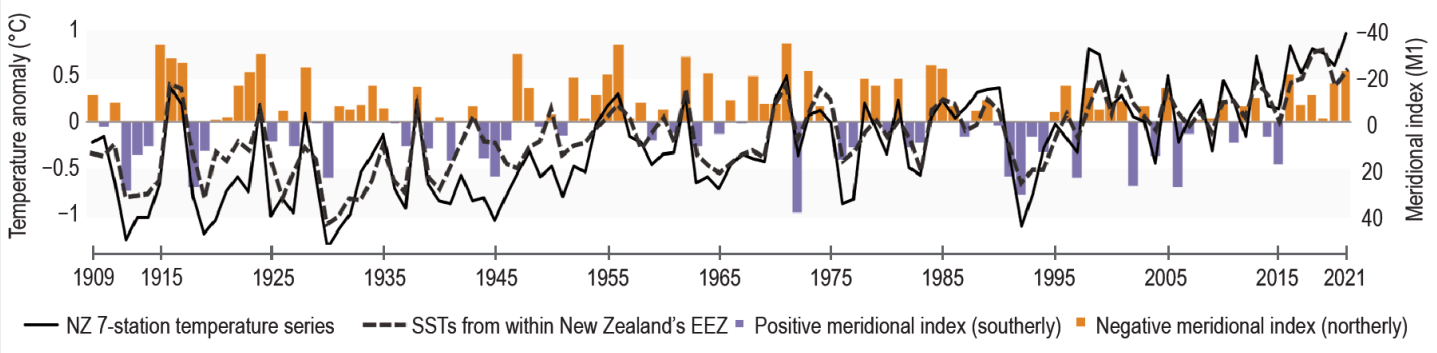

Fig. SB7.7. Timeseries of New Zealand seven-station temperature anomalies (°C, solid black line), sea surface temperature anomalies based on the New Zealand Exclusive Economic Zone (°C, dotted black line), and the Trenberth meridional index (M1) where negative values (orange bars) correspond with more northerly winds and positive values (purple bars) with more southerly winds. Note: the meridional index scale is reversed on the y-axis.

wet weather during September to more northeasterly winds during October–December, bringing frequent warm and humid weather and contributing to the country's fifth-warmest October, record warmest November, and fourth-warmest December. A warm end to the year was partially attributable to increasing coastal SSTs around New Zealand, particularly in November when marine heatwave (MHW) conditions emerged and persisted through the end of the year. During December, daily SSTs reached as high as 4–5°C above average around the western and northern North Island, qualifying as one of the strongest MHW events in the last four decades in the North Island's coastal waters. An area-weighted annual average of SSTs from within New Zealand's Exclusive Economic Zone based on ERSSTv5 (Huang et al. 2017) shows that SSTs for 2021 ranked third-warmest since at least 1909 (Fig. SB7.7).

Increasing global temperatures due to climate change are another key contributor to New Zealand's climate. The linear warming trend across the seven-station series from 1909–2021 is 1.07 ± 0.24°C century^{-1}. A study to discern the contribution of anthropogenic emissions to New Zealand's warmest year has not yet been carried out; however, seven of the past nine years have been among New Zealand's warmest on record.

Acknowledgments

Africa

- We would like to acknowledge the national and/or hydrometeorological services/bureaus of Morocco, Algeria, Egypt, Senegal (National Aviation and Meteorology Agency), Nigeria, South Africa, Madagascar, Seychelles, Comoros Mayotte (France), Reunion (France), and Mauritius.
- We acknowledge support by the NOAA-CPC International Desk. Global datasets from NCEP/NCAR and GPCP are acknowledged.
- Samson Hagos and Zhe Feng are supported by the U.S. Department of Energy Office of Science Biological and Environmental Research as part of the Atmospheric Systems Research (ASR) Program.

Europe

- Much of the information in this section is based on national climate reports kindly provided by the National Meteorological and Hydrological Services (NMHSs) of the WMO RA VI Region. The information has been compiled at the WMO RA VI Regional Climate Centre (RCC) Node on Climate Monitoring, located at Deutscher Wetterdienst (DWD) in Germany. The national contributions have been provided as part of the cooperation between NMHSs and the RCC.
- Specifically, we acknowledge the Instytut Meteorologii i Gospodarki Wodnej (IMGW) PIB in Poland for its kind cooperation with RCC in this subject.

APPENDIX 1: Chapter 7 – Acronyms

AGCD	Australian gridded climate data
AMJ	April–June
AWAP	Australian Water Availability Project
BNGRC	National Office for Risk and Disaster Management
CA	Central Africa
CA	Central America
CAMS	Climate Anomaly Monitoring System
CA-NWS	Central America National Weather Services
CAR	Central Africa Republic
CMORPH CPC	Morphing Technique
CONUS	contiguous United States
COSPPac	Climate and Oceans Support Program in the Pacific
CP	central Pacific
CPC	Climate Prediction Center
DJF	December–February
DRC	Democratic Republic of Congo
ECCC	Environment and Climate Change Canada
ENSO	El Niño–Southern Oscillation
GHA	Greater Horn of Africa
GHCN	Global Historical Climate Network
GPCC	Global Precipitation Climatology Centre
IDI	Integrated Drought Index
INPE	National Institute for Space Research
IO	Indian Ocean
ISMR	Indian summer monsoon rainfall
ITCZ	intertropical Convergence Zone
JAS	July–September
JFM	January–March
JJ	June–July
JJAS	June–September
JTWC	Joint Typhoon Warning Center
LTA	long-term average
MAM	March–May
NCEP/NCAR	National Centers for Environmental Prediction/ National Center for Atmospheric Research
NEM	Northeast monsoon
NH	Northern Hemisphere
NIWA	National Institute of Water and Atmospheric Research
OND	October–December
PNG	Papua New Guinea
RCC-CM	Regional Climate Centre on Climate Monitoring
RFE2	rainfall estimates version 2

SH	Southern Hemisphere
SON	September–November
SPCZ	South Pacific Convergence Zone
SPI	standardized precipitation index
SSA	Southern South America
SST	sea surface temperature
SSTA	sea surface temperature anomaly
TC	tropical cyclone
UN OCHA	United Nations Office for the Coordination of Humanitarian Affairs
WNPSH	western North Pacific Subtropical High

APPENDIX 2: Supplemental Materials

Table A7.1. Temporal coverage of nationally-averaged temperature and precipitation in-situ observations for Europe/WMO RA VI Region[5]. For some countries, only one station (preferably with long time series) has been used (name of the location in brackets). All records extend to the present. Missing values: no information available. Annual anomalies have been calculated from the 1991–2020 average if not otherwise mentioned in footnotes. Ranks are ordered for temperature from highest to lowest and for precipitation in green from wettest to driest and in red from driest to wettest.

Nation	Temperature start of record	Precipitation start of record	Source	Temperature Anomaly	Rank	Precipitation Anomaly	Rank
European average	1950	1950	GHCN[1], data	—	—	—	—
Albania (Korce)	1963	1963	CLIMAT[2]	—	—-	—	—
Andorra	1950	1950	NMHS[3]	—	—	—	—
Armenia	1935	1935	NMHS	+2.1[6]	3	80%[6]	23
Austria	1767	1858	NMHS	−0.2	18	93%	12
Azerbaijan (Astara)	1991	1991	CLIMAT	—	—	—	—
Belarus	1881	1945	NMHS	+0.3[4]	26	112%[4]	9
Belgium (Ukkel-Uccle)	1883	1981	NMHS	−0.3	23	124%	7
Bosnia & Herzegovina (Banja Luka)	1955	1955	CLIMAT	—	—	—	—
Bulgaria	1930	1954 (Burgas)	NMHS/CLIMAT	+0.4	12	120%	7
Croatia (Split/Marjan)	1949	1949	CLIMAT	—	—	—	—
Cyprus (Nicosia)	1899	1899	NMHS	+1.3[4]	3	48%[4]	41
Czechia	1961	1961	NMHS	−0.3	26	100%	51
Denmark	1873	1874	NMHS	−0.4[4]	15	98%[4]	51
Estonia	1961	1961	NMHS	+1.2	8	102%	45
Finland (Helsinki)	1900	1961	NMHS	−0.1	32	104%	15
France	1900	1959	NMHS	+0.4[4]	20	99%[4]	32
Georgia	1956	1881 (Tbilisi)	NMHS	+1.0	6	126%	33
Germany	1881	1881	NMHS	−0.1	21	101%	53
Greece	1960	1949 (Athens)	NMHS/CLIMAT	+1.2[7]	4	105%[7]	42
Hungary	1901	1901	NMHS	+0.1	19	83%	20
Iceland (Stykkishólmur)	1846	1856	NMHS	+0.2	21	92%	84
Ireland	1900	1900	NMHS	+0.34	8	94%	41
Israel	1951	1950)	NMHS	+0.8	4	88%	24
Italy	1961	1949 (Alghero)	NMHS/CLIMAT	+1.36[6]	7	38%[6]	25
Jordan (Amman)	1981	1981	NMHS	+1.3	2	81%	23
Kazakhstan	1941	1941	NMHS	+1.5	5	47%	3
Latvia	1924	1924	NMHS	+0.2	20	99%	55
Lebanon (Beirut)	1949	1949	CLIMAT	—	—	—	—
Lithuania	1961	1887 (Vilnius)	NMHS	−0.1	21	101%	26
Luxembourg (Findel)	1947	1947	NMHS	−0.6	42	154%	52
Malta	1923	1923	NMHS/CLIMAT	+0.8	2	98%	46
Moldova (Chisinau)	1886	1891	NMHS	−0.2	12	111%	16
Monaco	not available	not available	—	—	—	—	—
Montenegro (Plevlja)	1955	1955	CLIMAT	—	—	—	—
Netherlands	1901	1901	NMHS	−0.1	21	106%	38

Table A7.1. Temporal coverage of nationally-averaged temperature and precipitation in-situ observations for Europe/WMO RA VI Region[5]. For some countries, only one station (preferably with long time series) has been used (name of the location in brackets). All records extend to the present. Missing values: no information available. Annual anomalies have been calculated from the 1991–2020 average if not otherwise mentioned in footnotes. Ranks are ordered for temperature from highest to lowest and for precipitation in green from wettest to driest and in red from driest to wettest.

Nation	Temperature start of record	Precipitation start of record	Source	Temperature Anomaly	Rank	Precipitation Anomaly	Rank
North Macedonia (Bitola)	1955	1955	CLIMAT	+0.7[4]	14	114%[4]	11
Norway	1900	1900	NMHS	−0.1	28	90%	50
Poland	1951	1951	NMHS (IMGW)[8]	−0.1	22	116%	25
Portugal	1931	1931	NMHS	+0.4[7]	25	78%[7]	17
Romania	1961	1954 (Bistrita)	NMHS/CLIMAT	+0.9	14	98%	36
Russia, European part	1936	1936	NMHS	+0.7	19	103%	28
Serbia	1951	1951	NMHS	—	—	96%	22
Slovakia	1951	1961	NMHS	+0.5[6]	18	98%[6]	28
Slovenia	1961	1961	NMHS	+0.1	17	93%	50
Spain	1961	1961	NMHS	+0.5[4]	10	89%[4]	14
Sweden	1860	1860	NMHS	+0.05	26	103%	24
Switzerland	1864	1864	NMHS	+0.2	21	105%	47
Syrian Arab Republic (Aleppo)	1960	1960	CLIMAT	+1.8	3	17%	2
Türkiye	1971	1949 (Adana)	NMHS	+1.0	4	91%	14
Ukraine	1891	1891	NMHS	+0.9	17	105%	50
United Kingdom	1884	1862	NMHS	+0.1	18	93%	80

[1] GHCN = Global Historical Climatology Network (Menne et al. 2018)
[2] CLIMAT station data as reported worldwide via the WMO Global Telecommunication System
[3] NMHS = National Meteorological and Hydrological Service; for individual names of NMHSs see https://public.wmo.int/en/about-us/members
[4] normal refers to 1981–2010
[5] https://public.wmo.int/en/about-us/members
[6] normal refers to 1961–1990
[7] normal refers to 1971–2000
[8] IMGW = Instytut Meteorologii i Gospodarki Wodnej PIB

References

Amador, J. A., 1998: A climatic feature of the tropical Americas: The trade wind easterly jet. *Top. Meteor. Oceanogr.*, **5**, 91–102.

——, 2008. The Intra-Americas Seas Low-Level Jet (IALLJ): Overview and future research. *Ann. N. Y. Acad. Sci.*, **1146**, 153–188, https://doi.org/10.1196/annals.1446.012.

——, E. J. Alfaro, H. G. Hidalgo, and B. Calderón, 2011: Central America [in "State of the Climate in 2010"]. *Bull. Amer. Meteor. Soc.*, **92**, S182–S183, https://doi.org/10.1175/1520-0477-92.6.S1.

——, E. R. Rivera, A. M. Durán-Quesada, G. Mora, F. Sáenz, B. Calderón, and N. Mora, 2016a: The easternmost tropical Pacific. Part I: A climate review. *Int. J. Trop. Biol*, **64** (S1), 1–22, https://doi.org/10.15517/rbt.v64i1.23407.

——, A. M. Durán-Quesada, E. R. Rivera, G. Mora, F. Sáenz, B. Calderón, and N. Mora, 2016b: The easternmost tropical Pacific. Part II: Seasonal and intraseasonal modes of atmospheric variability. *Int. J. Trop. Biol*, **64** (S1), 23–57, https://doi.org/10.15517/rbt.v64i1.23409.

——, H. G. Hidalgo, E. J. Alfaro, B. Calderón, and N. Mora, 2018: Central America [in "State of the Climate 2017"]. *Bull. Amer. Meteor. Soc.*, **99** (8), S199–S200, https://doi.org/10.1175/2018BAMSStateoftheClimate.1.

ANA, 2021a: HIDROWEB v3.2.6. Agência Nacional de Águas, https://www.snirh.gov.br/hidroweb/apresentacao.

——, 2021b: Sistema HIDRO – Telemetria. Agência Nacional de Águas, http://www.snirh.gov.br/hidrotelemetria/Mapa.aspx.

Ashok, K., Z. Guan, and T. Yamagata, 2003: Influence of the Indian Ocean dipole on the Australian winter rainfall. *Geophys. Res. Lett.*, **30**, 1821, https://doi.org/10.1029/2003GL017926.

——, H. Nakamura, and T. Yamagata, 2007: Impacts of ENSO and Indian Ocean dipole events on the Southern Hemisphere storm-track activity during austral winter. *J. Climate*, **20**, 3147–3163, https://doi.org/10.1175/JCLI4155.1.

Barichivich, J., E. Gloor, P. Peylin, R. J. W. Brienen, J. Schöngart, J.-C. Espinoza, and K. C. Pattnayak, 2018: Recent intensification of Amazon flooding extremes driven by strengthened Walker circulation. *Sci. Adv.*, **4**, eaat8785, https://doi.org/10.1126/sciadv.aat8785.

Branstator, G., and H. Teng, 2017: Tropospheric waveguide teleconnections and their seasonality. *J. Atmos. Sci.*, **74**, 1513–1532, https://doi.org/10.1175/JAS-D-16-0305.1.

Capotondi, A., and Coauthors, 2015: Understanding ENSO diversity. *Bull. Amer. Meteor. Soc.*, **96**, 921–938, https://doi.org/10.1175/BAMS-D-13-00117.1.

CLIMATEMPO, 2021: São Paulo registra duplo recorde de frio. 30 June, accessed 20 January 2022, https://www.climatempo.com.br/noticia/2021/06/30/sao-paulo-registra-duplo-recorde-de-frio-0627.

Cunha, A. P. M. A., and Coauthors, 2019: Extreme drought events over Brazil from 2011 and 2019. *Atmosphere*, **10**, 642, https://doi.org/10.3390/atmos10110642.

Espinoza, J.-C., J. A. Marengo, J. Ronchail, J. M. Carpio, L. N. Flores, and J. L. Guyot, 2014: The extreme 2014 flood in south-western Amazon basin: The role of tropical-subtropical South Atlantic SST gradient. *Environ. Res. Lett.*, **9**, 124007, https://doi.org/10.1088/1748-9326/9/12/124007.

——, ——, J. Schöngart, and J. C. Jimenez, 2022: The new historical flood of 2021 in the Amazon River compared to major floods of the 21st century: Atmospheric features in the context of the intensification of floods. *Wea. Climate Extremes*, **35**, 100406, https://doi.org/10.1016/j.wace.2021.100406.

Evans, A., D. Jones, R. Smalley, and S. Lellyett, 2020: An enhanced gridded rainfall analysis scheme for Australia. Bureau of Meteorology Research Rep. 041, 39 pp., www.bom.gov.au/research/publications/researchreports/BRR-041.pdf.

FAN, 2021: La sequedad de la vegetación a causa de las heladas aumentan el riesgo de incendios forestales en la Chiquitania. Fundación Amigos de la Naturaleza, 13 July, accessed 12 January 2022, http://incendios.fan-bo.org/Satrifo/la-sequedad-de-la-vegetacion-a-causa-de-las-heladas-aumentan-el-riesgo-de-incendios-forestales-en-la-chiquitania/.

Fauchereau, N., B. Pohl, and A. Lorrey, 2016: Extratropical impacts of the Madden–Julian oscillation over New Zealand from a weather regime perspective. *J. Climate*, **29**, 2161–2175, https://doi.org/10.1175/JCLI-D-15-0152.1.

Filizola, N., E. M. Larubesse, P. Fraizy, R. Souza, V. Guimarães, and J.-L. Guyot, 2014: Was the 2009 flood the most hazardous or the largest ever recorded in the Amazon? *Geomorphology*, **215**, 99–105, https://doi.org/10.1016/j.geomorph.2013.05.028.

Funk, C., and Coauthors, 2015a: The Climate Hazards Infrared Precipitation with Stations—A new environmental record for monitoring extremes. *Sci Data*, **2**, 150066, https://doi.org/10.1038/sdata.2015.66.

——, and Coauthors, 2015b: Climate Hazards InfraRed Precipitation with Station data-2.0 global monthly data. Climate Hazards Center, accessed 27 December 2021, https://data.chc.ucsb.edu/products/CHIRPS-2.0/global_monthly/netcdf/.

Harrigan, S., and Coauthors, 2020: GloFAS-ERA5 operational global river discharge reanalysis 1979–present. Earth Syst. *Sci. Data*, **12**, 2043–2060, https://doi.org/10.5194/essd-12-2043-2020.

——, and Coauthors, 2021: River discharge and related historical data from the Global Flood Awareness System, v3.1, Copernicus Climate Change Service (C3S) Climate Data Store (CDS), accessed 4 January 2022, https://cds.climate.copernicus.eu/cdsapp#!/dataset/cems-glofas-historical, https://doi.org/10.24381/cds.a4fdd6b9.

Hendon, H. H., D. W. Thompson, and M. C. Wheeler, 2007: Australian rainfall and surface temperature variations associated with the Southern Hemisphere annular mode. *J. Climate*, **20**, 2452–2467, https://doi.org/10.1175/JCLI4134.1.

Hidalgo, H. G., E. J. Alfaro, J. A. Amador, and A. Bastidas, 2019: Precursors of quasi-decadal dry-spells in the Central America Dry Corridor. *Climate Dyn.*, **53**, 1307–1322, https://doi.org/10.1007/s00382-019-04638-y.

Huang, B., and Coauthors, 2017: NOAA Extended Reconstructed Sea Surface Temperature (ERSST), version 5. NOAA National Centers for Environmental Information, accessed 2 February 2022, https://doi.org/10.7289/V5T72FNM.

Jones, D. A., W. Wang, and R. Fawcett, 2009: High-quality spatial climate datasets for Australia. *Aust. Meteor. Oceanogr. J.*, **58**, 233–248, https://doi.org/10.22499/2.5804.003.

Kidston, J., J. A. Renwick, and J. McGregor, 2009: Hemispheric-scale seasonality of the southern annular mode and impacts on the climate of New Zealand. *J. Climate*, **22**, 4759–4770, https://doi.org/10.1175/2009JCLI2640.1.

Koren, G., and Coauthors, 2018: Widespread reduction in sun-induced fluorescence from the Amazon during the 2015/2016 El Niño. *Philos. Trans. Roy. Soc.*, **B373**, 20170408, https://doi.org/10.1098/rstb.2017.0408.

Lehner, B., and G. Grill, 2013: Global river hydrography and network routing: baseline data and new approaches to study the world's large river systems. *Hydrol. Processes*, **27**, 2171–2186, https://doi.org/10.1002/hyp.9740.

Lewis, S. L., P. M. Brando, O. L. Phillips, G. M. F. van der Heijden, and D. Nepstad, 2011: The 2010 Amazon Drought. *Science*, **331**, 554, https://doi.org/10.1126/science.1200807.

Libonati, R., and Coauthors, 2022: Assessing the role of compound drought and heatwave events on unprecedented 2020 wildfires in the Pantanal. *Environ. Res. Lett.*, **17**, 015005, https://doi.org/10.1088/1748-9326/ac462e.

Magaña, V., J. A. Amador, and S. Medina, 1999: The midsummer drought over Mexico and Central America. *J. Climate*, **12**, 1577–1588, https://doi.org/10.1175/1520-0442(1999)012<1577:TMDOMA>2.0.CO;2.

Marengo, J. A., and Coauthors, 2021: Extreme drought in the Brazilian Pantanal in 2019–2020: Characterization, causes, and impacts. *Front. Water*, **3**, 639204, https://doi.org/10.3389/frwa.2021.639204.

Menne, M. J., C. N. Williams, and B. E. Gleason, 2018: The Global Historical Climatology Network monthly temperature dataset, version 4. *J. Climate*, **31**, 9835–9854, https://doi.org/10.1175/JCLI-D-18-0094.1.

Merrifield, M. A., P. R. Thompson, and M. A. Lander, 2012: Multidecadal sea level anomalies and trends in the western tropical Pacific. *Geophys. Res. Lett.*, **39**, L13602, https://doi.org/10.1029/2012GL052032.

Mol, A., A. Tait, and G. Macara, 2017: An automated drought monitoring system for New Zealand. *Wea. Climate*, **37**, 23–36, https://doi.org/10.2307/26735444.

Mullan, A. B., S. J. Stuart, M. G. Hadfield, and M. J. Smith, 2010: Report on the review of NIWA's "seven-station" temperature series. NIWA Information Series 78, 175 pp., https://niwa.co.nz/sites/niwa.co.nz/files/import/attachments/Report-on-the-Review-of-NIWAas-Seven-Station-Temperature-Series_v3.pdf.

Naumann, G., and Coauthors, 2021: The 2019–2021 extreme drought episode in La Plata Basin : A joint report from EC-JRC, CEMADEN, SISSA and WMO. EUR 30833 EN, Publications Office of the European Union, 44 pp.,https://data.europa.eu/doi/10.2760/773.

NOAA, 2022: U.S. billion-dollar weather and climate disasters. NOAA/National Centers for Environmental Information, https://www.ncei.noaa.gov/access/billions/.

ReliefWeb, 2021: Brazil: Floods - Dec 2021. Accessed 8 January 2022, https://reliefweb.int/disaster/fl-2021-000204-bra.

Rodriguez, A., R. Camargo, and V. Ibarnegaray, 2021: Cuantificación de áreas quemadas en Bolivia, con información de enero a octubre de 2021. Fundación Amigos de la Naturaleza, https://incendios.fan-bo.org/Satrifo/areas-quemadas-ago-2021/.

Saji, N. H., and T. Yamagata, 2003: Possible impacts of Indian Ocean Dipole mode events on global climate. *Climate Res.*, **25**, 151–169, https://doi.org/10.3354/cr025151.

Salinger, J. M., and A. B. Mullan, 1999: New Zealand climate: Temperature and precipitation variations and their links with atmospheric circulation. *Int. J. Climatol.*, **19**, 1049–1071, https://doi.org/10.1002/(SICI)1097-0088(199908)19:10<1049::AID-JOC417>3.0.CO;2-Z.

Satyamurty, P. C. P. Wanzeler da Costa, A. O. Manzi, and L. A. Candido, 2013: A quick look at the 2012 record flood in the Amazon Basin. *Geophys. Res. Lett.*, **40**, 1396–1401, https://doi.org/10.1002/grl.50245.

Schneider, U., P. Finger, A. Meyer-Christoffer, M. Ziese, and A. Becker, 2018: Global precipitation analysis products of the GPCC. Deutscher Wetterdienst, 15 pp., https://opendata.dwd.de/climate_environment/GPCC/PDF/GPCC_intro_products_v2018.pdf

Smith, A. B., 2020: U.S. billion-dollar weather and climate disasters, 1980–present (NCEI Accession 0209268). NOAA/National Centers for Environmental Information, accessed 27 March 2022, https://doi.org/10.25921/stkw-7w73.

——, 2022: 2021 U.S. billion-dollar weather and climate disasters in historical context. Climate.gov, https://www.climate.gov/news-features/blogs/beyond-data/2021-us-billion-dollar-weather-and-climate-disasters-historical.

Taylor, M., D. Enfield, and A. Chen, 2002: Influence of the tropical Atlantic versus the tropical Pacific on Caribbean rainfall. *J. Geophys. Res.*, **107**, 3127, https://doi.org/10.1029/2001JC001097. Trenberth, K. E., 1976: Fluctuations and trends in indices of the Southern Hemispheric circulation. *Quart. J. Roy. Meteor. Soc.*, **102**, 65–75, https://doi.org/10.1002/qj.49710243106.

Trewin, B., 2018: The Australian Climate Observations Reference Network–Surface Air Temperature (ACORN-SAT) version 2. Bureau of Meteorology Research Rep. No. 032, 57 pp., www.bom.gov.au/research/publications/researchreports/BRR-032.pdf.

van Schaik, E., L. Killaars, N. E. Smith, G. Koren, L. P. H. van Beek, W. Peters, and I. T. van der Laan-Luijkx, 2018: Changes in surface hydrology, soil moisture and gross primary production in the Amazon during the 2015/2016 El Niño. *Philos. Trans. Roy. Soc.*, **B373**, 20180084, https://doi.org/10.1098/rstb.2018.0084.